AD NUMBER

ADB012440

LIMITATION CHANGES

TO:

Approved for public release; distribution is unlimited.

FROM:

Distribution authorized to U.S. Gov't. agencies only; Test and Evaluation; APR 1976. Other requests shall be referred to Air Force Wright Laboratory, LRO, Kirtland AFB, NM 87117.

AUTHORITY

afwl ltr 7 nov 1986

AD B012440

AUTHORITY:
AFWL ctc,
7 NOV 86

AFWL-TR-74-331

AFWL-TR-74-331

AIRBORNE POINTING AND TRACKING SYSTEMS OPEN PORT DESIGN AND MODIFICATION ANALYSIS

Hughes Aircraft Company
Electro-Optical and Data Systems Group
Culver City, CA 90230

April 1976

Final Report

AIR FORCE WEAPONS LABORATORY
Air Force Systems Command
Kirtland Air Force Base, NM 87117

AFWL-TR-74-331

This final report was prepared by Hughes Aircraft Company, Culver City, California, under Contract F29601-73-C-0080, Job Order 317J1304 with the Air Force Weapons Laboratory, Kirtland Air Force Base, New Mexico. Major Dennis L. Boesen (LRO) was the Laboratory Project Officer-in-Charge.

When US Government drawings, specifications, or other data are used for any purpose other than a definitely related Government procurement operation, the Government thereby incurs no responsibility nor any obligation whatsoever, and the fact that the Government may have formulated, furnished, or in any way supplied the said drawings, specifications, or other data, is not to be regarded by implication or otherwise, as in any manner licensing the holder or any other person or corporation, or conveying any rights or permission to manufacture, use, or sell any patented invention that may in any way be related thereto.

This technical report has been reviewed and is approved for publication.

DENNIS L. BOESEN
Major, USAF
Project Officer

FOR THE COMMANDER

LAWRENCE SHER
Chief, ALL Beam Control Branch

RUSSELL K. PARSONS
Colonel, USAF
Chief, Laser Development Division

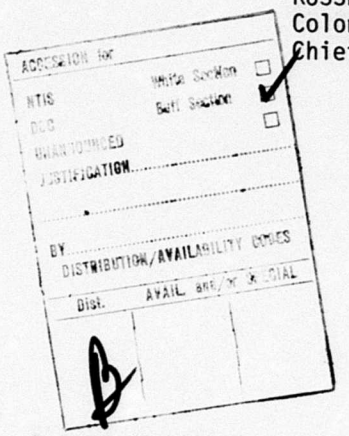

DO NOT RETURN THIS COPY. RETAIN OR DESTROY.

UNCLASSIFIED

SECURITY CLASSIFICATION OF THIS PAGE (When Data Entered)

REPORT DOCUMENTATION PAGE

READ INSTRUCTIONS BEFORE COMPLETING FORM

1. REPORT NUMBER: AFWL-TR-74-331
2. GOVT ACCESSION NO.
3. RECIPIENT'S CATALOG NUMBER
4. TITLE (and Subtitle): AIRBORNE POINTING AND TRACKING SYSTEMS OPEN PORT DESIGN AND MODIFICATION ANALYSIS.
5. TYPE OF REPORT & PERIOD COVERED: FINAL REPORT.
6. PERFORMING ORG. REPORT NUMBER
7. AUTHOR(s)
8. CONTRACT OR GRANT NUMBER(s): F29601-73-C-0080 NEW
9. PERFORMING ORGANIZATION NAME AND ADDRESS: Hughes Aircraft Company, Electro-Optical and Data Systems Group, Culver City, CA 90230
10. PROGRAM ELEMENT, PROJECT, TASK AREA & WORK UNIT NUMBERS: 63605F; AF-317J/13/04; 13
11. CONTROLLING OFFICE NAME AND ADDRESS: Air Force Weapons Laboratory, Kirtland Air Force Base, New Mexico 87117
12. REPORT DATE: Apr 76
13. NUMBER OF PAGES: 157
14. MONITORING AGENCY NAME & ADDRESS (if different from Controlling Office): 212 p.
15. SECURITY CLASS. (of this report): UNCLASSIFIED
15a. DECLASSIFICATION/DOWNGRADING SCHEDULE

16. DISTRIBUTION STATEMENT (of this Report)

Distribution limited to US Government agencies only because of test and evaluation of military systems (Apr 76). Other requests for this document must be referred to AFWL (LRO), Kirtland Air Force Base, New Mexico 87117.

17. DISTRIBUTION STATEMENT (of the abstract entered in Block 20, if different from Report)

18. SUPPLEMENTARY NOTES

19. KEY WORDS (Continue on reverse side if necessary and identify by block number)

Open Port
Open Aperture
Laser

20. ABSTRACT (Continue on reverse side if necessary and identify by block number)

The Open Port modification to the Airborne Pointer Tracker (APT) system makes possible system operation without a sealed aperture window. This is accomplished by a protective shroud that prevents direct airstream impingement on critical internal turret components and a porous aperture aerofence that reduces acoustical coupling of the turret cavity to the airstream. An extensive instrumentation of the Open Port components has been accomplished. Data obtained will include dynamic pressure, static pressure, temperature and structural stress. The instrumentation signals are conditioned by a (OVER)

DD FORM 1 JAN 73 1473 EDITION OF 1 NOV 65 IS OBSOLETE

409 084

UNCLASSIFIED

SECURITY CLASSIFICATION OF THIS PAGE (When Data Entered)

ABSTRACT (Cont'd)

compact turret mounted, electronic amplifier before they are delivered to the recording system of the Airborne Laser Laboratory (ALL) aircraft. A general description of the physical and operational characteristics of the Open Port modification is provided in the following text. The design analyses undertaken as part of the modification work task directive and the resultant conclusions are also provided.

CONTENTS

CONTENTS (Continued)

LIST OF ILLUSTRATIONS

LIST OF TABLES

SECTION I

SYSTEM DESCRIPTION AND OBJECTIVES

The Airborne Pointing and Tracking (APT) Open Port modification design and analysis was performed to demonstrate that the APT can be safely tested in airborne operation with an Open Port modification which incorporates protective structural elements.

This design and analysis task was performed and detail elements of the structural components were drawn in preparation for final fabrication. An instrumentation system concept was formulated for the required testing in the Airborne Laser Laboratory.

The major objectives to be accomplished with the hardware designed for this system are

- Fly Open Port, all configurations and determine restrictions
- Measure torque on gimbal axes
- Verify wind tunnel data
- Determine improvements which can be incorporated into high power Open Port modification
- Determine propagation characteristics

This report deals with the design and analysis which demonstrates that it is feasible and safe to fly and test the APT Pointing assembly with an open port.

BACKGROUND

The pointing assembly of the APT system is currently designed to operate as a sealed, environmentally conditioned unit. Temperature is maintained at approximately 70°F. Internal pressure is maintained at 3 psi above external ambient pressure. Input and output windows fabricated with zinc selenide optical material will be installed in the Pointing Assembly (PA)

in order to allow the PA to retain its environmental seal while propagating a low power carbon dioxide laser beam. It has become apparent, however, that certain inflight experiments will be required with the output window removed. The objective of the technical design was, therefore, to design modifications to the pointing assembly that will allow safe operation of the APT system with the output window removed.

To back up the feasibility of open port operation of the APT, the Airforce performed wind tunnel testing* on a 0.3 scale model of the APT with an open port. The results of data reduction from this test indicated that open port operation would result in satisfactory system performance if the inner gimbal mounted telescope was properly shrouded from wind loading, and a suitable aerodynamic fence was used around the periphery of the open port.

The existing plexiglass window assembly and the Low Power Window assembly and its ancillary equipment bound the approximate weight and cg location for an Open Port modification weight. Since this weight is relatively high, it was decided early in the design phase of Open Port that a very conservative approach was feasible that would result in an economical flight safe design.

FUNCTIONAL DESCRIPTION AND OPERATION

The APT Open Port modification Figure 1-1 consists of structural shrouds which are designed to reduce or eliminate wind load torques on the fine gimbal-mounted elements of the APT pointing assembly when it is flown with the eyelid retracted. The modification also incorporates an instrumentation system which will measure residual wind load torques and collect pressure distribution data on the shroud elements for comparison with the 0.3 scale wind tunnel model. In order to decrease aerodynamic disturbances inside the open cavity, the modification includes a 50 percent porous fence around the periphery of the open port. Since the pointing assembly is still thermally conditioned, it was necessary to design a positive eyelid pressure

*Reference AFWL-TR-73-17, "0.3 Scale Open Port ALL Turret Wind Tunnel Test Results" Volume 1, April 1973 (Confidential).

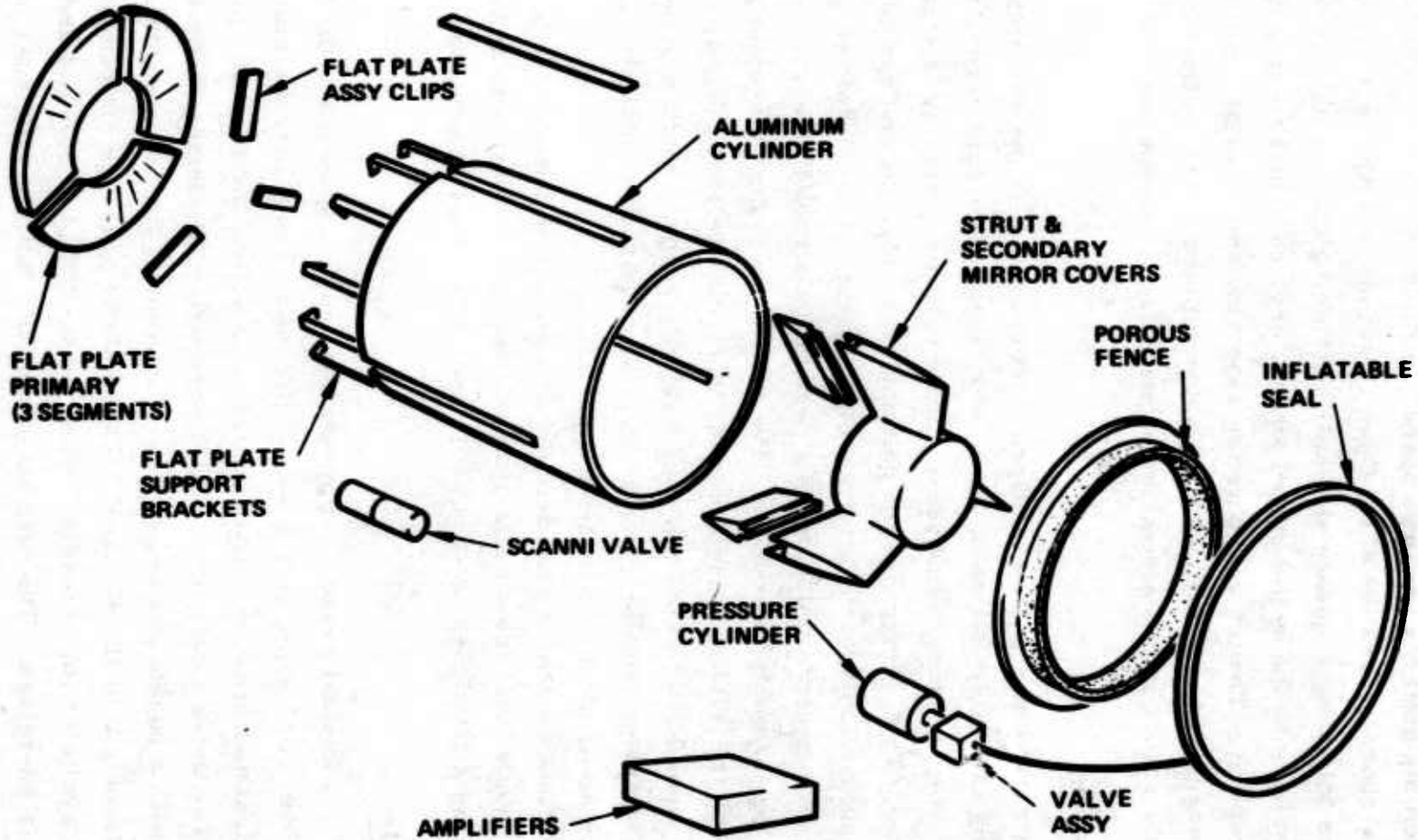

Figure 1-1. Open Port modification kit.

sealing system so that the environmental control system could condition the pointing assembly until the port was opened in flight.

The airborne operation of the Open Port modified APT system will consist of the following sequence of events, assuming that the APT is functioning normally with the eyelid closed and the environmental control system operating properly. The internal pointing assembly should be at a nominal 70°F and pressurized to a nominal 3 psi above ambient. The instrumentation system should read steady-state values of pressure, temperature, and strain.

De-compression

The first event required for Open Port operation is the de-compression of the pointing assembly to a point where very little ΔP occurs across the eyelid seal. The pressure transducers should indicate a new lower steady-state pressure. To de-compress the pointing assembly, the environmental control pressurization system is turned off. A vent valve solenoid (Figure 1-2) in the turret is energized which opens a port to the aircraft exterior, exhausting the pointing assembly to ambient. The vent valve is then closed to prevent airflow through the APT pointing assembly when the eyelid is opened.

If the eyelid fails to open or only partially opens, switches in the existing eyelid system should indicate the failure. Analysis indicates that a partially open aperture does not affect flight safety.

The inflatable seal is then deflated and the eyelid opened. This deflation method should limit the amount of debris that moves past optical surfaces since the major airflow will be out of the base of the pointing assembly.

Data Recording

Power is applied to the Instrumentation and Signal Conditioning Module (ISCM) whenever APT secondary power is present. Thus, turret temperature, strain, and dynamic pressure instrumentation is active and available for recording. The drive motor to the static pressure multiplexing "Scanivalve" is activated with a pushbutton switch that is located on the Instrumentation and Signal Conditioning Unit (ISCU) panel. Thus, static pressure instrumentation is active and available for recording whenever the ICOM is powered and the drive motor is energized. The position of the APT turret eyelid does not have any control over instrumentation operational status.

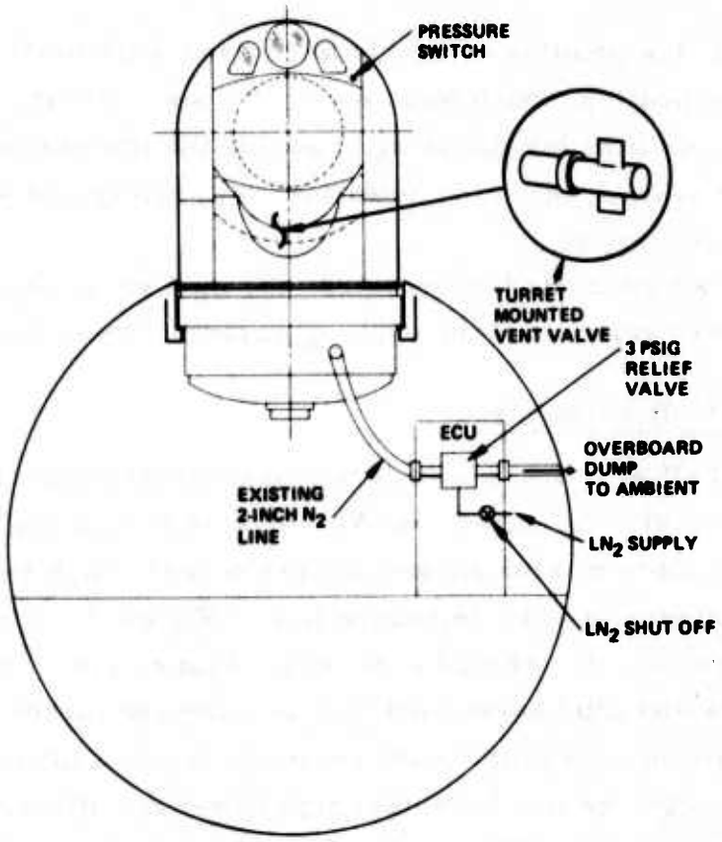

Figure 1-2. Open Port overboard dump.

Re-compression

After the data required are recorded, the unit is re-pressurized by closing the eyelid. The pneumatic seal is inflated after receiving a lid closed signal. The environmental control system is then activated to recondition the pointing assembly.

MECHANICAL MODIFICATION KIT

The Open Port mechanical modification kit was designed with the primary emphasis on a kit that could be installed without removal of the APT pointing assembly from the aircraft and with minimum disassembly of the pointing assembly. As designed, all of the elements of the mod kit can be inserted through the front opening of the pointing assembly after removal of the plexiglass window or the lower power window assembly.

Initially, the pointing assembly must have work performed on it that anticipates modification. Such work would include installing the required signal harness, drilling the mounting holes for the instrumentation mod kit, and drilling the several mounting holes for transducers and brackets for the inflatable seal assembly.

With these elements incorporated, the mod kit as presently designed, should not require removal of the pointing assembly from the ALL aircraft.

Mechanical Mod Kit Elements

Figure 1-3* is a breakdown of the mechanical elements of the Open Port modification kit. As shown, the kit contains two (2) major shroud elements, the secondary mirror shroud and the covers which surround the three (3) strut elements and a telescope liner. Except for the exposed secondary mirror(s), this shroud assembly, (Figure 1-4) completely covers all exposed area and eliminates wind load torquer and forces on these elements. The trailing edge of the strut shroud is tapered to simulate a mirror which might be required in an eventual high power modification of the APT.

The telescope liner (Figure 1-5) is a right circular cylinder which lines the inside of the telescope assembly from the front opening of the coarse elevation shroud back to the auto alignment reference mirror. The front flange of the liner is bolted to the existing holes which mount the low power window and has several screened holes in its periphery which provide a path for exhausting the air from the pointing assembly.

The cylindrical portion of the assembly has three (3) slots which allow the assembly to be installed over the secondary mirror struts of the telescope. After installation, the three cover plates are bolted over the slots so that the assembly acts as a homogeneous structure. The bottom of the cylinder has attachment holes for the brackets which support the primary mirror shroud cover (backplate).

This backplate assembly is designed to be installed in three segments around the beam steering assembly, and is bolted together in place with three doublers. A protective cover for the beam steering mirror assembly (Figure 1-6) must be installed prior to installation of the three primary mirror cover parts.

*Figure 1-3 is a foldout and appears at the end of this report.

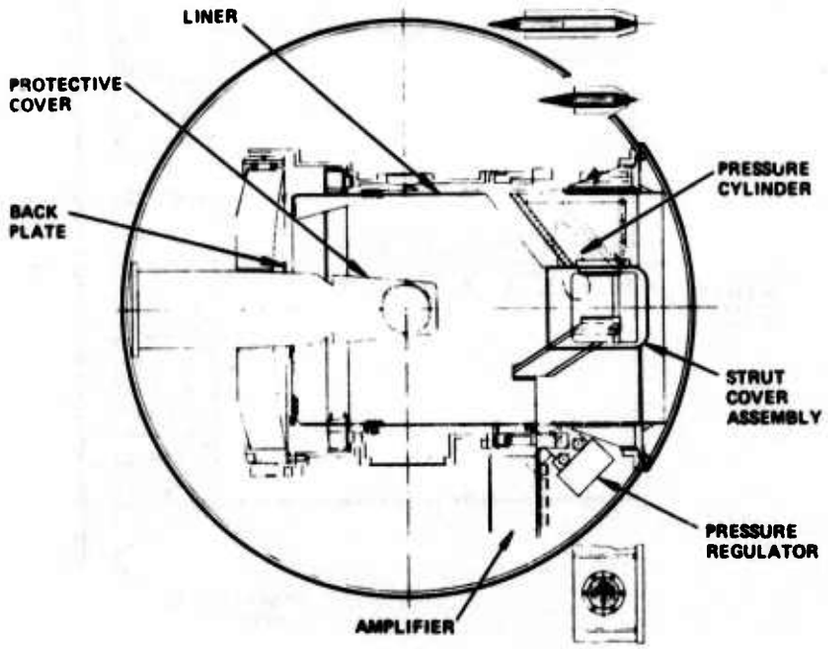

Figure 1-4. Open Port layout.

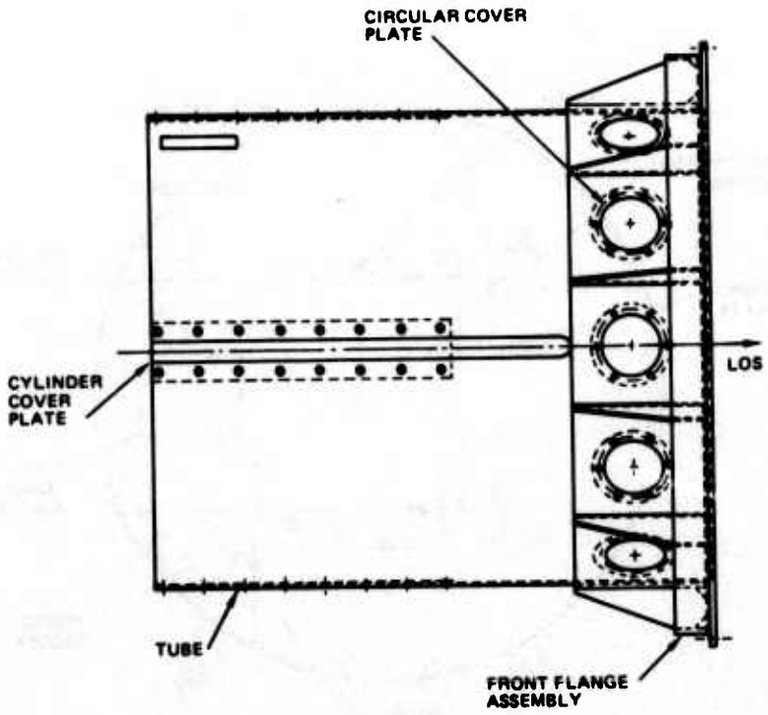

Figure 1-5. Telescope liner.

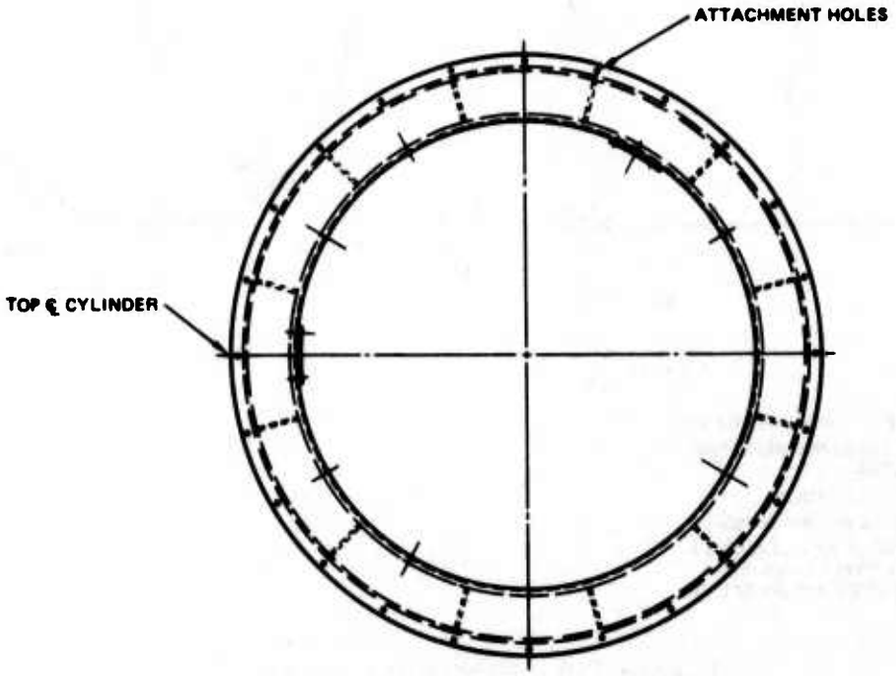

Figure 1-5. Telescope liner. (Continued)

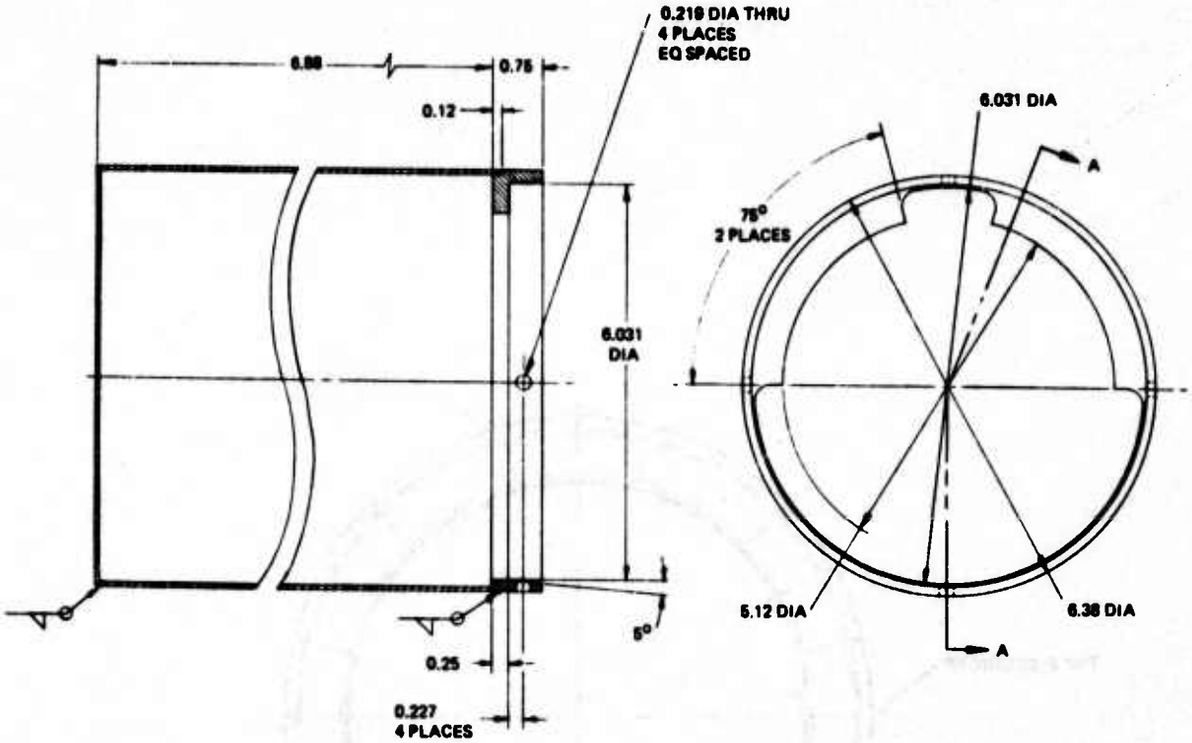

NOTES: UNLESS OTHERWISE SPECIFIED

1 REMOVE ALL BURRS AND BREAK SHARP EDGES

2 SURFACE FINISH 125√

3 FUSION WELD PER MIL-W-8604

(4) MARK CODE IDENT AND PART NO PER HP8-5, TYPE I, CLASS 3, GRA, FORM 2, LOCATE APPROX AS SHOWN

Figure 1-6. Protective cover.

The mechanical modification kit also includes two aerodynamic fences which are mounted external to the pointing assembly aperture. One fence is designed to extend as far from the aperture as possible without interference with the eyelid of the pointing assembly. The second fence sticks out a minimum of 1.65 inches from the aperture and is basically a minimum design which was scaled from the 0.3 wind tunnel model. Only one fence at a time is installed on the pointing assembly for the Open Port tests.

The eyelid seal assembly on both the plexiglass and the low power window assembly is designed to act only as a dust seal. The Open Port modification requires a seal which must withstand differential air pressure without leakage. Figure 1-7 is an inflatable seal assembly which is required for the modification. It consists of a pneumatic seal, a seal mounting ring,

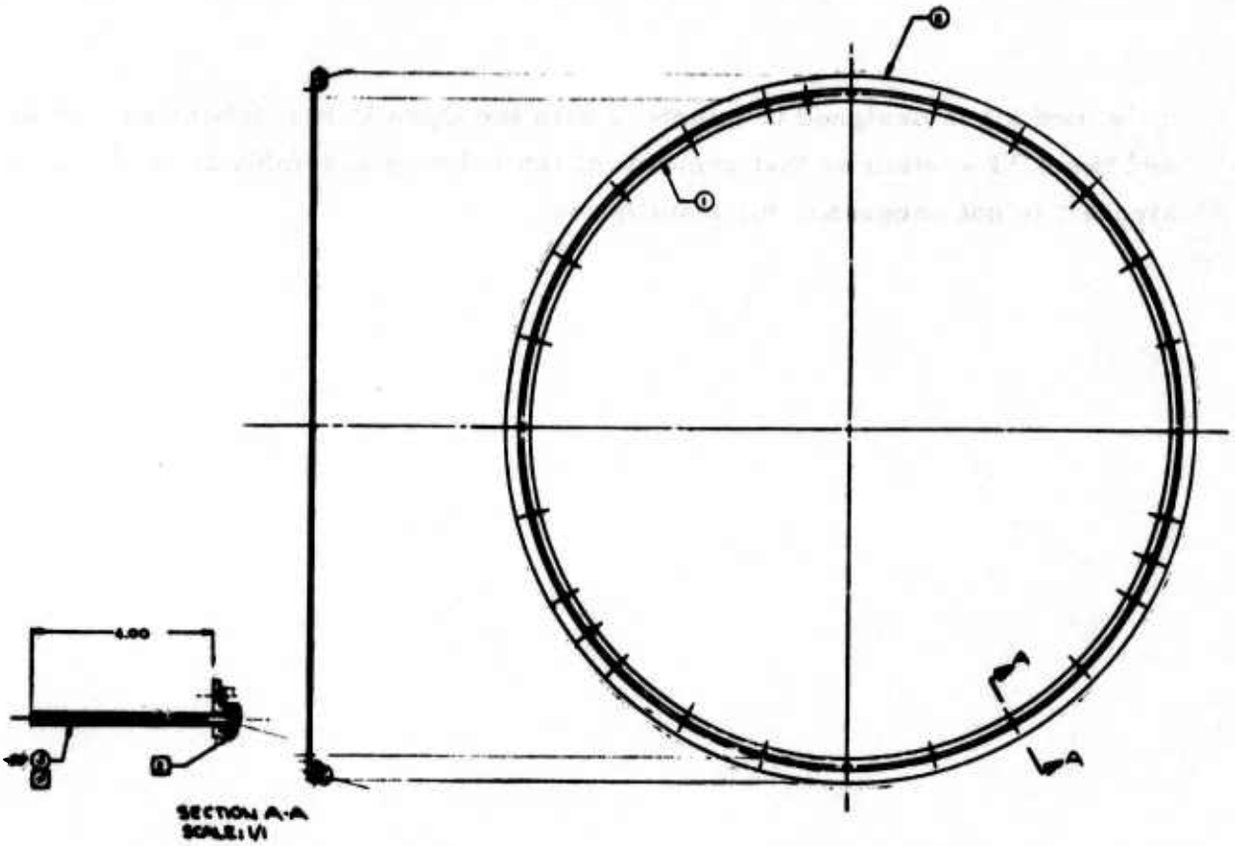

Figure 1-7. Seal, inflatable.

a pressure regulator, a pressure bottle, and a fill valve with a pressure gauge. The seal operates with a 20 to 26 psig inflation pressure and seals against the inside of the spherical eyelid assembly. The seal pressurization equipment is mounted by brackets to the inside ball structure of the APT pointing assembly. They are designed so that they can be inserted into the opening of the APT pointing assembly and fastened with screws.

SYSTEM DESCRIPTION, INSTRUMENTATION MOD KIT

The instrumentation mod kit is designed to measure static and dynamic pressures, temperature, and mechanical stresses in and around the open port cavity. The mod kit incorporates three functional sub assemblies, 1) transducers and attendant interconnections, 2) pointing assembly mounted signal conditioning module with interface leads to an off gimbal connection bulkhead and 3) lid sequence package contained in the pointing assembly.

This mod kit is designed to interface with the Open Port mechanical mod kit and the APT system so that removal of the pointing assembly from the ALL aircraft is not necessary for installation.

SECTION II

DESIGN REQUIREMENTS AND CRITERIA

The design requirements and criteria are covered in the ALL Manual, the statement of work, the data and results from the 0.3 scale wind tunnel model test, and from initial design review technical direction.

ALL MANUAL REQUIREMENTS ARE OUTLINED IN ATTACHMENT I DESIGN CRITERIA AND INCLUDE:

Acceleration;	8g crash load in all directions since the pointing assembly Open Port can nearly look in all directions.
	2g limit load in all directions – flight.
Safety Factors;	1.5 for ultimate
	1.15 for yield
Altitude;	Sea Level to 40,000 feet
Temperature;	-65°F to 130°F* Operating
Vibration;	Power spectral density of Figure 20F ALL Manual

CRITERIA FROM 0.3 WIND TUNNEL MODEL TEST

The 0.3 scale wind tunnel model test results when scaled up to the APT size add additional environmental requirements for the Open Port modification. The Open Port adds a dynamic input to the fine gimbal elements which is not present with a windowed turret. It also presents additional torque loads to the coarse gimbal axes.

The 0.3 scale model data were evaluated (see analysis section) and basically it was found that the additional loads were insignificant compared

---

*Revised by technical direction to -40°F to +130°F. See the last paragraph in this Section.

to the 5-psi static load and the 8g crash landing loads from a structural design standpoint.

INITIAL DESIGN REVIEW AND OTHER TECHNICAL DIRECTION

At the initial design review held at Hughes Culver City, further design criteria direction was given.

1. The design of the porous fence was to assume that 4.0 psi acted on the entire fence area including the holes.
2. The design of the liner and strut covers was to be based on a pressure of 1-1/2 times the maximum recovery pressure or 5 psi.
3. The temperature, operating, was limited for the APT structure elements from -40°F to +130°F. The shroud for the secondary mirror, struts, and the cylinder was analyzed for -65°F to +130°F.
4. The low power input window was to be re-analyzed using Weibull analysis criteria.
5. The eyelid analysis was to be re-analyzed for Open Port loads.

SECTION III

SYSTEM DESIGN

This section covers the description of the instrumentation design, and the mechanical design of the open port elements.

INSTRUMENTATION DESIGN

The instrumentation package design comprises primarily three parts: (See Figure 3-5 for block diagram)

1. transducers and interconnections,
2. signal conditioning module with output leads for off gimbal interface to ALL aircraft recording equipment, and
3. turret lid sequencer package.

There are 14 dynamic pressure transducers that will measure RMS pressure from 0.01 psi to 1.0 psi over a frequency of 5 to 1000 hertz. Static pressure is measured at 11 points and mechanically time multiplexed to a single pressure transducer. Temperature is measured at 16 locations. A reference pressure transducer is provided for turret ambient pressure. Four strain gauges will measure stress conditions in the open port structure. All transducers are connected to the signal conditioner by wiring harnesses organized according to type of measurement; e.g., pressure sensors in one bundle etc.

The instrumentation signal conditioning module (ICOM) provides power to drive the transducers and amplifies the resulting output signals. A two value gain programming capability is provided for the dynamic pressure channels. This capability allows the setting of all amplifiers in each of three amplifier groups to either of two different gains. A calibrate function is provided that puts a known reference voltage at the input of each

conditioning channel. Conditioned signals will be in the 0-5 volt range with low output impedance.

The lid sequence module (LSM) controls the opening and closing of the turret's protective eyelid. Upon receipt of an eyelid open/close instruction, the sequencer will generate the control signals and monitor the responses that prepare the turret for the eyelid action. When the turret has been properly prepared, the sequencer will issue the eyelid open/close instruction to the drive motor. Proper turret preparation actions involve the pressurization state of the turret, the gaseous nitrogen supply, the system abort interlocks, and the inflatable open port seal. A motor driven valve is located in the turret to control venting operations.

MECHANICAL DESIGN

Design of the Strut Covers and the Telescope Liner

The strut cover elements consist of a diamond shaped enclosure constructed of aluminum sheet with solid leading and trailing edges. The non-removable leading edge portions are fastened with monel rivets while the trailing edge and the attachments to the periphery of the cylindrical liner are fastened together with screws. The strut covers support in 3 places a can-shaped cover surrounding the secondary mirror. A 0.125 inch thick solid aluminum cylindrical liner extends back into the telescope cavity and has a bottom structure attached to the liner which simulates the primary mirror. This entire bucket shaped device is cantilevered off of the front face of the APT opening and forms a shroud for most of the exposed area of the telescope assembly. Figure 3-1 is the detail design of the shroud.

Porous Fence

The porous fence or aerodynamic fence consists of a thin rim or ring into which a uniform hole pattern is drilled such that the complete periphery has approximately half the metal removed. The purpose of the fence is to decrease air turbulence and dynamic pressures within the cavity. Figure 3-2 is the detail design drawing of the fence.

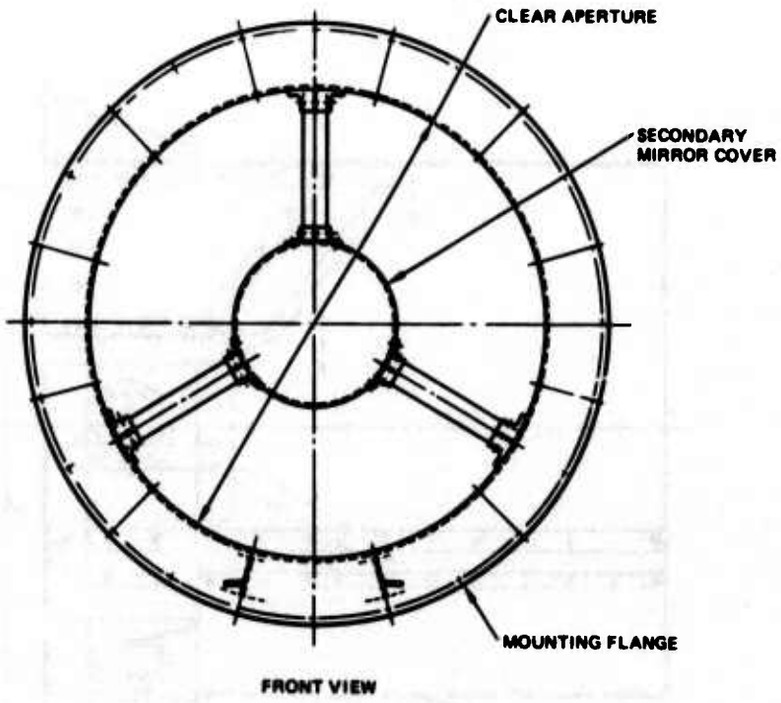

Figure 3-1. Shrouds.

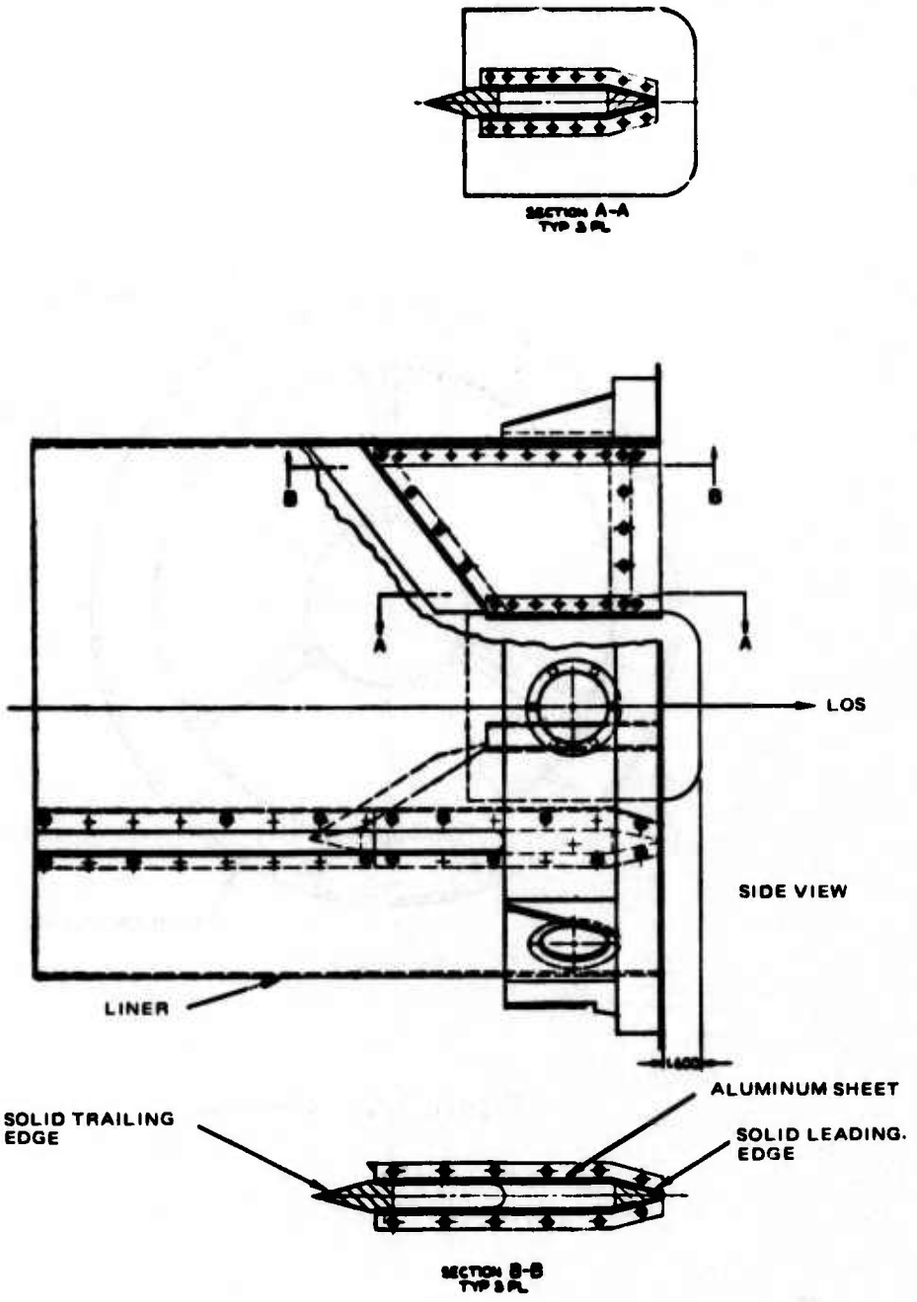

Figure 3-1. Shrouds. (Continued)

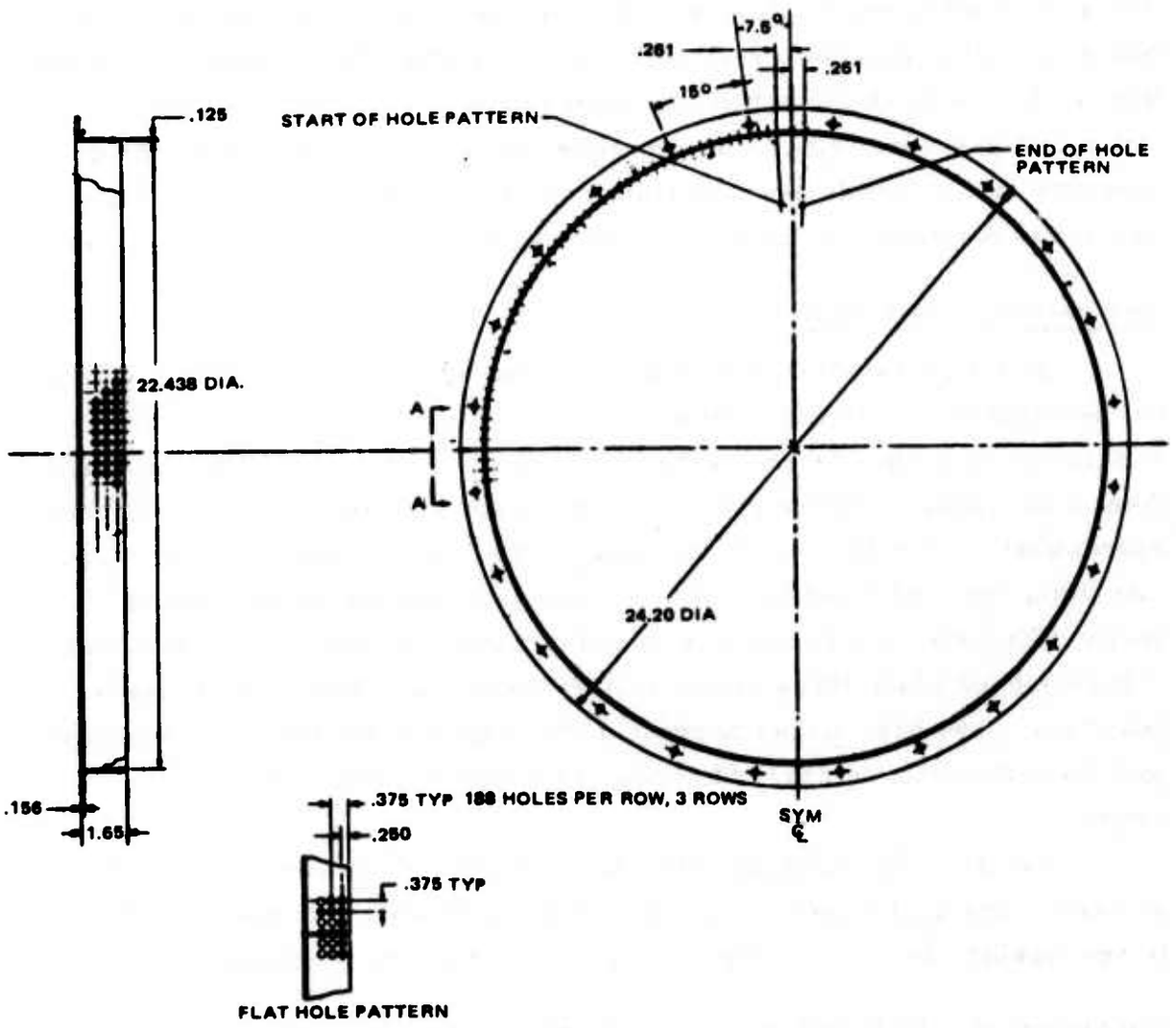

Figure 3-2. Porous fence.

Sealing System

The sealing system consists basically of an inflatable type seal which presses against the closed lid thus allowing the entire turret to be pressurized. The seal itself is pressurized with dry nitrogen from a 2100 psi pressure bottle through a step down regulator. The seal operating pressure is 26 psi. The bottle can be easily refilled through a special filler valve adjacent to which is a pressure gage. The pressure reading can be monitored through a window and is visible near the front rim of the shroud assembly. Figure 3-3 is the detail design of the sealing system.

Depressurization System

The depressurization system is shown in Figure 1-2. The sequence of operation is as follows. The overboard vent valve for the entire turret is actuated to permit returning the turret internal pressure from a positive 3 psi over outside ambient pressure back to ambient pressure. It will take approximately 8 to 10 seconds to depressurize the pointing assembly. At this time, the seal itself is depressurized which allows any remaining cavity differential air pressure to bleed out pass the seal. The eyelid door is then opened which takes approximately 3 seconds. The aircraft overboard dump has been closed to prevent circulation of air due to the open air path from the pointing assembly opening through the turret, to the vent valve.

The pressurization sequence is a reversal of the depressurization process. The eyelid door is closed, and the inflatable seal portion inflated to seal against the door, and the turret pressurization reactivated.

Instrumentation Installation on the Telescope Shroud

The shroud instrumentation consists of static pressure sensing tubes and dynamic low level pressure transducers. The latter devices are capable of measuring pressure levels down to 0.01 psi RMS.

The static tubes are connected to a mechanical multiplexed Scanivalve that is also mounted on the shroud.

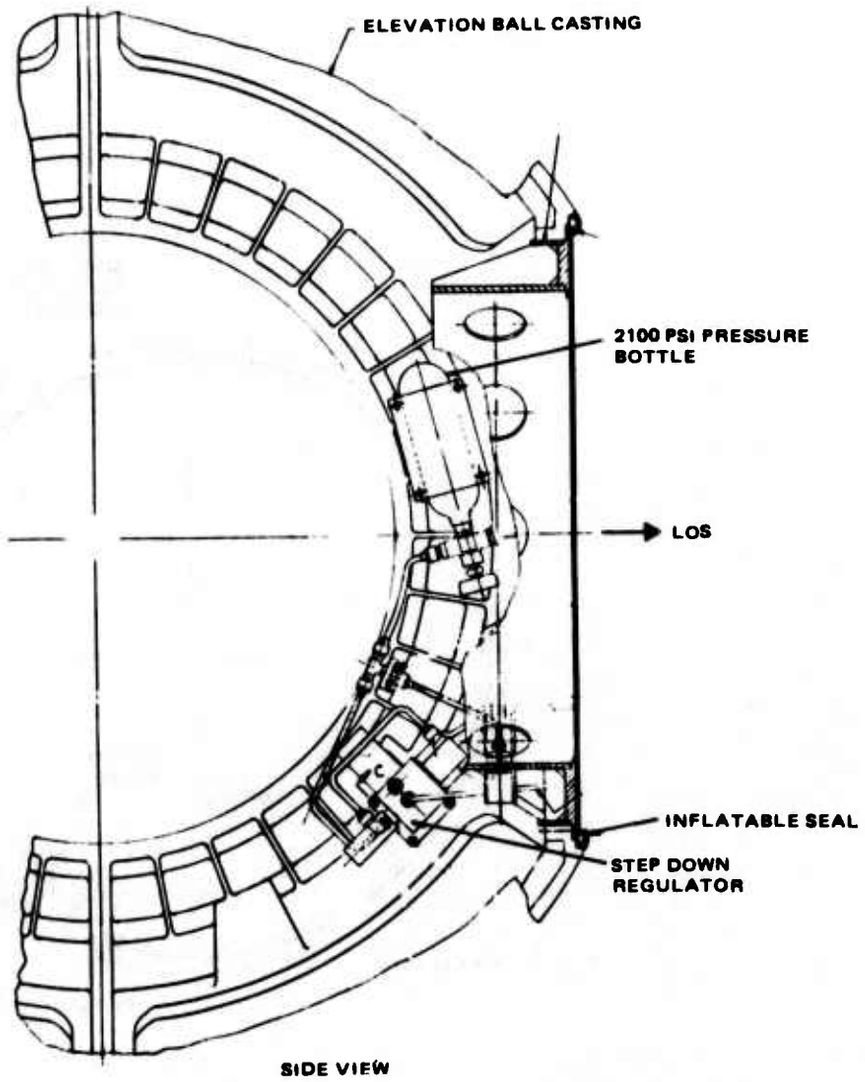

Figure 3-3. Seal inflation system.

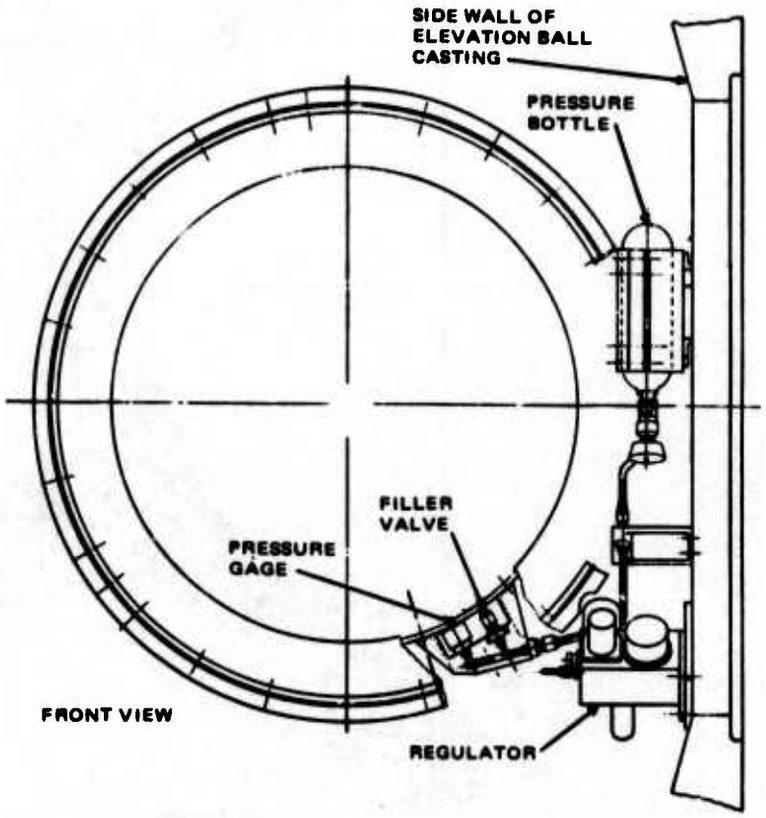

Figure 3-3. Seal inflation system. (Continued)

The shroud instrumentation is located in approximately the same location as similar transducers on the 1/3 scale wind tunnel model. In addition, there are temperature sensing elements and strain gages mounted in key structural areas. The strain gauges sense the torsional forces on the secondary mirror shroud which result from air loads on the 3 strut covers. Figure 3-4 depicts the installation of the transducers and Figure 3-5 shows the associated interconnection lines. Figure 3-6 provides further information on instrumentation sensor locations.

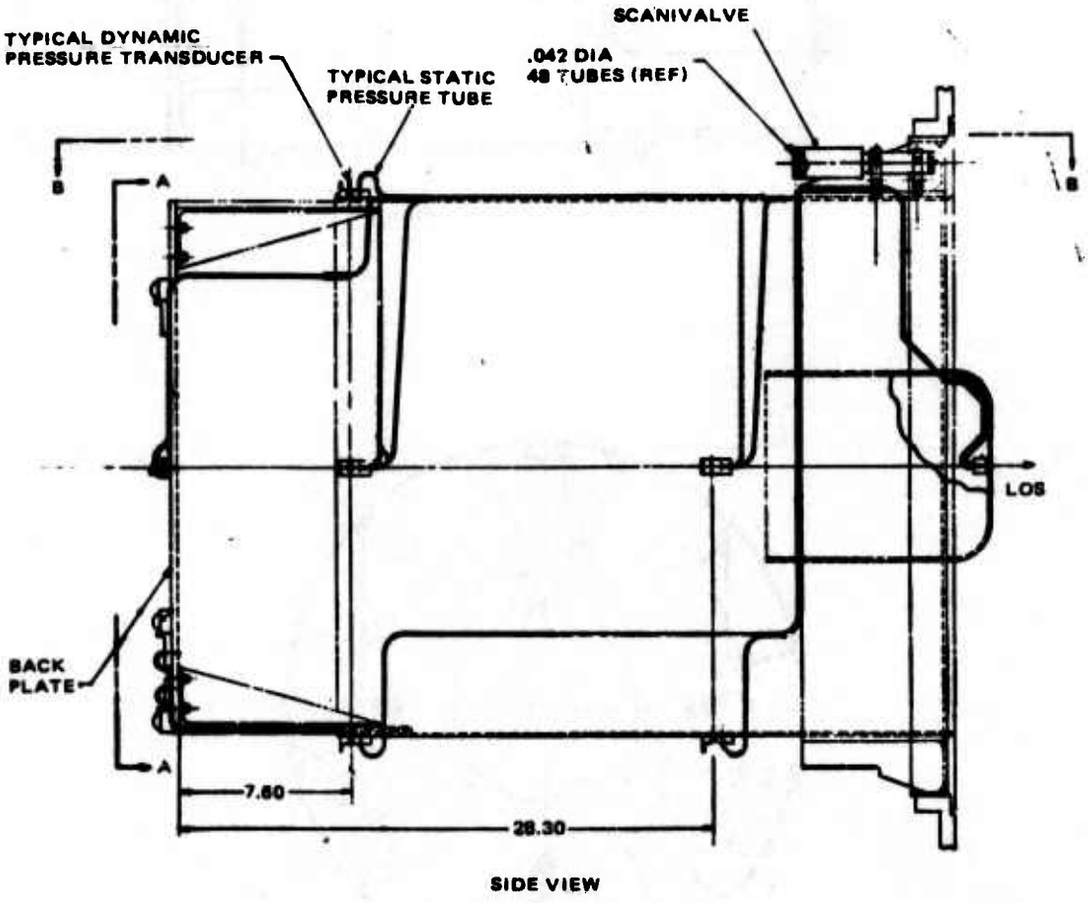

Figure 3-4. Instrumentation installation.

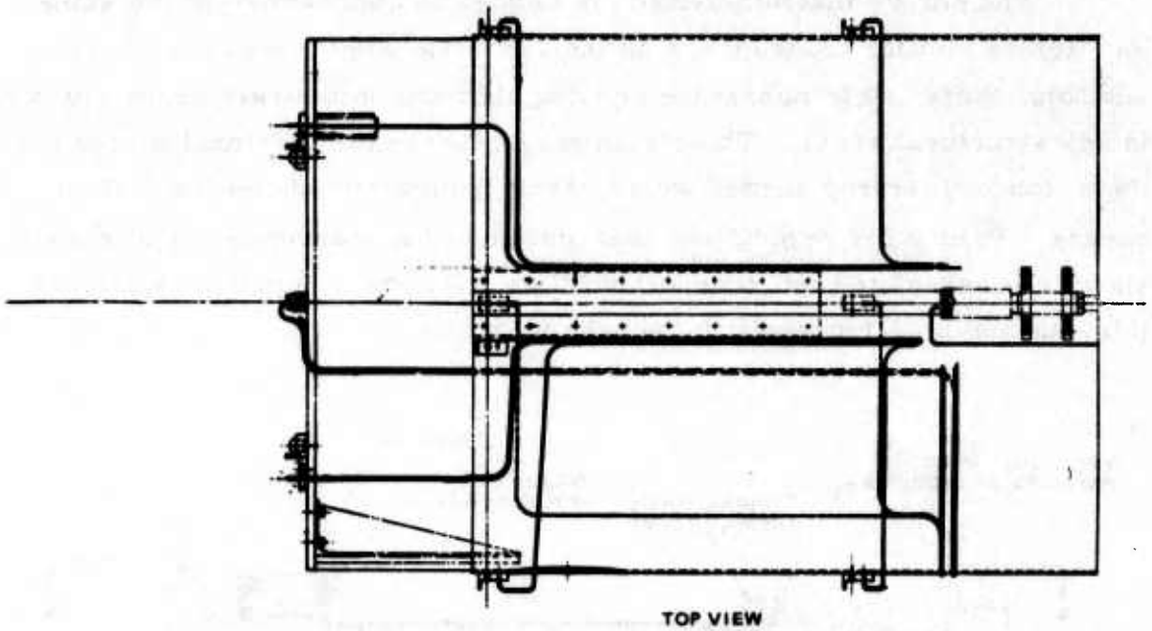

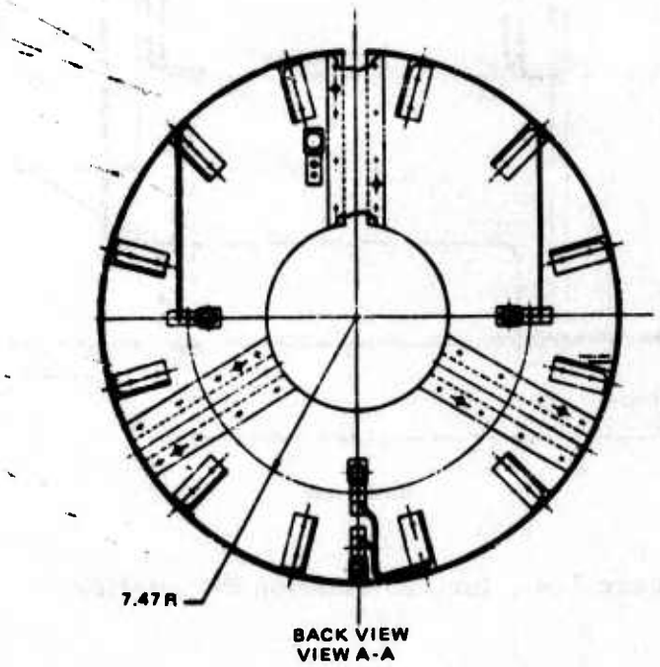

Figure 3-4. Instrumentation installation. (Continued)

OPEN PORT CABLE LIST

QTY	CABLE NO.	PART NUMBER	NAME
1	W1090	3459528	LAW BULKHEAD TO LSM & ICOM
2	W1091	3459727	LSM CONTROL
3	W1092	3459530	TURRET TEMP SENSORS
4	W1093	3459529	ICOM POWER INPUT
5	W1094	3459531	TI BULKHEAD TO ICOM
6	W1095	3459728	STRAIN SENSORS
7	W1096	3459533	PRESSURE SENSORS
8	W1097	3459729	SHROUD TEMP SENSORS
9	W1098	3459668	LSM TO W1022
10	XW1091	3459634	SCANI EXTENDER
11	XW1095	3459616	STRAIN EXTENDER
12	XW1096	3459617	PRESSURE EXTENDER
13	XW1097	3459618	SHROUD TEMP EXTENDER

APT OPEN PORT MODIFICATION INTERCONNECTION BLOCK DIAGRAM

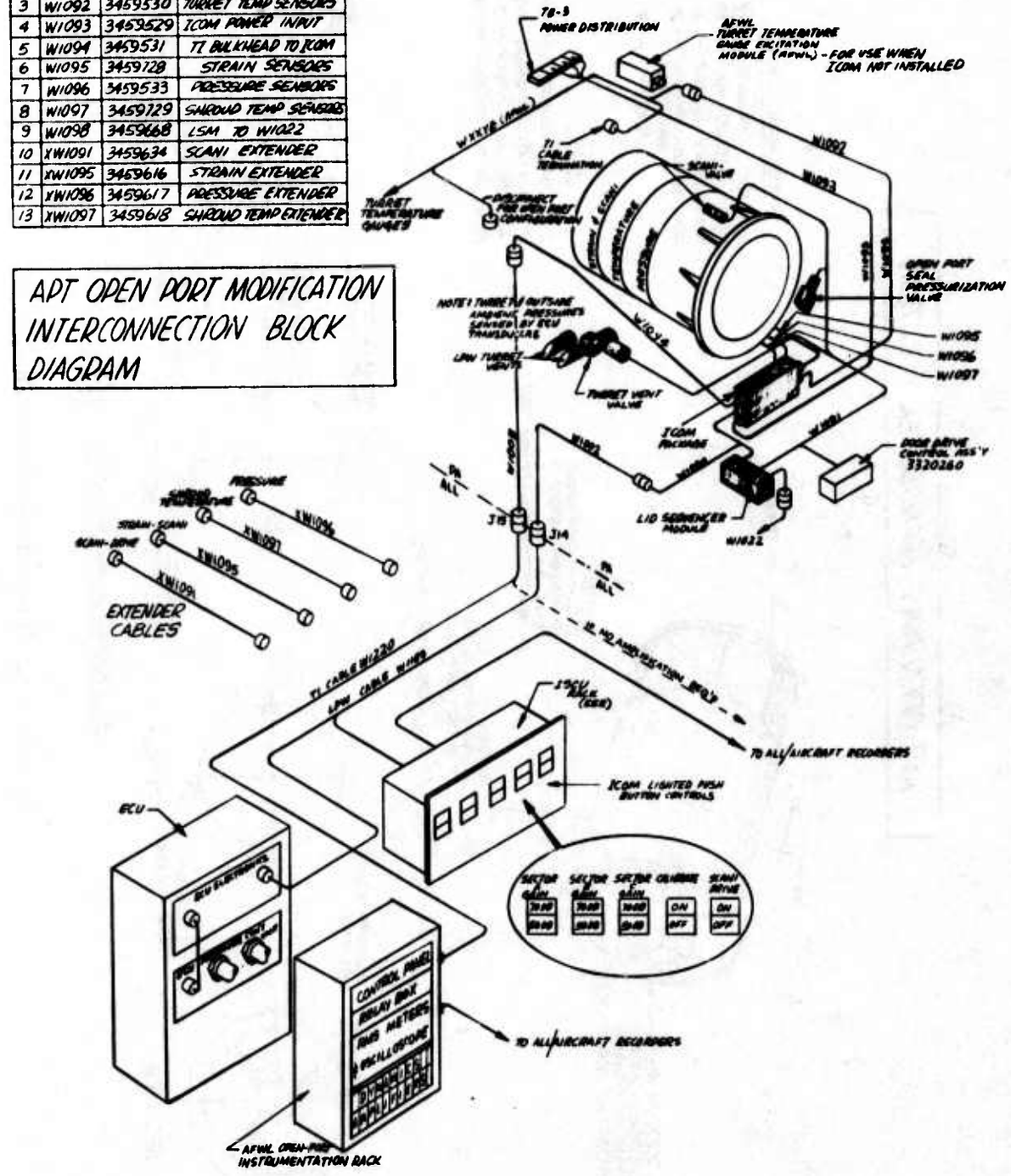

Figure 3-5. Interconnection block diagram.

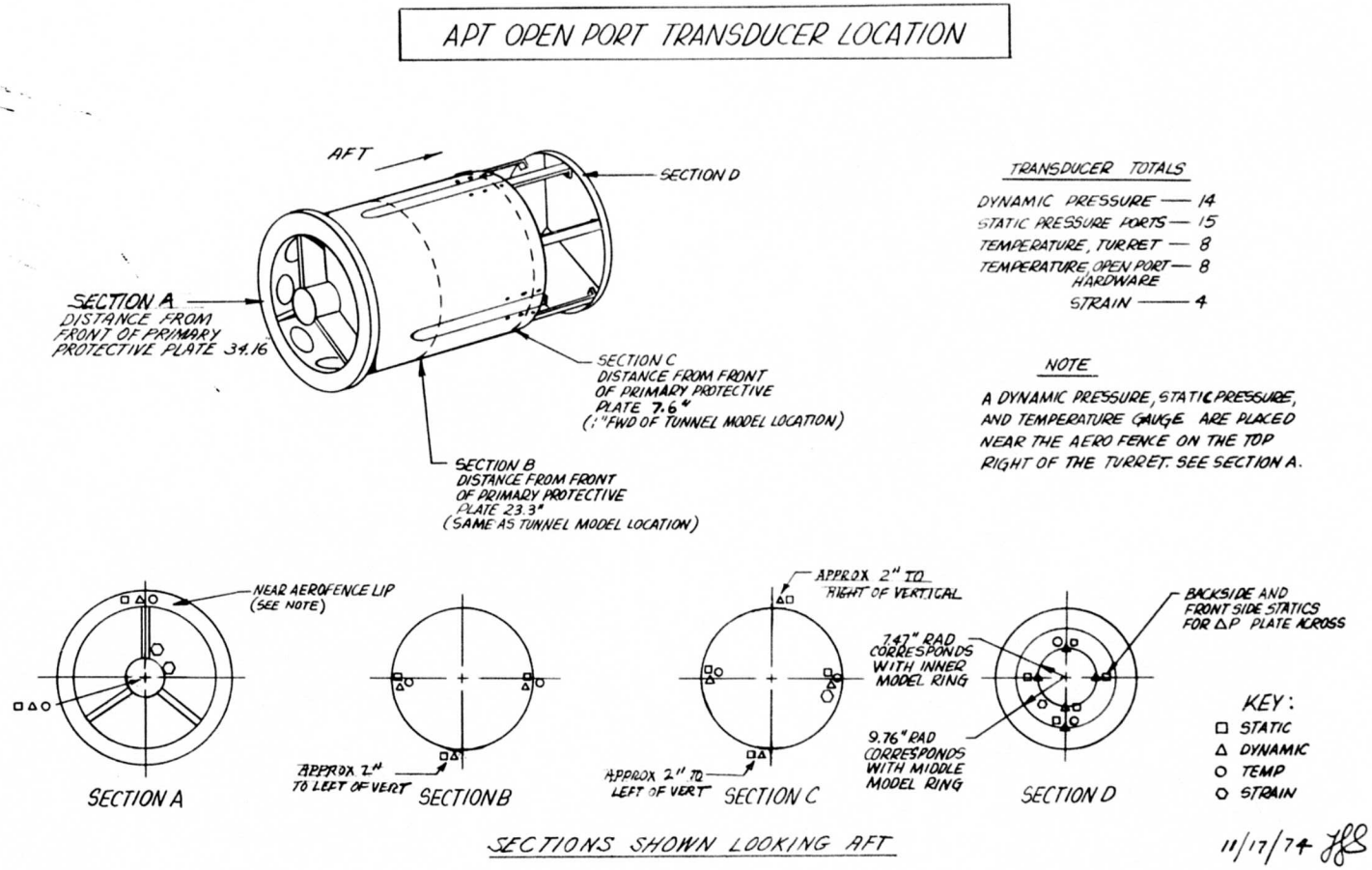

Figure 3-6. Transducer location.

SECTION IV

SYSTEM ANALYSIS

INSTRUMENTATION SYSTEM ANALYSIS

The system analysis tasks (with reference to the criteria and requirements discussed in Section 2) will be made available in a separate report.

STATIC AND DYNAMIC STRUCTURAL ANALYSIS

This section summarizes the results of the structural analysis performed to demonstrate structural adequacy of the APT Open Port Modification and the APT Protective Door (Eyelid).

APT Open Port Modification Environmental Design Criteria

All components of the APT Open Port Modification have been designed to satisfactorily withstand the static loading conditions presented in Table 4-1 and the unsteady pressure power spectral density plot shown in Figure 4-3.

The three 8g acceleration load cases are those for the crash landing condition in each of three mutually perpendicular directions.

The four pressure load cases represent hypothetical worst case pressure distributions. The magnitude of the peak pressure, 5 psi, is two times the stagnation pressure differential existing on the nose of an object in a Mach 0.50 sea level air stream. This stagnation pressure is consistent with the steady pressures measured in 0.3-scale Open Port ALL Turret Wind Tunnel test results for a forward-looking port. (HAC IDC 2712.22/527, dated 6 February 1974).

TABLE 4-1. ENVIRONMENTAL DESIGN REQUIREMENTS

Load Condition	
A1 – A3	8G crash landing load in any direction
P1	5 psi proof pressure
P2	$P_r(\theta)$ = 5 psi uniform radial pressure acting on the liner shell combined with a P_z = 5 psi normal pressure on the primary mirror cover and a P_s = 5 psi normal pressure acting on one side of each of the secondary mirror support struts. See Figure 4-1.
P3	Same as load condition P2 except $P_r(\theta)$ = 5 cos θ psi
P4	Same as load condition P2 except $P_r(\theta)$ = 5|cos θ| psi
T1	Cold soak at -65°F

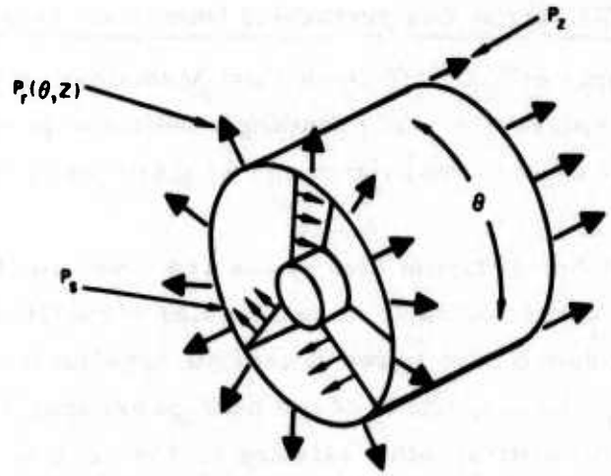

Figure 4-1. Definition of pressure distributions.

The - 65°F cold soak case represents the worst case temperature differential condition, relative to a +70°F installation temperature, that can be approached by the liner in flight. This is substantiated by Figures 4-2 and 4-3, taken from the APT Open Port thermal analysis (HAC IDC 277740.1/292, dated March 1974), which show that the liner cylinder and the secondary mirror cover cool uniformly and rapidly reach their steady state values for the Open Port Condition.

The unsteady pressure data are presented in Figure 4-4 as a power spectral density versus frequency plot for the maximum rms pressure condition found in the 0.3-scale Open Port ALL Turret Wind Tunnel test results for Open Port Configuration 11 at sea level at Mach 0.75 (HAC IDC 271222/527, dated 6 February 1974). This worst-case condition envelopes all test data. It occurs on the primary mirror when the APT orientation is at 0° elevation and 45° azimuth. This data can be scaled to sea level operation at Mach 0.50 using the following conversions:

$$PSD_2 = \left(\frac{L_2}{L_1}\right)\left(\frac{V_1}{V_2}\right)\left(\frac{q_2}{q_1}\right)^2 PSD_1$$

$$= \left(\frac{L_2}{L_1}\right)\left(\frac{V_2}{V_1}\right)^3 PSD_1$$

$$= 1.0 \times \left(\frac{0.5}{0.75}\right)^3 PSD_1 = 0.29630\ PSD_1$$

$$f_2 = \left(\frac{L_1}{L_2}\right)\left(\frac{V_2}{V_1}\right) f_1$$

$$= 1.0 \times \left(\frac{0.75}{0.5}\right) f_1 = 1.5 f_1$$

All loading conditions are considered to be limit loading conditions. Maximum working stresses and loads must not, therefore, exceed 2/3 (1/1.15) of their minimum guaranteed ultimate (yield) values as published in MIL-HDBK-5B.

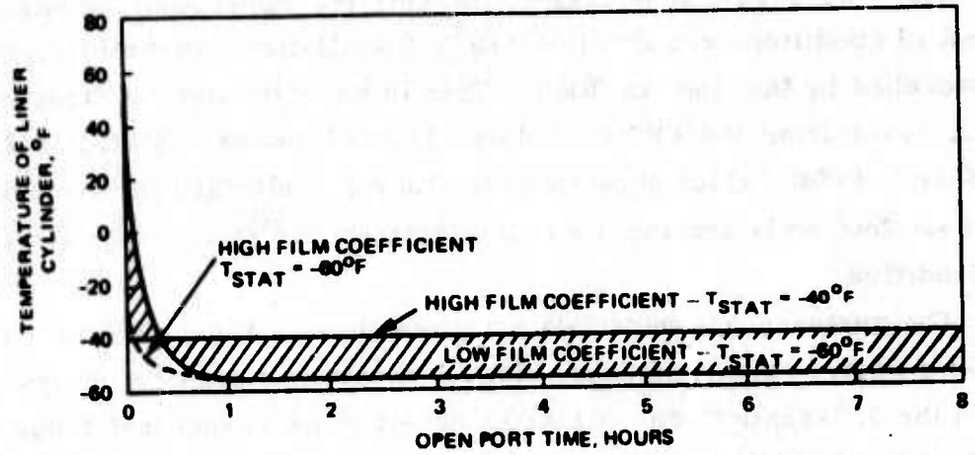

Figure 4-2. Temperature of cylindrical liner.

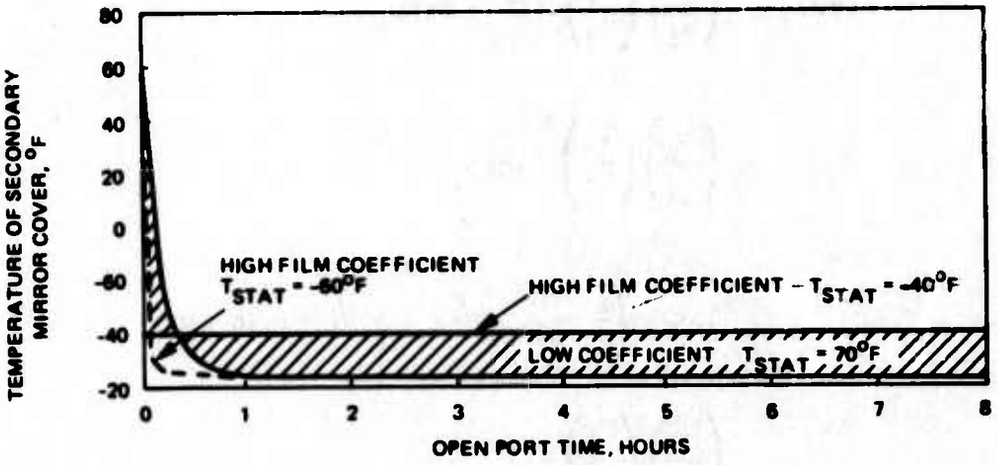

Figure 4-3. Temperature of secondary mirror cover.

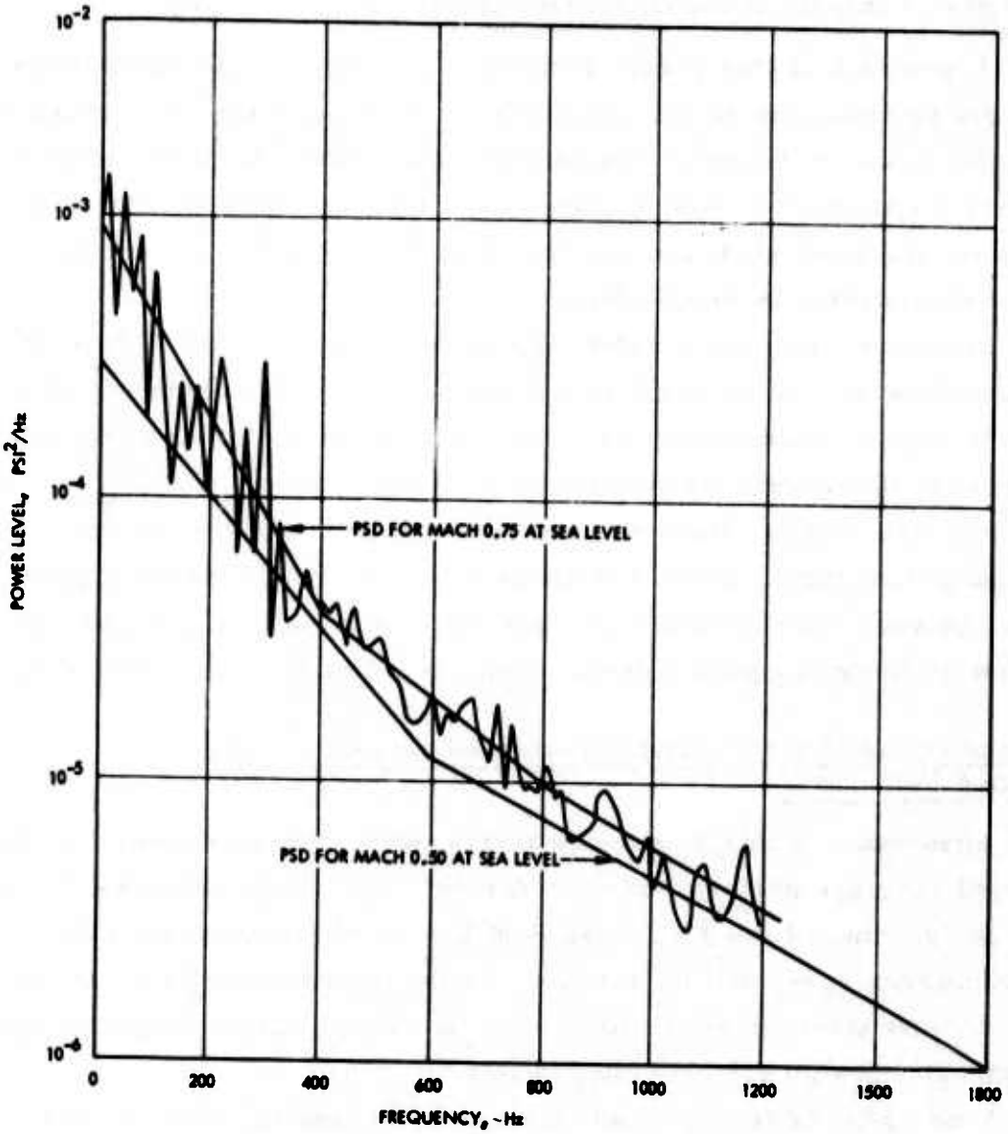

Figure 4-4. Full scale APT primary mirror unsteady pressure power spectral density for sea-level flight at Mach 0.75.

Hand Stress Analysis of the Open Port Liner

Appendix 1 of this report documents the hand stress calculations performed to demonstrate structural adequacy of the following components of the APT Open Port Liner: the aerodynamic fence, the primary mirror cover and its support straps, the secondary mirror cover and its support struts, and the liner shell and its mounting provisions for the environmental design criteria cited in this Section.

Minimum margins of safety are summarized in Table 4-2 for the three acceleration (A1-A3), the four 5 psi pressure (P1-P4) conditions, and the -65°F cold soak condition (T1). The three acceleration loading conditions are considered non-critical because the equivalent pressures, $P_{eq} = 8\rho t = 0.8t$ psi, are small. Since all minimum margins of safety are greater than zero, the aerodynamic fence, the primary mirror cover and its support straps, the secondary mirror cover and its support struts, and the liner shell and its mounting provisions are considered structurally adequate.

Static and Dynamic STARDYNE Structural Analysis of the APT Open Port Liner

Appendix 2 of this report documents the static and dynamic STARDYNE structural analyses performed to demonstrate structural adequacy of the following components of the APT Open Port Liner: the aerodynamic fence, the primary mirror cover and its support straps, the secondary mirror cover and its support struts, and the liner shell and its mounting flange for the environmental design criteria cited in this Section.

Peak nodal deflections and elemental stresses are summarized in Table 4-3 for the three 8g acceleration (A1 - A3), the four 5 psi pressure (P1 - P4), and the -65°F cold soak temperature (T1) load cases. Since these peak deflections and stresses do not exceed their allowable values, the aerodynamic fence, the liner shell and its mounting flange, the secondary mirror cover and its support struts, and the primary mirror cover and its support straps are considered structurally adequate.

The extremely high stresses predicted for the -65°F cold soak condition are due to the fact that the perimeter nodes of the mounting flange, nodes N136 through N147, were restrained against translation along the

TABLE 4-2. SUMMARY OF RESULTS OF APT OPEN PORT LINER HAND STRESS ANALYSIS

Component	Material	Allowable Stress*	Allowable Deflection	Peak Stresses and Deflections								
				8G Acceleration			5 PSI Steady Pressure				-65°F Temp	Unsteady Pressure
				A1	A2	A3	P1	P2	P3	P4	T1	
Aerofence	0.063 inches thick 6061-T6 Al	28 ksi	-	0.20 ksi	0.17 ksi	0.21 ksi	-	8.8 ksi	8.8 ksi	8.8 ksi	26.3 ksi	0.24 ksi
Liner Cylinder	0.125 inches thick 2024-T4 Al	36.5 ksi	- 0.0625 in.	0.20 ksi 0.00032 in.	0.17 ksi 0.00056 in.	0.21 ksi 0.00056 in.	- -	11.2 ksi 0.00296 in.	10.5 ksi 0.220 in.	9.2 ksi 0.0130 in.	26.3 ksi 0.0596 in.	0.24 ksi 0.0027 in.
Liner Flange	0.500 inches thick 6061-T6 Al	28 ksi	-	0.01 ksi	0.02 ksi	0.02 ksi	-	0.22 ksi	0.37 ksi	0.35 ksi	22.9 ksi	0.02 ksi
Liner Flange Gussets	0.125 inches thick 6061-T6 Al	28 ksi	-	0.13 ksi	0.15 ksi	0.14 ksi	-	2.8 ksi	5.3 ksi	4.0 ksi	6.4 ksi	0.29 ksi
Secondary Mirror Cover	0.125 inches thick 6061-T6 Al	28 ksi	-	0.21 ksi	0.16 ksi	0.14 ksi	-	9.2 ksi	11.3 ksi	9.8 ksi	26.0 ksi	0.30 ksi
Secondary Mirror Cover Support Struts	0.063 inches thick 2024-T4 Al	36.5 ksi	-	0.04 ksi	0.09 ksi	0.09 ksi	-	1.9 ksi	2.9 ksi	2.1 ksi	27.4 ksi	0.16 ksi
Primary Mirror	0.312 inches thick 6061-T6 Al	28 ksi	-	0.60 ksi	1.2 ksi	1.2 ksi	-	11.9 ksi	11.9 ksi	11.9 ksi	4.2 ksi	0.26 ksi
Primary Mirror Support Straps	0.125 inches thick 2024-T4 Al	36.5 ksi	-	0.95 ksi	1.8 ksi	1.8 ksi	-	18.9 ksi	18.9 ksi	18.9 ksi	6.3 ksi	0.56 ksi

*The allowable strength is the lesser of the minimum guaranteed ultimate strengths ÷ 1.5 or yield strength ÷ 1.15.

three global axes to conservatively simulate the flexibility of the liner to outer elevation gimbal interface. This is equivalent to applying radial forces to nodes N136 - N147 of sufficient magnitude to move these nodes outward radially a distance δ_b:

$$\delta_b = \alpha_{AL} R_b \Delta T = 13 \times 10^{-6} \times 14.188 \times 135 = 0.0249 \text{ in.}$$

where α_{AL} is the coefficient of thermal expansion for the aluminum liner, R_b is the flange bolt circle radius, and ΔT is the temperature differential. In reality, the distance δ_b will be less than:

$$\delta_b = \left(\alpha_{AL} - \alpha_{FE} \right) R_b \Delta T = \left(13 - 5.5 \right) \times 10^{-6} \times 14.88 \times 135 = 0.0144 \text{ in.}$$

where α_{FE} is the coefficient of thermal expansion for the glass epoxy shell of the outer elevation gimbal. The actual stress levels will therefore be less than 58 percent of the predicted stress levels cited in Table 4-3.

The results of the Householder -QR eigenvalue extraction are presented in Table 4-4. Those results indicate that the in-plane rotation and translation modes of the primary mirror occur at 82 Hz and 95 Hz, respectively, while its out-of-plane translation mode occurs at 224 Hz. The results also indicate that the first four symmetric breathing modes of the liner cylinder occur at 291 Hz, 317 Hz, 365 Hz, and 455 Hz, respectively, while its first two asymmetric breathing modes occur at 318 Hz and 365 Hz.

The results of the random response analysis, also summarized in Table 4-3, indicate the three-sigma responses and stresses are small compared to those for the static loading conditions. These results were obtained using the 10 modes described above, assuming 5 percent viscous modal damping, suppressing response cross-covariances, and assuming that the random pressure power spectral density used in this analysis (the PSD shown in Figure 4-4 for Mach 0.5 flight at sea-level) is spacially correlated.

TABLE 4-3. SUMMARY OF RESULTS OF THE STARDYNE STATIC AND DYNAMIC ANALYSIS OF THE APT OPEN PORT LINER

Component	Material	Allowable Strength (Note 3)	Minimum Margins of Safety								Page
			8G Acceleration			5 psi Pressure				-65°F Temp T1	
			A1	A2	A3	P1	P2	P3	P4		
Aerofence			(Note 1)	(Note 1)	(Note 1)					(Note 2)	
Screen	6061-T6A1	28 ksi				+2.17	+2.17	+2.17	+2.17		
Flange	6061-T6A1	28 ksi				+1.64	+1.64	+1.64	+1.64		
Attach Bolts	10-32 160 ksi bolt	1928 lb				HI	HI	HI	HI		
Primary Mirror Cover											
Cover	6061-T6A1	28 ksi				+1.36	+1.36	+1.36	+1.36		
Doublers	6061-T6A1	28 ksi				+0.52	+0.52	+0.52	+0.52		
Doubler Attach Bolts	10-32 160 ksi bolt	1928 lb				+0.25	+0.25	+0.25	+0.25		
Support Straps	2024-T4A1	36.5 ksi				+0.93	+0.93	+0.93	+0.93		
Support Strap Attach Bolts	10-32 160 ksi bolt	1928 lb				+1.77	+1.77	+1.77	+1.77		
Secondary Mirror Cover and Support Struts											
Liner Cylinder	2024-T4A1	36.5 ksi				-	-	-	HI		
Secondary Mirror Cylinder	6061-T6A1	28 ksi				-	-	-	+1.36		
Struts	2024-T4A1	36.5 ksi				-	-	-	HI		
Strut Bracketa	2024-T4A1	36.5 ksi				-	-	-	+2.08		
Strut Bracket Rivets	MS20427M4C rivet	297 lb				-	-	-	+1.05		
Secondary Mirror Cap	6061-T6	28 ksi				+0.20	+0.20	+0.20	+0.20		
Liner											
Liner	2024-T4A1	36.5 ksi				HI	HI	+0.00	HI	HI	
Doublers	2024-T4A1	36.5 ksi				HI	HI	+0.00	HI	Note 2	
Doubler Attach Bolts	10-32 160 ksi bolt	1928 lb				HI	HI	+1.59	HI	Note 2	
Liner Mounting Bolts	10-32 180 ksi bolt	2363 lg				HI	HI	HI	HI	+0.04	
Liner Mounting Flange	6061-T6A1	28 ksi				HI	HI	+0.57	HI	+0.01	
Outer Elevation Gimbla	Glass-Epoxy	21.3 ksi	-	-	-	-	-	-	-	+0.06	

Note 1. The 8G acceleration cases are considered non-critical since the equivalent pressures are $8\rho t = 0.8t$ psi.
Note 2. The -65°F cold soak condition is considered critical only at the liner flange/outer elevation gimbal interface.
Note 3. The allowable strength is the lesser of the minimum guaranteed ultimate strength 1.5 or yield strength 1.15.

TABLE 4-4. APT OPEN PORT LINER MODES AND FREQUENCIES

Mode Number	Frequency Hz	Mode Shape Description
1	82	In-plane (X4) rotation of primary mirror cover
2	95	In-plane vertical (X3) translation of primary mirror cover
3	95	In-plane horizontal (X2) translation of primary mirror cover
4	224	Out-of-plane (X1) translation of primary mirror cover
5	291	First liner cylinder symmetric breathing mode
6	317	Second liner cylinder symmetric breathing mode
7	318	First liner cylinder asymmetric breathing mode
8	365	Second liner cylinder asymmetric breathing mode
9	365	Third liner cylinder symmetric breathing mode
10	455	Fourth liner cylinder symmetric breathing mode

Static STARDYNE Structural Analysis of the APT Protective Door

Appendix 3 of this report documents the results of an analysis of the protective door or eyelid which covers the Airborne Pointer and Tracker (APT) telescope window. MRI's STARDYNE Structural Analysis System of computer programs was used to evaluate the deflections and stresses induced by an 8 psi internal pressure on a 3/8 inch thick solid 2024-T4 aluminum eyelid.

The results of the analysis indicate that the eyelid can satisfactorily withstand a proof pressure of 1.5 x 8 = 12 psi without permanent set and a burst pressure of 3 x 8 = 24 psi without rupture. Tables 4-5 and 4-6

TABLE 4-5. SUMMARY OF RESULTS OF THE STARDYNE ANALYSIS OF THE APT EYELID

Critical Stress Levels and Margins of Safety for the 8 psi Peak Working Pressure Load Condition

Element Group	Material	Allowable Axial Stress*	Peak Axial Stress	Location	Allowable Shear Stress**	Peak Shear Stress	Location	M.S.
T1-T120	6061-T6	14,000	8,333	T119	9,000	4,000	T119	+0.35
B1-B20	2024-T4	20,000	10,483	B10	12,000	4,230	B10	+0.58
Mounting Screws***	160 Ksi Steel	1,780	—	—	1,553	1,441	Corner of Eyelid (T120)	+0.08

*The allowable axial stress is defined as the lesser of $F_{tu}/3$ or $F_{ty}/(1.5 \times 1.15)$.

**The allowable shear stress is defined as $F_{su}/3$.

***Modified as noted in the text.

TABLE 4-6. SUMMARY OF RESULTS OF THE STARDYNE ANALYSIS OF THE APT EYELID

Critical Deflections for the 8 psi Peak Working Pressure Load Condition

Node Number	Deflection Normal to Eyelid Surface (inches)	Rotation about Axis Tangent to Surface in X-Z Plane (radians)	Y-Axis Deflection (inches)
N1	0.1081	0.0	0.0
N15	0.0621	0.0	0.0
N36	0.0458	0.0	0.0
N57	0.0695	0.0	0.0
N71	0.1236	0.0	0.0
N4	0.0548	0.0116	-0.0153
N18	0.0339	0.0051	-0.0056
N39	0.0315	0.0029	-0.0029
N60	0.0389	0.0057	-0.0062
N74	0.0464	0.0125	-0.0147
N7	0.0063	-0.0023	-0.0227
N21	0.0021	-0.0017	-0.0216
N42	0.0022	-0.0013	-0.0216
N63	0.0020	-0.0017	-0.0231
N77	0.0067	-0.0023	-0.0244

present stress levels and deflections for critical sections of the eyelid. Maximum deflection normal to the eyelid surface for the 8 psi peak operating pressure was 0.12 inches. The minimum margin of safety was 0.08 for the mounting screw on the outer corner.

These results are predicated on a design with 160 ksi steel 1/4-28 screws replacing the existing 10-32 screws and an additional 1/4-28 screw added at each corner.

WEIBULL ANALYSIS OF THE APT ZnSe AUTO ALIGNMENT INPUT WINDOW

The results of theoretical studies on the effect of nonuniform multiaxial stress fields encountered in simply-supported, uniformly loaded circular plates on the fracture of brittle materials are described in Appendix 4. Derivations were carried out to determine the risk of rupture assuming the material obeyed the Weibull distribution function for volumetric flaw distribution.

The method has been used to predict the risk of rupture in the APT Zinc Selenide Auto Alignment Input Window for various pressures. The results of the analysis, using both the von Mises and maximum shear criteria for equivalent uniaxial stresses for multiaxial stress systems, is presented in Table 4-7.

The values of the Weibull parameters used in this analysis were derived by Dr. J.C. Wurst of the University of Dayton by performing a Weibull analysis on flexural strengths of 83 Raytheon CVD Zinc Selenide test bars obtained in four-point bending tests.

THERMAL ANALYSIS

The thermal analysis for the APT Open Port modification (Appendix 5) was limited to analysis required for inputs to the structural analysis and to determine if any damage could occur to APT internal components due to thermal effects of an Open Port.

As shown in the analysis, the temperature of the added shroud elements rapidly decreased toward ambient due to their relatively low mass, but the structural elements of the telescope very slowly approached ambient due to their high mass.

TABLE 4-7. WEIBULL ANALYSIS OF UNIFORMLY LOADED, SIMPLY-SUPPORTED CIRCULAR PLATE

PLATE RADIUS RO = 3.15
PLATE THICKNESS TO = .3
POISSON'S RATIO VO = .3
WEIBULL SHAPE PARAMETER M = 7.3
WEIBULL SCALE PARAMETER SO = 3545
WEIBULL LOCATION PARAMETER SU = O

PRESSURE	PLATE RELIABILITY VON MISES CRITERION	PLATE RELIABILITY MAX SHEAR CRITERION
1	1	1
2	1	1
3	1	1
4	1.	1.
5	.999999	.999999
6	.999998	.999997
7	.999994	.999992
8	.999983	.999978
9	.999961	.999949
10	.999916	.999889
11	.999831	.999778
12	.999681	.999581
13	.999428	.999249
14	.999018	.998711
15	.998376	.997868
16	.9974	.996587
17	.995956	.994691
18	.993868	.991954
19	.990914	.988083
20	.986814	.982718
21	.981226	.975415
22	.973735	.965646
23	.96385	.952792
24	.951006	.936151
25	.934565	.914951
26	.913831	.888385
27	.888082	.855653
28	.856603	.816041
29	.818754	.769015
30	.774047	.714342

The very low heat transfer to the main telescope structure results from the insulation provided by the required shroud elements. Figure 4-5 and Figure 4-6 are two temperature versus time curves for a linear versus. the strut element shielded by the liner.

The thermal analysis demonstrates that Open Port operation for up to 30 minutes results in only a 20°F drop in temperature of any of the structural elements of the pointing assembly. The APT pointing assembly was designed to operate within optical specifications over a range of ±30°F. It is structurally safe to fly the pointing assembly much lower than 0°F so flight safety of the APT would not be affected by a failed Open Port. If the aircraft were landed in less than one (1) hour from the time of failure even water cooled mirrors would probably not be damaged.

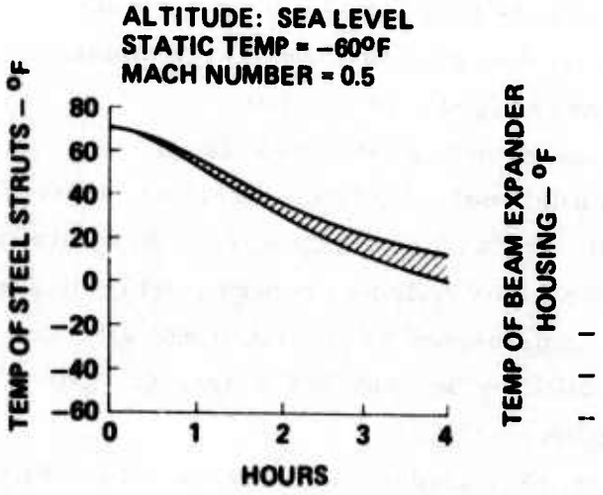

Figure 4-5. Temperature region of steel struts.

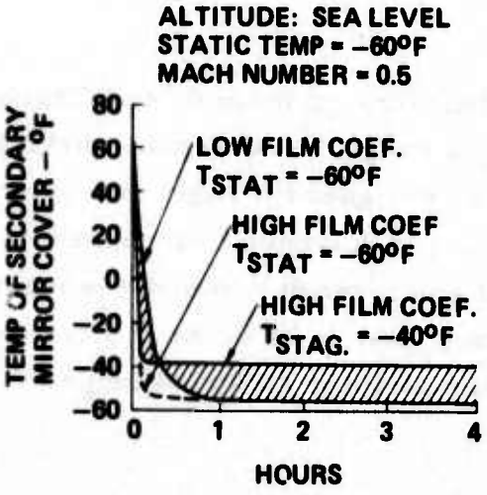

Figure 4-6. Temperature of secondary mirror cover.

ELECTRICAL LOAD ANALYSIS

The anticipated loading of APT power supplies by the instrumentation package is 20 watts of +20 VDC power, 10 watts of -20 VDC power, 140 watts of +28 VDC power on an intermittent basis, 34 watts of +28 VDC power on a continuous basis.

Power will be obtained from existing sources in the pointing assembly. The increased load can be handled by the present APT supplies.

ELECTROMAGNETIC COMPATIBILITY ANALYSIS

No problems are anticipated with the instrumentation as a receiver of EM noise. All signal input leads will be properly shielded. The conditioner electronics will be packaged in a shielded enclosure. Differential input techniques will be used for low level signals to minimize common mode noise. The conditioner amplifier will be designed to allow a high signal to noise ratio before transmitting the sensor signals off gimbal.

The instrumentation modification provides three new EM noise sources. The static pressure mechanical multiplexer (Scanivalve) is driven by a 28 VDC motor. Shielding and filtering will be accomplished to minimize the EM effects. The inflatable seal has a 28V Solenoid control. Shielding and diode suppression techniques will be implemented to minimize EM effects. The turret de-pressurization is controlled by another 28V Solenoid. The same EM suppression techniques will be used here.

The instrumentation system will be tested after installation to verify the efficiency of the suppression techniques used.

SYSTEM SAFETY ANALYSIS

The APT Open Port modification to the Airborne Pointing and Tracking System must be designed so as to minimize the danger to personnel working on the equipment in the laboratory and must be designed for flight safe operation when installed into the aircraft. The major task from a flight safety standpoint, is the determination of the actual environment to which the modification must be designed and to instrument any weak links in the system so that operation can be curtailed until the unsafe condition either no longer

exists or the aircraft is landed. The major task from a laboratory standpoint is to evaluate all potentially hazardous conditions and to either design out the hazard or unmistakably flag the hazard so that a operator unfamiliar with the equipment is aware of potential danger.

Subsystem Hazard Analysis

The environmental criteria for the open port modification of APT is covered in detail in Section 2 of this report. The criteria comes from the ALL Design Manual, the 0.3 scale wind tunnel testing, the Statement of Work, and from specific technical direction from AFWL. The pointing assembly has been previously designed to meet closed port airborne environment and has flown in the ALL aircraft during cycle I testing. This hazard analysis therefore, covers only the Open Port modification of the PA and its effects on the PA and on airborne and laboratory safety.

The extensive test data from the 0.3 scale model testing and the ALL requirements manual have been analyzed and incorporated into the detailed stress and structural dynamic analysis of the Open Port modification. This analysis is covered in detail in Appendices 1, 2, 3 and 4, and demonstrates that all margins are positive and that the resultant modification is flight safe. Since the Open Port modification does differ from the 0.3 model tested (see Figure 4-7), additional aerodynamic analysis was performed (Appendix 6) to determine the effects of these differences. The major difference is that the APT-PA is not a clean closed cavity like the 0.3 scale model, so it has some different characteristics. It has several volumes that are coupled to the

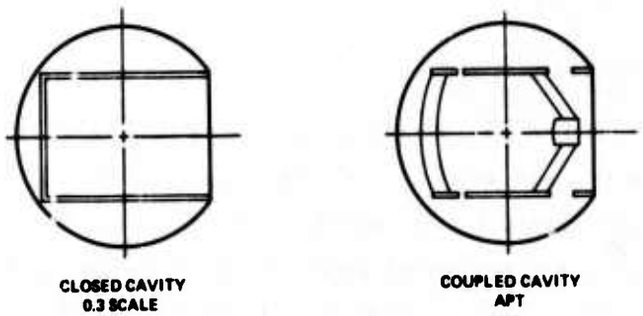

Figure 4-7. 0.3 scale model compared with APT.

main telescope cavity which in effect suppresses the normal sharp fundamental tonal frequencies of a clean cavity and results in less of a dynamic disturbance on the pointing assembly. As indicated by the aerodynamic analysis, there will be some acoustic noise or "Tones" which might be audible inside the aircraft. This noise will in no way affect the flight safety of the pointing assembly as is demonstrated by the structural and dynamic analysis.

Laboratory operation of the APT pointing assembly with the Open Port modification incorporated does add a potential hazard. Since there is no window in the PA aperture, the eyelid could be a hazard to personnel working on or near the secondary mirror. To negate this hazard, the hydraulic drive source to the eyelid could be disabled, or a warning flag could be attached to the PA which hangs across the open cavity. This flag should also be used when the pointing system is installed on the aircraft.

The Open Port modification also requires the use of a pressurization system for an inflatable seal. This pressurization system is periodically filled from a high pressure nitrogen source. A fill valve and a pressure gauge which monitors the seal supply pressure are available. A warning decal should be mounted adjacent to the fill valve and/or pressure gauge which indicates the maximum pressure allowed for safe operation.

The electrical equipment used in conjunction with the open port modification is mostly of low voltage signal level. All 28 VDC power to solenoids and other equipment is routed through connectors with the source as the female side of the connections so that potential shock hazard is eliminated. All wiring harnesses and pneumatic equipment is designed to meet the ALL manual requirements.

Detail System Safety Analysis

A major effort of the preliminary hazard analysis was the search for a weak link in the system which could be instrumented such that an indication of impending failure could be detected. The analysis indicates that there is no such weak link. Two potential weak links were thought to be the exterior structural covers of the unit and the low power input window.

The analysis of the structural covers (with Open Port incorporated into the pointing assemblies) quickly demonstrates that the structural load on the covers actually decreases with Open Port operation. The major structural load on the covers occurs when the output port is closed and the unit is pressurized. The low power input window was analyzed using a Weibull analysis (Appendix 4) and was found to be structurally adequate and not a weak link.

All structures of the APT and the elements of the Open Port modification are designed for the 8 g crash landing load case, and for a static 5 psi load. These cases result in loads which are much higher than any structural loads measured on the 0.3 scale wind tunnel loads imposed by flying open port i.e., loads measured on the 0.3 scale wind tunnel model extrapolated to full scale.

APPENDIX 1

APT OPEN PORT LINER STRESS ANALYSIS IDC 27122/599

A1.1 INTRODUCTION

This section of the report documents the hand stress calculations performed to demonstrate structural adequacy of the following components of the APT Open Port Modification: the aerodynamic fence, the primary mirror cover and its support straps, the secondary mirror cover and its support struts, and the liner shell and its mounting provisions.

A1.2 ENVIRONMENTAL DESIGN CRITERIA

All components of the APT Open Port Liner have been designed to satisfactorily withstand the landing conditions presented in Table A1.2.1.

The three 8g acceleration load cases are those for the crash landing condition in each of three mutually perpendicular directions.

The four pressure load cases represent hypothetical worst case pressure distributions. The magnitude of the peak pressure, 5 psi, is two times the stagnation pressure at sea level at Mach 0.50.

The -65°F cold soak case represents the worst case temperature differential condition, relative to a +70°F installation temperature, that can actually be seen in flight.

All loading conditions are considered to be limit loading conditions. Maximum working stresses and loads must not, therefore, exceed 2/3 (1/1.15) of their minimum guaranteed ultimate (yield) values as published in MIL-HDBK-5B.

A1.3 SUMMARY OF RESULTS

Minimum margins of safety are summarized in Table A1.3.1 for the three acceleration (A1-A3), the four 5 psi pressure (P1-P4), and the -65°F cold soak condition (T1). The three acceleration loading conditions are considered non-critical because the equivalent pressures, $P_{eq} = 8\rho t = 0.8t$ psi, are small. Since all minimum margins of safety are greater than zero, the aerodynamic fence, the primary mirror cover and its support straps, the secondary mirror cover and its support struts, and the liner shell and its mounting provisions are considered structually adequate.

TABLE A1.2.1 ENVIRONMENTAL DESIGN CRITERIA

Load Condition	Load Condition Description
A1-A3	8G crash landing load in any direction
P1	5 psi proof pressure
P2	$P_r(\theta)$ = 5 psi uniform radial pressure acting on the liner shell combined with a P_z = 5 psi normal the primary mirror cover and a P_s = 5 psi normal pressure acting on one side of each of the secondary mirror support struts. See Figure A1.2.1.
P3	Same as load Condition P2 except $P_r(\theta) = 5 \cos \theta$ psi
P4	Same as load Condition P2 except $P_r(\theta) = 5 \lvert \cos \theta \rvert$ psi
T1	Cold soak at -65°F

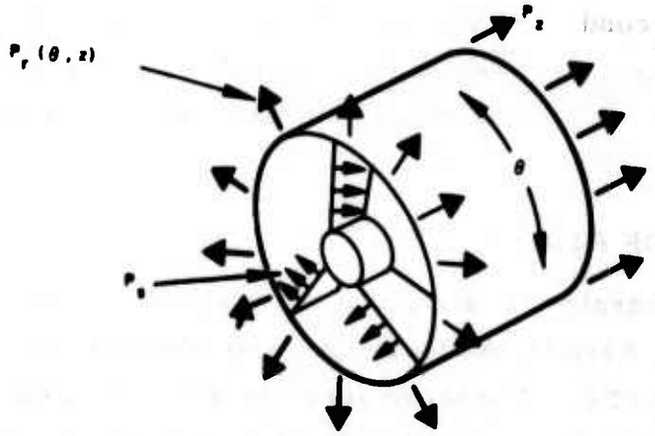

Figure A1.2.1 Definition of Pressure Distributions

TABLE A1.3.1 SUMMARY OF RESULTS OF APT OPEN PORT LINER HAND STRESS ANALYSIS

Component	Material	Allowable Strength (Note 3)	Minimum Margins of Safety								Page
			8G Acceleration			5 psi Pressure				-65°F Temp	
			A1	A2	A3	P1	P2	P3	P4	T1	
Aerofence			(Note 1)	(Note 1)	(Note 1)					(Note 2)	
Screen	6061-T6A1	28 ksi				+ 2. 17	+ 2. 17	+ 2. 17	+ 2. 17		
Flange	6061-T6A1	28 ksi				+ 1. 64	+ 1. 64	+ 1. 64	+ 1. 64		
Attach Bolts	10-32 160 ksi bolt	1928 lb				HI	HI	HI	HI		
Primary Mirror Cover											
Cover	6061-T6A1	28 ksi				+ 1. 36	+ 1. 36	+ 1. 36	+ 1. 36		
Doublers	6061-T6A1	28 ksi				+ 0. 52	+ 0. 52	+ 0. 52	+ 0. 52		
Doubler Attach Bolts	10-32 160 ksi bolt	1928 lb				+ 0. 25	+ 0. 25	+ 0. 25	+ 0. 25		
Support Straps	2024-T4A1	36. 5 ksi				+ 0. 93	+ 0. 93	+ 0. 93	+ 0. 93		
Support Strap Attach Bolts	10-32 160 ksi bolt	1928 lb				+ 1. 77	+ 1. 77	+ 1. 77	+ 1. 77		
Secondary Mirror Cover and Support Struts											
Liner Cylinder	2024-T4A1	36. 5 ksi				-	-	-	HI		
Secondary Mirror Cylinder	6061-T6A1	28 ksi				-	-	-	+ 1. 36		
Struts	2024-T4A1	36. 5 ksi				-	-	-	HI		
Strut Brackets	2024-T4A1	36. 5 ksi				-	-	-	+ 2. 08		
Strut Bracket Rivets	MS20427M4C rivet	297 lb				-	-	-	+ 1. 05		
Secondary Mirror Cap	6061-T6	28 ksi				+ 0. 20	+ 0. 20	+ 0. 20	+ 0. 20		
Liner											
Liner	2024-T4A1	36. 5 ksi				HI	HI	+ 0. 00	HI	HI	
Doublers	2024-T4A1	36. 5 ksi				HI	HI	+ 0. 00	HI	Note 2	
Doubler Attach Bolts	10-32 160 ksi bolt	1928 lb				HI	HI	+ 1. 59	HI	Note 2	
Liner Mounting Bolts	10-32 180 ksi bolt	2363 lb				HI	HI	HI	HI	+ 0. 04	
Liner Mounting Flange	6061-T6A1	28 ksi				HI	HI	+ 0. 57	HI	+ 0. 01	
Outer Elevation Gimbal	Glass-Epoxy	21. 3 ksi	-	-	-	-	-	-	-	+ 0. 06	

Note 1. The 8G acceleration cases are considered non-critical since the equivalent pressures are $8p_t$ = 0. 8t psi.
Note 2. The -65°F cold soak condition is considered critical only at the liner flange/outer elevation gimbal interface.
Note 3. The allowable strength is the lesser of the minimum guaranteed ultimate strength ÷ 1. 5 or yield strength ÷ 1. 15.

A1.4 STRESS ANALYSIS OF AERODYNAMIC FENCE (P/N 3432706)

A1.4.1 Screen

It is conservative to assume that the porous screen behaves as a cantilever, with effective width a function of hole size (d = 0.250 inch) and spacing (s = 0.375 inch), because the beneficial effect of hoop membrane action in the cylinder is ignored.

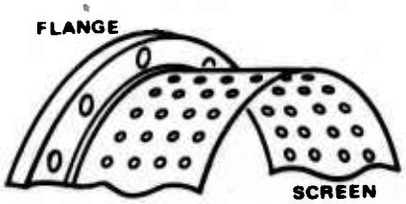

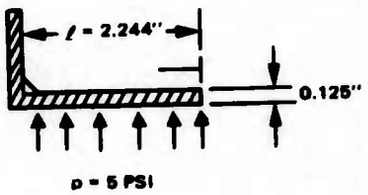

The bending stress at the flange, where there are no holes, is

$$\sigma = \frac{3psx^2}{st^2} = \frac{3 \times 5 \times 0.375 \times 2.244^2}{0.375 \times 0.125^2} = 4834 \text{ psi}$$

The bending stress at the innermost hole is

$$\sigma = \frac{3psx^2}{(s-d)t^2} = \frac{3 \times 5 \times 0.375 \times 1.75^2}{(0.375 - 0.25) \times 0.125^2} = 8820 \text{ psi}$$

The minimum margin of safety in the 6061-T6 aluminum, screen per MIL-HDBK-5B, is

$$MS = \frac{F_{tu}(6061\text{-}T6)}{1.5\sigma} - 1 = \frac{42000}{1.5 \times 8820} - 1 = \underline{+2.17 > 0}$$

A1.4.2 Flange

It is again conservative to assume that the cantilever moment M from the screen acting over an effective width a is reacted by the flange with a bolt load P_B and a heel reaction acting over an effective width b.

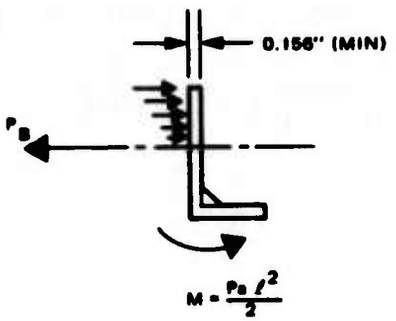

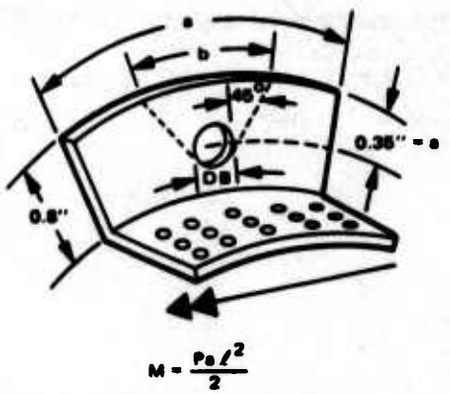

The effective width a is assumed to be π times the fence diameter D_F divided by the number of attach bolts n_B so

$$a = \frac{\pi D_F}{n_B} = \frac{22.5\pi}{24} = 2.95 \text{ in.}$$

The effective width b is assumed to be the sum of the 10-32 attach bolt head diameter $2D_B$ and twice the edge distance e so

$$b = (2D_B + 2e) = 2 \times 0.19 + 2 \times 0.35) = 1.08 \text{ in.}$$

The maximum bending stress in the flange then becomes

$$\sigma = \frac{6M}{(b-D_B)t^2} = \frac{3pa\ell^2}{(b-D_B)t^2} = \frac{3 \times 5 \times 2.95 \times 2.275^2}{(1.08 - 0.19) \times 0.156^2} = 10570 \text{ psi}$$

The margin of safety in the 6061-T6 aluminum flange, per MIL-HDBK-5B, is

$$MS = \frac{F_{tu}(6061\text{-}T6)}{1.5\sigma} - 1 = \frac{42000}{1.5 \times 10570} - 1 = \underline{1.64 > 0}$$

A1.4.3 Attach Bolts

The attach bolt load P_B is

$$P_B = \frac{3M}{2e} = \frac{3\ pa\ell^2}{4e} = \frac{3 \times 5 \times 2.95 \times 2.275^2}{4 \times 0.35} = 164 \text{ lbs}$$

The margin of safety in the 10-32 160 ksi UTS bolt, per MIL-HDBK-5B, is

$$MS = \frac{P_{ult}(10\text{-}32\ @\ 160\ ksi)}{1.5P_B} - 1 = \frac{2892}{1.5 \times 164} - 1 = \underline{HI>0}$$

A1.5 STRESS ANALYSIS OF PRIMARY MIRROR COVER (P/N 3432818)

A1.5.1 Cover

Assuming the primary mirror cover behaves as an annular plate simply supported along its outer radius and subjected to a uniform normal pressure, the maximum stress, per case 13 in Table X of Roark's Formulas for Stress and Strain, is

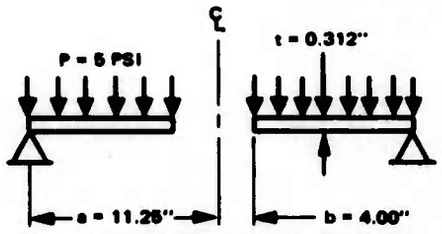

$$\sigma_{max} = \frac{3p}{4t^2(a^2-b^2)}\left[a^4(3+v) + b^4(1-v) - 4a^2b^2\left|1 + (1+v)\log\frac{a}{b}\right|\right]$$

$$= \frac{3 \times 5}{4 \times 0.312^2\,(11.25^2-4^2)}\left[11.25^4 \times 3.3 + 4^4 \times 0.7 - 4 \times 11.25^2 \times 4^2\right.$$

$$\left.\left|1 + 1.3\log\left(\frac{11.25}{4}\right)\right|\right] = 11870 \text{ psi}$$

The margin of safety in the 2024-T4 aluminum cover, per MIL-HDBK-5B, is

$$MS = \frac{F_{tu}(2024\text{-}T4)}{1.15\sigma} - 1 = \frac{42000}{1.15 \times 11870} - 1 = +\underline{2.08}$$

A1.5.2 Primary Mirror Cover Doublers

The doublers and their attach bolts must be capable of carrying a moment M, where

$$M = \frac{\sigma_p t_p^2}{6} = \frac{11870 \times .312^2}{6} = 192.5 \text{ in-lb/in}$$

as shown in the sketch below

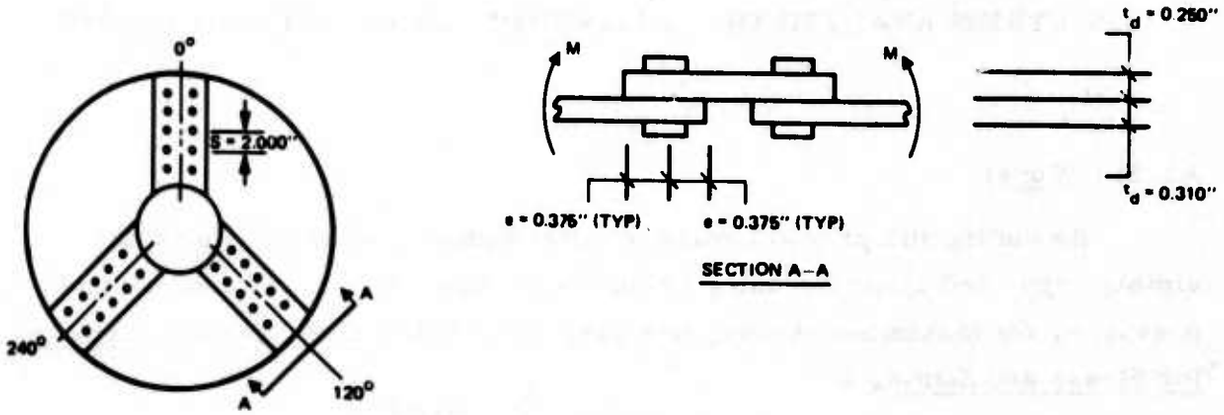

Assuming the doubler free-body diagram takes the form

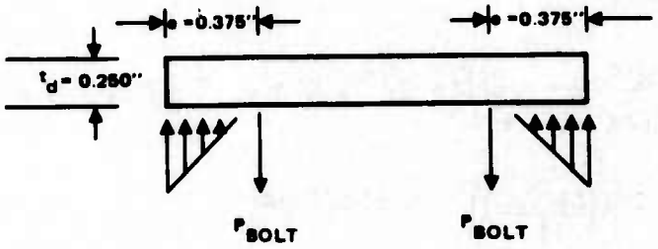

the bending stress in the doubler becomes

$$\sigma_d = \frac{6M}{t_d^2} = \frac{6 \times 192.5}{.250^2} = 18480 \text{ psi}$$

The margin of safety in the 2024-T4 aluminum doubler, per MIL-HDBK-5B, is

$$MS = \frac{F_{tu}(2024\text{-}T4)}{1.15\sigma} - 1 = \frac{42000}{1.15 \times 18480} - 1 = \underline{+0.98}$$

A1.5.3 Doubler Attach Bolts

Referring again to the doubler free-body diagrams, the bolt loads, for spacing s, become

$$P_B = \frac{3Ms}{2e} = \frac{3 \times 192.5 \times 2.000}{2 \times 0.375} = 1540 \text{ lbs}$$

The margin of safety in the 10-32 160 ksi UTS bolts, per MIL-HDBK-5B, is

$$MS = \frac{P_{ult}(10\text{-}32 \text{ at } 160 \text{ ksi})}{1.5\ P_B} - 1 = \frac{2892}{1.5 \times 1540} - 1 = \underline{+.25 > 0}$$

A1.5.4 Support Straps (P/N 3432710)

The primary mirror cover is supported by twelve 2024-T4 aluminum support straps as shown below.

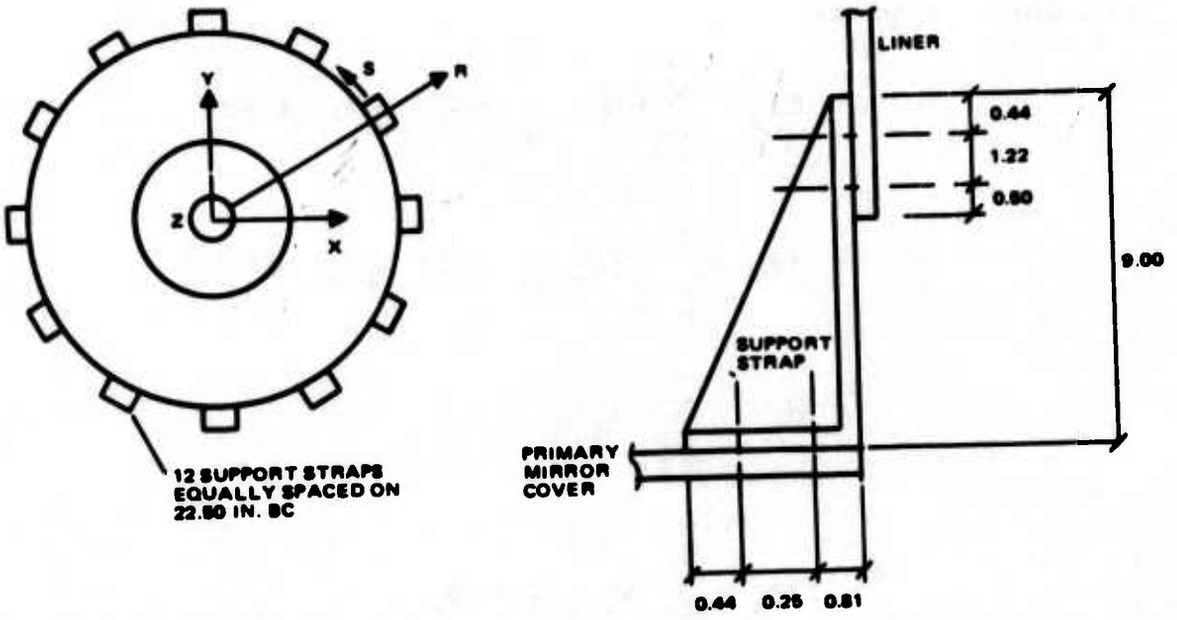

Strap Spring Rates

The spring rates of the support strap suspension system can be obtained using the following procedure

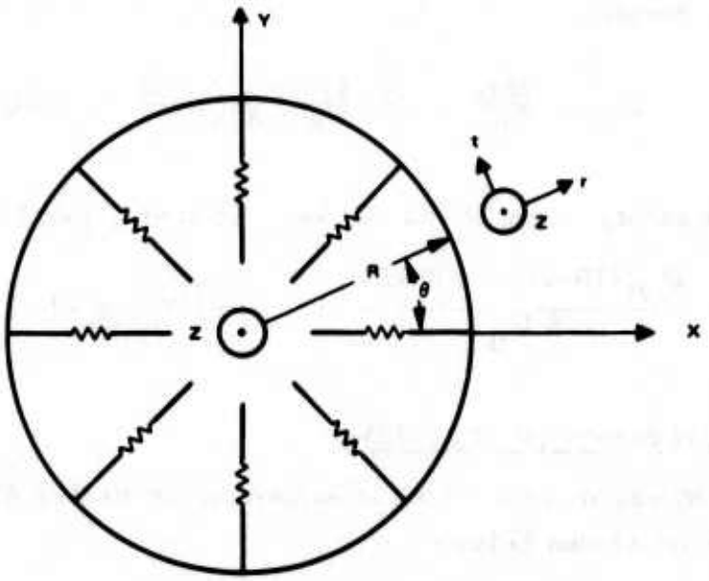

Equilibrium requires

$$\Sigma F_x = \sum_{i=1}^{n} (k_r \, \delta_{r_i} \cos\theta_i - k_t \, \delta_{t_i} \sin\theta_i)$$

$$\Sigma F_y = \sum_{i=1}^{n} (k_r \, \delta_{r_i} \sin\theta_i + k_t \, \delta_{t_i} \cos\theta_i) \qquad (1)$$

$$\Sigma F_z = \sum_{i=1}^{n} k_z \, \delta_{z_i}$$

$$\Sigma M_x = \sum_{i=1}^{n} k_z \, \delta_{z_i} \, R \sin\theta_i$$

$$\Sigma M_y = - \sum_{i=1}^{n} k_z \delta_{z_i} R \cos\theta_i$$

$$\Sigma M_z = \sum_{i=1}^{n} k_t \delta_{t_i} R$$

Compatibility requires

$$\delta_{r_i} = \delta_x \cos\theta_i + \delta_y \sin\theta_i$$

$$\delta_{t_i} = - \delta_x \sin\theta_i + \delta_y \cos\theta_i + R\theta_z \qquad (2)$$

$$\delta_{z_i} = \delta_z + \theta_x R \sin\theta_i - \theta_y R \cos\theta_i$$

The subsitution of Equation 2 into 1 gives

$$\Sigma F_x = \sum_{i=1}^{n} [\delta_x(k_r\cos^2\theta_i + k_t \sin^2\theta_i) + \delta_y(k_r-k_t)\sin\theta_i \cos\theta_i - \theta_z k_t R \sin\theta_i]$$

$$\Sigma F_y = \sum_{i=1}^{n} [\delta_x(k_r-k_t) \sin\theta_i \cos\theta_i + \delta_y(k_r\cos^2\theta_i + k_t \sin^2\theta_i) + \theta_z k_t R \cos\theta_i]$$

$$\Sigma F_z = \sum_{i=1}^{n} k_z(\delta_z + \theta_x R \sin\theta_i - \theta_y R \cos\theta_i) \qquad (3)$$

$$\Sigma M_x = \sum_{i=1}^{n} k_z (\delta_z R \sin\theta_i + \theta_x R^2\sin^2\theta_i - \theta_y R^2\sin\theta_i \cos\theta_i)$$

$$\Sigma M_y = \sum_{i=1}^{n} k_z(-\delta_z R \cos\theta_i - \theta_x R^2 \sin\theta_i \cos\theta_i + \theta_y R^2\cos^2\theta_i)$$

$$\Sigma M_z = \sum_{i=1}^{n} k_t(-\delta_x R \sin\theta_i + \delta_y R \cos\theta_i + \theta_z R^2)$$

If the n springs are equally spaced, then

$$\sum_{i=1}^{n} \sin\theta_i = \sum_{i=1}^{n} \cos\theta_i = \sum_{i=1}^{n} \sin\theta_i \cos\theta_i = 0 \tag{4}$$

and

$$\sum_{i=1}^{n} \sin^2\theta_i = \sum_{i=1}^{n} \cos^2\theta_i = \frac{n}{2} \tag{5}$$

And Equation 3 reduces to

$$\begin{aligned}
\Sigma F_x &= \frac{n}{2}(k_r + k_t)\,\delta_x \\
\Sigma F_y &= \frac{n}{2}(k_r + k_t)\,\delta_y \\
\Sigma F_z &= nk_z\,\delta_z \\
\Sigma M_x &= \frac{n}{2}k_z R^2\,\theta_x \\
\Sigma M_y &= \frac{n}{2}k_z R^2\,\theta_y \\
\Sigma M_z &= nk_t R^2
\end{aligned} \tag{6}$$

The system spring rates therefore become

$$\begin{aligned}
k_{F_x} &= k_{F_Y} = \frac{n}{2}(k_r + k_t) \\
k_{F_z} &= nk_z \\
k_{M_x} &= k_{M_Y} = \frac{n}{2}k_z R^2 \\
k_{M_z} &= nk_t R^2
\end{aligned} \tag{7}$$

The spring rates of the individual support straps, assuming they behave as fixed-pinned beams, are

$$k_r = \frac{3EI_s}{L^3(1 + \Phi_s)}$$

$$k_s = \frac{3EI_r}{L^3(1 + \Phi_r)} \qquad (8)$$

$$k_z = \frac{EA}{L}$$

where

$$\Phi_r = \frac{3EI_r}{L^2 A_r} \qquad (9)$$

$$\Phi_s = \frac{3EI_s}{L^2 A_s G}$$

Assuming the effective length L = 7.95 inches and the effective cross-section of the support straps to be

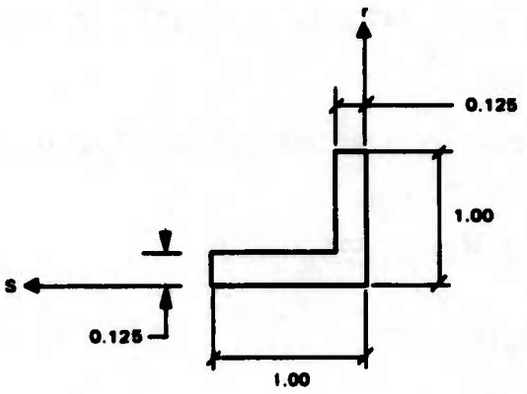

so

$$A_r = A_s = 1.875 \times .125 = 0.234 \text{ in}^2$$

$$\bar{r} = \bar{s} = (0.875 \times .125^2 + 1.00^2 \times .125)/(2A_r) = 0.296 \text{ in}$$

$$I_r = I_s = \frac{1}{3}(.875 \times .125^3 + 1.000^3 \times .125) - A_r \bar{r}^2 = .0218 \text{ in}^4$$

$$I_{rs} = 2 \times 1^2 \times .125^2/2 - A_r \bar{r}\,\bar{s} = -4.887 \times 10^{-3} \text{ in}^4$$

and

$$\Phi_r = \Phi_s = \frac{3 \times 10^7 \times .0218}{7.95^2 \times 0.234 \times 0.24 \times 10^7} = .0184$$

$$k_r = k_s = \frac{3 \times 10^7 \times .0218}{7.95^3 \times 1.0184} = 1278 \text{ lb/in}$$

$$k_z = \frac{10^7 \times .234}{7.94} = 2.947 \times 10^5 \text{ lb/in}$$

Then

$$k_{F_x} = k_{F_y} = 6 \times 2 \times 1278 = 1.534 \times 10^4 \text{ lb/in}$$

$$k_{F_z} = 12 \times 2.947 \times 10^5 = 3.537 \times 10^6 \text{ lb/in}$$

$$k_{M_x} = k_{M_y} = 6 \times 2.947 \times 10^5 \times 11.25^2 = 2.238 \times 10^8 \text{ in-lb/rad}$$

$$k_{M_z} = 12 \times 1278 \times 11.25^2 = 1.941 \times 10^6 \text{ in-lb/rad}$$

Primary Mirror Cover Weight and Inertia

$$W_x = W_y = W_z = \pi \rho t_p (a^2 - b^2) = \pi \times .1 \times .3125\,(11.25^2 - 4.00^2) = 10.85 \text{ lbs}$$

$$I_z = 2I_x = 2I_y = \frac{W}{2}(a^2 + b^2) = \frac{10.85}{2}(11.25^2 + 4.00^2) = 774 \text{ lb-in}^2$$

Strap Natural Frequencies

$$f_{F_x} = f_{F_y} = 3.13\sqrt{\frac{K_{F_x}}{W_x}} = 3.13\sqrt{\frac{1.543 \times 10^4}{10.85}} = 118 \text{ Hz}$$

$$f_{F_z} = 3.13\sqrt{\frac{K_{F_z}}{W_z}} = 3.13\sqrt{\frac{3.537 \times 10^6}{10.85}} = 1790 \text{ Hz}$$

$$f_{M_x} = f_{M_y} = 3.13\sqrt{\frac{K_{M_x}}{I_x}} = 3.13\sqrt{\frac{2.238 \times 10^8}{387}} = 2380 \text{ Hz}$$

$$f_{M_z} = 3.13\sqrt{\frac{K_{M_z}}{I_z}} = 3.13\sqrt{\frac{1.941 \times 10^6}{774}} = 157 \text{ Hz}$$

Strap Stress Levels

A conservative estimate of stress levels in the straps can be obtained by considering a cylinder with a flat head closure for which the free-body diagram is shown below

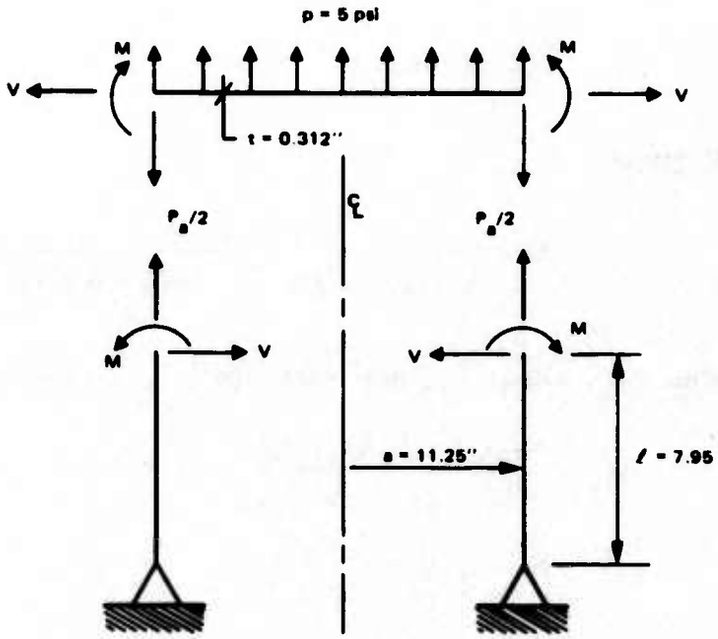

The load deflection relation for the flat head closure, per cases 1 and 12 in Table X of R. J. Roark's Formulas for Stress and Strain, is

$$\theta = \left[\frac{3pa^3}{2Et^3} - \frac{12Ma}{Et^3}\right](1-v)$$

$$= \frac{3 \times 5 \times 11.25^3 \times (1-0.3)}{2 \times 10^7 \times .312^3} - \frac{12 \times 11.25 \times (1-0.3)M}{10^7 \times .312^3}$$

$$= 0.024612 - 3.11149 \times 10^{-4} M$$

The load deflection relation for the $n_s = 12$ straps per linear inch of circumference is

$$\theta = \frac{M\ell}{3EI_s} \cdot \frac{n_s}{2\pi a}$$

$$= \frac{7.95 \times 12M}{3 \times 10^7 \times .0218 \times 2\pi \times 11.25}$$

$$= 2.06366 \times 10^{-6} M$$

Solving for M gives

$$M = \frac{0.024612}{3.11149 \times 10^{-4} + 2.06366 \times 10^{-6}} = 78.6 \text{ in-lb/in}$$

The end moment M_s, shear V_r, and axial load P_z on each strap becomes

$$M_s = \frac{2\pi a M}{n_s} = \frac{2\pi \times 11.25}{12} \times 78.6 = 463 \text{ in-lb}$$

$$V_r = \frac{M_s}{L} = \frac{463}{7.95} = 58.2 \text{ lb}$$

$$P_z = \frac{2\pi a}{n_s} \cdot \frac{pa}{2} = \frac{2\pi}{12} \times 5 \times 11.25^2 = 331 \text{ lb}$$

The stress levels in the effective cross-section shown below can be analyzed using the method of effective bending moments as outlined in F.R. Shanley's Strength of Materials.

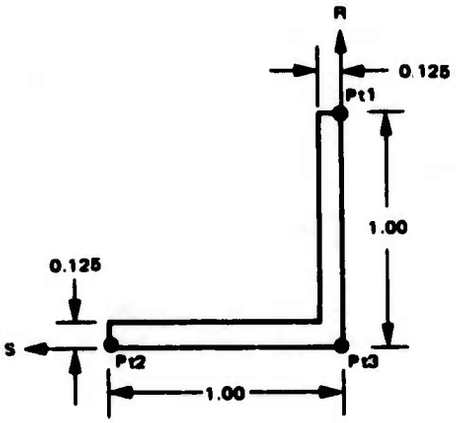

$A = 0.234\ IN^2$
$r = s = 0.296\ IN$
$I_r = I_s = 0.0218\ IN^4$
$I_{rs} = -0.004887\ IN^4$

$$k_1 = k_2 = I_{rs}/I_s = -0.22417$$

$$k_3 = 1 - k_1 k_2 = 0.94975$$

$$M_r^* = \frac{M_r + k_1 M_s}{k_3} = -\frac{0.22417}{0.94975} \times 463 = -109\ \text{in-lb}$$

$$M_s^* = \frac{M_s + k_2 M_r}{k_3} = \frac{1}{0.94975} \times 463 = 487\ \text{in-lb}$$

$$\sigma_i = \frac{P_z}{A} + \frac{M_r^*}{I_r} s_i - \frac{M_s^*}{I_s} r_i$$

Pt_i	r_i	s_i	σ_i
1	0.704	-.296	-15792
2	-0.296	-.296	+9507
3	-0.296	.704	+4507

The minimum margin of safety in the 2024-T4 aluminum strap, per MIL-HDBK-5B, is

$$MS = \frac{F_{ty}(2024\text{-}T4)}{1.15\sigma} - 1 = \frac{42000}{1.15 \times 15792} - 1 = \underline{+1.31}$$

A1.5.5 Support Strap Attach Bolts

The support strap attach bolt loads are

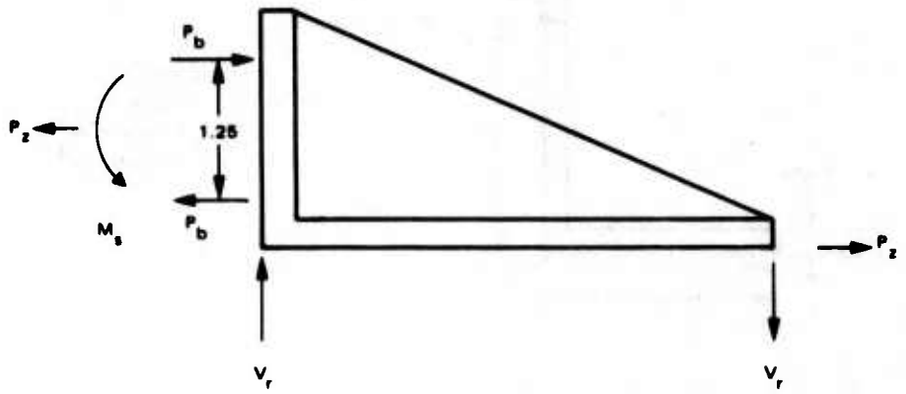

$$P_b = \frac{P_z}{2} + \frac{M_s}{1.25} = \frac{331}{2} + \frac{463}{1.25} = 536 \text{ lbs}$$

$$V_b = \frac{V_r}{2} = \frac{58.2}{2} = 29.1 \text{ lbs}$$

The margin of safety in the 10-32 160 ksi UTS bolts, per MIL-HDBK-5B, is

$$MS = \frac{P_{tu}}{1.5P_b}(10\text{-}32 \text{ @ } 160 \text{ ksi}) - 1 = \frac{2892}{1.5 \times 538} - 1 = \underline{+2.60}$$

A1.6 STRESS ANALYSIS OF SECONDARY MIRROR COVER AND SUPPORT STRUTS (P/N 3432705)

A free body diagram for worst case loading of the secondary mirror support struts is shown below.

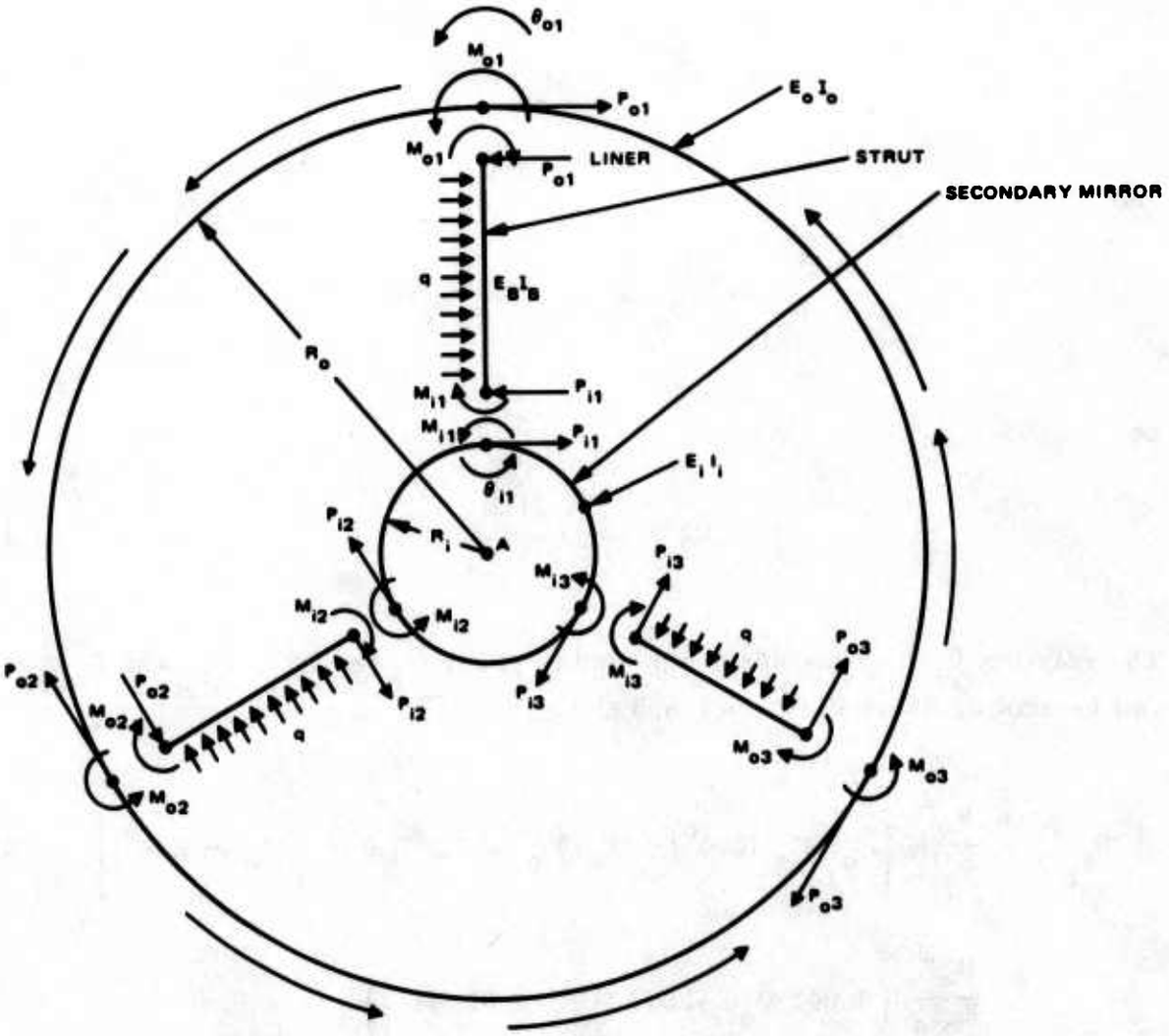

Figure A1.6.1 Free-body diagram for worst case loading of secondary mirror support struts.

The rotation $\theta_{o_1}{}^{M}$ of the outer ring due to moments M_{o_1}, M_{o_2}, and M_{o_3} can be shown, using Figure A1.6.2, to be

$$o^{M} = \frac{R_o}{E_o I_o}\left[M_{o_1} K_\theta\,(\phi=0^o) + M_{o_2} K_\theta\,(\phi=120^o) + M_{o_3} K_\theta\,(\phi=240^o)\right] \qquad 1)$$

$$= \frac{R_o}{E_o I_o}\left(.25\, M_{o_1} - .025\, M_{o_2} - .025\, M_{o_3}\right)$$

Symmetry requires

$$M_{o_1} = M_{o_2} = M_{o_3} = M_o \qquad 2)$$

and

$$\theta_{o_1}{}^{M} = \theta_{o_2}{}^{M} = \theta_{o_3}{}^{M} = \theta_o{}^{M} \qquad 3)$$

so

$$\theta_o{}^{M} = 0.2\,\frac{M_o R_o}{E_o I_o} \qquad 4)$$

The rotation $\theta_{o_1}{}^{P}$ of the outer ring due to shear forces P_{o_1}, P_{o_2} and P_{o_3} can be shown, using Figure A1.6.3, to be

$$\theta_{o_1}{}^{P} = \frac{R_o{}^2}{E_o I_o}\left[P_{o_1} K_\theta\,(\phi=0^o) + P_{o_2} K_\theta\,(\phi=120^o) + P_{o_3} K_\theta\,(\phi=240^o)\right] \qquad 5)$$

$$= \frac{R_o{}^2}{E_o I_o}\left(0.043\, P_{o_1} - .013\, P_{o_2} - 0.013\, P_{o_3}\right)$$

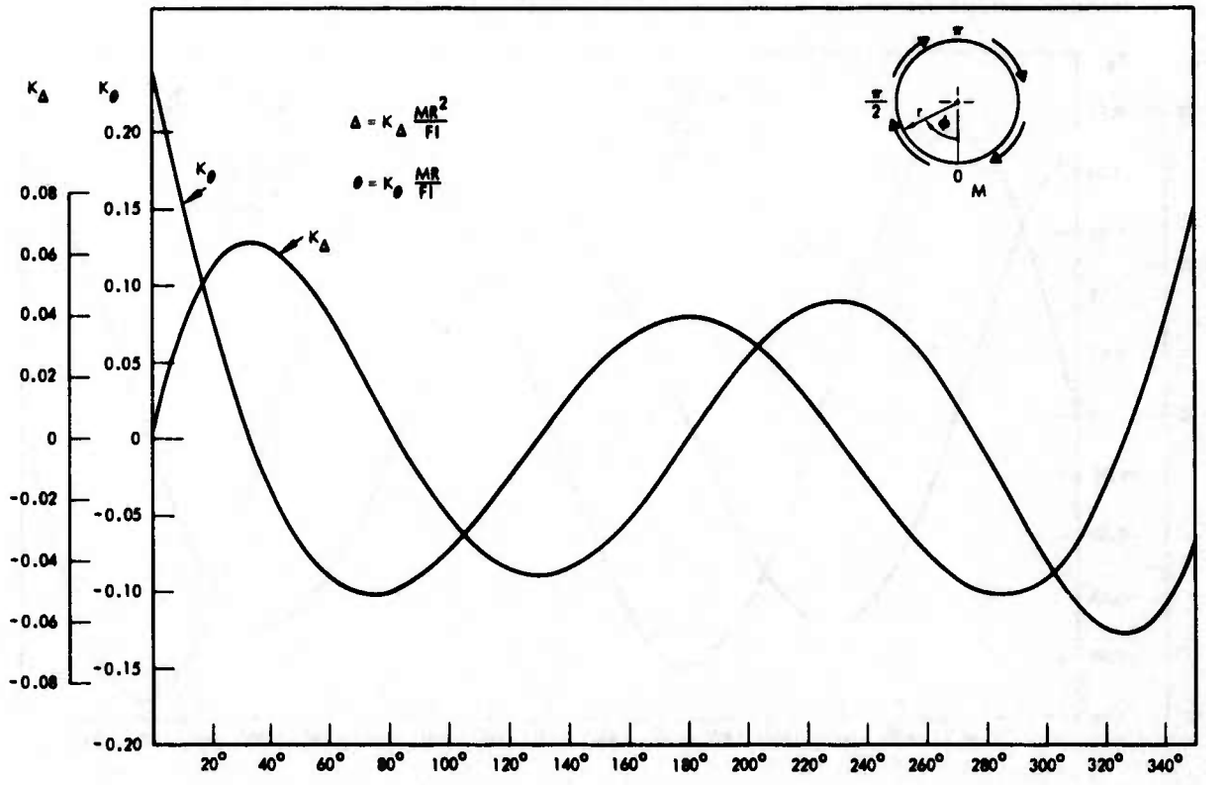

Figure A1.6.2. Load Deflection Relations for Moment Loading of Rings.

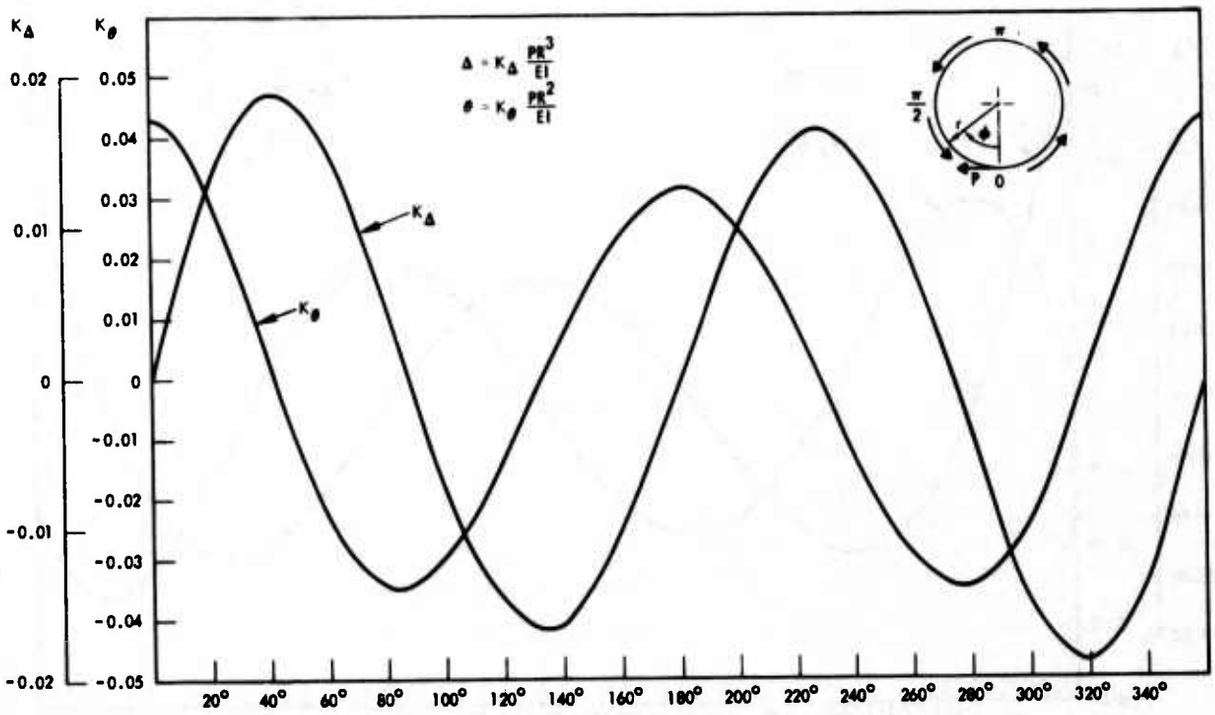

Figure A1.6.3. Load Deflection Relations for Shear Loading of Rings.

Symmetry requires

$$P_{o_1} = P_{o_2} = P_{o_3} = P_o \tag{6}$$

and

$$\theta_{o_1}{}^{P} = \theta_{o_2}{}^{P} = \theta_{o_3}{}^{P} = \theta_o{}^{P} \tag{7}$$

so

$$\theta_o^P = .017 \frac{P_o R_o{}^2}{E_o I_o} \tag{8}$$

Combining Equations 4 and 7 gives

$$\theta_o = \theta_o{}^{M} + \theta_o{}^{P} = .2 \frac{M_o R_o}{E_o I_o} + 0.017 \frac{P_o R_o{}^2}{E_o I_o} \tag{9}$$

Since the same considerations apply to the inner ring we may write

$$\theta_i = 0.2 \frac{M_i R_i}{E_i I_i} + 0.017 \frac{P_i R_i{}^2}{E_i I_i} \tag{10}$$

For the inner ring, equilibrium requires

$$\Sigma M = 0 = R_i \left(P_{i_1} + P_{i_2} + P_{i_3} \right) - M_{i_1} - M_{i_2} - M_{i_3} \tag{11}$$

This expression, in view of Equations 2 and 6, may be recast in the form

$$P_i = \frac{M_i}{R_i} \qquad 12)$$

For the struts, shear and moment equilibrium require, respectively,

$$\Sigma V = 0 = P_o + P_i - q(R_o - R_o) \qquad 13)$$

and

$$M = 0 = M_o + M_i + P_i (R_o - R_i) - \frac{q}{2} (R_o - R_i)^2 \qquad 14)$$

The Dummy Load Method can now be used to obtain the load deflection relation for the struts. Consider the figure

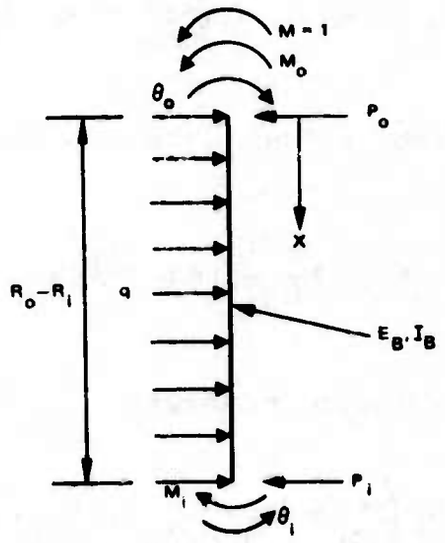

The Dummy Load method requires

$$\theta_o - \theta_i = \int_0^{R_o - R_i} \frac{M(x)m}{E_B I_B} \, dx \qquad 15)$$

where

$$M(x) = - M_o + P_o x - \frac{qx^2}{2} \qquad 16)$$

Evaluation of this integral yields

$$\theta_o - \theta_i = \frac{1}{E_B I_B} \left[\frac{P_o}{2} (R_o - R_i)^2 - M_o (R_o - R_i) - \frac{q}{6} (R_o - R_i)^3 \right] \qquad 17)$$

Equations 9, 10, 12, 13, 14, and 17 may be recast in the matrix form

$$[A] \left| X \right| = \left| B \right| \qquad 18)$$

where

$$\left| X \right| = \begin{Bmatrix} M_i \\ P_i \\ \theta_i \\ M_o \\ P_o \\ \theta_o \end{Bmatrix} \qquad 19)$$

$$\left|B\right| = \left\{ \begin{array}{l} 0 \\ 0 \\ 0 \\ q(R_o - R_i) \\ \frac{q}{2}(R_o - R_i)^2 \\ -\frac{q}{6}(R_o - R_i)^3 \end{array} \right\} \qquad (20)$$

$$[A] = \begin{bmatrix} 1 & -R_i & 0 & 0 & 0 & 0 \\ 0 & 0 & 0 & 0.2R_o & 0.017R_o^2 & -E_oI_o \\ 0.2R_i & 0.017R_i^2 & -E_iI_i & 0 & 0 & 0 \\ 0 & 1 & 0 & 0 & 1 & 0 \\ 1 & (R_o - R_i) & 0 & 1 & 0 & 0 \\ 0 & 0 & -F_BI_B & (R_o - R_i) & -\frac{1}{2}(R_o - R_i)^2 & E_BI_B \end{bmatrix} \qquad (21)$$

Solving for $\left|X\right|$ gives

$$\left|X\right| = \left|A\right|^{-1} \left|B\right| \qquad (23)$$

A GE 265 Time Sharing computer program has been developed to evaluate the vector $\left|X\right|$ and compute stresses in the inner and outer rings.

The program listing is:

```
10 DIM A(6,6),B(6,1),C(6,6),X(6,1)
15 MAT A=ZER(6,6)
20 MAT B=ZER(6,1)
25 MAT C=ZER(6,6)
30 MAT X=ZER(6,1)
35 READ R0,B0,T0,R1,B1,T1,I2,Q
40 E0=E1=E2=10.5E6
45 I0=B0*T0↑3/12
50 I1=B1*T1↑3/12
55 L=R0-R1
60 A(1,1)=A(4,2)=A(4,5)=A(5,1)=A(5,4)=1
65 A(5,2)=A(6,4)=L
70 A(1,2)=-R1\A(2,4)=.2*R0\A(2,5)=.017*R0↑2
75 A(2,6)=-E0*I0\A(3,1)=.2*R1\A(3,2)=.017*R1↑2
80 A(3,3)=-E1*I1\A(6,3)=-E2*I2\A(6,5)=-L↑2/2
85 A(6,6)=-A(6,3)
90 MAT C=INV(A)
95 B(4,1)=Q*L\B(5,1)=B(4,1)*L/2\B(6,1)=-B(5,1)*L/3
100 MAT X=C*B
105 PRINT "STRESS ANALYSIS ØF APT ØPEN-PØRT STRUTS"\PRINT
110 PRINT "RI ="R1,"BI ="B1,"TI ="T1
115 PRINT "RO ="R0,"BO ="B0,"TO ="T0
120 PRINT "I2 ="I2,"Q ="Q
125 PRINT "MI ="X(1,1),"PI ="X(2,1),"AI ="X(3,1),"SI ="6*X(1,1)/B1/T1↑2
130 PRINT "MO ="X(4,1),"PO ="X(5,1),"AO ="X(6,1),"SO ="6*X(4,1)/B0/T0↑2
135 DATA 11.3,12.4,.156
140 DATA 3.9,7.4,.125
145 DATA .480,61
150 END
```

For the case when the inner ring properties are

$$R_i = 3.9 \text{ in}$$

$$b_i = 7.4 \text{ in}$$

$$t_i = 0.125 \text{ in}$$

$$I_i = \frac{b_i t_i^3}{12} = 0.001204 \text{ in}^4$$

$$E_i = 10^7 \text{ psi}$$

and the outer ring properties are

$$R_o = 11.3 \text{ in}$$

$$b_o = 12.4 \text{ in}$$

$$t_o = 0.156 \text{ in}$$

$$I_o = \frac{b_o t_o^3}{12} \quad 0.003923 \text{ in}^4$$

$$E_o = 10^7 \text{ psi}$$

and the strut properties are

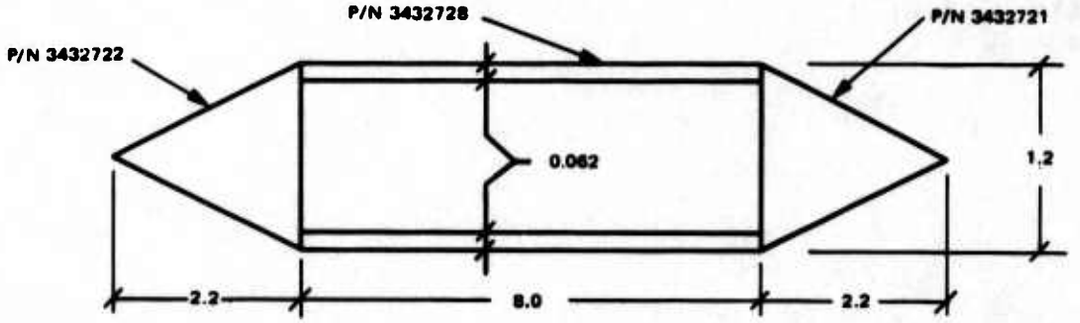

$$I_B = \frac{2}{48} \times 1.2^3 \times 2.2 + \frac{2}{4}(1.2 - 0.062)^2 \times 8.00 \times 0.062 = 0.480 \text{ in}^4$$

$$E_B = 10^7 \text{ psi}$$

$$q = 5 \times 12.2 = 61 \text{ psi}$$

the results become

STRESS ANALYSIS ØF APT ØPEN-PØRT STRUTS

RI = 3.9	BI = 7.4	TI = .125		
RO = 11.3	BO = 12.4	TO = .156		
I2 = .48	Q = 61			
M1 = 479.814	PI = 123.029	AI = 3.21091E-02	SI = 24898.5	
MO = 279.948	PO = 328.371	AO = 3.26645E-02	SO = 5566.2	

The stress levels σ_i, σ_o, and σ_B in the inner and outer rings and the struts are

$$\sigma_i = \frac{3M_i}{b_i t_i^2} = \frac{3 \times 479.814}{7.4 \times 0.125^2} = 12449 \text{ psi}$$

$$\sigma_o = \frac{3M_o}{b_o t_o^2} = \frac{3 \times 279.948}{12.4 \times 0.156^2} = 2783 \text{ psi}$$

$$\sigma_s = \frac{M_i \, c_B}{I_B} = \frac{479.814 \times .6}{0.480} = 600 \text{ psi}$$

The stress levels σ_B in the 3432787 (3432790) angle brackets and the axial load P_B in the Monel rivets at spacing s_B securing the inner (outer) cylinders to the strut are

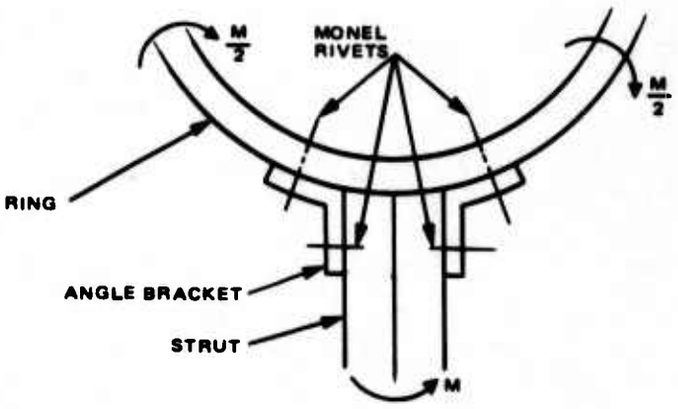

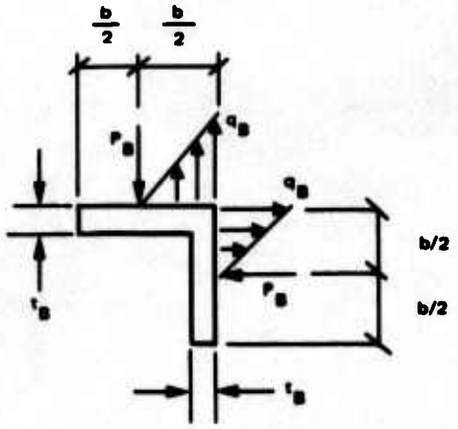

$$\sigma_B^{\,i} = \frac{3M_i}{b_i t_B^2} = \frac{3 \times 479.814}{7.4 \times 0.125^2} = 12449 \text{ psi}$$

$$P_B^i = \frac{3M_i s_B}{2b_i b} = \frac{3 \times 479.814 \times 1.00}{2 \times 7.4 \times 0.32} = 304 \text{ lbs}$$

$$\sigma_B = \frac{3M_o}{b_o t_B^2} = \frac{3 \times 279.948}{12.4 \times 0.156^2} = 2783 \text{ psi}$$

$$P_B^o = \frac{3M_o s_B}{2b_o b} = \frac{3 \times 279.948 \times 1.8}{2 \times 12.4 \times 0.38} = 160 \text{ lb}$$

The minimum margin of safety in the 6061-T6 aluminum outer and 6061-T6 aluminum inner cylinders, per MIL-HDBK-5B, is

$$MS = \frac{F_{tu}\,(6061\text{-}T6)}{1.5\sigma_i} - 1$$

$$= \frac{42000}{1.5 \times 12449} - 1 = \underline{+1.25}$$

The minimum margin of safety in the 2024-T4 aluminum struts and angle brackets, per MIL-HDBK-5B, is

$$MS = \frac{F_{ty}\,(2024\text{-}T4)}{1.15 \times \sigma_B^i} - 1$$

$$= \frac{42000}{1.15 \times 12449} - 1 = +1.93$$

The minimum margin of safety in the MS20427M4C Monel rivets, per Northrup Structural Design Manual Section 201.1, is

$$MS = \frac{P_{ult}}{1.5\ P_B^i} - 1$$

$$= \frac{446}{1.5 \times 304} - 1 = \underline{-0.02 \simeq 0}$$

A conservative estimate of the peak stress level in the 6061-T6 aluminum 3432709 secondary mirror cover cap shown below may be obtained by treating it as a uniformly loaded circular plate with fixed edges (Case 6 in Table X of R.J. Roark's Formulas for Stress and Strain)

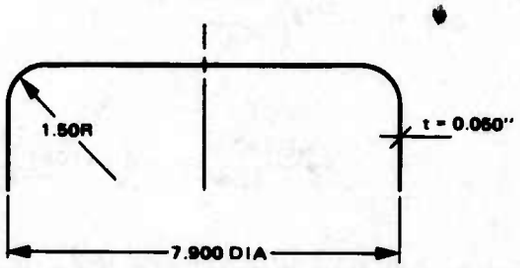

$$\sigma = \frac{3pR^2}{4t^2} = \frac{3 \times 5 \times 3.95^2}{4 \times .05^2} = 23400 \text{ psi}$$

The margin of safety becomes

$$MS = \frac{F_{tu}(6061\text{-}T6)}{1.5\sigma} - 1$$

$$= \frac{42000}{1.5 \times 23400} - 1 = \underline{+0.20 > 0}$$

A1.7 STRESS ANALYSIS OF LINER AND DOUBLERS

A1.7.1 Uniform Internal Pressure

For the uniform internal pressure condition ($p(\phi)$ = 5 psi) shown below

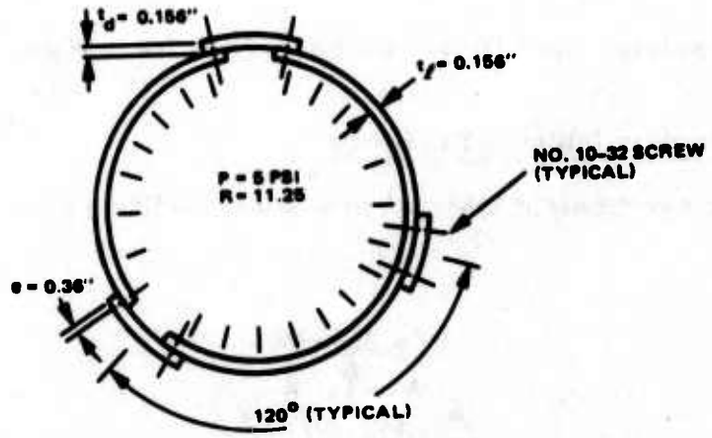

the combined membrane and offset bending stress in the 0.156" thick 6061-T6 aluminum liner and doublers becomes

$$\sigma = \frac{pR}{t} + \frac{6pRt}{t^2} = \frac{7pR}{t}$$

$$= \frac{7 \times 5 \times 11.25}{0.156} = 2524 \text{ psi}$$

The corresponding margin of safety, per MIL-HDBK-5B, is

$$MS = \frac{F_{tu}(6061\text{-}T6)}{1.5\sigma} - 1 = \frac{42000}{1.5 \times 2524} - 1 = \underline{HI}$$

The axial P_b and shear V_b bolt loads for s = 2" spacing are

$$P_b = \frac{3pRts}{2e} = \frac{3 \times 5 \times 11.25 \times 0.156 \times 2}{2 \times 0.36} = 73.1 \text{ lbs}$$

$$V_b = pRs = 5 \times 11.25 \times 2 = 112.5 \text{ lbs}$$

The margin of safety in the 10-32 160 ksi UTS bolts is high.

A1.7.2 Asymmetric Internal Pressure

For the asymmetric internal pressure condition ($p(\phi) = 5\cos\phi$ psi) shown below

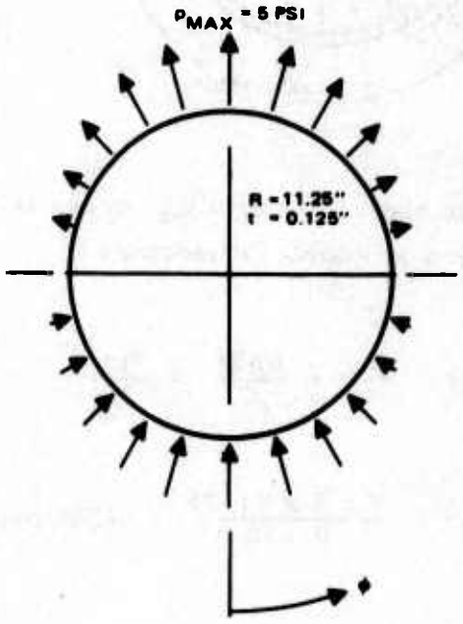

The internal load distribution is

$$\left.\begin{aligned} M(\phi) &= Q(\phi) = 0 \\ N(\phi) &= -pR\cos\phi \end{aligned}\right\} \quad \text{See Figure A1.7.1}$$

The combined membrane and offset bending stress in the 0.156" thick 6061-T6 aluminum line and doublers becomes

$$\sigma = \frac{pR}{t} + \frac{6pRt}{t^2} = \frac{7pR}{t}$$

$$= \frac{7 \times 5 \times 11.25}{0.156} = 2524 \text{ psi}$$

The corresponding margin of safety, per MIL-HDBK-5B, is

$$MS = \frac{F_{tu}(6061\text{-}T6)}{1.5\sigma} - 1 = \frac{42000}{1.5 \times 2524} - 1 = \textbf{HI}$$

The axial P_b and shear V_b bolt loads for s = 2" spacing are

$$P_b = \frac{3pRts}{2e} = \frac{3 \times 5 \times 11.25 \times 0.125 \times 2}{2 \times .36} = 73.1 \text{ lbs}$$

$$V_b = pRs = 5 \times 11.25 \times 2 = 112.5 \text{ lbs}$$

The margin of safety in the 10-32 160 ksi UTS bolts is high.

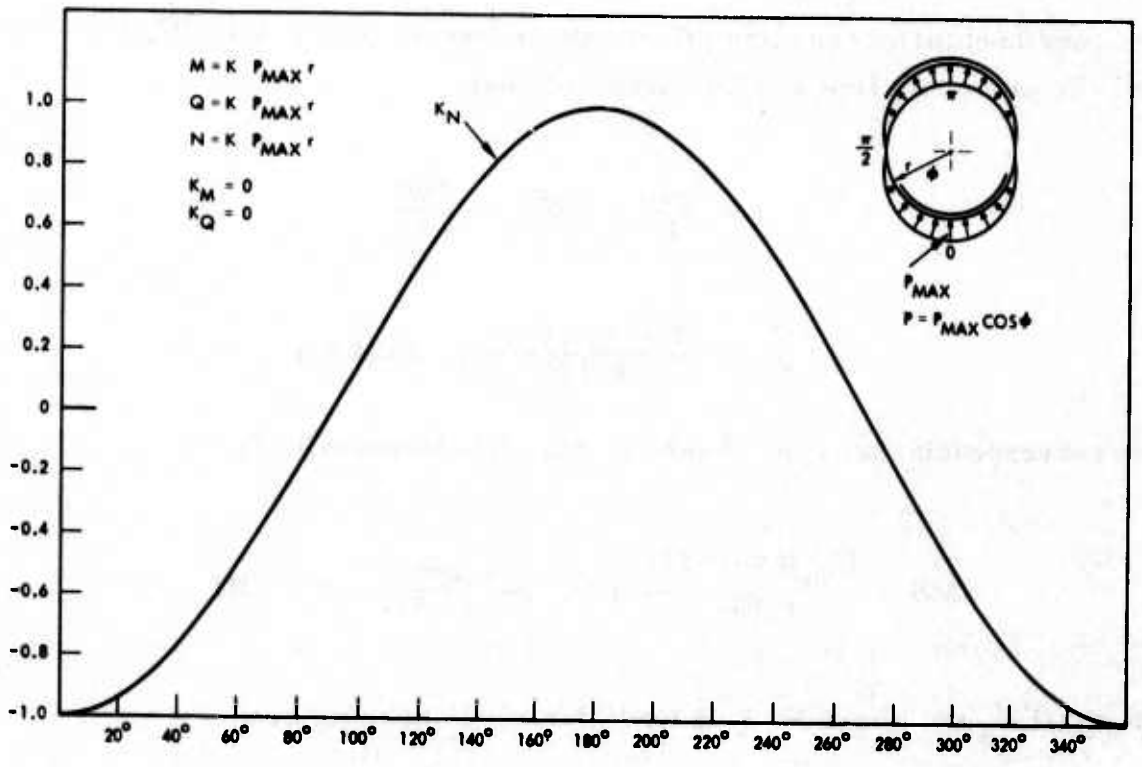

Figure A1.7.1. Internal Ring Load Distribution for $p = P_{max} \cos \theta$.

A1.7.3 Symmetric Internal Pressure

For the symmetric internal pressure condition ($p(\phi) = 5|\cos\phi|$psi) shown below

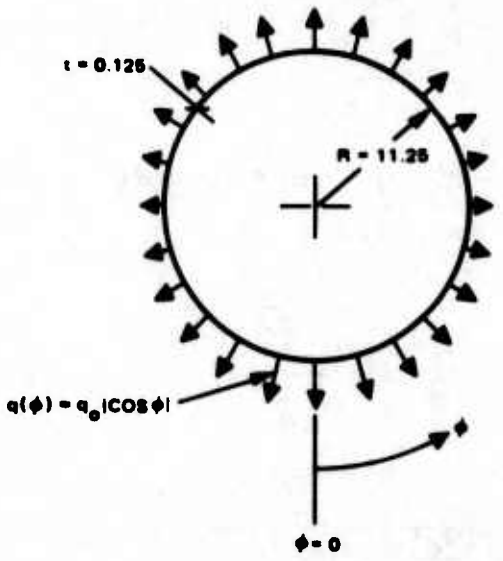

symmetry permits us to consider a quadrant for which the free-body is shown below.

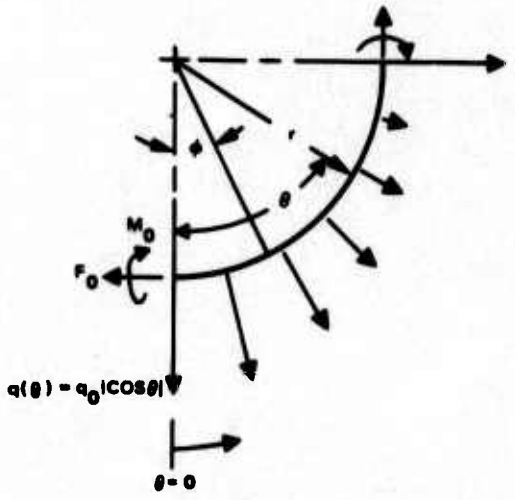

Equilibrium requires

$$F_o = \int_0^{\frac{\pi}{2}} q(\theta) \sin\theta \, r \, d\theta$$

$$= q_o r \int_0^{\frac{\pi}{2}} \sin\theta \cos\theta \, d\theta$$

$$= \frac{q_o r}{2} \sin^2\theta \Big|_0^{\frac{\pi}{2}}$$

$$= \frac{q_o r}{2}$$

The moment at any point may be written as

$$M(\theta) = M_o + Fr(1 - \cos\theta)$$

$$- \int_0^\theta q \cos\phi \, rd\phi \sin\phi \, r(\cos\phi - \cos\theta)$$

$$- \int_0^\theta q \cos\phi \, rd\phi \cos\phi \, r(\sin\theta - \sin\phi)$$

$$= M_o + Fr(1 - \cos\theta) - qr^2 \int_0^\theta (\cos\theta \cos\phi \sin\phi - \sin\theta \cos^2\phi) d\phi$$

$$= M_o + Fr(1 - \cos\theta) - qr^2 \left[\frac{\cos\theta \sin^2\phi}{2} - \sin\theta \left(\frac{\phi}{2} + \frac{\sin\phi \cos\phi}{2} \right) \right]_0^\theta$$

$$M(\theta) = M_o + Fr(1 - \cos\theta) - q\frac{r^2}{2}(\theta \sin\theta)$$

Symmetry requires rotation at $\theta = 0$ and $\frac{\pi}{2}$ be zero so Castigliano's Theorems can be used to determine the unknown M_o; thus

$$U = \frac{1}{2} \int_o^{\frac{\pi}{2}} \frac{M^2(\theta)}{EI} \, rd\theta$$

$$\frac{\partial U}{\partial M_o} = \frac{r}{EI} \int_o^{\frac{\pi}{2}} M(\theta) \frac{\partial M(\theta)}{\partial M_o} \, dr$$

$$\frac{\partial U}{\partial M_o} = 0 = \frac{r}{EI}\int_o^{\frac{\pi}{2}} [M_o + Fr(1 - \cos\theta) - q_o\frac{r^2}{2}(\theta \sin\theta)]d\theta$$

Divide by r/EI and integrate:

$$\left[M_o\theta + Fr(\theta - \sin\theta) - \frac{q_o r^2}{2}(\sin\theta - \theta\cos\theta)\right]\Bigg|_o^{\frac{\pi}{2}} = 0$$

$$M_o\frac{\pi}{2} + Fr\left(\frac{\pi}{2} - 1\right) - \frac{q_o r^2}{2} = M_o\frac{\pi}{2} + \frac{q_o r^2}{2}\left(\frac{\pi}{2} - 2\right) = 0$$

$$M_o = \frac{2}{\pi}\frac{q_o r^2}{2}\left(2 - \frac{\pi}{2}\right) = q_o r^2\left(\frac{2}{\pi} - \frac{1}{2}\right) = 0.1366\ q_o r^2$$

The maximum moment occurs at

$$\frac{\partial M(\theta)}{\partial\theta} = 0 = Fr\sin\theta - \frac{qr^2}{2}(\theta\cos\theta + \sin\theta)$$

$$= \frac{qr^2}{2}\sin\theta - \frac{qr^2}{2}(\theta\cos\theta + \sin\theta)$$

$$= \theta\cos\theta$$

It follows therefore that the maximum moments occur at $\theta = 0, \frac{\pi}{2}$ where

$$M(\theta = 0) = M_o = 0.1366\ q_o r^2$$

$$M\left(\theta = \frac{\pi}{2}\right) = -.14878\, q_o r^2$$

$$F(\theta = 0) = F_o = \frac{q_o r}{2}$$

$$F\left(\theta = \frac{\pi}{2}\right) = \int_o^{\frac{\pi}{2}} q(\theta) \cos\theta \, r\, do$$

$$= q_o r \int_o^{\frac{\pi}{2}} \cos^2\theta \, do$$

$$= \left(q_o r \frac{\theta}{2} + \frac{1}{4}\sin 2\theta\right)\Bigg|_o^{\frac{\pi}{2}}$$

$$= \frac{\pi}{4} q_o r$$

The combined membrane and bending stress in the 0.156" thick 6061-T6 aluminum liner and doublers becomes

$$\sigma_{max}\left(\phi = \frac{\pi}{2}\right) = \frac{\pi}{4} q_o \frac{r}{t} + .14878\, q_o r^2 \times \frac{6}{t^2}$$

$$\sigma_{max}\left(\phi = \frac{\pi}{2}\right) = \frac{\pi}{4} \cdot \frac{5 \times 11.25}{0.156} + \frac{0.14878 \times 5 \times 11.25^2 \times 6}{0.156^2}$$

$$= 23495 \text{ psi}$$

The corresponding margin of safety, per MIL-HDBK-5B, is

$$MS = \frac{F_{tu}(6061\text{-}T6)}{1.5\sigma} - 1 = \frac{42000}{1.5 \times 23495} - 1 = \underline{+0.19>0}$$

The axial P_b and shear V_b bolt loads for s = 2" spacing are

$$P_b = \frac{3M\left(\theta = \frac{\pi}{2}\right)s}{2e} = \frac{3 \times 0.14878 \times 5 \times 11.25^2 \times 2}{2 \times 0.38} = 743 \text{ lbs}$$

$$V_b = F\left(\theta = \frac{\pi}{2}\right)s = \frac{\pi}{4} \times 5 \times 11.25 \times 2 = 88.4 \text{ lbs}$$

The margin of safety in the 10-32 160 ksi UTS bolts, per MIL-HDBK-5B, is

$$MS = \frac{P_{ult}\ (10\text{-}32\ @\ 160\ ksi)}{1.5\ P_b} - 1 = \frac{2892}{1.5 \times 743} - 1 = \underline{+1.59>0}$$

A1.8 STRESS ANALYSIS OF LINER MOUNTING FLANGE AND ATTACH BOLTS

A1.8.1 Asymmetric Internal Pressure

The APT Open Port liner is secured to the APT Outer Elevation gimbal by $n_b = 24$ 10-32 180 ksi UTS bolts on a $2R_b = 28.375$ inch bolt circle.

The worst case pressure loading condition that the attach bolts can experience is that for the asymmetric pressure condition, $p(\theta) = 5 \cos\theta$ psi, acting along the entire liner length L = 27.1 inch. For this case the overturning moment is

$$M = \frac{L^2}{2} \int_0^{2\pi} q(\theta) \cos\theta r d\theta$$

$$= q_o r \frac{L^2}{2} \int_0^{2\pi} \cos^2 \theta d\theta$$

$$= q_o r \frac{L^2}{2} \left(\frac{\theta}{2} + \frac{1}{4} \sin 2\theta \right) \Bigg|_0^{2\pi}$$

$$= \frac{\pi}{2} q_o r L^2 = \frac{\pi}{2} \times 5 \times 11.25 \times 27.1^2 = 64900 \text{ in-lb}$$

The bolt load becomes

$$P_b = \frac{2M}{n_b R_b} = \frac{2 \times 64900}{24 \times 14.188} = 381 \text{ lbs}$$

The margin of safety in the 10-32 180 ksi UTS bolts, per MIL-HDBK-5B, is

$$MS = \frac{P_{ult}(10\text{-}32 \ @ 160 \text{ ksi})}{1.5 \, P_b} - 1 = \frac{3253}{1.5 \times 381} - 1 = \underline{\text{HI}}$$

The stress level in the mounting flange, assuming the effective width of the flange fans out at 45^o from the bolt head diameter $D_b = 0.38''$, is

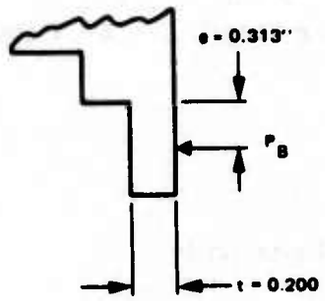

$$\sigma = \frac{6P_B e}{(2e + D_b)t^2} = \frac{6 \times 381 \times 0.313}{(2 \times 0.313 + 0.38) \times 0.200^2} = 17860 \text{ psi}$$

The margin of safety in the 6061-T6 aluminum liner flange, per MIL-HDBK-5B, then becomes

$$MS = \frac{F_{tu}(6061\text{-}T6)}{1.5\sigma} - 1 = \frac{42000}{1.5 \times 17860} - 1 = \underline{+0.57 > 0}$$

A1.8.2 -65°F Cold Soak Condition

For the -65°F cold soak condition, the free radial displacement of the liner mounting flange is restrained by the outer elevation gimbal. The free thermal contractions of the aluminum liner δ_ℓ^o and the glass-epoxy skin of the outer elevation gimbal δ_s^o are

$$\delta_\ell^o = -\alpha_{AL} R_b \Delta T = -13 \times 10^{-6} \times 14.188 \times (-65 - 70) = 0.02490 \text{ in.} \tag{1}$$

$$\delta_s^o = -\alpha_{FE} R_b \Delta T = -5.5 \times 10^{-6} \times 14.188 \times (-65 - 70) = 0.01053 \text{ in.}$$

Consider the figure

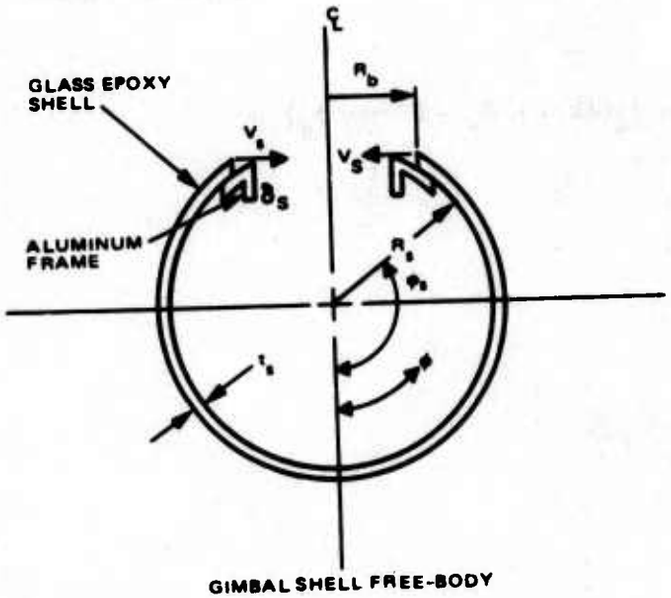

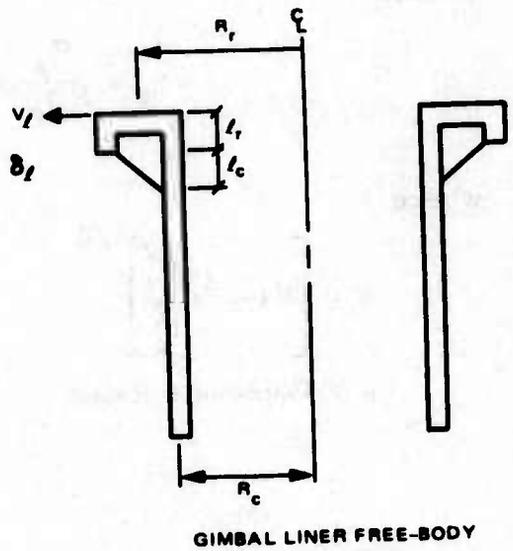

Compatibility requires

$$\delta_s^o + \delta_s = \delta_n^o - \delta_\ell \tag{2}$$

Equilibrium requires

$$V_s = V_\ell = V_b \tag{3}$$

The load deflection relations for both shell and liner may be expressed in the form

$$\delta_s = a_s V_s \tag{4}$$

$$\delta_\ell = a_\ell V_\ell \tag{5}$$

Solving for V_b liner gives

$$V_b = \frac{\delta_\ell^o - \delta_s^o}{a_\ell + a_s} \tag{6}$$

The shell flexibility a_s, per Table 2.33-2 of E. H. Baker's Shell Analysis Manual (NASA CR-912) is

$$a_s = \frac{R_s}{E_s t_s} \sin \phi_s (2k \sin \phi_s - \mu \cos \phi_s) \tag{7}$$

where

$$k = \left[3(1-\mu^2) \frac{R_s^2}{t_s^2} \right]^{1/4}$$

μ = Poisson's Ratio

The liner stiffness k_l will be developed as follows. Consider the figure

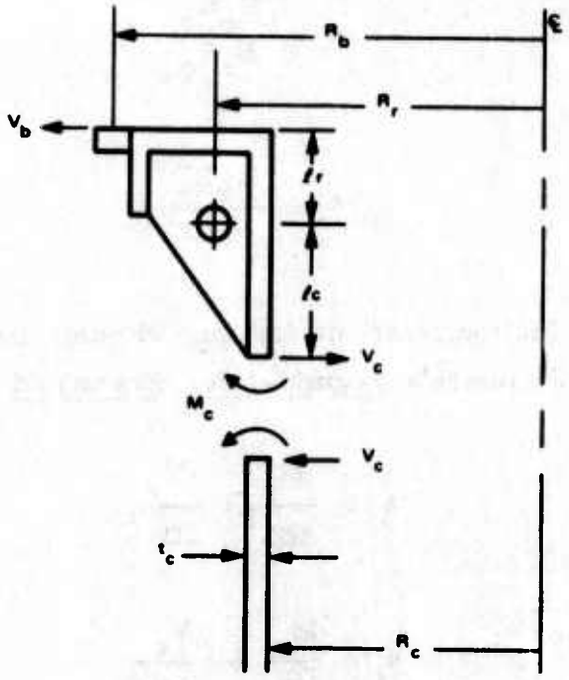

Liner Flange/Cylinder Free-Body

Compatibility requires

$$\theta_r = \theta_c \tag{8}$$

$$\delta_r = \delta_\ell - \theta_r \ell_r \tag{9}$$

$$\delta_c = \delta_\ell - \theta_r(\ell_r + \ell_c) \tag{10}$$

Equilibrium requires that the flange rolling moment M_r and shear V_r be

$$M_r = V_b \ell_r + V_c \ell_c - M_c \tag{11}$$

$$V_r = V_b - V_c \tag{12}$$

The load-deflection relations for the flange are

$$\delta_r = \frac{V_r R_r^2}{E_r A_r} \tag{13}$$

$$\theta_r = \frac{M_r R_r^2}{E_r I_r} \tag{14}$$

The load deflection relations for the cylinder, per Cases 10 and 11 in Table XIII of R. J. Roark's Formulas for Stress and Strain, are

$$\delta_c = \frac{M_c}{2D\lambda^2} + \frac{V_c}{2D\lambda^3} \tag{15}$$

$$\theta_c = \frac{M_c}{D\lambda} + \frac{V_c}{2D\lambda^2} \tag{16}$$

where

$$\lambda = \left[\frac{3(1-\mu^2)}{R_c^2 t_c^2}\right]^{1/4}$$

$$D = \frac{\left[E_c t_c^3\right]}{12(1-\mu^2)}$$

Equations 8 - 16 may be expressed in matrix form as

$$[A]\{x\} = \{B\}.$$

where

$$
\begin{bmatrix}
-1 & 0 & 0 & \frac{R_r^2}{E_r A_r} & 0 & 0 & 0 & 0 & 0 \\
0 & -1 & \frac{R_r^2}{E_r I_r} & 0 & 0 & 0 & 0 & 0 & 0 \\
0 & 0 & 0 & 0 & -1 & 0 & \frac{1}{2D\lambda^2} & \frac{1}{2D\lambda^3} & 0 \\
0 & 0 & 0 & 0 & 0 & -1 & \frac{1}{D\lambda} & \frac{1}{2D\lambda^2} & 0 \\
0 & 1 & 0 & 0 & 0 & -1 & 0 & 0 & 0 \\
1 & \ell_r & 0 & 0 & 0 & 0 & 0 & 0 & 0 \\
0 & \ell_r + \ell_c & 0 & 0 & 1 & 0 & 0 & 0 & 0 \\
0 & 0 & 1 & 0 & 0 & 0 & 1 & -\ell_c & -\ell_r \\
0 & 0 & 0 & 1 & 0 & 0 & 0 & 1 & -1
\end{bmatrix}
\begin{Bmatrix} \delta_r \\ \theta_r \\ M_r \\ V_r \\ \delta_c \\ \theta_c \\ M_c \\ V_c \\ V_b \end{Bmatrix}
=
\begin{Bmatrix} 0 \\ 0 \\ 0 \\ 0 \\ 0 \\ \delta_\ell \\ \delta_\ell \\ 0 \\ 0 \end{Bmatrix}
$$

[A] {X} {B}

Solving for $\{X\}$ gives

$$\{X\} = [A]^{-1}\{B\}$$

The listing of the GE265 Time-Sharing Computer program developed to evaluate the vector $\{X\}$ is

```
HØLMAN      8:33    THURS. 06/06/74

5 DIM A(9,9),K(9,9),B(9,1),X(9,1)
10 PRINT "STRESS ANALYSIS ØF THE APT ØPEN PØRT LINER/FLANGE"
15 PRINT "FØR THE CØLD SØAK CØNDITIØN"
20 READ R1,E1,A1,I1,L1,R2,E2,T2,L2,TO
25 PRINT
30 PRINT "R1 ="R1,"E1 ="E1,"A1 ="A1,"I1 ="I1,"L1 ="L1
35 PRINT "R2 ="R2,"E2 ="E2,"T2 ="T2,"L2 ="L2,"TO ="TO
40 PRINT
45 D=E2*T2↑3/12/(1-.3↑2)
50 L=(3*(1-.3↑2)/R2↑2/T2↑2)↑(1/4)
55 MAT A=ZER(9,9)
60 MAT K=ZER(9,9)
65 MAT X=ZER(9,1)
70 MAT B=ZER(9,1)
75 A(1,1)=-1
80 A(1,4)=R1↑2/E1/A1
85 A(2,2)=-1
90 A(2,3)=R1↑2/E1/I1
95 A(3,5)=-1
100 A(3,7)=1/2/D/L↑2
105 A(3,8)=1/2/D/L↑3
110 A(4,6)=-1
115 A(4,7)=1/D/L
120 A(4,8)=1/2/D/L↑2
125 A(5,2)=1
130 A(5,6)=-1
135 A(6,1)=1
140 A(6,2)=L1
145 A(7,2)=L1+L2
150 A(7,5)=1
155 A(8,3)=1
160 A(8,7)=1
165 A(8,8)=-L2
170 A(8,9)=-L1
175 A(9,4)=1
180 A(9,8)=1
185 A(9,9)=-1
190 B(6,1)=TO
195 B(7,1)=TO
```

```
200 MAT K=INV(A)
205 MAT X=K*B
210 PRINT "FLANGE:","T1 ="X(1,1),"R1 ="X(2,1),"M1 ="X(3,1),"V1 ="X(4,1)
215 PRINT "LINER:","T2 ="X(5,1),"R2 ="X(6,1),"M2 ="X(7,1),"V2 ="X(8,1)
220 PRINT "BOLT SHEAR:","VO ="X(9,1)
225 DATA 12.2,1E7,3.1118,13.1518,1.64,11.25,1E7,.125,4.9,1
230 END
```

The flange section properties are

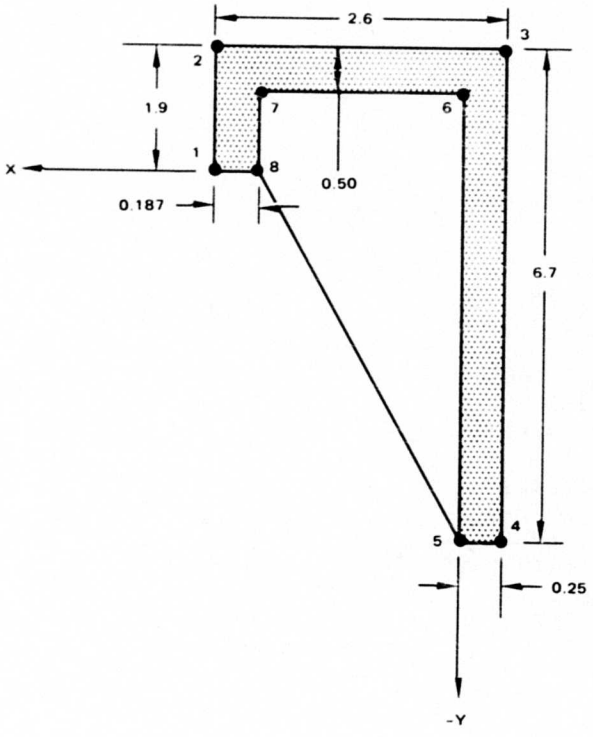

CRSEC* 13:02 TUES. 06/04/74

CRØSS-SECTIØNAL PRØPERTIES PRØGRAM

SECTIØN 1

VERTEX	ENVELØPE X CØØRD	Y CØØRD.
1	2.35	0
2	2.35	1.9
3	-.25	1.9
4	-.25	-4.8
5	0	1.4
6	0	1.4
7	2.163	0
8	2.163	

AREA= 3.1118
IX[CG] = 13.1518
IY[CG] = 2.53397
IXY[CG] = 3.16884
PHI= -15.4163
IMAX[CG] = 14.0256
IMIN[CG] = 1.66016
RHØ[MAX]= 2.12303
RHØ[MIN] = .730413
X-BAR= .566232
Y-BAR= -9.85732E-02
IXX= 13.182
IYY= 3.53167

Subbing values

$R_b = 14.188$ in.

$R_s = 27.80$ in.

$E_s = 2.5 \times 10^6$ psi

$t_s = 0.400$ in.

$\phi_s = 180 - \arcsin \frac{R_b}{R_s} = 149.3^\circ$

$$R_r = 12.2 \text{ in.}$$

$$E_r = 10^7 \text{ psi}$$

$$A_r = 3.1118 \text{ in.}$$

$$I_r = 13.1518 \text{ in.}^4$$

$$\ell_r = 1.64 \text{ in.}$$

$$R_c = 11.25 \text{ in.}$$

$$E_c = 10^7 \text{ psi}$$

$$t_c = 0.125 \text{ in.}$$

$$\ell_c = 4.9 \text{ in.}$$

$$\delta_\ell = 1$$

gives for the gimbal shell

$$k = \left[3(1 - 0.3^2)\,\frac{27.8^2}{0.4^2}\right]^{1/4} = 10.716$$

$$k_s = \frac{27.8}{2.5 \times 10^7 \times 0.4} \sin 149.3^\circ (2 \times 10.716 \sin 149.3^\circ - 0.3 \cos 149.3^\circ)$$

$$= 1.58849 \times 10^{-5} \text{ psi}$$

and for the liner gives

HOLMAN 8:36 THURS. 06/06/74

STRESS ANALYSIS ØF THE APT ØPEN PØRT LINER/FLANGE
FØR THE CØLD SØAK CØNDITIØN

R1 = 12.2	E1 = 10000000		A1 = 3.1118	I1 = 13.1518
L1 = 1.64				
R2 = 11.25	E2 = 10000000		T2 = .125	L2= 4.9
TO = 1				
FLANGE:	T1 = .647963	R1 = .214656	M1 = 189675	V1 = 135470.
LINER:	T2 =-.403853	R2 = .214656	M2 = 2529.7	V2 =-4581.95
BØLT SHEAR:	V0 = 130888.			

$$k_\ell = \frac{1}{VO} = \frac{1}{130888} = 7.64013 \times 10^{-6} \text{ psi}$$

The shear V_b then becomes

$$V_b = \frac{0.0249 - 0.01053}{7.64013 \times 10^{-6} + 1.26174 \times 10^{-5}} = 611 \text{ lb/in.}$$

The shell loads at $\phi = \phi_s$, per Table 2.33-2 of E. H. Baker's Shell Analysis Manual (NASA CR-912) are

$$Q_\phi(\phi_s) = V_b \left\{ -\sqrt{2} \sin \phi_s \, e^{-k(\phi_s - \phi)} \cos\left[k(\phi_s - \phi) + \frac{\pi}{4}\right] \right\}_{\phi = \phi_s}$$

$$= -V_b \sin \phi_s = -312 \text{ lb/in.}$$

$$N_\phi(\phi_s) = -\phi(\phi) \cot\phi \Big|_{\phi = \phi_s}$$

$$= V_b \sin \phi_s \cot \phi_s = -525 \text{ lb/in.}$$

$$N_\theta(\phi_s) = 2V_b k \sin\phi_s \, e^{-k(\phi_s-\phi)} \cos k(\phi_s - \phi)\Big|_{\phi=\phi_s}$$

$$= 2V_b k \sin\phi_s = 6679 \text{ lb/in.}$$

$$M_\phi(\phi_s) = V_b \frac{R_s}{k} \sin\phi_s \, e^{-k(\phi_s-\phi)} \sin k(\phi_s - \phi)\Big|_{\phi=\phi_s}$$

$$= 0$$

$$M_\theta(\phi_s) = \left\{ -\frac{V_b R_s}{k^2\sqrt{2}} \sin\phi_s \cot\phi \, e^{-k(\phi_s-\phi)} \sin\left[k(\phi_s - \phi) + \frac{\pi}{4}\right] + \mu M_\phi \right\}\Big|_{\phi=\phi_s}$$

$$= -\frac{V_b R_s}{2k^2} \sin\phi_s \cot\phi_s = 63.6 \text{ in-lb/in.}$$

The corresponding stresses become

$$\sigma_\phi = \frac{N_\phi}{t_s} + \frac{6M_\phi}{t_s^2} = \frac{525}{0.4} = 1310 \text{ psi}$$

$$\sigma_\phi = \frac{N_\theta}{t_s} + \frac{6M_\theta}{t_s^2} = \frac{6679}{0.4} + \frac{6 \times 63.6}{0.4^2} = 19080 \text{ psi}$$

$$\tau_\phi = \frac{Q_\phi}{t} = \frac{312}{0.4} = 780 \text{ psi}$$

The equivalent uniaxial stress for this combined stress condition per the von Mises Criterion is

$$\sigma^* = \sqrt{\frac{(\sigma_1 - \sigma_2)^2 + (\sigma_1 - \sigma_3)^2 + (\sigma_2 - \sigma_3)^2}{2}} = 20160 \text{ psi}$$

where

$$\tau = \sqrt{\frac{\sigma_\phi^2}{4} + \tau_\phi^2} = 1019 \text{ psi}$$

$$\sigma_1 = \frac{\sigma_\phi}{2} + \tau = 1674 \text{ psi}$$

$$\sigma_2 = \frac{\sigma_\phi}{2} - \tau = -364 \text{ psi}$$

$$\sigma_3 = \sigma_\rho = 19080$$

The minimum margin of safety for the glass epoxy gimbal shell, per HP16-107, Grade B, using MIL-C-9084, Type VIII, glass cloth, is

$$MS = \frac{F_{tu}}{1.5\sigma^*} - 1 = \frac{0.67 \times 48000}{1.5 \times 20160} - 1 = \underline{+0.6 > 0}$$

The shear load on each of the 24 attach volts on the 28.375 inch B.C. is

$$V_b^* = \frac{\pi}{24} \times 28.375 V_b = 3.71441 \times 611 = 2268 \text{ lbs.}$$

The margin of safety in these 10-32 180 ksi UTS attach bolts, per MIL-HDBK-5B, is

$$MS = \frac{V_{ult}}{1.5V_b^*} (10\text{-}32 \text{ @ } 180 \text{ ksi}) - 1 = \frac{3544}{1.5 \times 2268} - 1 = \underline{+0.04 > 0}$$

The shear-out stress in the 0.200 in. thick liner flange is

$$\tau = \frac{V_b}{(2e - d)t_s} = \frac{2268}{(2 \times 0.412 - 0.19) \times 200} = 17860 \text{ psi}$$

The margin of safety in the 6061-T6 aluminum flange, per MIL-HDBK-5B, is

$$MS = \frac{F_{su}(6061\text{-}T6)}{1.5\tau} = \frac{27000}{1.5 \times 17860} - 1 = \frac{+\ 0.01\quad 0}{}$$

The combined axial stress in the liner flange due to the hoop tension force $P_z = V_r R_r$ and flange rolling moment $M_x = M_r R_r$:

$$P_z = V_b\left(\frac{V_1}{VO}\right) R_r = 611\left(\frac{135470}{130888}\right) \times 12.2 = 7710 \text{ lbs}$$

$$M_z = V_b\left(\frac{M_1}{VO}\right) R_r = 611\left(\frac{189675}{130888}\right) \times 12.2 = 10795 \text{ in-lbs}$$

is

CRSEC* 8:40 THURS. 06/06/74

CRØSS-SECTIØNAL PRØPERTIES PRØGRAM

SECTION 1

VERTEX	ENVELOPE X COORD.	Y COORD.
1	2.35	0
2	2.35	1.9
3	-.25	1.9
4	-.25	-4.8
5	0	-4.8
6	0	1.4
7	2.163	1.4
8	2.163	0

AREA= 3.1118
IX[CG] = 13.1518
IY[CG] = 2.53397
IXY[CG] = 3.16884
PHI= -15.4163
IMAX[CG] = 14.0256
IMIN[CG] = 1.66016
RHØ[MAX]= 2.12303
RHØ[MIN] = .730413
X-BAR= .566232
Y-BAR= -9.85732E-02
IXX= 13.182
IYY= 3.53167

LØAD CASE 1 MX= 10795 MY= Ø FZ= 7710

CØMPØNENT	NØDE	X CØØRD.	Y CØØRD.	CØMBINED STE
1	1	-.25	1.9	-1069.33
1	2	2.35	1.9	2750.34
1	3	2.35	0	4982.4
1	4	2.163	0	4707.68
1	5	2.163	1.4	3063.
1	6	0	1.4	-114.665
1	7	0	-4.8	7168.91
1	8	-.25	-4.8	6801.63

The margin of safety in the 6061-T6 aluminum flange, per MIL-HDBK-5B, is

$$M = \frac{F_{tu}(6061\text{-}T6)}{1.5\sigma_7} - 1 = \frac{42000}{1.5 \times 7169} - 1 = \underline{\text{HI}}$$

The liner cylinder loads M_c and V_c are

$$M_c = V_b \left(\frac{M2}{VO}\right) = 611 \times \left(\frac{2530}{130888}\right) = 11.80 \text{ in-lb/in.}$$

$$V_c = V_b \left(\frac{V2}{VO}\right) = 611 \times \left(\frac{-4582}{130888}\right) = -21.38 \text{ lb/in.}$$

The liner cylinder stresses at x = 0, per Cases 10 and 11 in Table XIII of R. J. Roark's Formulas for Stress and Strain, are

$$\lambda = \left[\frac{3(1-\mu^2)}{R_c^2 t_c^2}\right]^{1/4} = \left[\frac{3(1-0.3^2)}{11.25^2 \times 0.125^2}\right]^{1/4} = 1.08395$$

$$\sigma_x = \frac{6M_c}{t_c^2} = \frac{6 \times 11.80}{0.125^2} = 4531 \text{ psi}$$

$$\sigma_\theta = \frac{2R_c\lambda}{t_c}(V_c + \lambda M_c) + \mu\sigma_x$$

$$= \frac{2 \times 11.25 \times 1.08395}{0.125}(-21.38 + 1.08395 \times 11.80) + 0.3 \times 4531$$

$$= -317 \text{ psi}$$

$$\tau_x = \frac{V_c}{t_c} = \frac{-21.38}{0.125} = 171 \text{ psi}$$

The equivalent uniaxial stress for this combined stress condition per the Von Mises Criterion is

$$\sigma^* = \sqrt{\frac{(\sigma_1 - \sigma_2)^2 + (\sigma_1 - \sigma_3)^2 + (\sigma_2 - \sigma_3)^2}{2}} = 4707 \text{ psi}$$

where

$$\tau = \sqrt{\frac{\sigma_x^2}{4} + \tau_x^2} = 2272 \text{ psi}$$

$$\sigma_1 = \frac{\sigma_x}{2} + \tau = 4537 \text{ psi}$$

$$\sigma_2 = \frac{\sigma_x}{2} - \tau = -6 \text{ psi}$$

$$\sigma_3 = \sigma_\theta = -317 \text{ psi}$$

The minimum margin of safety in the 2024-T4 aluminum liner cylinder, per MIL-HDBK-5B, is

$$MS = \frac{F_{ty}}{1.5\sigma*} (2024\text{-}T4) - 1 = \frac{42000}{1.5 \times 4707} - 1 = \underline{HI}$$

APPENDIX 2

APT OPEN PORT LINER – STATIC AND DYNAMIC STARDYNE STRUCTURAL ANALYSIS

This section is a condensed version of:

IDC 271222/563, dated 5 April 1974
IDC 271222/577, dated 1 May 1974

A2.1 INTRODUCTION

This report documents the static and dynamic STARDYNE structural analyses performed to demonstrate structural adequacy of the following components of the APT Open Port Modification: the aerodynamic fence, the primary mirror cover and its support straps, the secondary mirror cover and its support struts, and the liner shell and its mounting flange.

A2.2 ENVIRONMENTAL DESIGN CRITERIA

All components of the APT Open Port Modification have been designed to satisfactorily withstand the static loading conditions presented in Table A2.2.1 and the unsteady pressure power spectral density plot shown in Figure A2.2.4.

The three 8g acceleration load cases are those for the crash landing condition in each of three mutually perpendicular directions.

The four pressure load cases represent hypothetical worst case pressure distributions. The magnitude of the peak pressure, 5 psi, is two times the stagnation pressure differential existing on the nose of an object in a Mach 0.50 sea level air stream. This stagnation pressure is consistent with the steady pressures measured in 0.3-scale Open Port ALL Turret Wind Tunnel test results for a forward looking port. (HAC IDC 271222/527, dated 6 February 1974).

The -65°F cold soak case represents the worst case temperature differential condition, relative to a +70°F installation temperature, that can be approached by the liner in flight. This is substantiated by Figures A2.2.2 and A2.2.3 taken from the APT Open Port thermal analysis (HAC IDC

277740.1/292, dated 27 March 1974), which show that the liner cylinder and the secondary mirror cover cool uniformly and rapidly reach their steady state values for the Open Port Condition.

The unsteady pressure data is presented in Figure A2.2.4 as a power spectral density versus frequency plot for the maximum rms pressure condition found in the 0.3-scale Open Port ALL Turret Wind Tunnel test results for Open Port Configuration 11 at sea level at Mach 0.75 (HAC IDC 271222/527, dated 6 February 1974). This worst case condition envelopes all test data. It occurs on the primary mirror when the APT orientation is at 0° elevation and 45° azimuth. This data can be scaled to sea level operation at Mach 0.50 using the following conversions:

$$PSD_2 = \left(\frac{L_2}{L_1}\right)\left(\frac{V_1}{V_2}\right)\left(\frac{q_2}{q_1}\right)^2 PSD_1$$

$$= \left(\frac{L_2}{L_1}\right)\left(\frac{V_2}{V_1}\right)^3 PSD_1$$

$$= 1.0 \times \left(\frac{0.5}{0.75}\right)^3 PSD_1 = 0.29630\ PSD_1$$

$$f_2 = \left(\frac{L_1}{L_2}\right)\left(\frac{V_2}{V_1}\right) f_1$$

$$= 1.0 \times \left(\frac{0.75}{0.5}\right) f_1 = 1.5 f_1$$

All loading conditions are considered to be limit loading conditions. Maximum working stresses and loads must not, therefore, exceed 2/3 (1/1.15) of their minimum guaranteed ultimate (yield) values as published in MIL-HDBK-5B.

TABLE A2.2.1. ENVIRONMENTAL DESIGN CRITERIA

Load Condition	Load Condition Description
A1 - A3	8G crash landing load in any direction
P1	5 psi proof pressure
P2	$P_r(\theta)$ = 5 psi uniform radial pressure acting on the linear shell combined with a P_z = 5 psi normal pressure on the primary mirror cover and a P_s = 5 psi normal pressure acting on one side of each of the secondary mirror support struts. See Figure A2.2.1.
P3	Same as load condition P2 except $P_r(\theta) = 5 \cos \theta$ psi
P4	Same as load condition P2 except $P_r(\theta) = 5\lvert\cos\theta\rvert$ psi
T1	Cold soak at -65°F

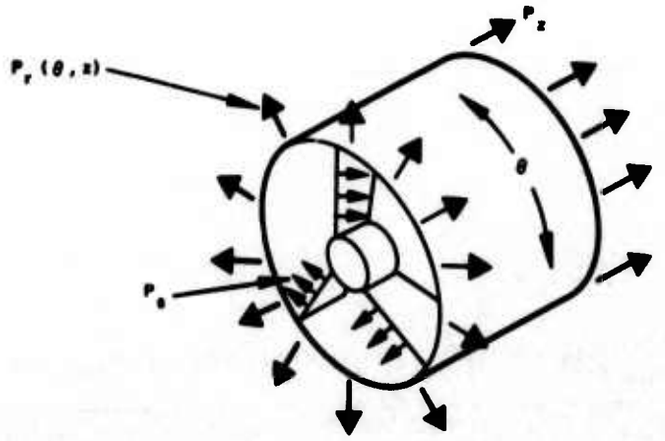

Figure A2.2.1. Definition of pressure distributions.

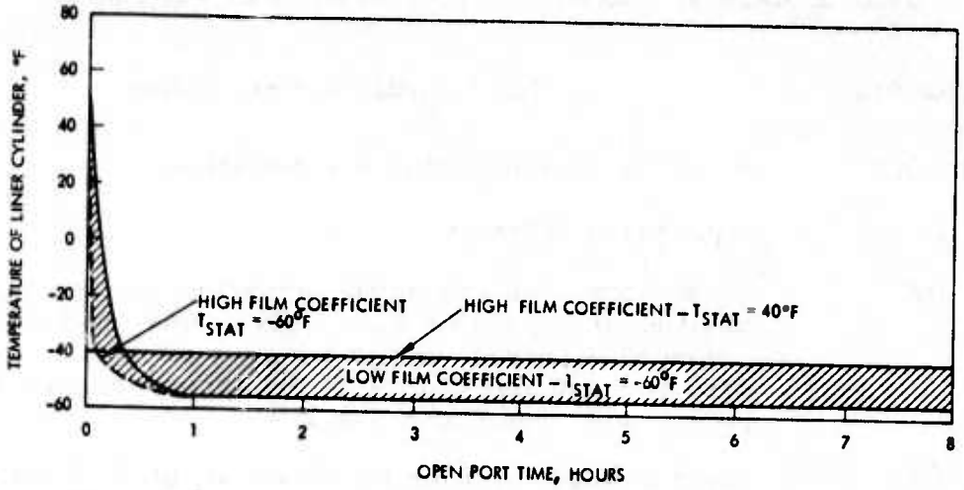

Figure A2.2.2. Temperature of cylindrical liner.

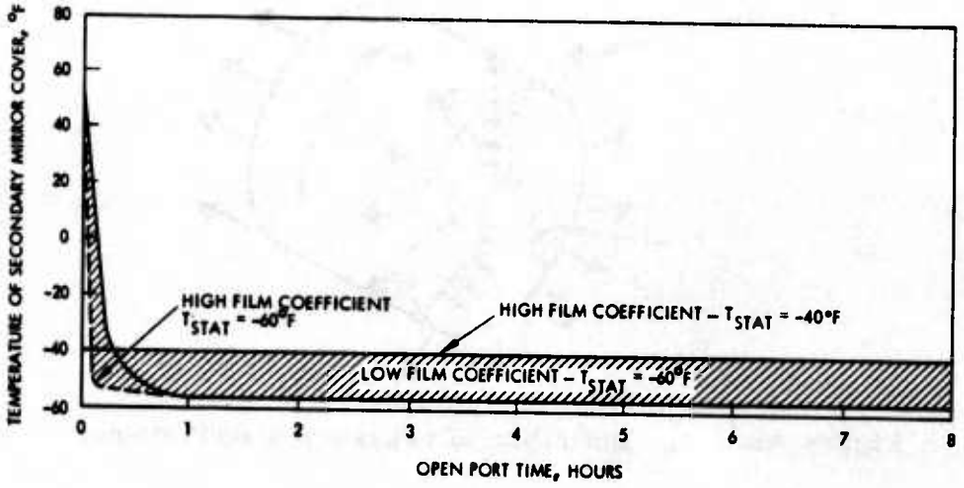

Figure A2.2.3. Temperature of secondary mirror cover.

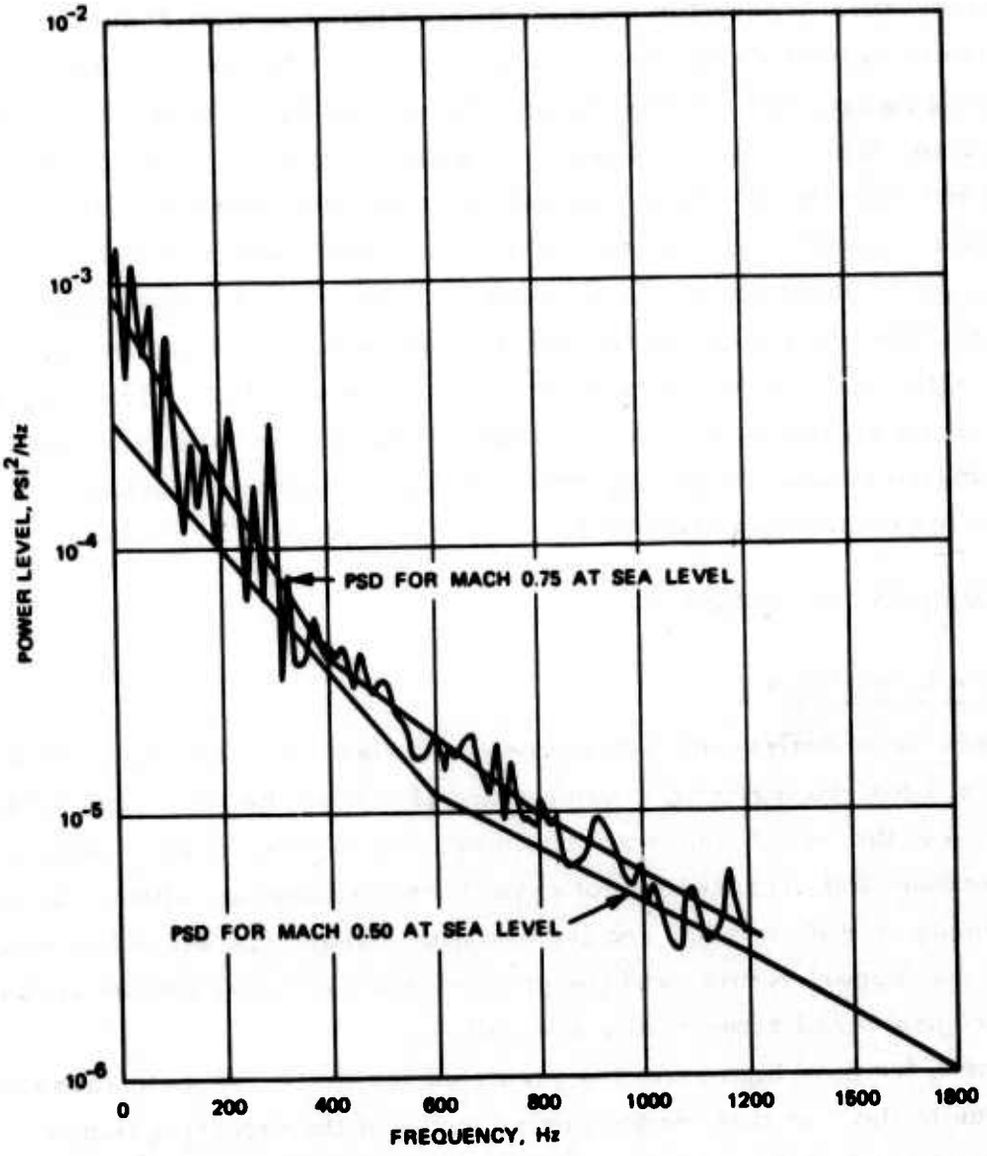

Figure A2.2.4. Full scale APT primary mirror unsteady pressure power spectral density for sea-level flight at Mach 0.75.

A2.3 METHOD OF ANALYSIS

MRI's STARDYNE Structural Analysis System, available on CDC's 6600 CYBERNET System, was used to analyze a combined model consisting of the aerodynamic fence, the primary mirror cover and its support straps, the secondary mirror cover and its support struts, and the liner shell and its mounting flange, for the loading conditions cited in Section A2.2. STARDYNE is a batch processing computer program that employs the finite element method wherein the three-dimensional continuous structure is represented mathematically by a system of finite elements interconnected at a finite number of nodal points where loads are applied and displacements are calculated. The finite element library includes beams, plates, cubes, tetrahedrons, rigid links, springs, and direct stiffness additions. The program uses the direct stiffness method to synthesize the elemental and system stiffness matrices and the normal mode method to determine dynamic responses for transient, sinusoidal, random, and acoustic excitation.

A2.4 SUMMARY OF RESULTS

A2.4.1 Static Analysis

Peak nodal deflections and elemental stresses are summarized in Table A2.4.1 for the three 8g acceleration (A1 - A3), the four 5 psi pressure (P1 - P4), and the -65°F cold soak temperature (T1) load cases. Since these peak deflections and stresses do not exceed their allowable values, the aerodynamic fence, the liner shell and its mounting flange, the secondary mirror cover and its support struts, and the primary mirror cover and its support straps are considered structurally adequate.

The extremely high stresses predicted for the -65°F cold soak condition are due to the fact that the perimeter nodes of the mounting flange, nodes N136 through N147, were restrained against translation along the three global axes to conservatively simulate the flexibility of the liner to outer elevation gimbal interface. This is equivalent to applying radial forces

to nodes N136 - N147 of sufficient magnitude to move these nodes outward radially a distance δ_b:

$$\delta_b = \alpha_{AL} R_b \Delta T = 13 \times 10^{-6} \times 14.188 \times 135 = 0.0249 \text{ in.}$$

where α_{AL} is the coefficient of thermal expansion for the aluminum liner, R_b is the flange bolt circle radius, and ΔT is the temperature differential. In reality, the distance δ_b will be less than:

$$\delta_b = (\alpha_{AL} - \alpha_{FE}) R_b \Delta T = (13 - 5.5) \times 10^{-6} \times 14.88 \times 135 = 0.0144 \text{ in.}$$

where α_{FE} is the coefficient of thermal expansion for the glass epoxy shell of the outer elevation gimbal. The actual stress levels will therefore be less than 58 percent of the predicted stress levels cited in Table A2.4.1.

A2.4.2 Dynamic Analysis

The results of the Householder - QR eigenvalue extraction are presented in Table A2.4.2. Computer plots of the three orthogonal projections of the mode shapes described in this table are given in Figures A2.4.1 through A2.4.30. These results indicate that the in-plane rotation and translation modes of the primary mirror occur at 82 Hz and 95 Hz, respectively, while its out-of-plane translation mode occurs at 224 Hz. The results also indicate that the first four symmetric breathing modes of the liner cylinder occur at 291 Hz, 317 Hz, 365 Hz, and 455 Hz, respectively, while its first two asymmetric breathing modes occur at 318 Hz and 365 Hz.

The results of the random response analysis, also summarized in Table A2.4.1, indicate the three-sigma responses and stresses are small compared to those for the static loading conditions. These results were obtained using the 10 modes described above, assuming 5 percent viscous modal damping, suppressing response cross-covariances, and assuming that the random pressure power spectral density used in this analysis (the PSD shown in Figure A2.2.4 for Mach 0.5 flight at sea-level) is spatially correlated.

TABLE A2.4.1. SUMMARY OF RESULTS OF THE STARDYNE STATIC AND DYNAMIC ANALYSIS OF THE APT OPEN PORT LINER

Component	Material	Allowable Stress	Allowable Deflection	Peak Stresses and Deflections								
				8G Acceleration			5 PSI Steady Pressure				-65°F Temp	Unsteady Pressure
				A1	A2	A3	P1	P2	P3	P4	T1	
Aerofence	0.063 inches thick 6061-T6 A1	28 ksi	-	0.20 ksi	0.17 ksi	0.21 ksi	-	8.8 ksi	8.8 ksi	8.8 ksi	26.3 ksi	0.24 ksi
Liner Cylinder	0.125 inches thick 2024-T4 A1	36.5 ksi	- 0.0625 in.	0.20 ksi 0.00032 in.	0.17 ksi 0.00056 in.	0.21 ksi 0.00056 in.	- -	11.2 ksi 0.00296 in.	10.5 ksi 0.220 in.	9.2 ksi 0.0130 in.	26.3 ksi 0.0596 in.	0.24 ksi 0.0027 in.
Liner Flange	0.500 inches thick 6061-T6 A1	28 ksi	-	0.01 ksi	0.02 ksi	0.02 ksi	-	0.22 ksi	0.37 ksi	0.35 ksi	22.9 ksi	0.02 ksi
Liner Flange Gussets	0.125 inches thick 6061-T6 A1	28 ksi	-	0.13 ksi	0.15 ksi	0.14 ksi	-	2.8 ksi	5.3 ksi	4.0 ksi	6.4 ksi	0.29 ksi
Secondary Mirror Cover	0.125 inches thick 6061-T6 A1	28 ksi	-	0.21 ksi	0.16 ksi	0.14 ksi	-	9.2 ksi	11.3 ksi	9.8 ksi	26.0 ksi	0.30 ksi
Secondary Mirror Cover Support Struts	0.063 inches thick 2024-T4 A1	36.5 ksi	-	0.04 ksi	0.09 ksi	0.09 ksi	-	1.9 ksi	2.9 ksi	2.1 ksi	27.4 ksi	0.16 ksi
Primary Mirror	0.312 inches thick 6061-T6 A1	28 ksi	-	0.60 ksi	1.2 ksi	1.2 ksi	-	11.9 ksi	11.9 ksi	11.9 ksi	4.2 ksi	0.26 ksi
Primary Mirror Support Straps	0.125 inches thick 2024-T4 A1	36.5 ksi	-	0.95 ksi	1.8 ksi	1.8 ksi	-	18.9 ksi	18.9 ksi	18.9 ksi	6.3 ksi	0.56 ksi

*The allowable strength is the leaser of the minimum guaranteed ultimate strengths ÷ 1.5 or yield strength ÷ 1.15.

TABLE A2.4.2. APT OPEN PORT LINER MODES AND FREQUENCIES

Mode Number	Frequency Hz	Mode Shape Description
1	82	In-plane (X4) rotation of primary mirror cover
2	95	In-plane vertical (X3) translation of primary mirror cover
3	95	In-plane horizontal (X2) translation of primary mirror cover
4	224	Out-of-plane (X1) translation of primary mirror cover
5	291	First liner cylinder symmetric breathing mode
6	317	Second liner cylinder symmetric breathing mode
7	318	First liner cylinder asymmetric breathing mode
8	365	Second liner cylinder asymmetric breathing mode
9	365	Third liner cylinder symmetric breathing mode
10	455	Fourth liner cylinder symmetric breathing mode

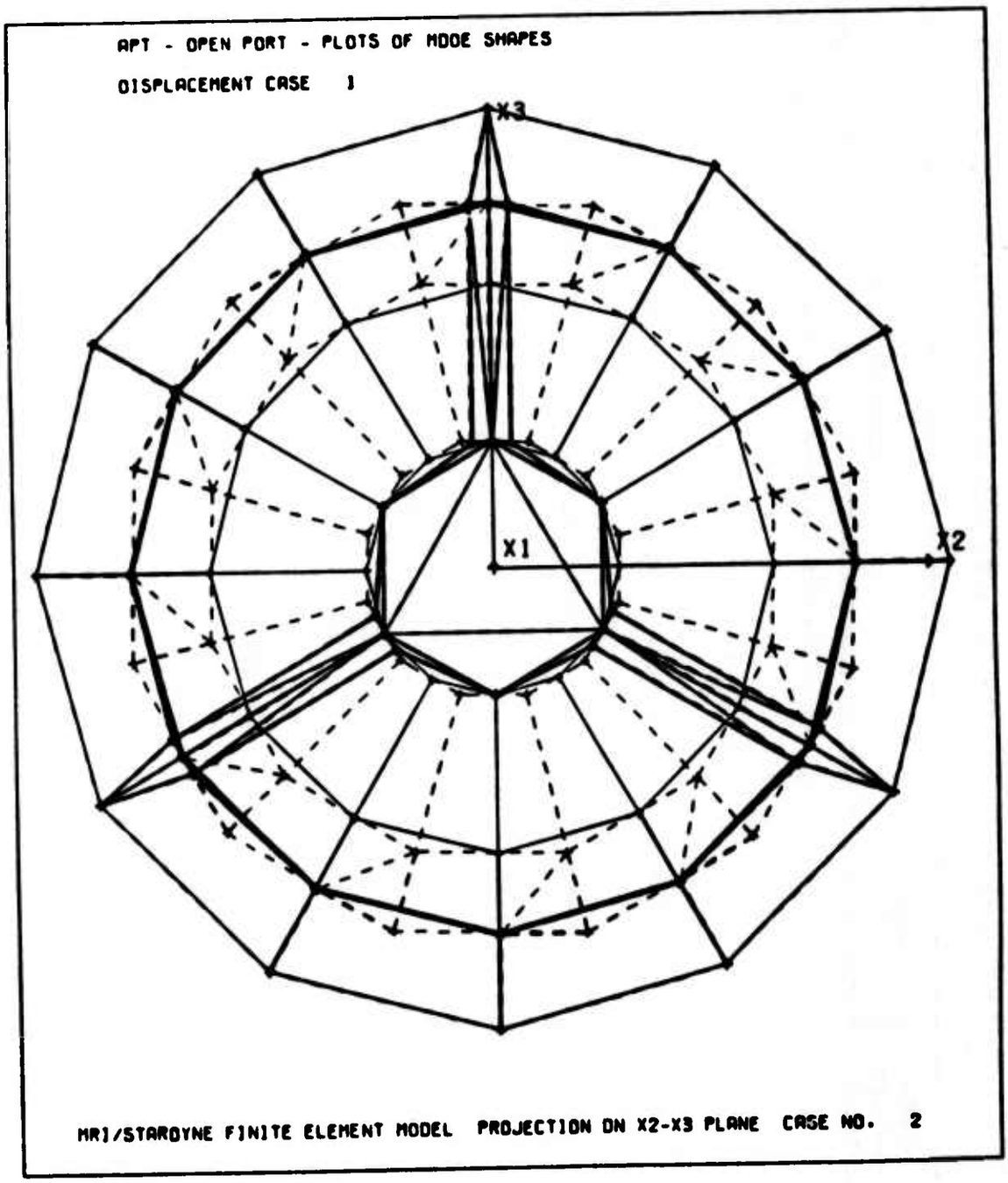

Figure A2.4.1. Computer plot of mode shape number 1 for STARDYNE analysis of APT open port liner.

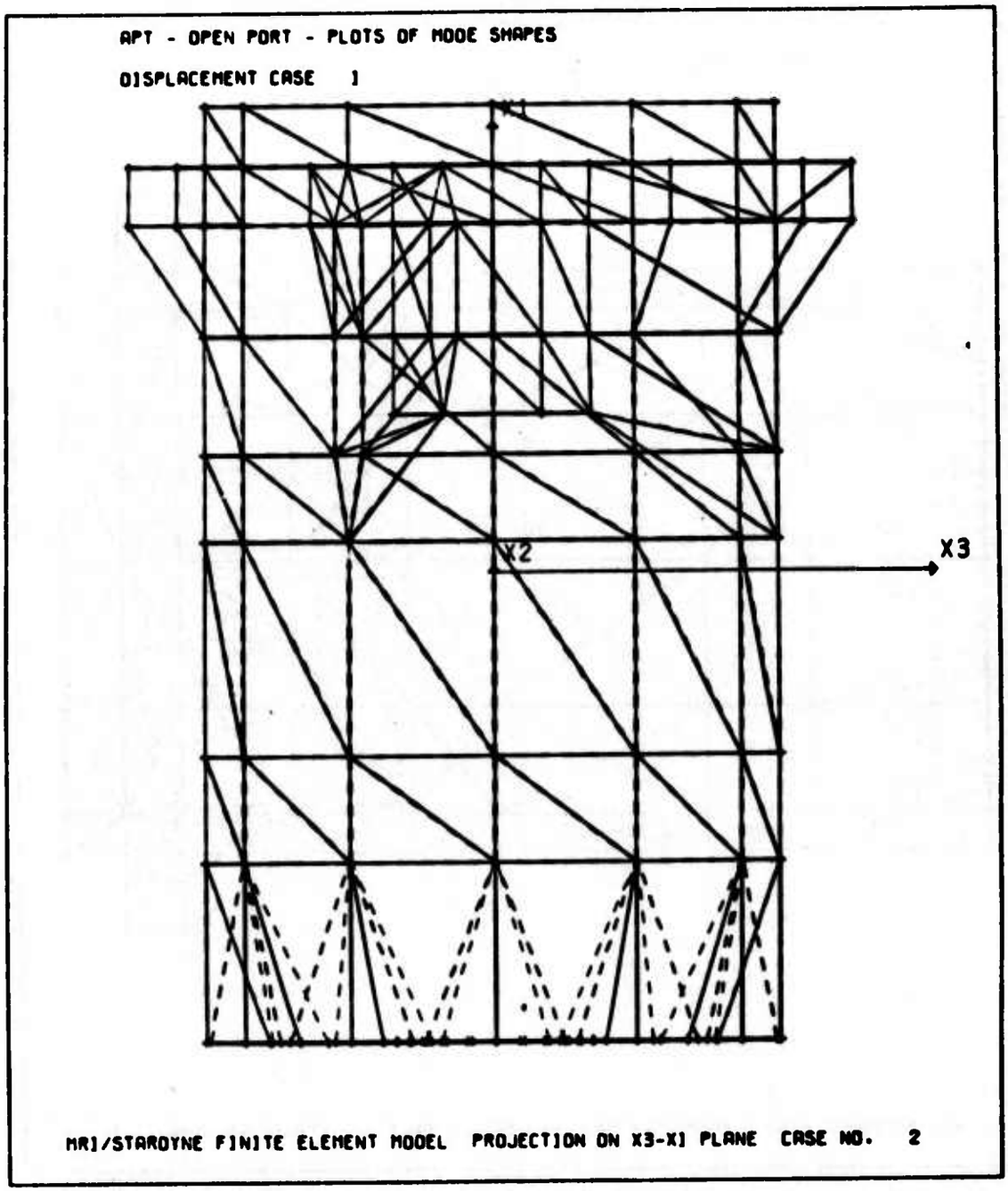

Figure A2.4.2. Computer plot of mode shape number 1 for STARDYNE analysis of APT open port liner.

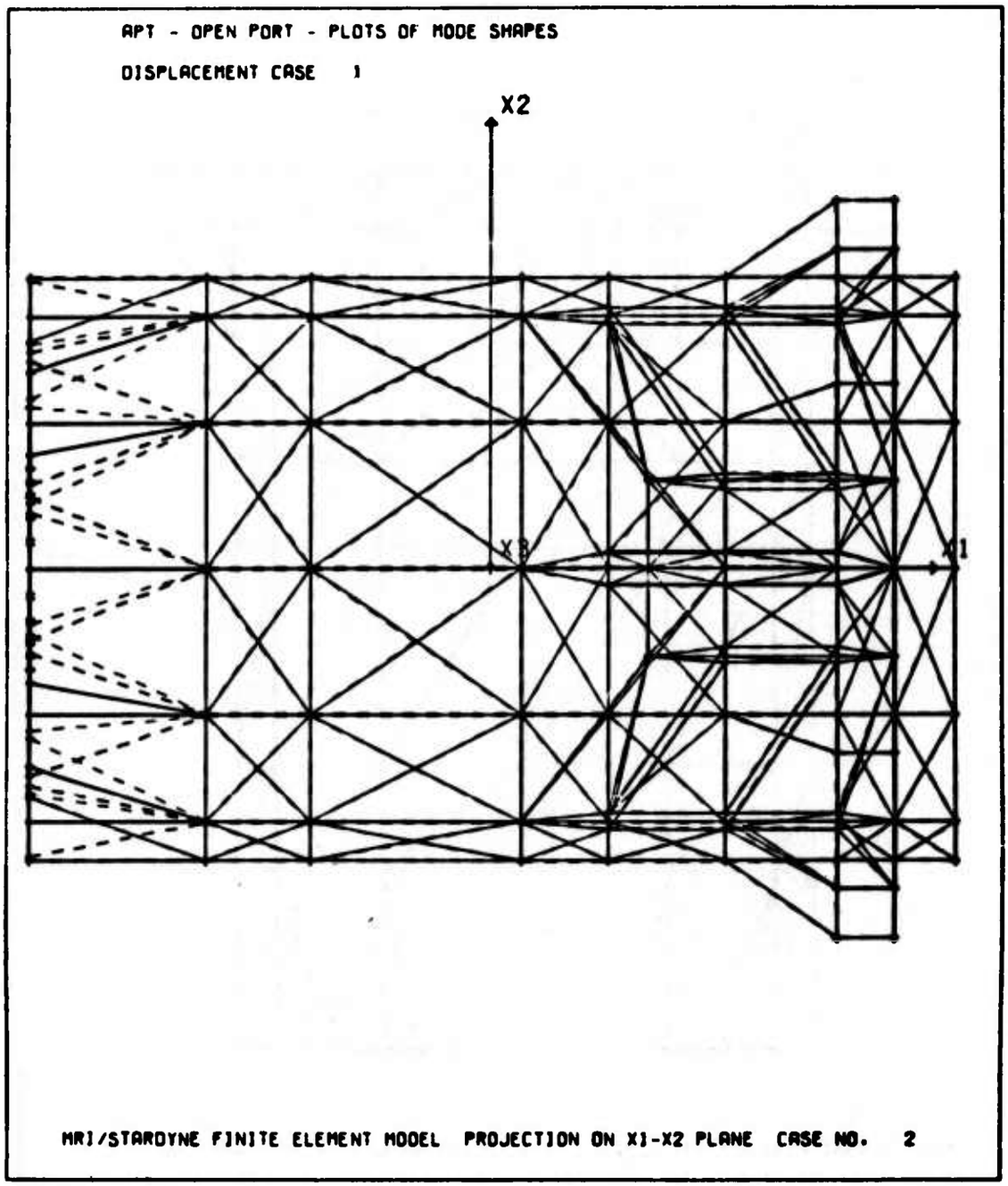

Figure A2.4.3. Computer plot of mode shape number 1 for STARDYNE analysis of APT open port liner.

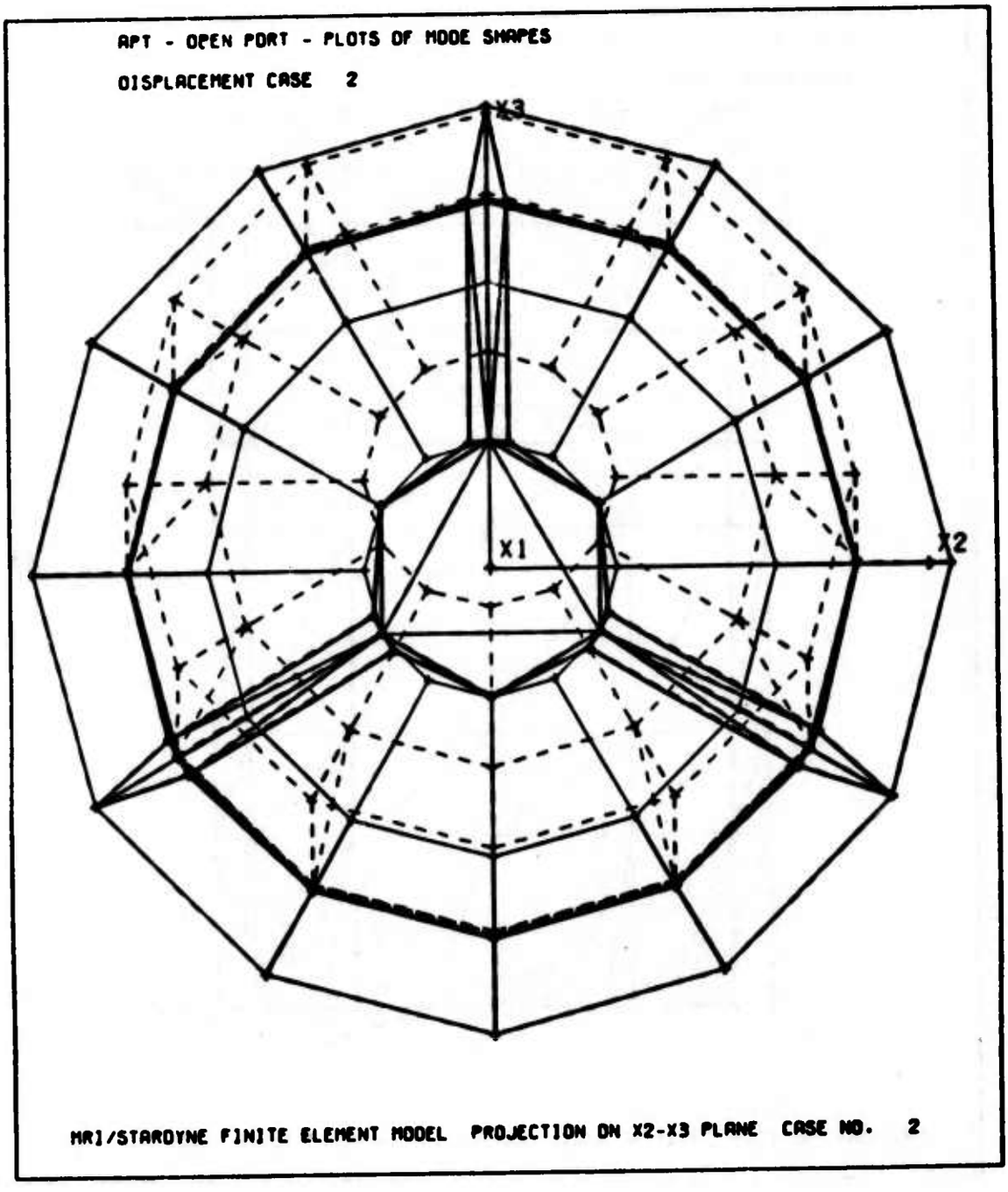

Figure A2.4.4. Computer plot of mode shape number 2 for STARDYNE analysis of APT open port liner.

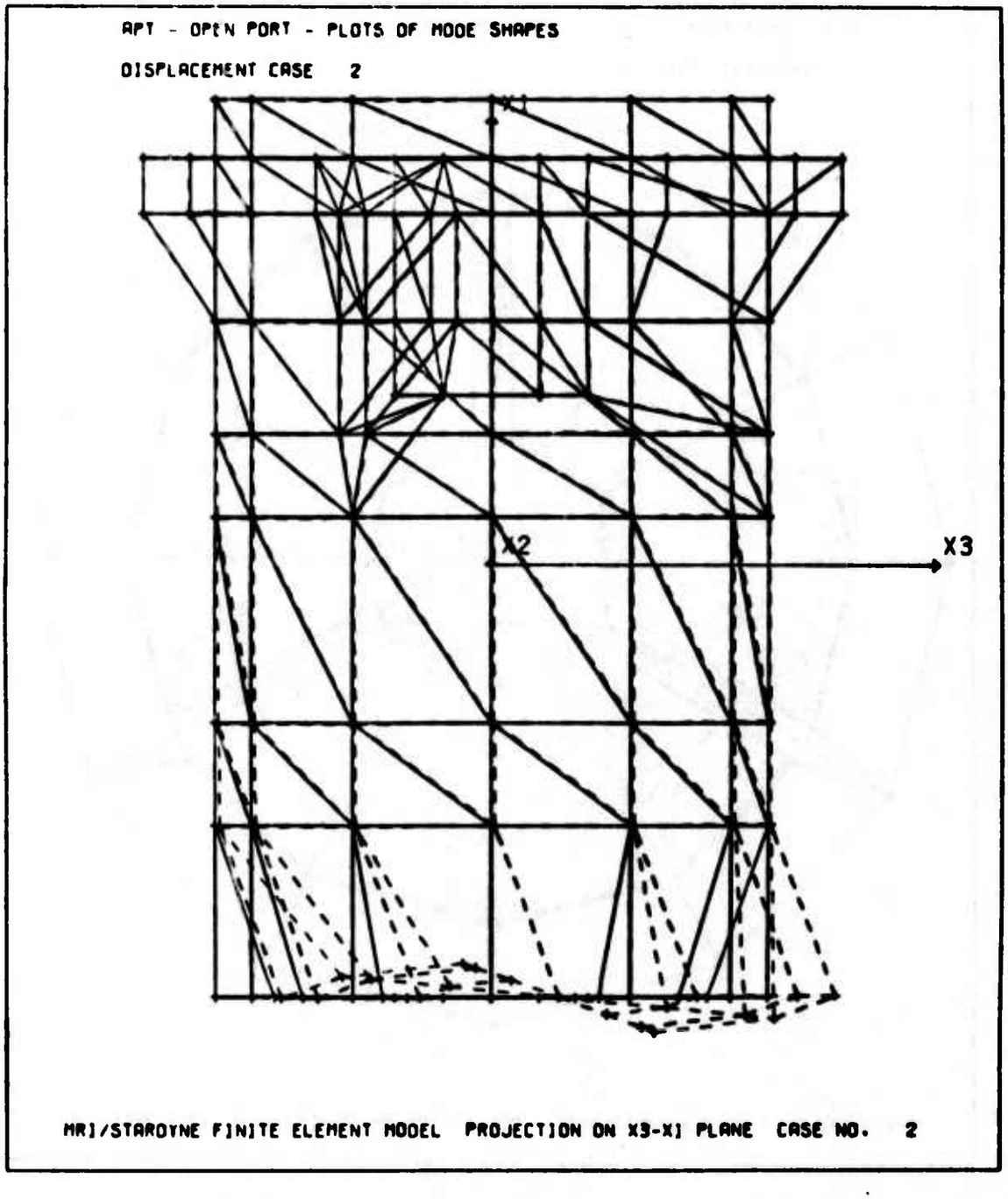

Figure A2.4.5. Computer plot of mode shape number 2 for STARDYNE analysis of APT open port liner.

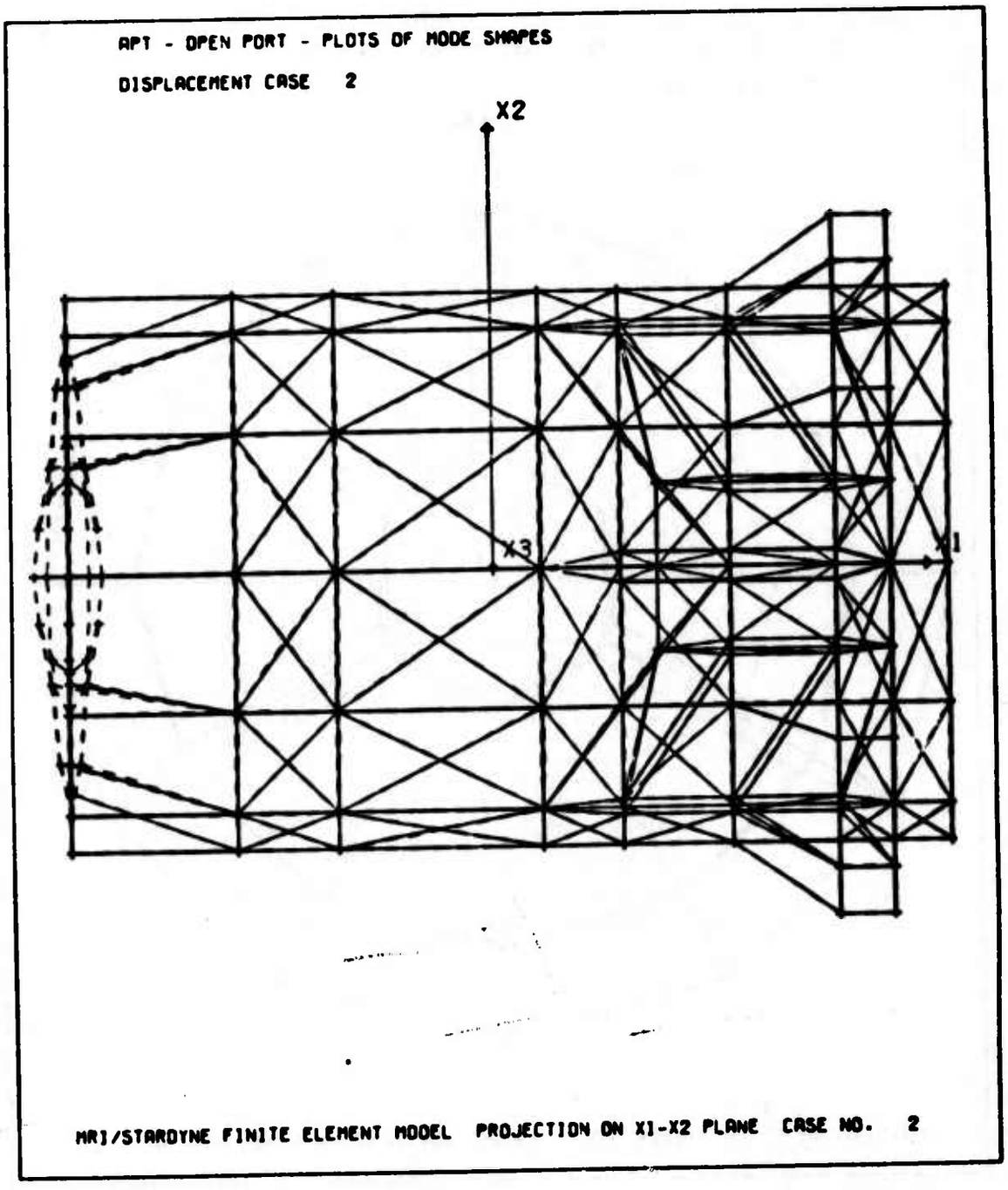

Figure A2.4.6. Computer plot of mode shape number 2 for STARDYNE analysis of APT open port liner.

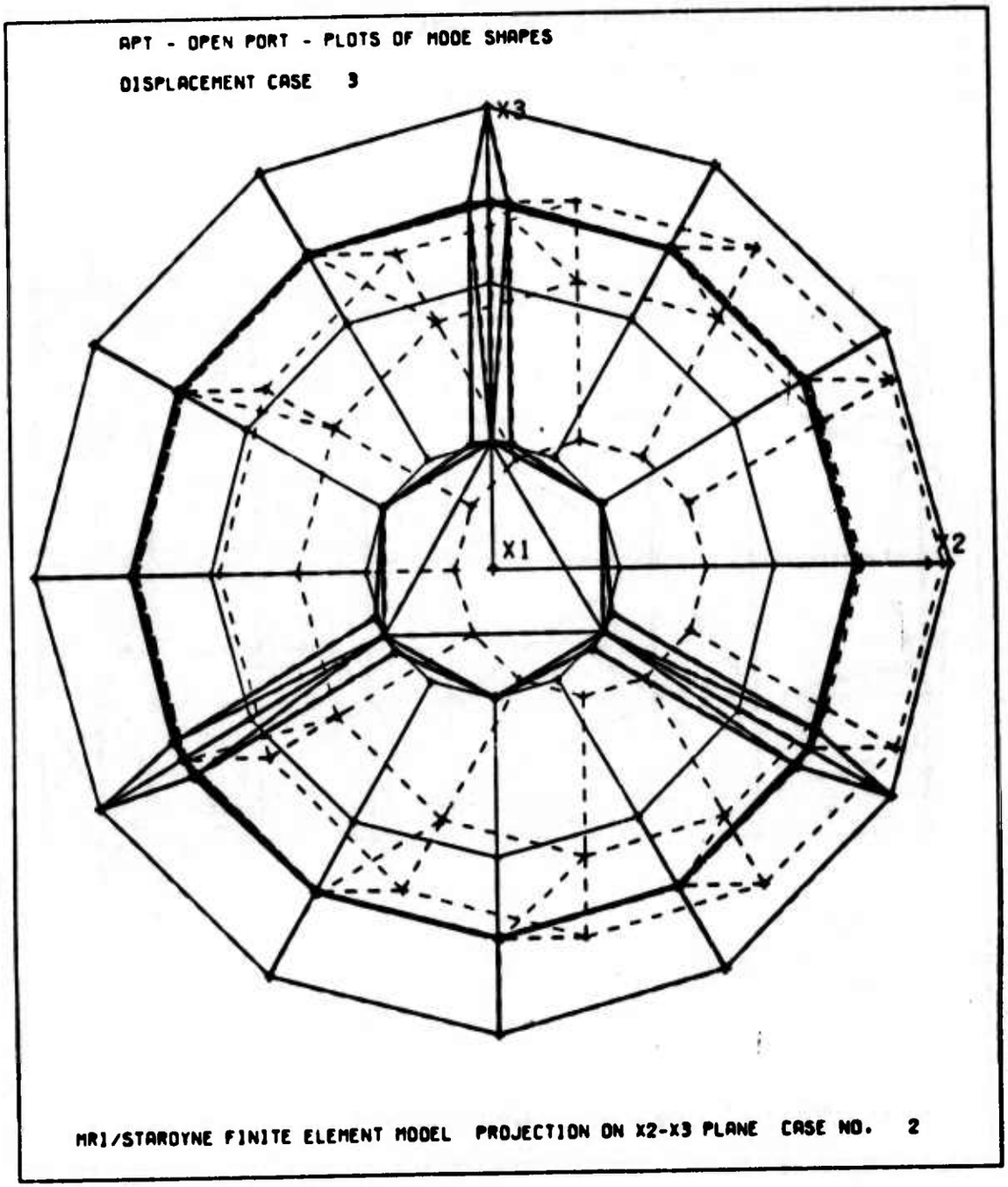

Figure A2.4.7. Computer plot of mode shape number 3 for STARDYNE analysis of APT open port liner.

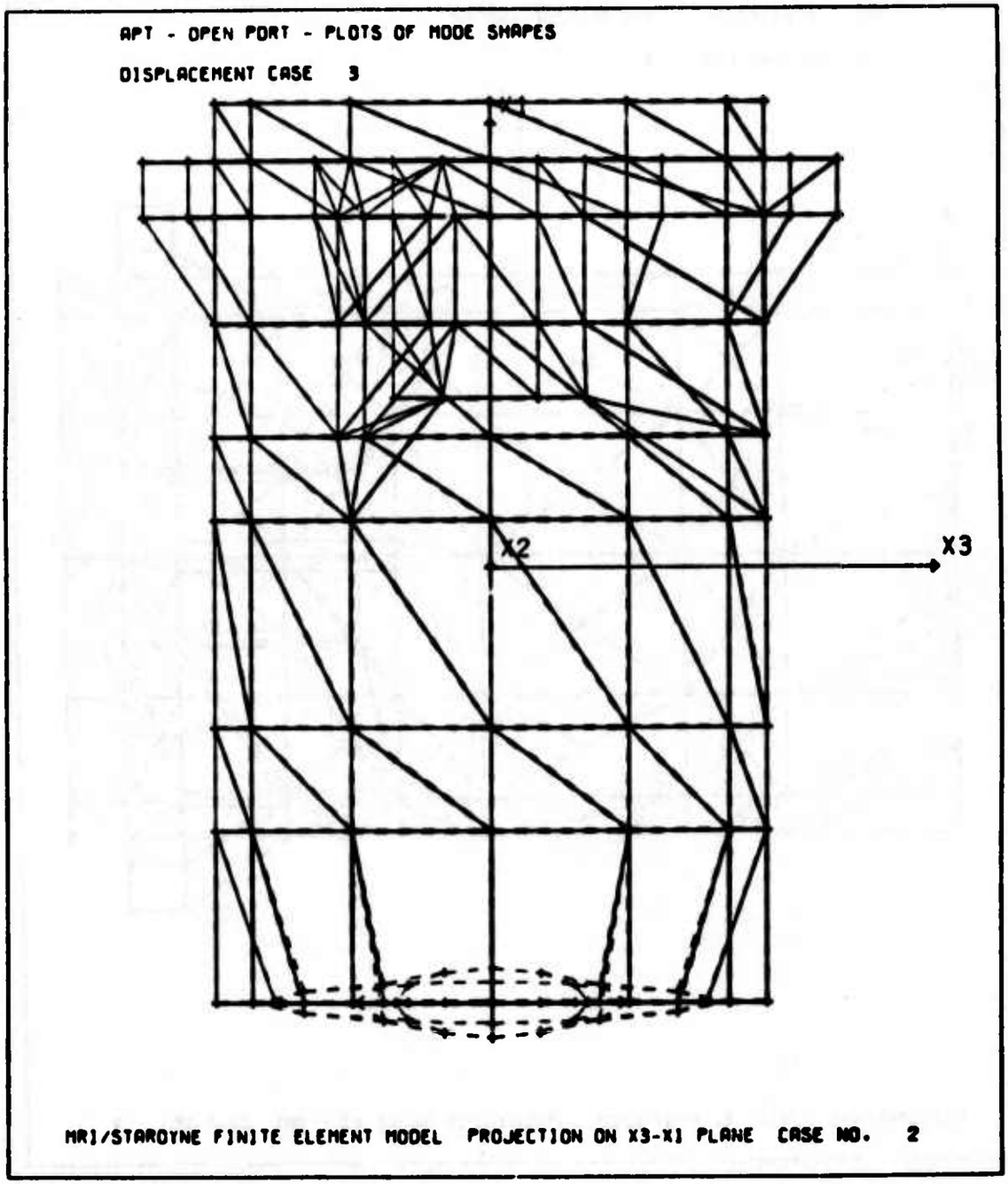

Figure A2.4.8. Computer plot of mode shape number 3 for STARDYNE analysis of APT open port liner.

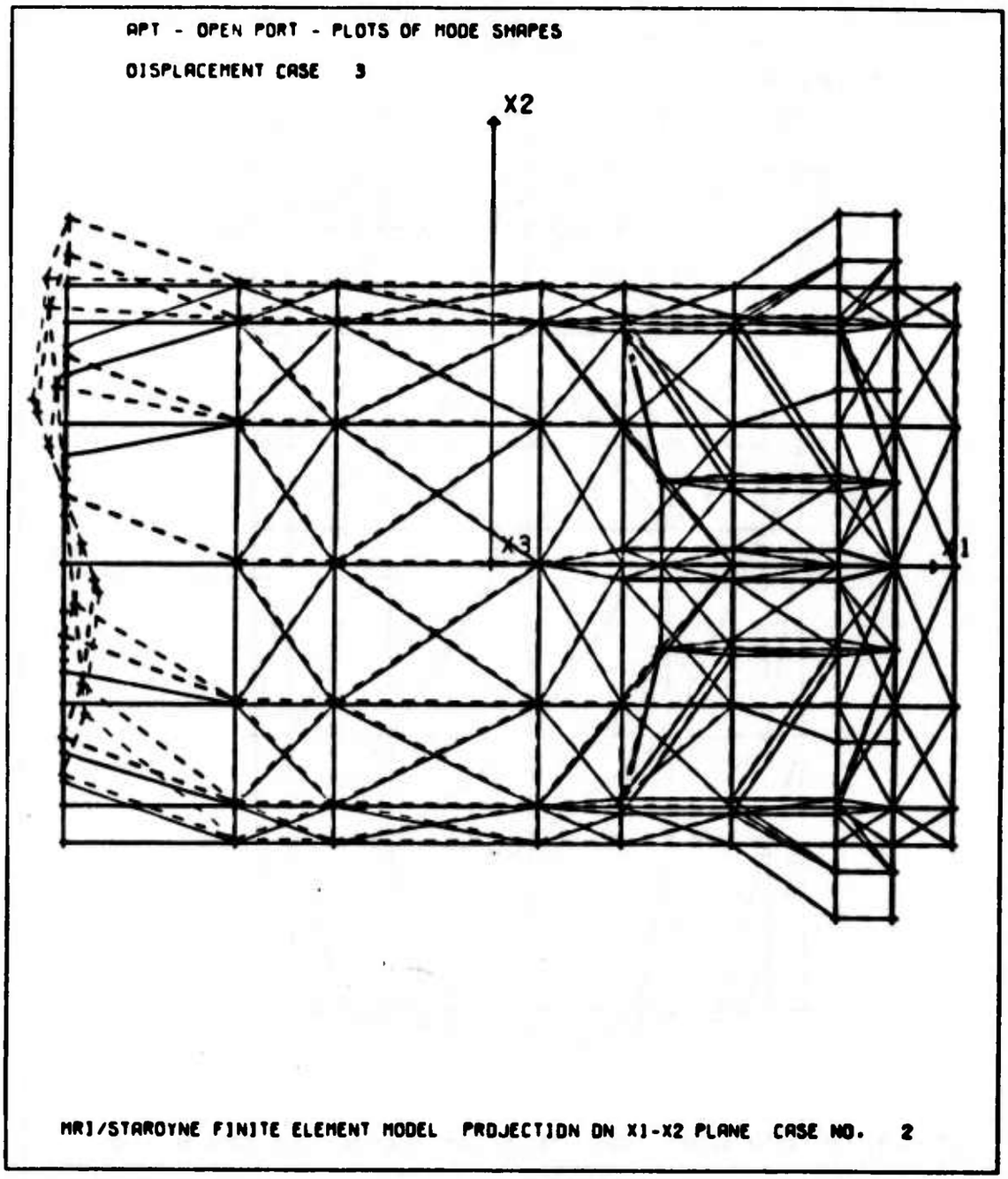

Figure A2.4.9. Computer plot of mode shape number 3 for STARDYNE analysis of APT open port liner.

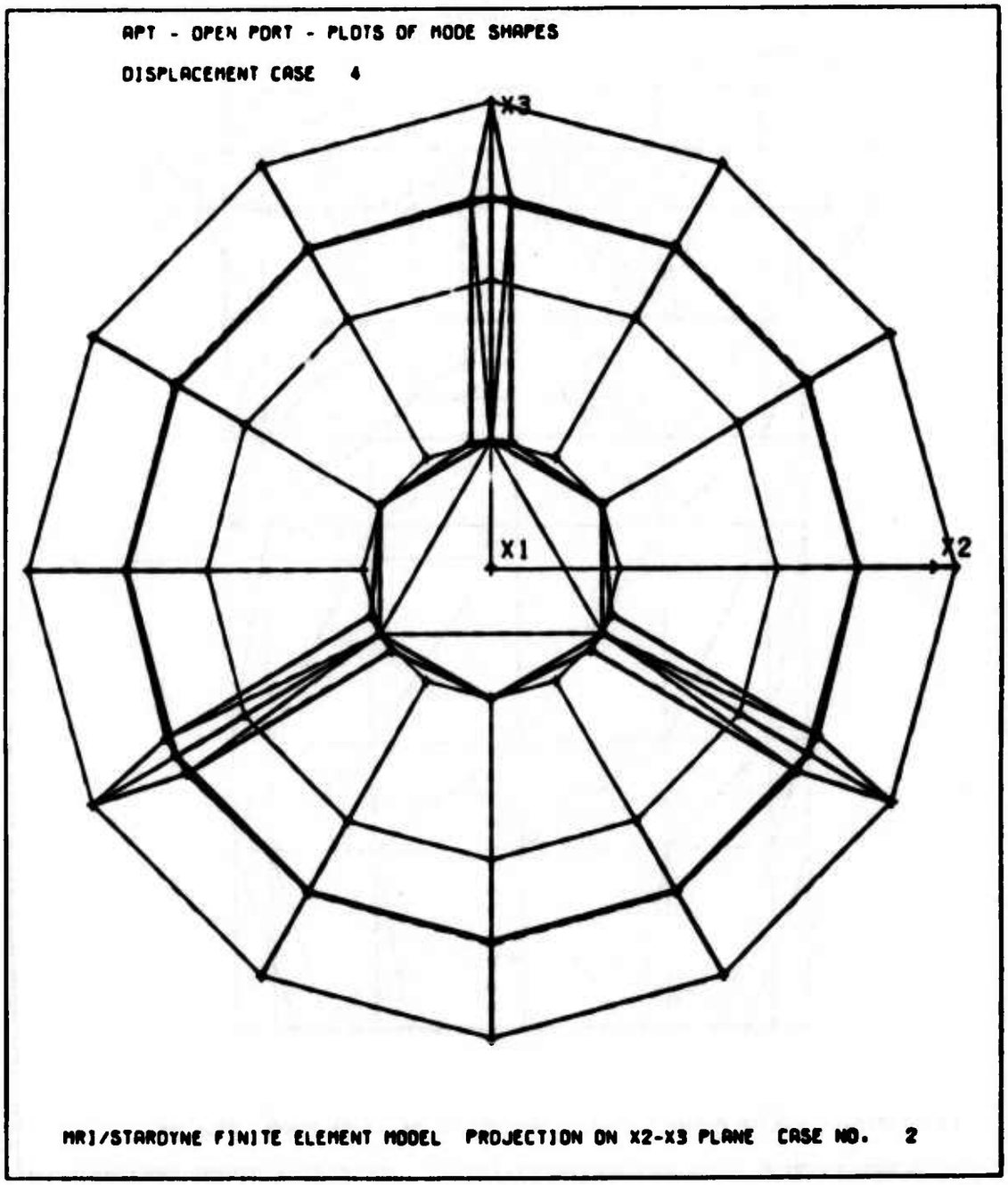

Figure A2.4.10. Computer plot of mode shape number 4 for STARDYNE analysis of APT open port liner.

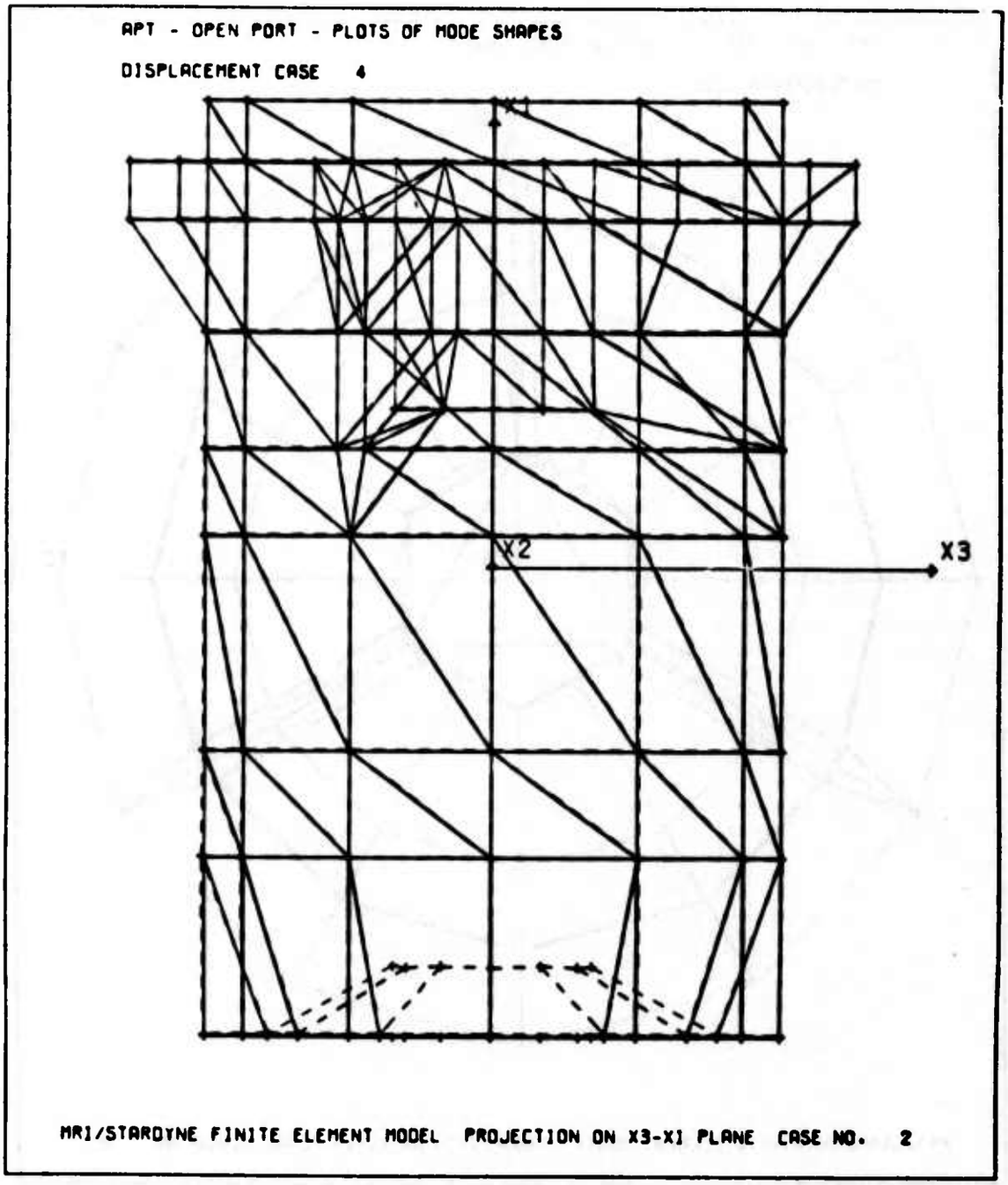

Figure A2.4.11. Computer plot of mode shape number 4 for STARDYNE analysis of APT open port liner.

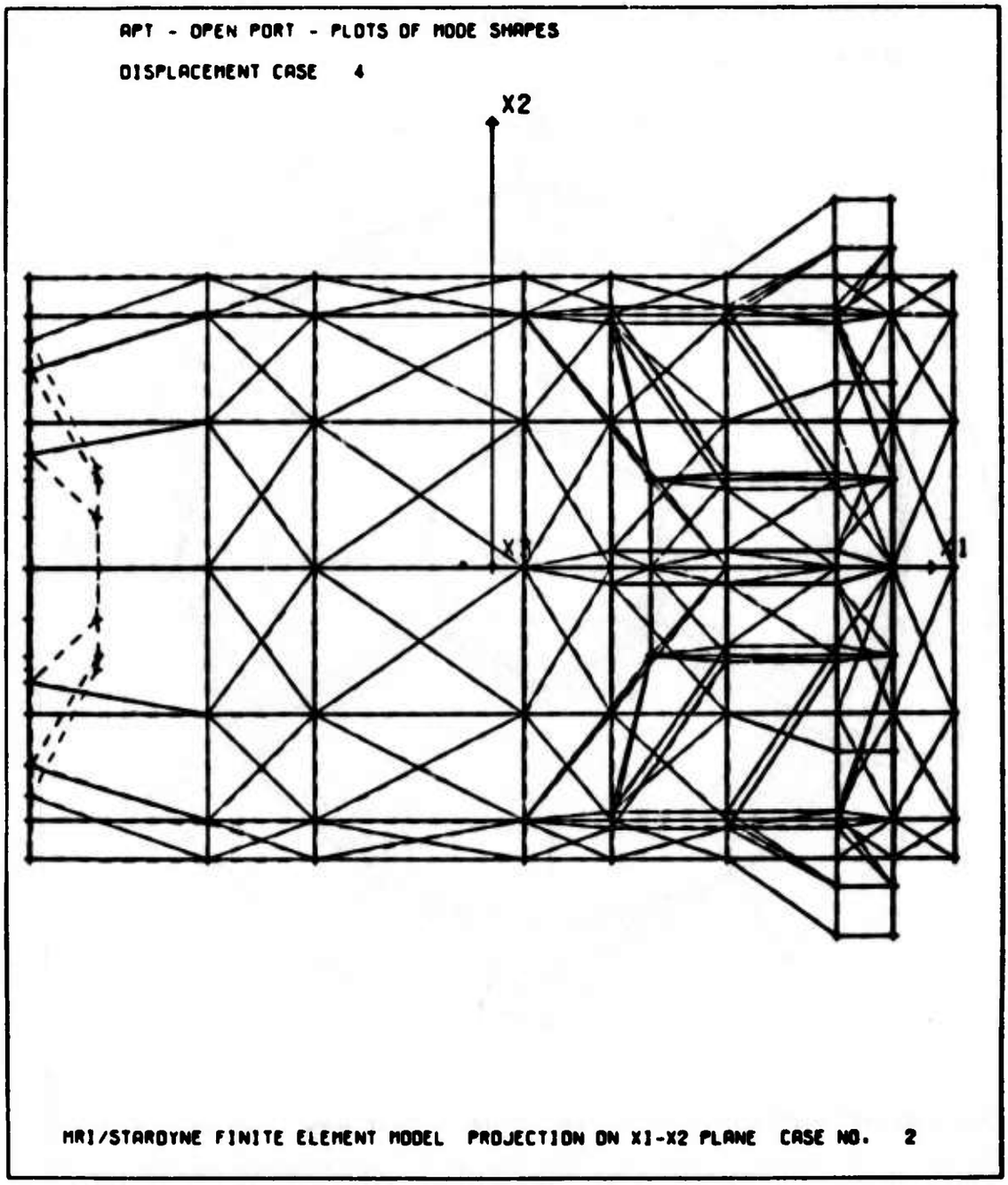

Figure A2.4.12. Computer plot of mode shape number 4 for STARDYNE analysis of APT open port liner.

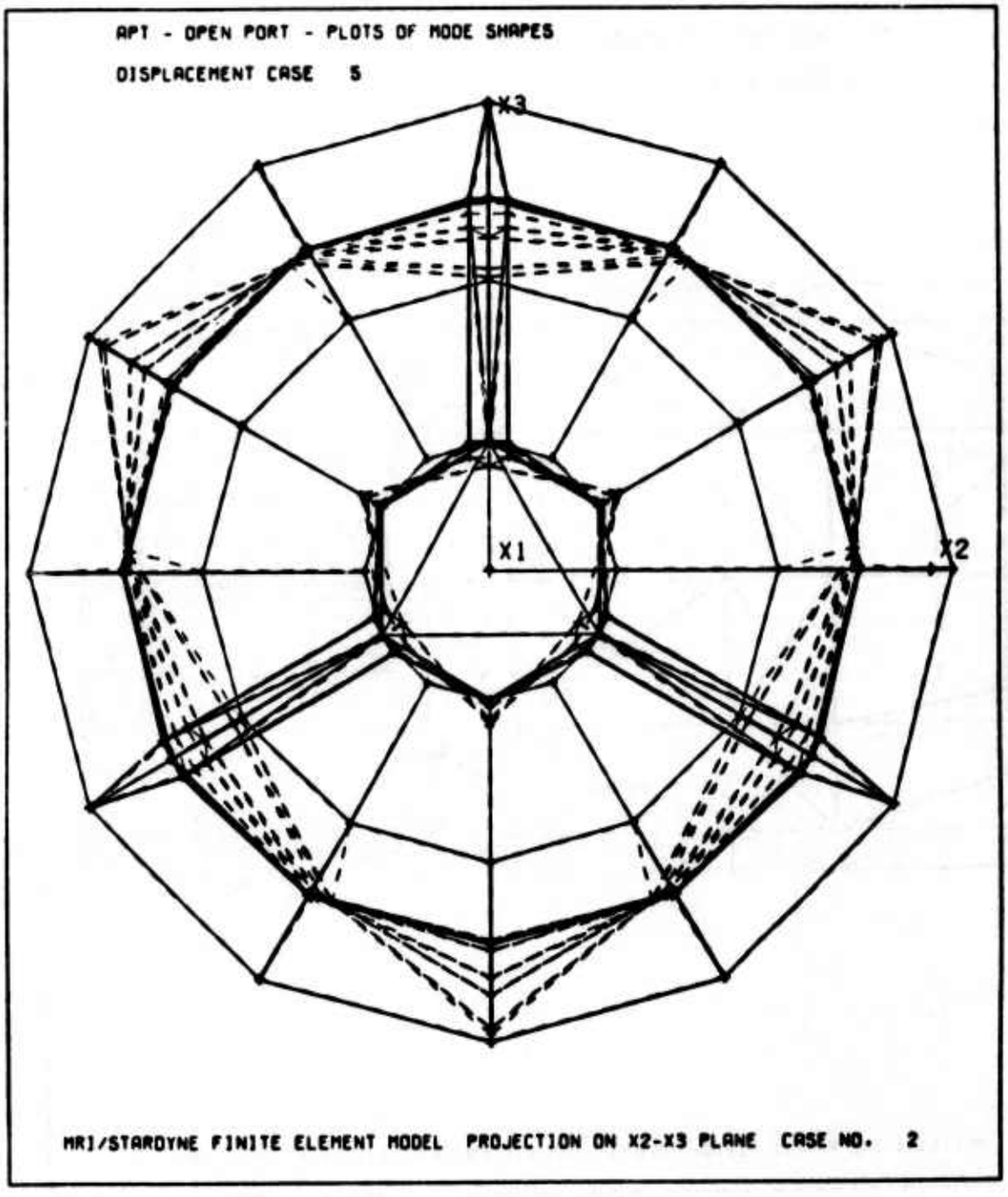

Figure A2.4.13. Computer plot of mode shape number 5 for STARDYNE analysis of APT open port liner.

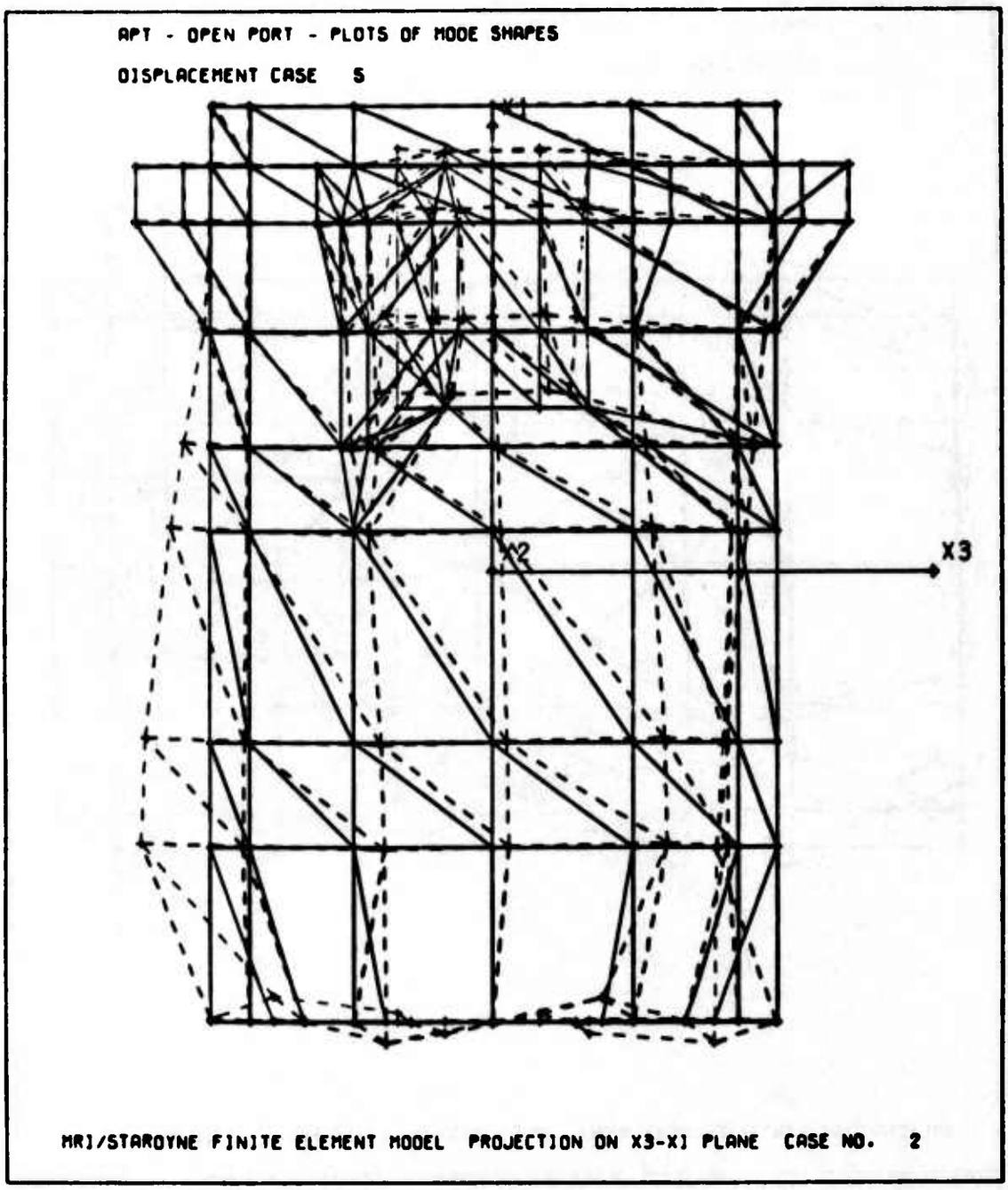

Figure A2.4.14. Computer plot of mode shape number 5 for STARDYNE analysis of APT open port liner.

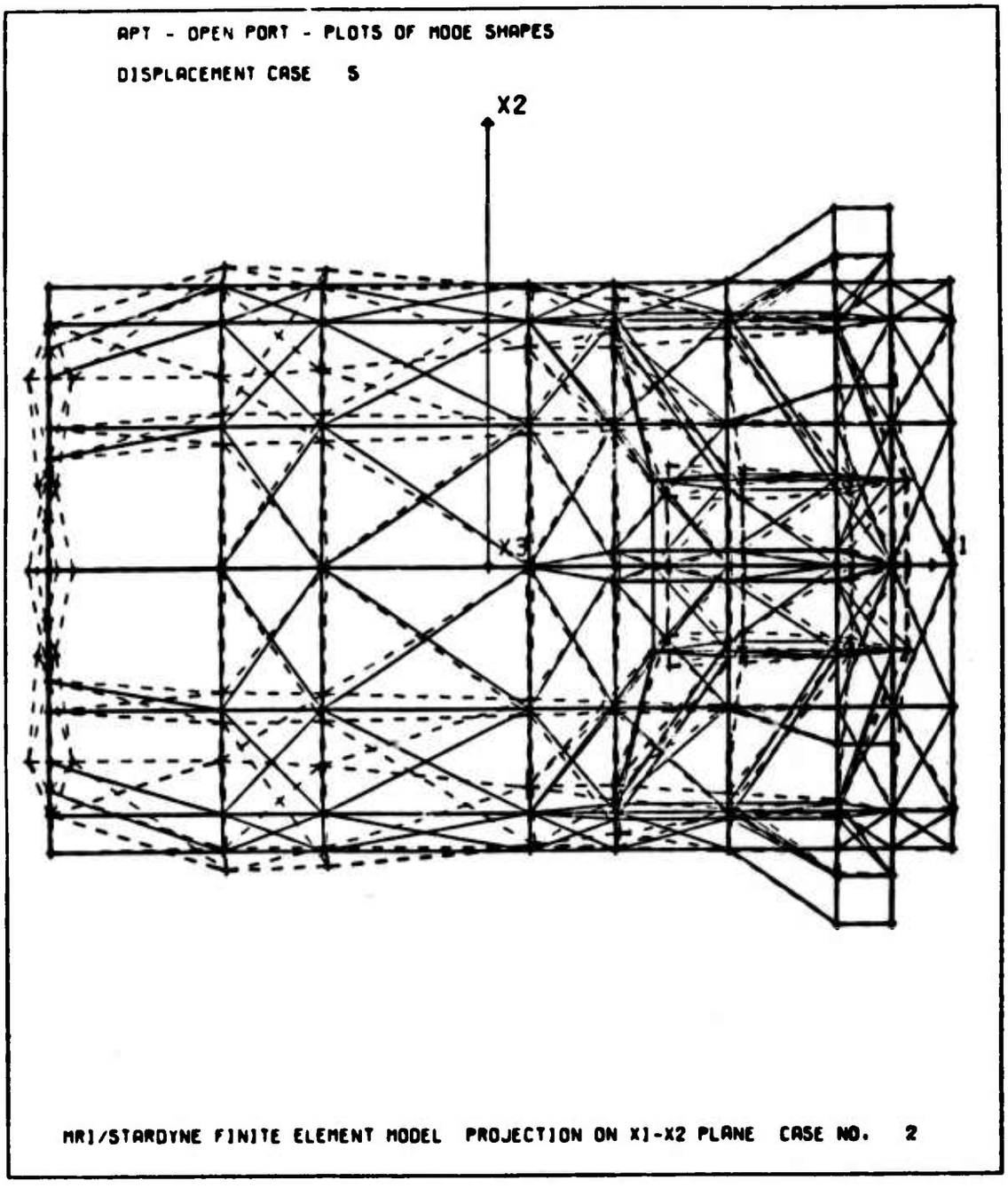

Figure A2.4.15. Computer plot of mode shape number 5 for STARDYNE analysis of APT open port liner.

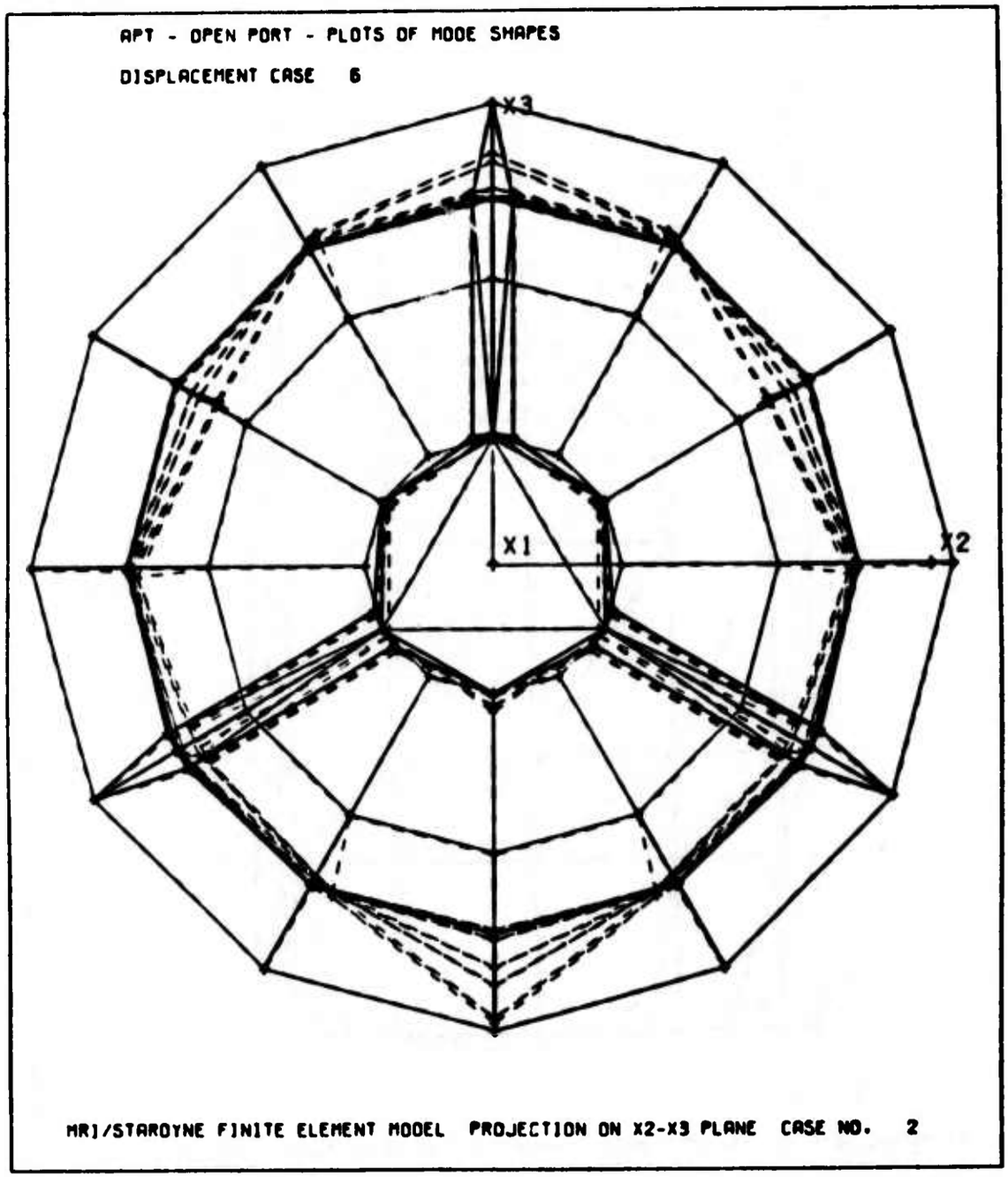

Figure A2.4.16. Computer plot of mode shape number 6 for STARDYNE analysis of APT open port liner.

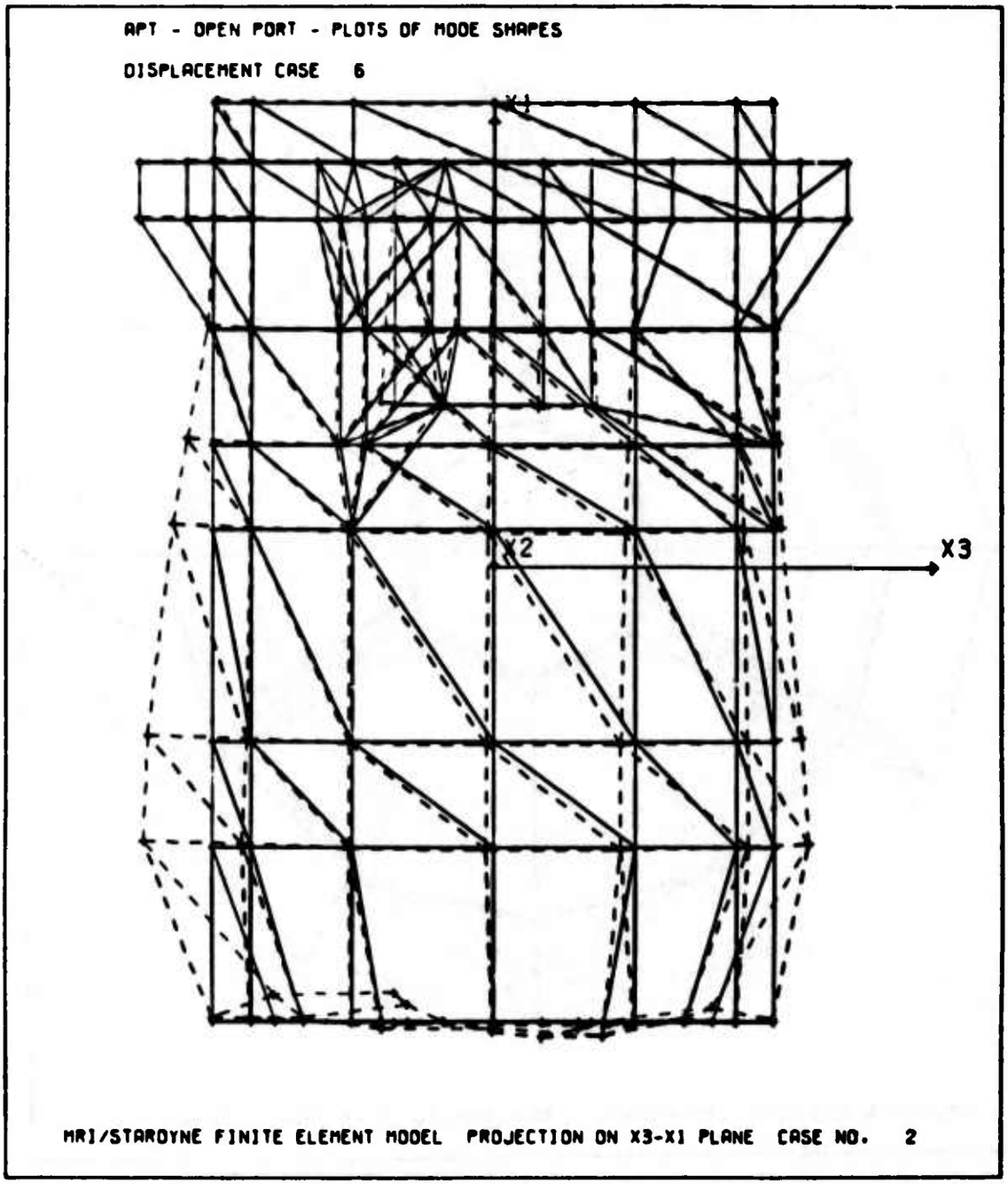

Figure A2.4.17. Computer plot of mode shape number 6 for STARDYNE analysis of APT open port liner.

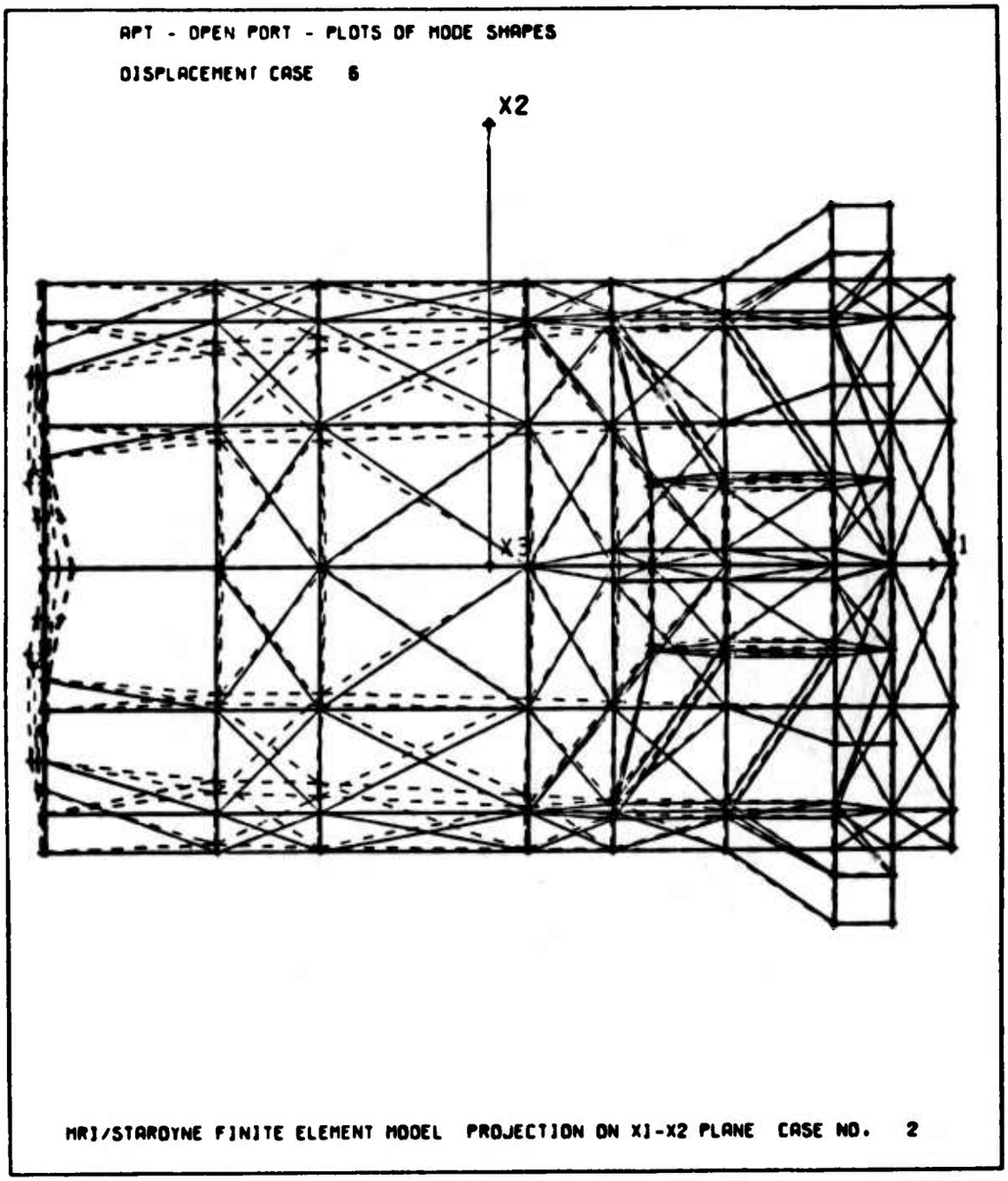

Figure A2.4.18. Computer plot of mode shape number 6 for STARDYNE analysis of APT open port liner.

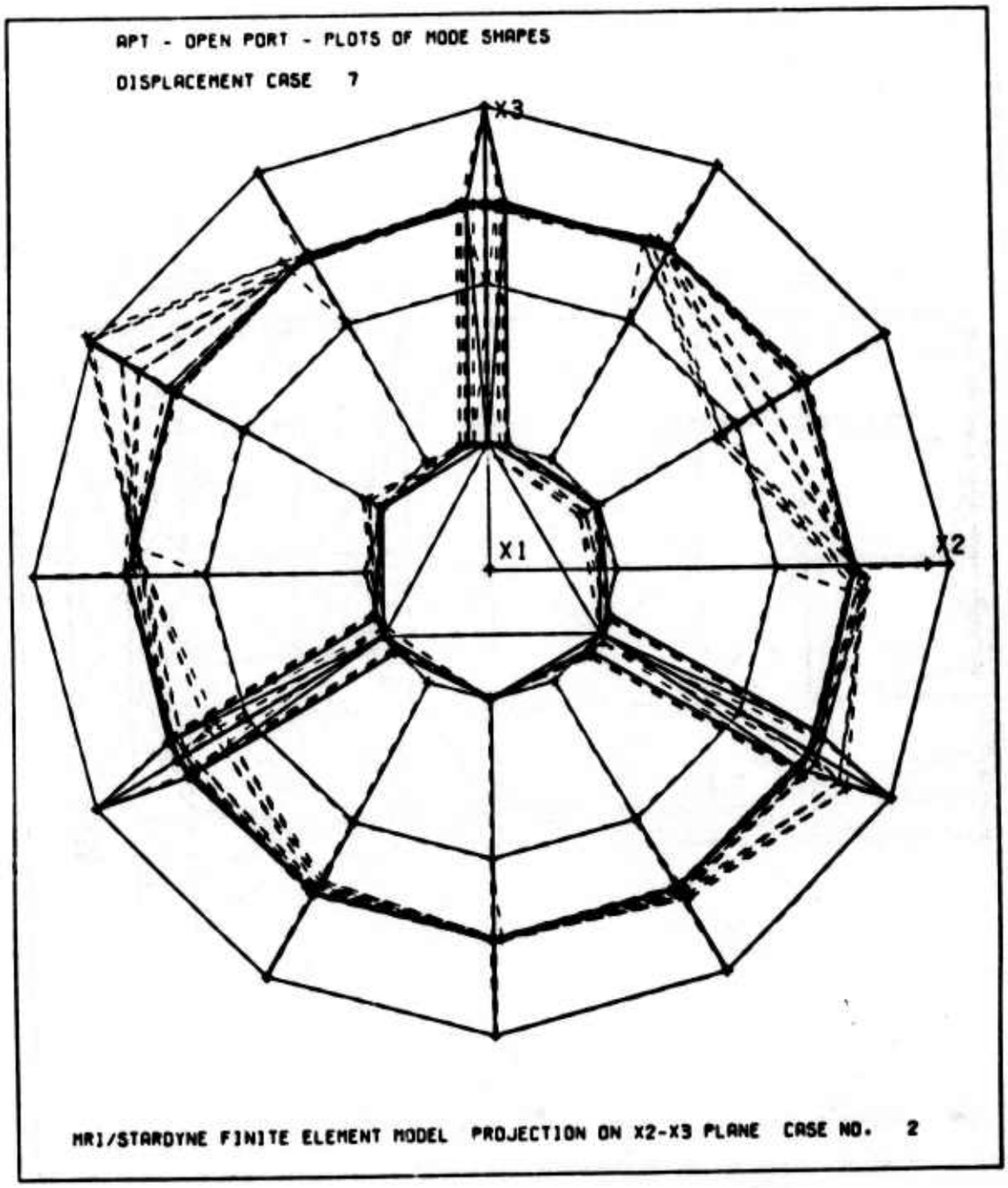

Figure A2.4.19. Computer plot of mode shape number 7 for STARDYNE analysis of APT open port liner.

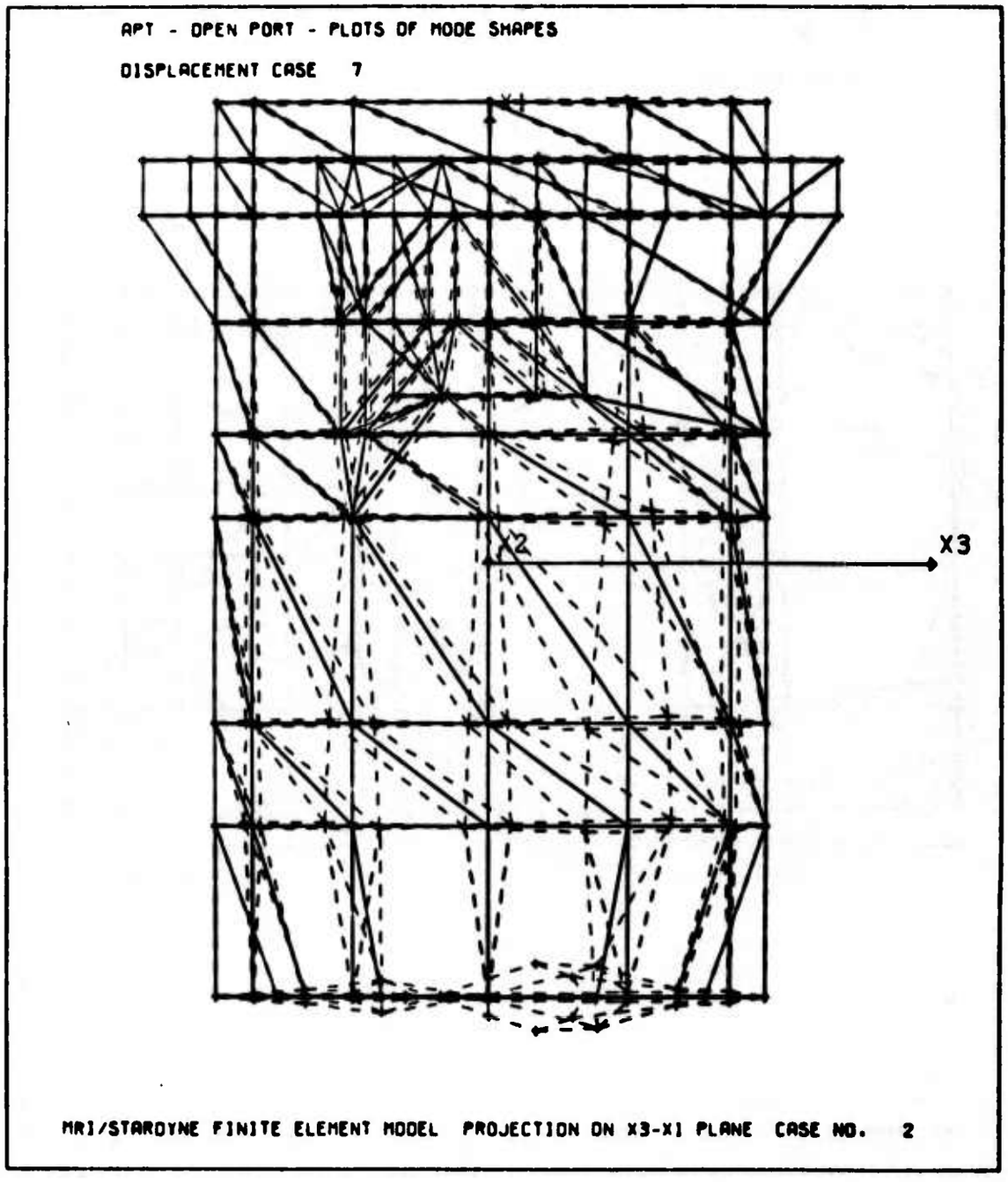

Figure A2.4.20. Computer plot of mode shape number 7 for STARDYNE analysis of APT open port liner.

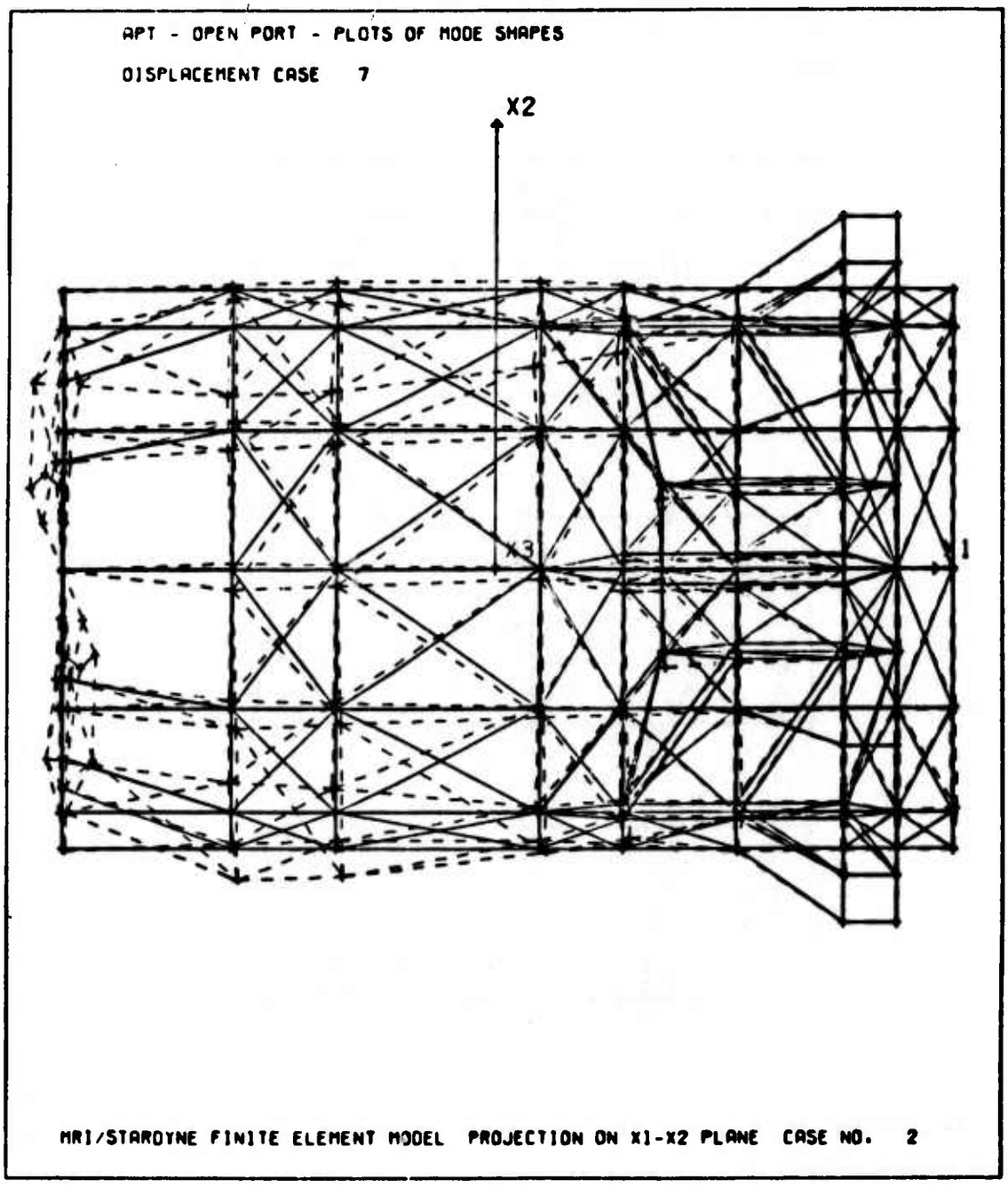

Figure A2.4.21. Computer plot of mode shape number 7 for STARDYNE analysis of APT open port liner.

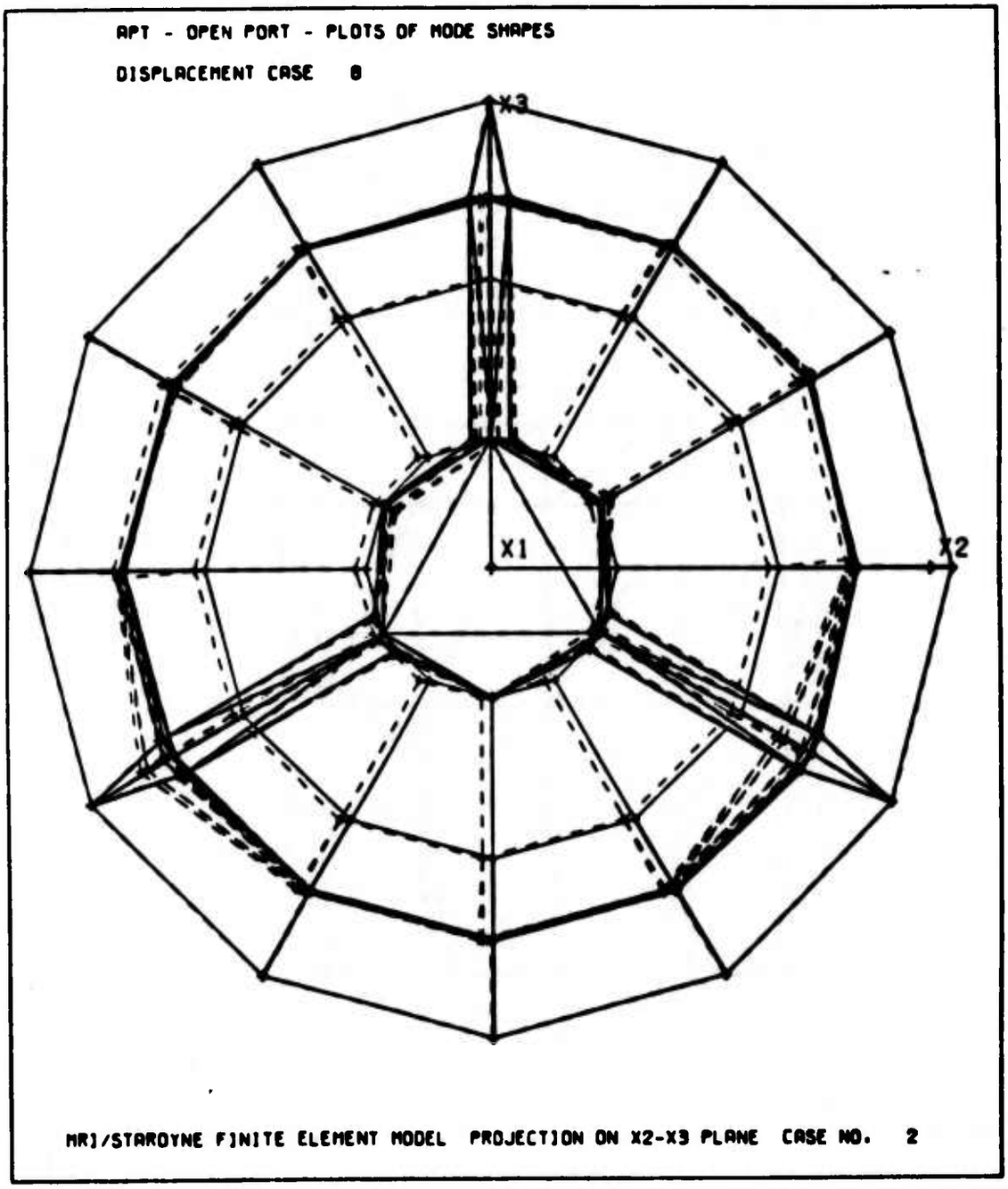

Figure A2.4.22. Computer plot of mode shape number 8 for STARDYNE analysis of APT open port liner.

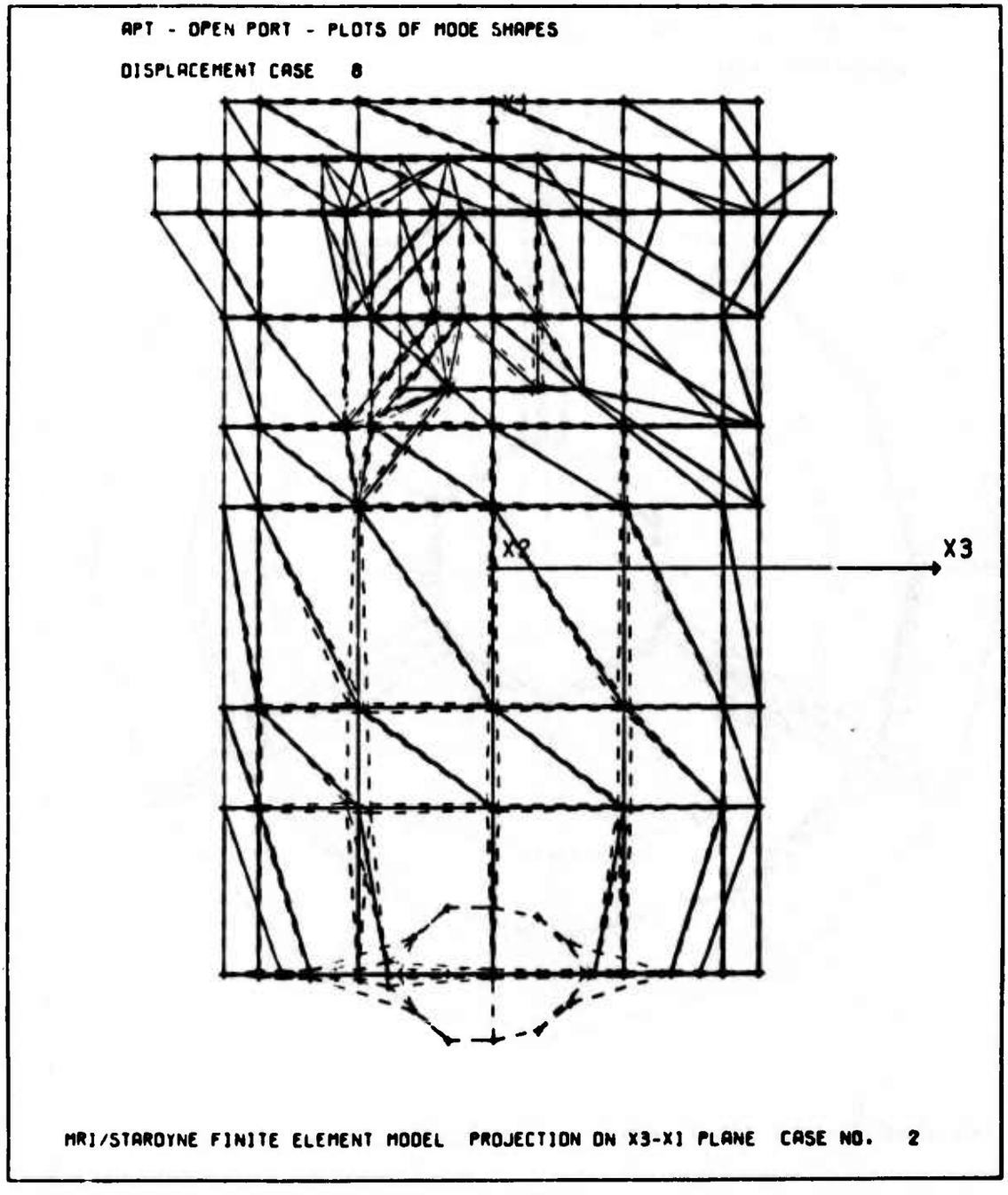

Figure A2.4.23. Computer plot of mode shape number 8 for STARDYNE analysis of APT open port liner.

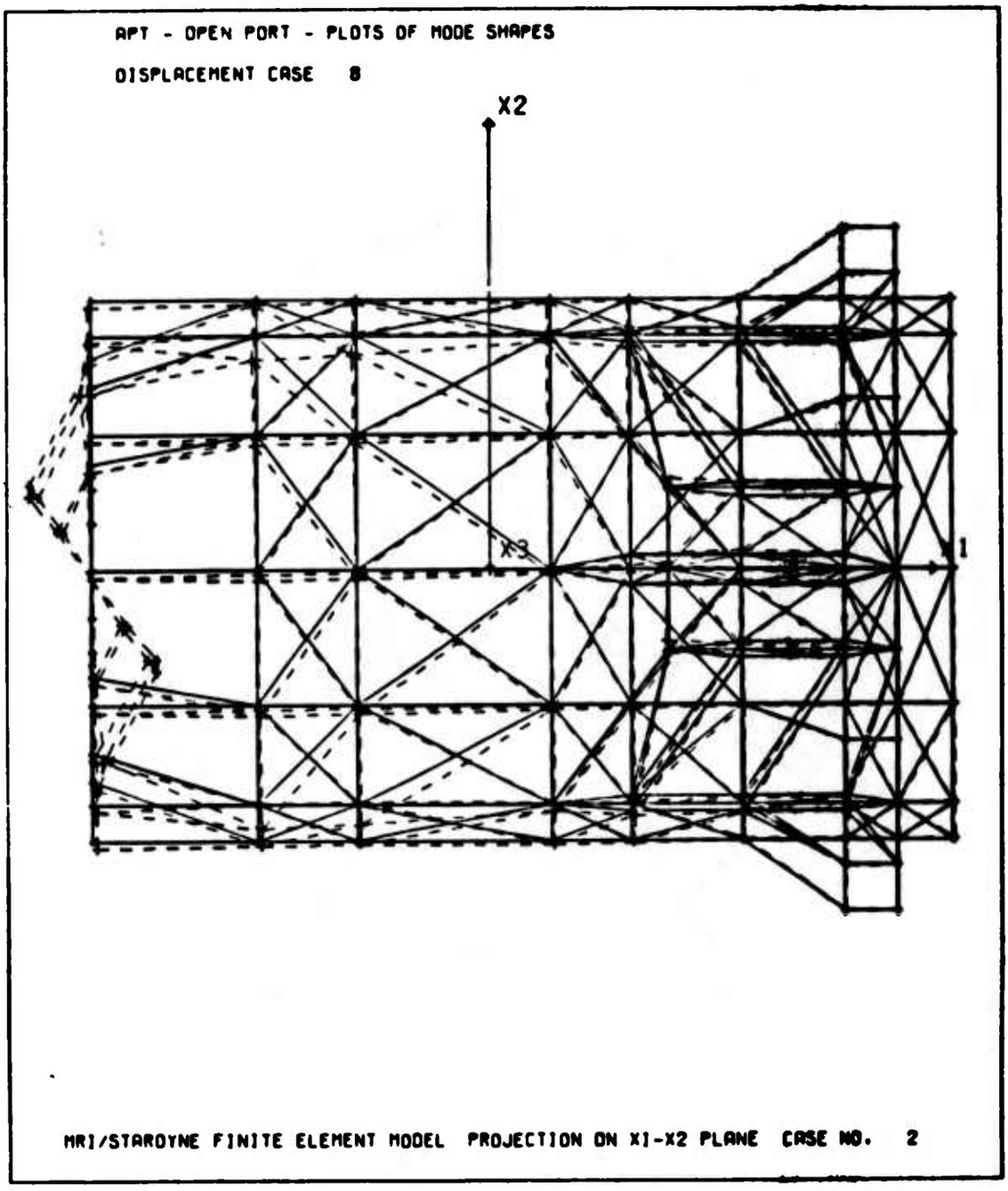

Figure A2.4.24. Computer plot of mode shape number 8 for STARDYNE analysis of APT open port liner.

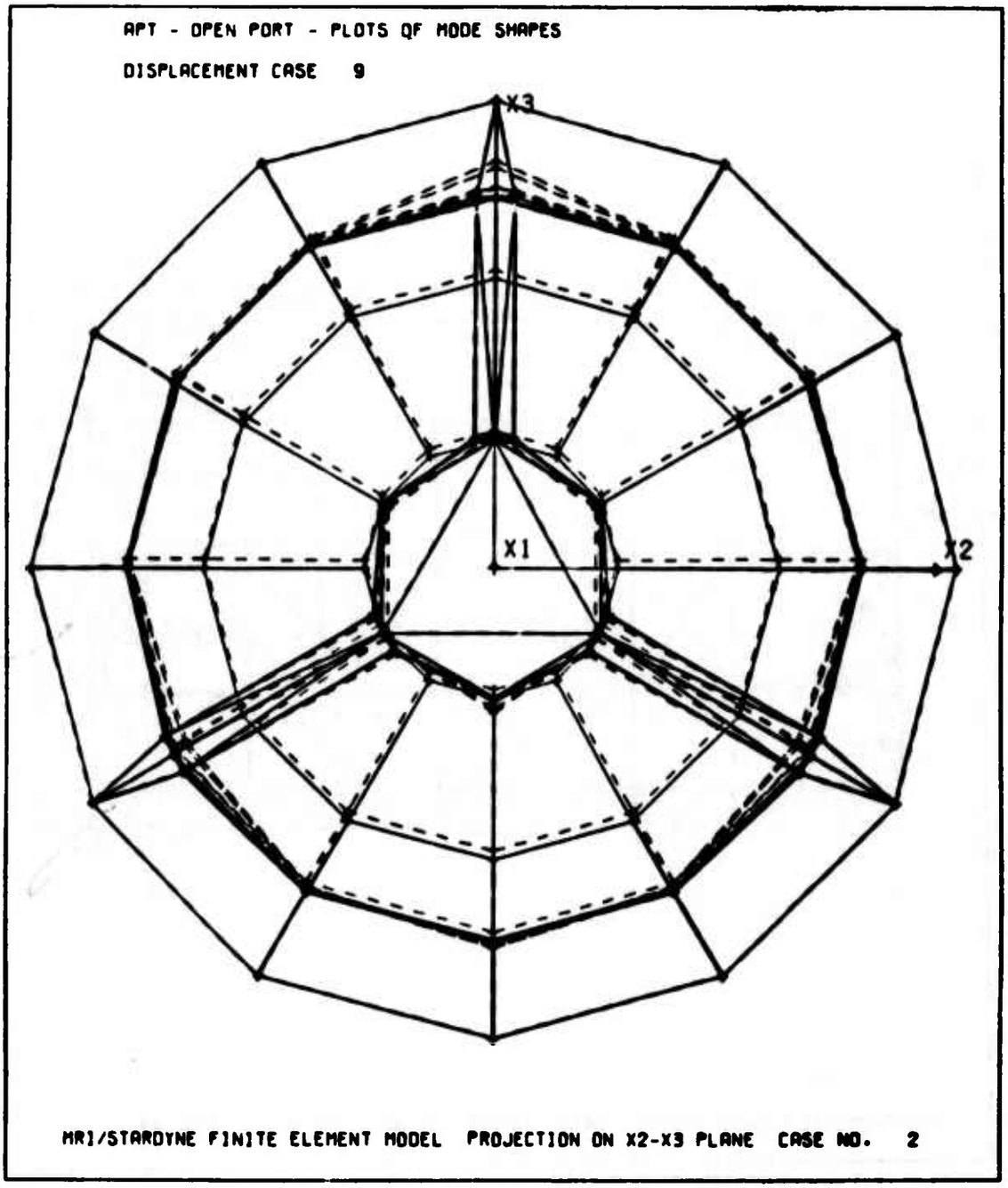

Figure A2.4.25. Computer plot of mode shape number 9 for STARDYNE analysis of APT open port liner.

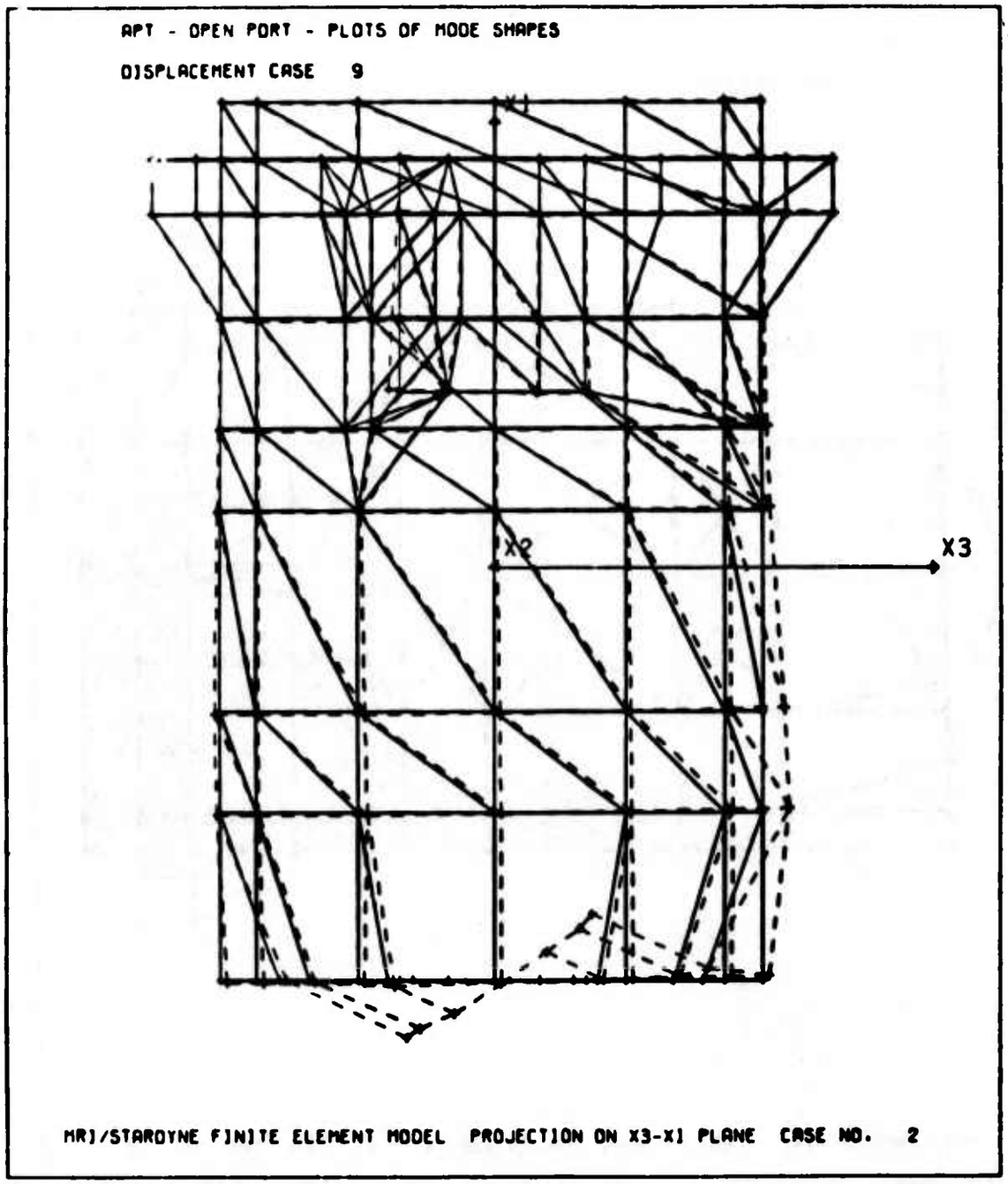

Figure A2.4.26. Computer plot of mode shape number 9 for STARDYNE analysis of APT open port liner.

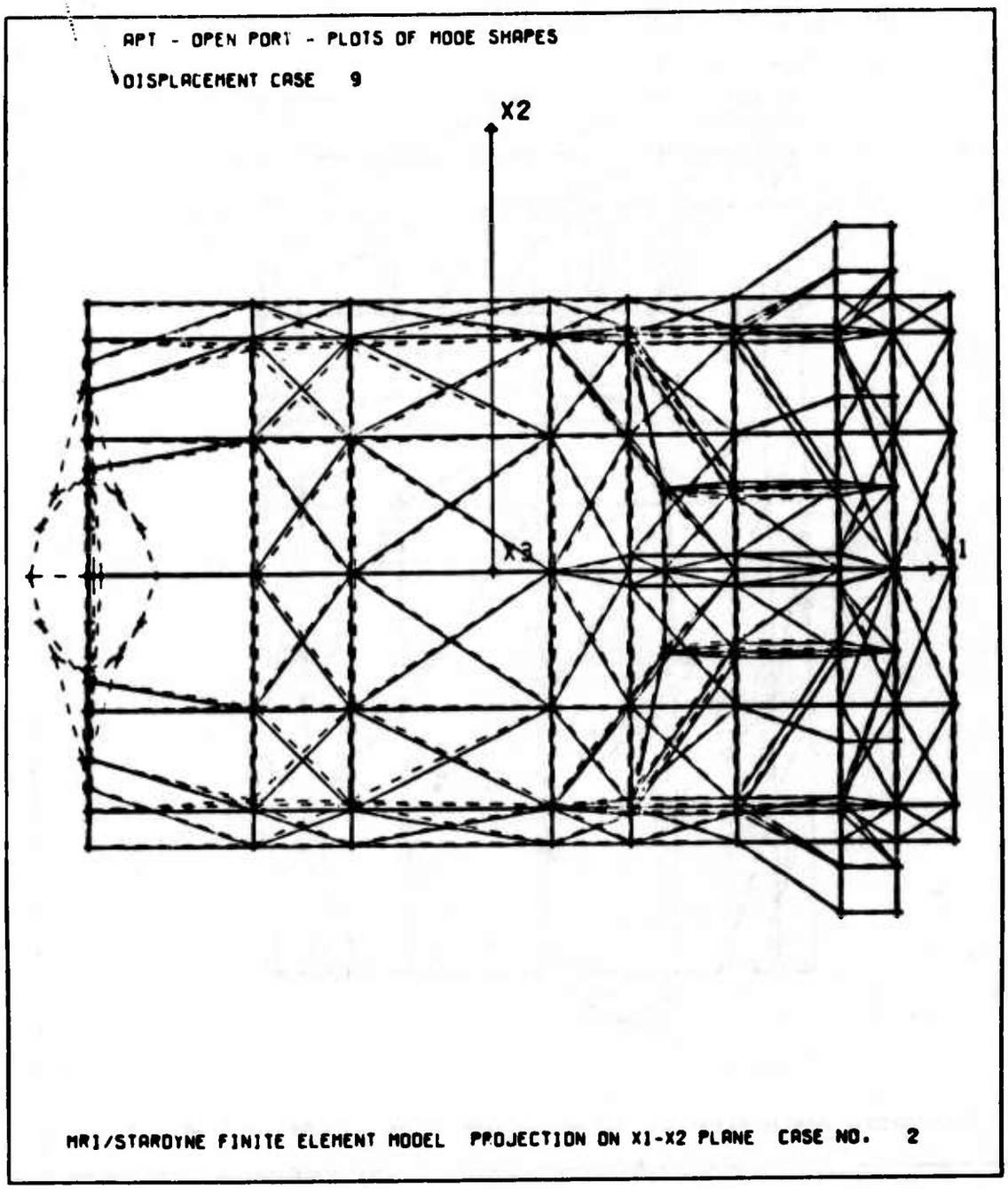

Figure A2.4.27. Computer plot of mode shape number 9 for STARDYNE analysis of APT open port liner.

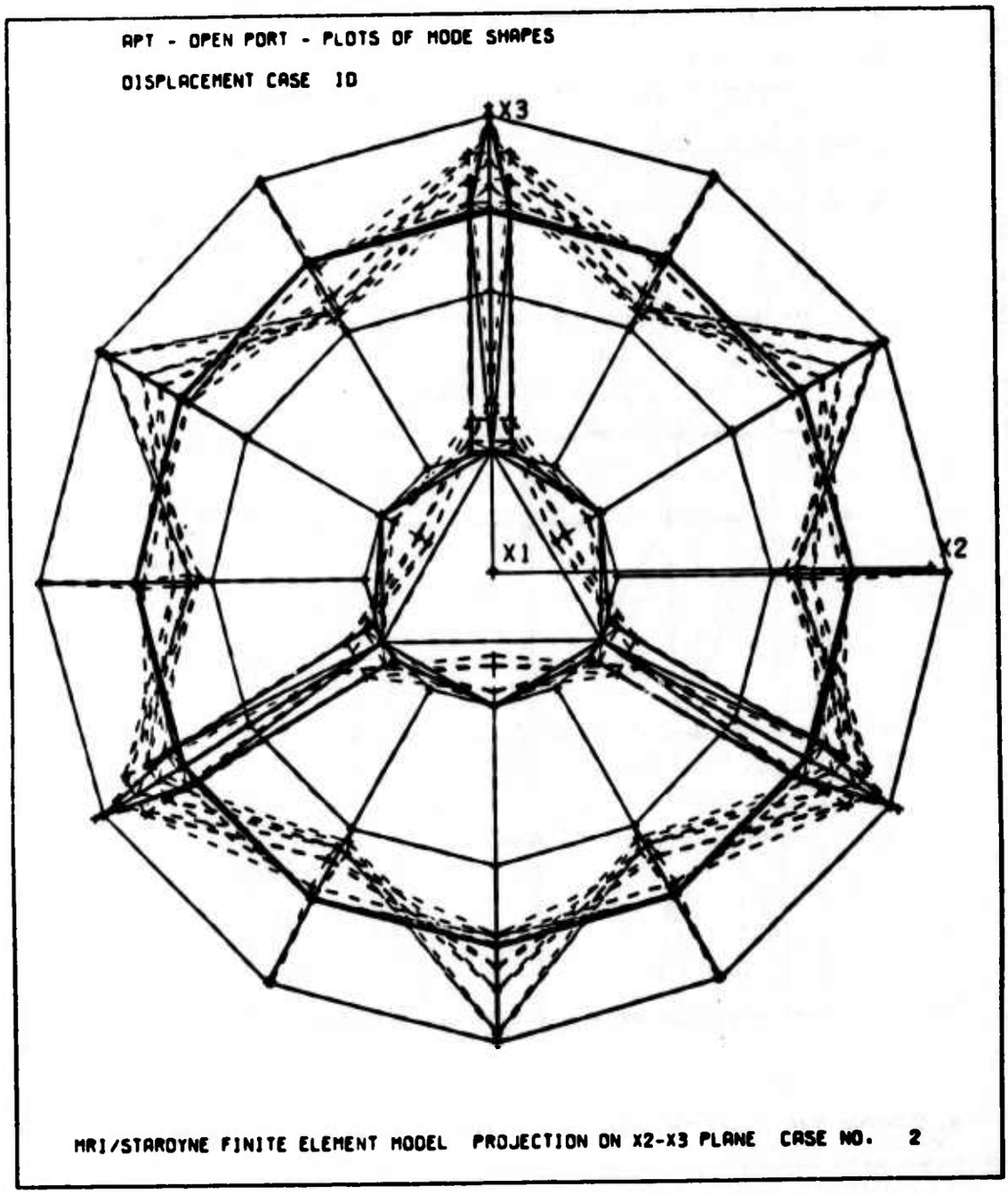

Figure A2.4.28. Computer plot of mode shape number 10 for STARDYNE analysis of APT open port liner.

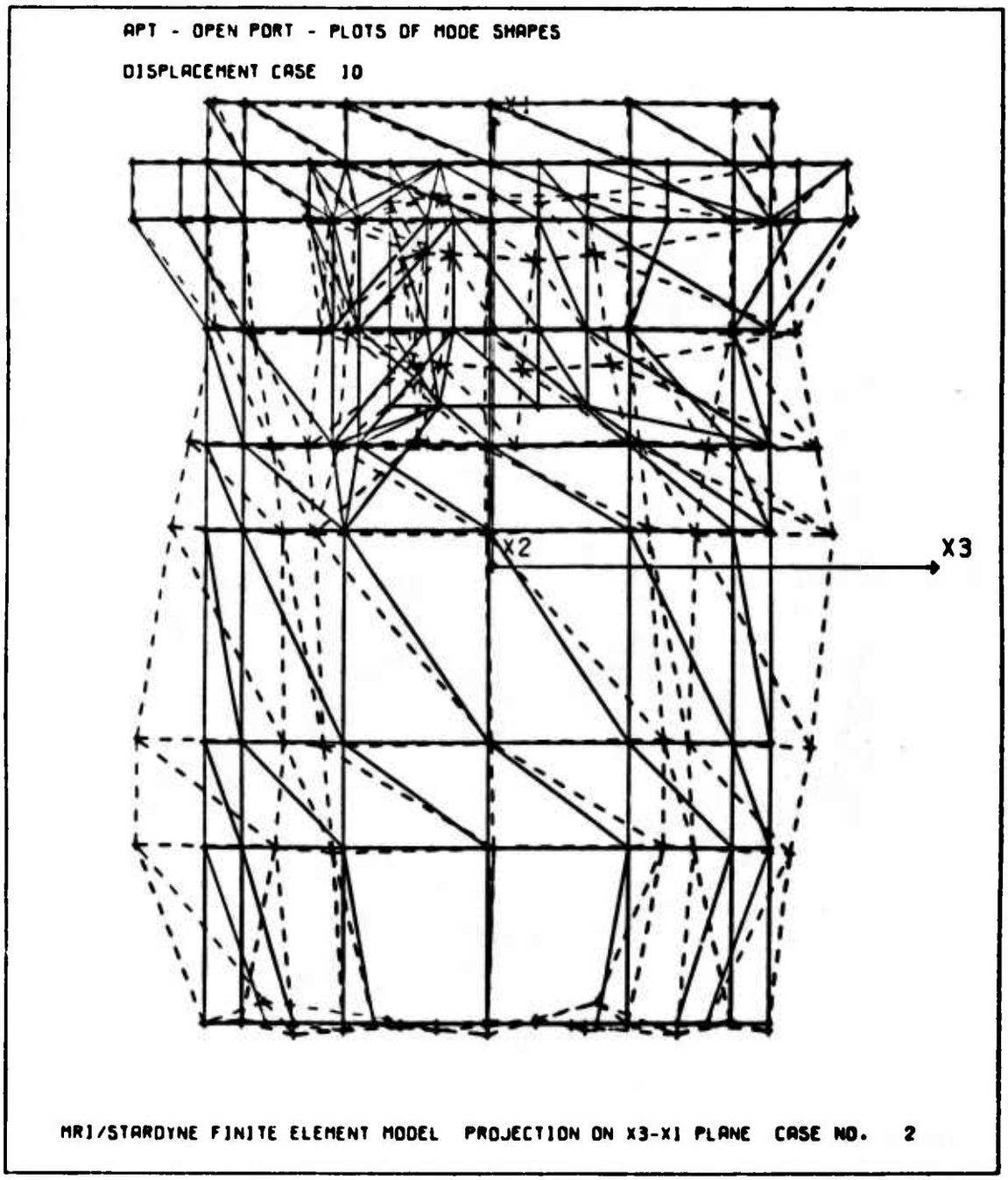

Figure A2.4.29. Computer plot of mode shape number 10 for STARDYNE analysis of APT open port liner.

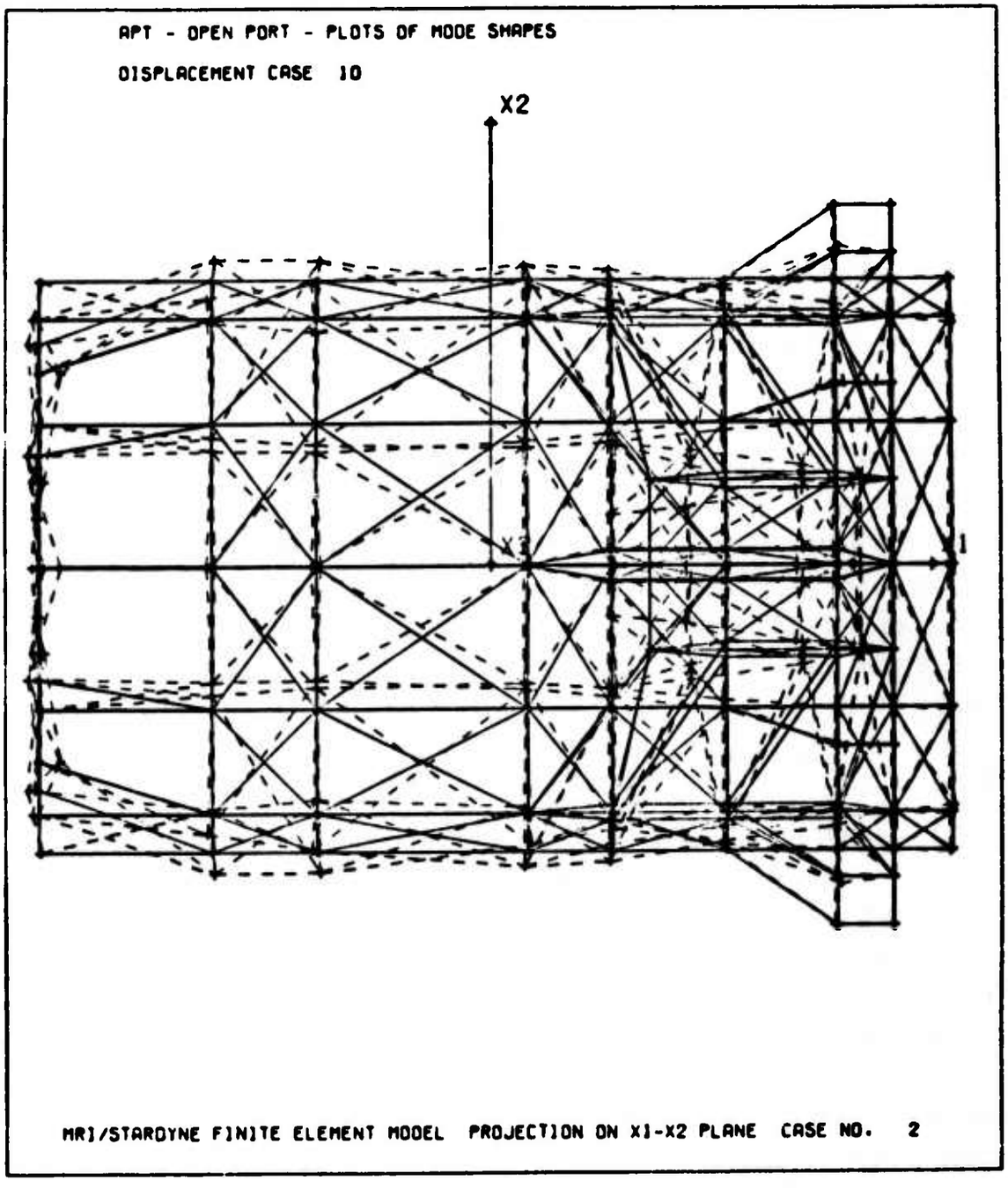

Figure A2.4.30. Computer plot of mode shape number 10 for STARDYNE analysis of APT open port liner.

A2.5 MATHEMATICAL MODELS

The finite element, lumped mass, mathematical model for both the static and dynamic STARDYNE analysis of the APT Open Port Liner consists of 202 nodes, 108 beams, 320 triangular plates, and 45 quadrilateral plates. Computer plots of three orthogonal and three rotated views of this model are shown in Figures A2.5.1 through A2.5.6.

Mathematical models of the major components of the liner, namely, the aerodynamic fence and liner cylinder, the liner flange, the secondary mirror cover, the secondary mirror cover support struts, and the primary mirror cover and its support straps, are shown in Figures A2.5.7 through A2.5.11, respectively. The schedule of associated beam and plate elements is presented in Table A2.5.1, and beam section properties are given in Table A2.5.2.

The flexibility of the liner mounting provisions were conservatively simulated by restraining the perimeter nodes of the mounting flange, nodes N136 through N147, against translation along the three global axes.

For the static base acceleration analyses, the automatic weight generation feature of the STARDYNE program was utilized. The STARDYNE program automatically computes the volume of each finite element, multiplies it by the associated material density, and distributes the weight so obtained equally to the associated nodes.

For the Householder - QR eigenvalue extraction analysis, the weights were lumped in manner that would minimize the dynamic degrees-of-freedom but would adequately represent the breathing modes of the liner and the in-plane rigid body translation and out-of-plane bending modes of the primary mirror cover. This task was accomplished first by creating individual coordinate systems for the liner and secondary mirror cover nodes in such a manner that the X1 direction of each of the individual coordinate systems would correspond to the radial direction at the nodes. Then the static nodal weights of the liner were lumped radially to every other node and the static nodal weights of the secondary mirror cover were lumped radially to six nodes, three at each end. One-fourth of the total primary mirror cover weight was lumped in the global X2 and X3 (in-plane) directions at each of

four equally spaced nodes on the outer perimeter of the cover. Half of the total primary mirror cover weight was distributed to six evenly spaced nodes on the inner perimeter of the cover in the global X1 (out-of-plane) direction. In this fashion, the model was reduced to 77 dynamic degrees-of-freedom.

For the random response analysis, the nodal areas of the liner and secondary mirror cover cylinder were lumped radially to every one of their respective nodes, while the nodal areas of the primary mirror cover were lumped to every one of its nodes in the global X1 (out-of-plane) direction.

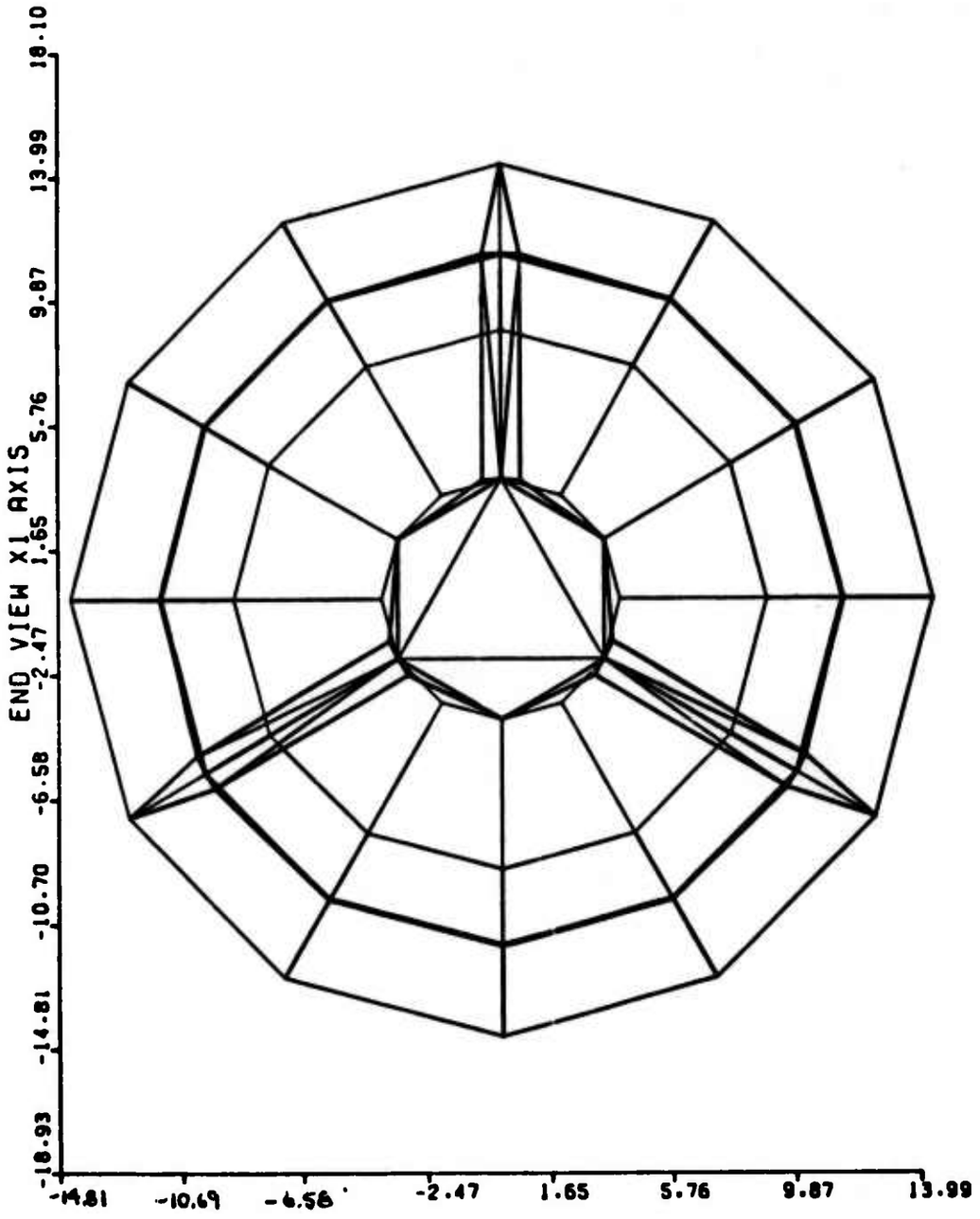

Figure A2.5.1. Computer plot of mathematical model for STARDYNE analysis of APT open port liner.

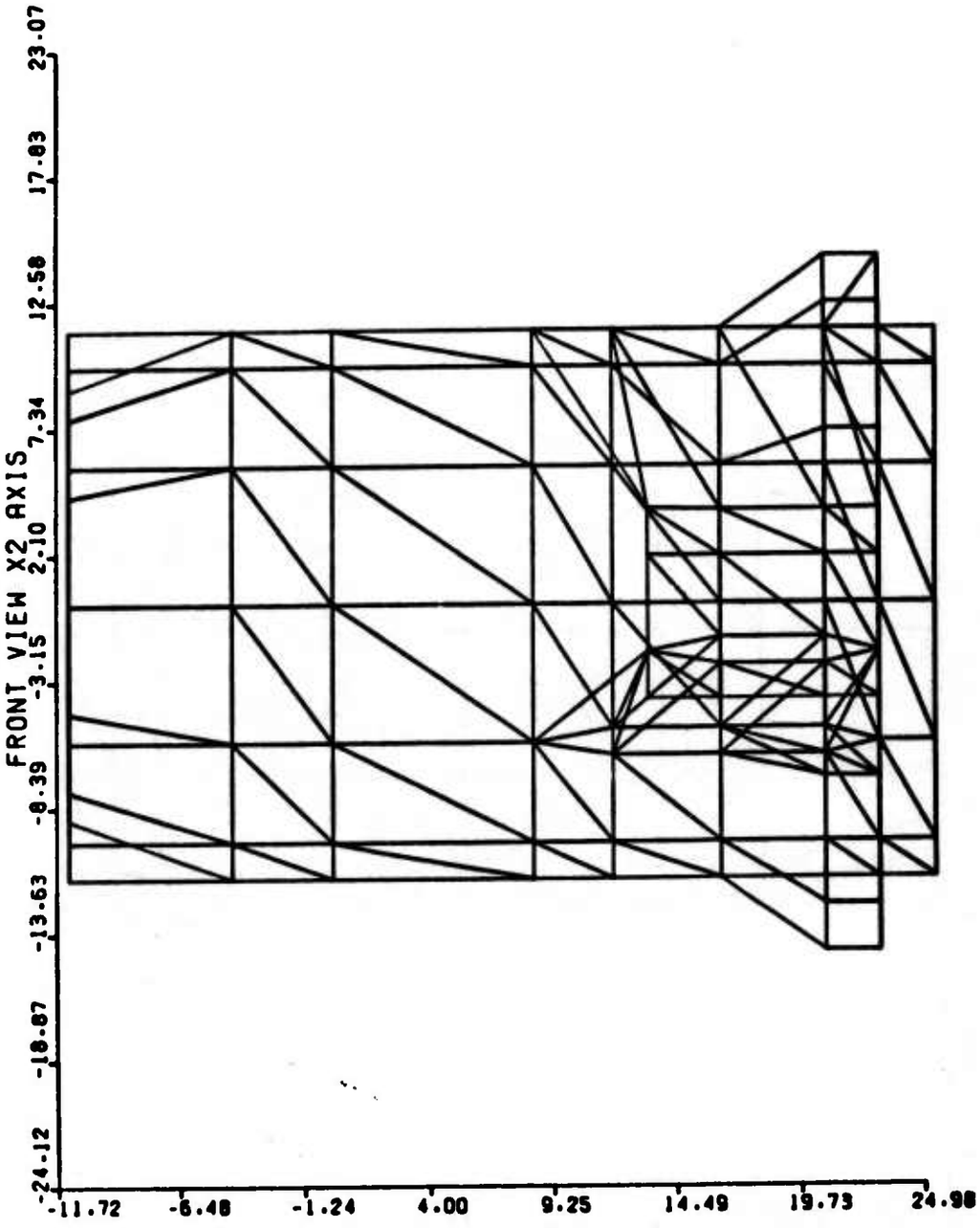

Figure A2.5.2. Computer plot of mathematical model for STARDYNE analysis of APT open port liner.

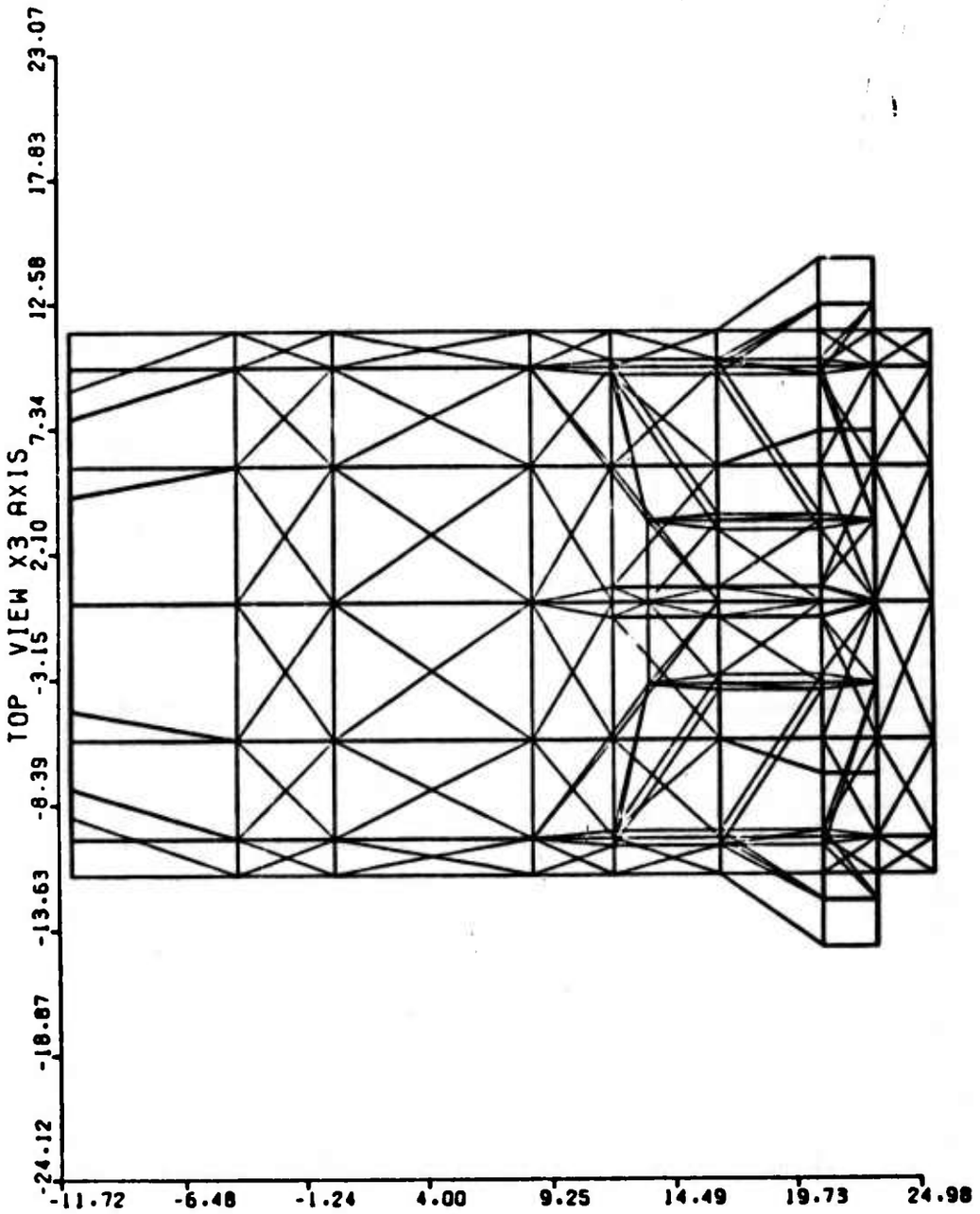

Figure A2.5.3. Computer plot of mathematical model for STARDYNE analysis of APT open port liner.

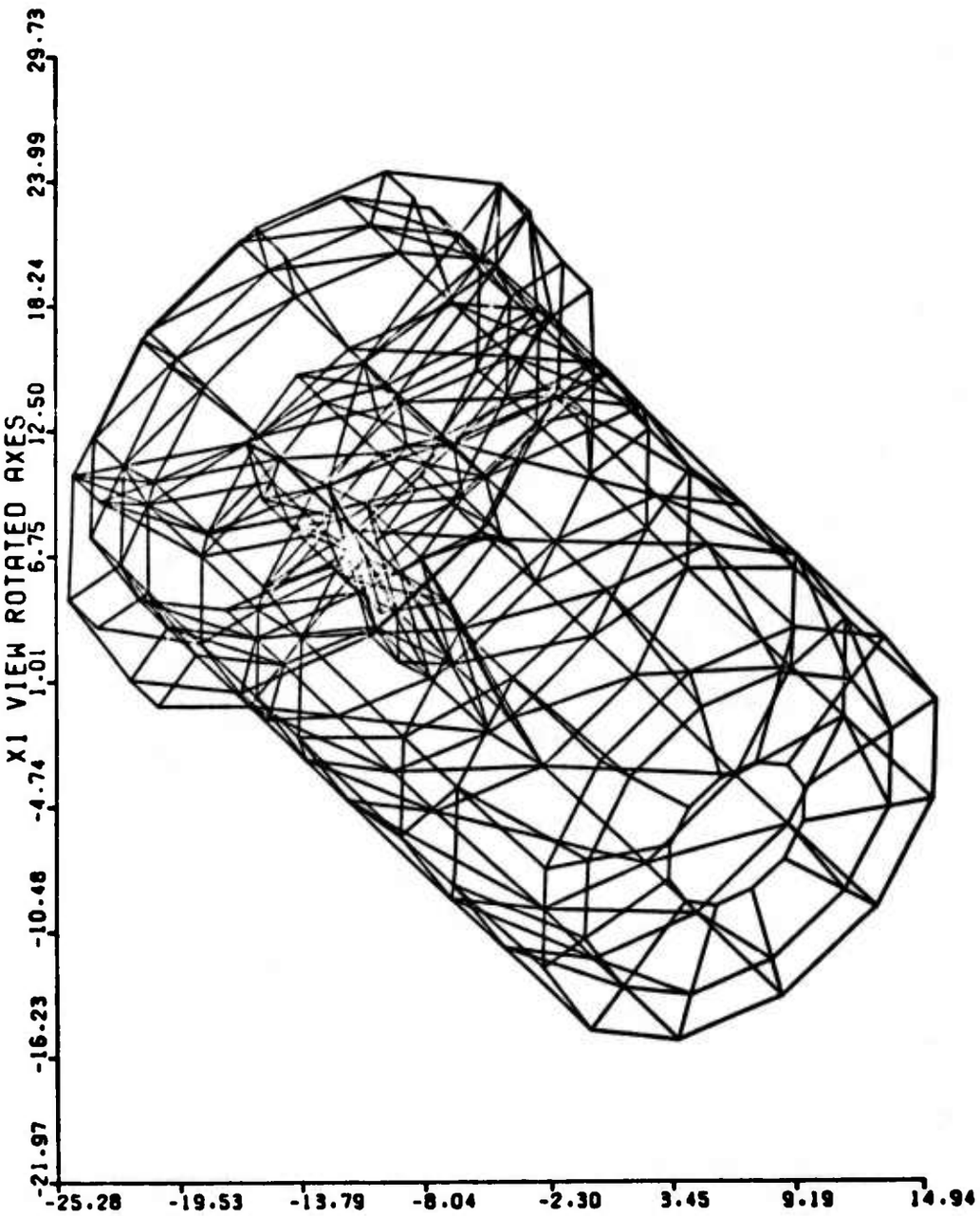

Figure A2.5.4. Computer plot of mathematical model for STARDYNE analysis of APT open port liner.

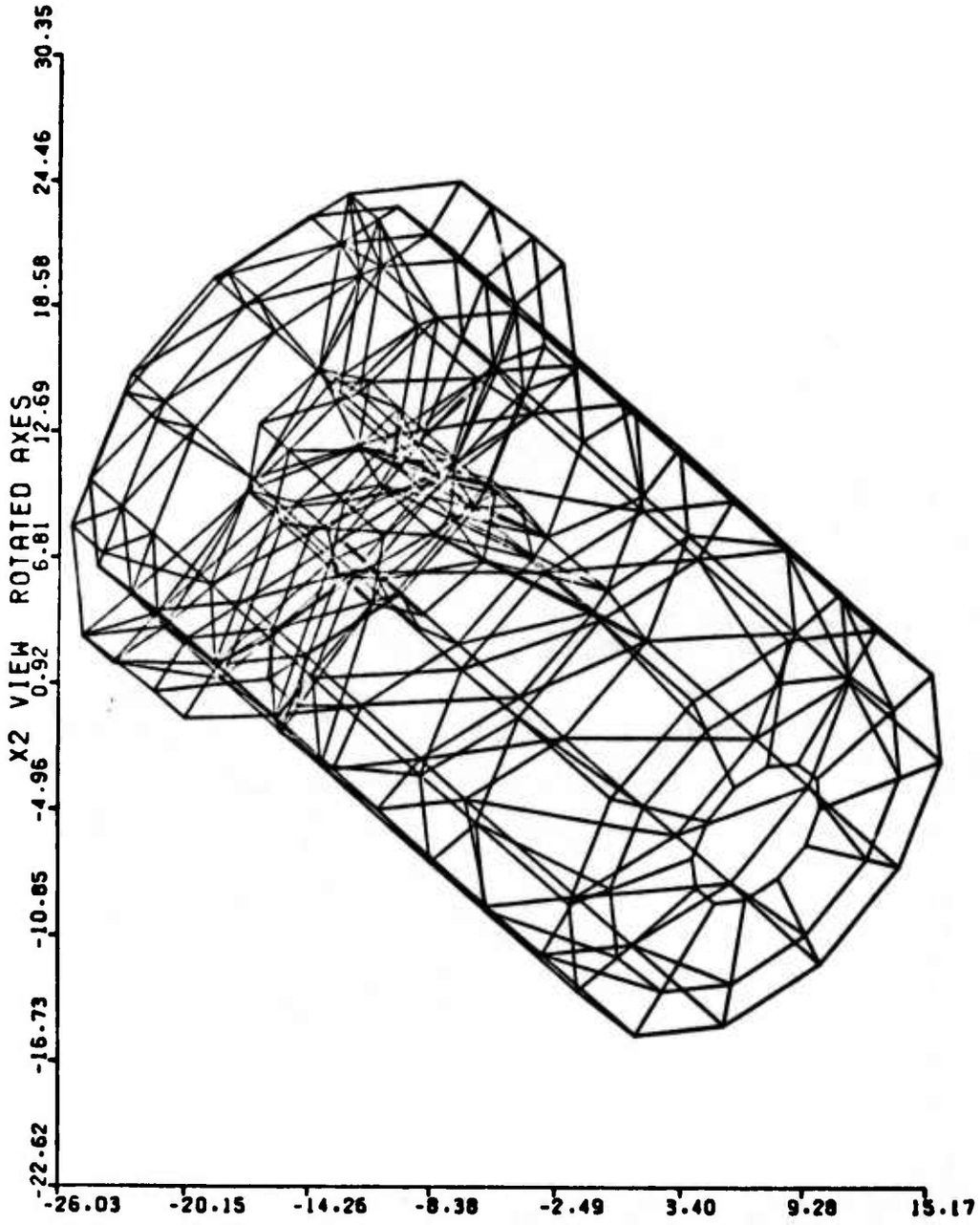

Figure A2.5.5. Computer plot of mathematical model for STARDYNE analysis of APT open port liner.

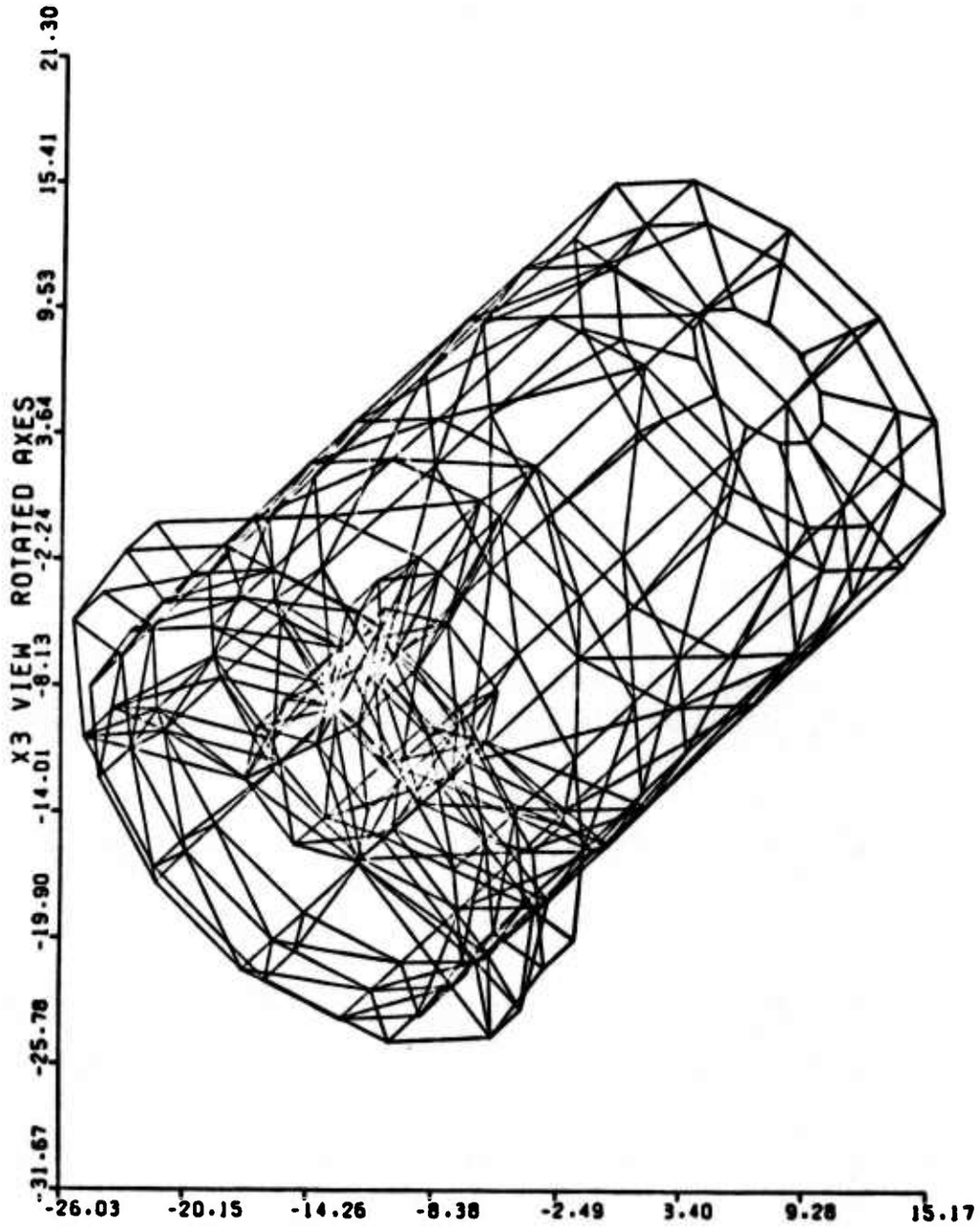

Figure A2.5.6. Computer plot of mathematical model for STARDYNE analysis of APT open port liner.

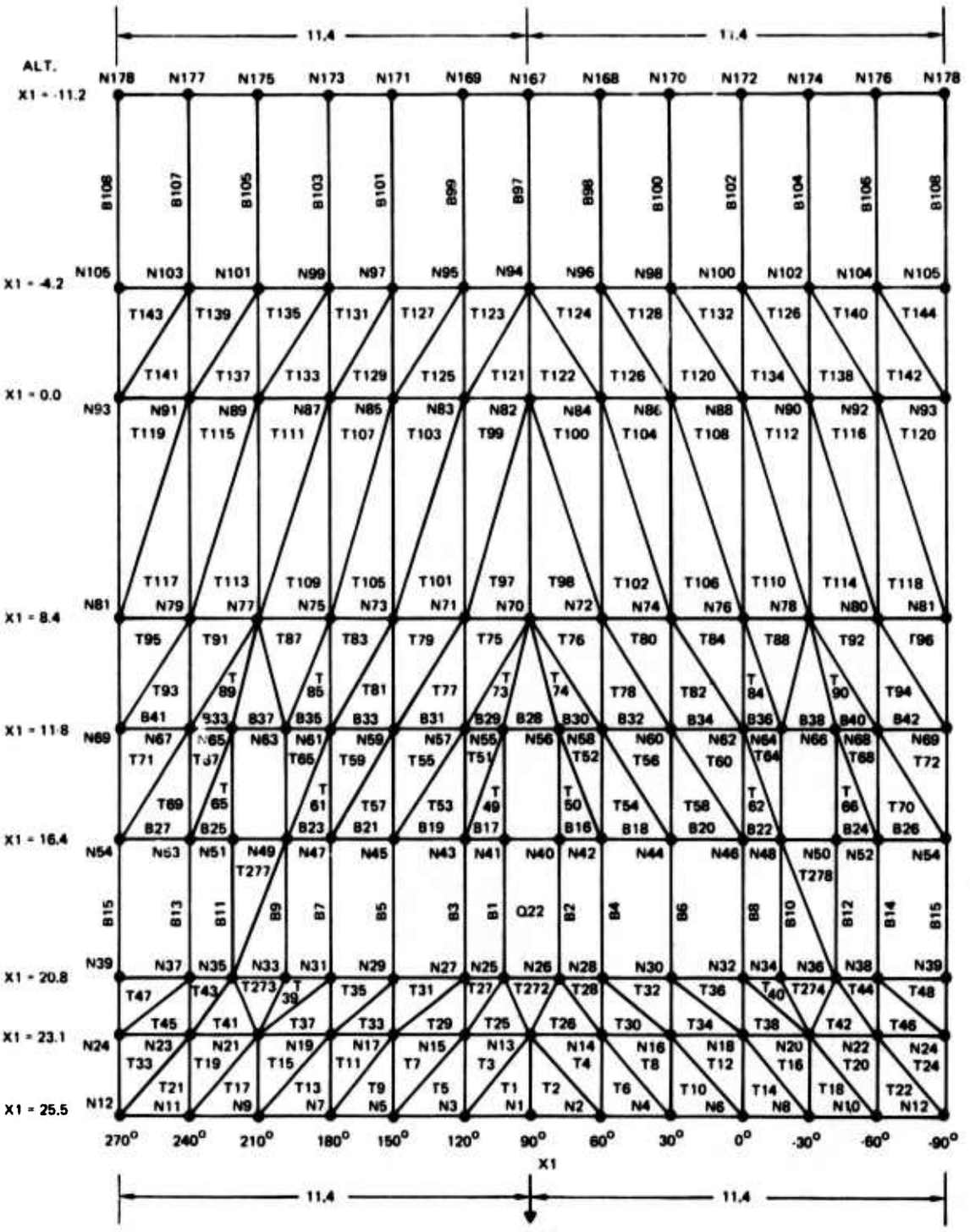

Figure A2.5.7. Mathematical model for STARDYNE analysis of APT open bit liner-unfolded aerofence and liner cylinder.

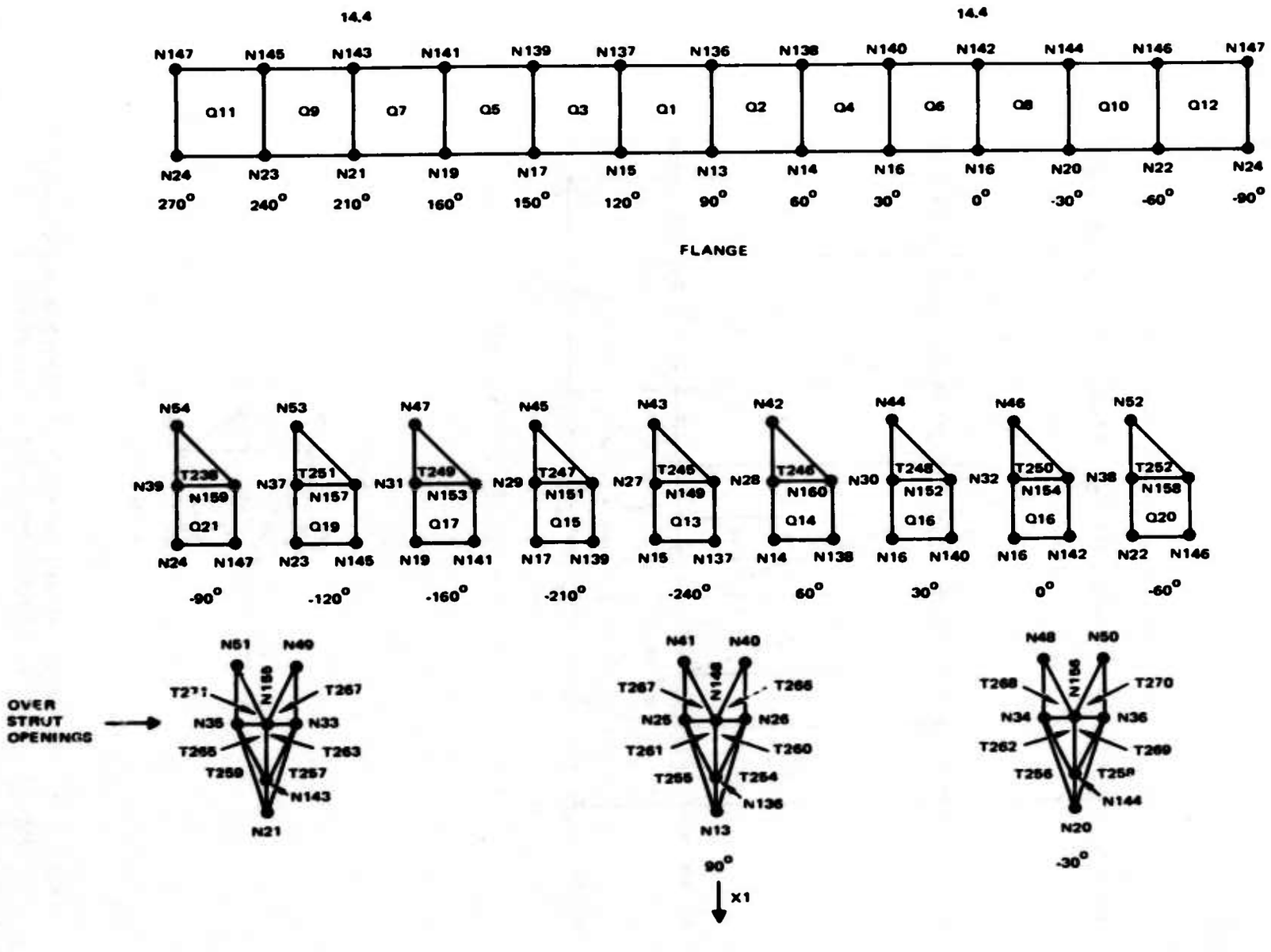

Figure A2.5.8. Mathematical model for STARDYNE analysis of APT open port liner-unfolded flange and flange gussets.

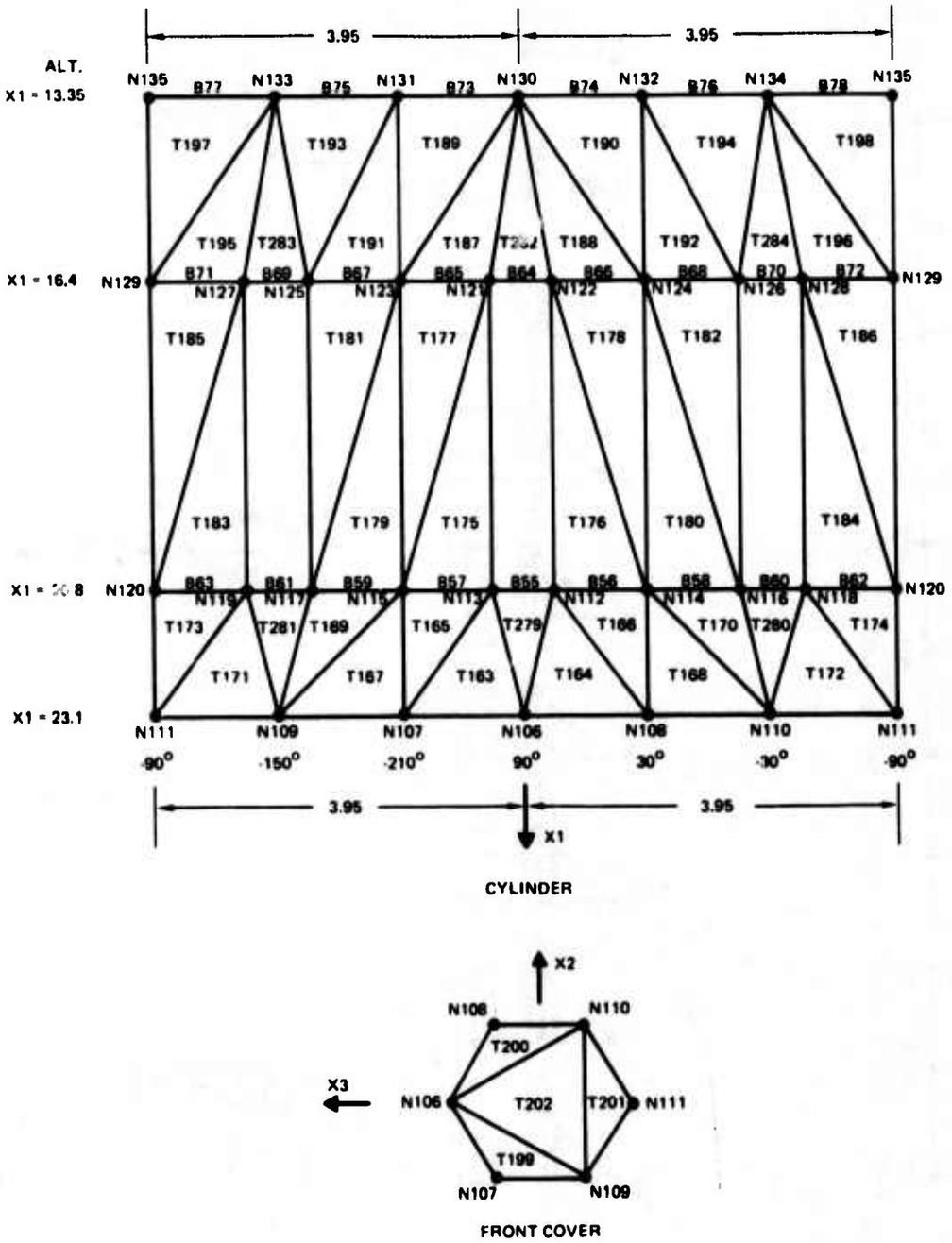

Figure A2.5.9. Mathematical model for STARDYNE analysis of APT open port liner-unfolded secondary mirror cover.

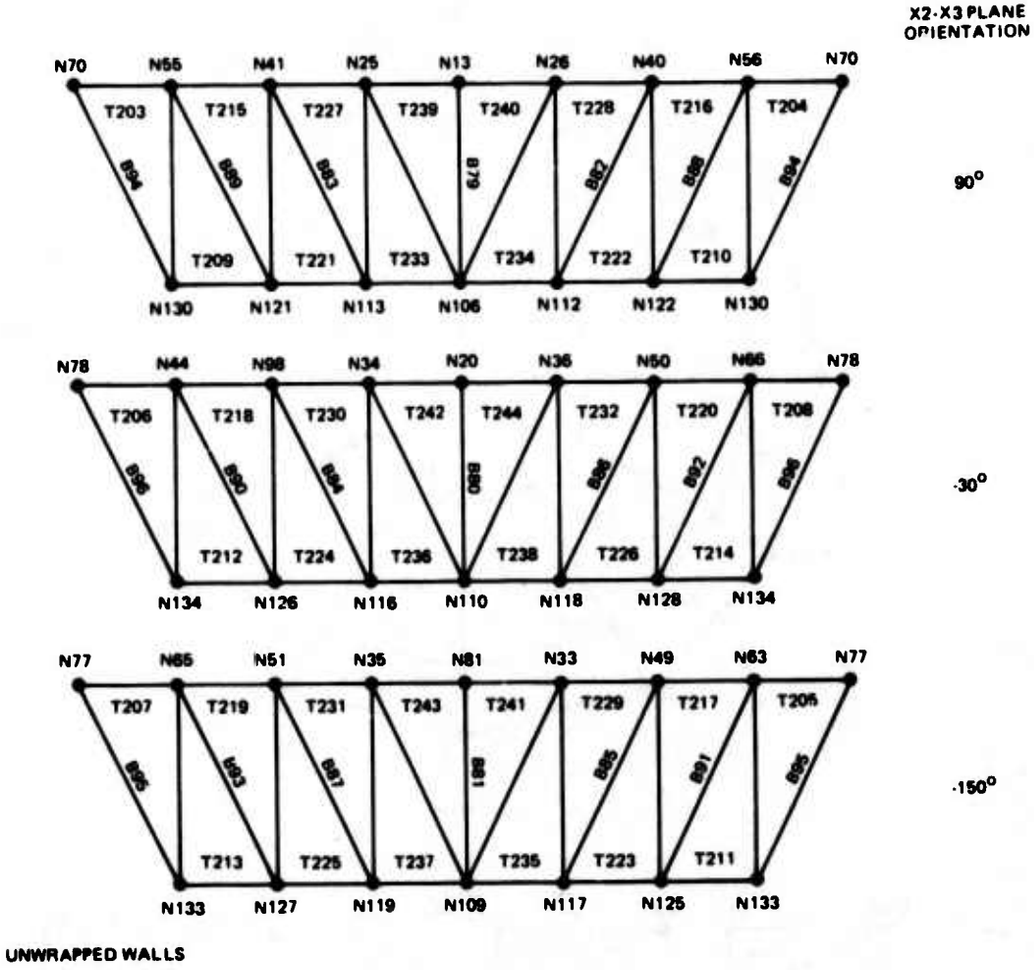

Figure A2.5.10. Mathematical model for STARDYNE analysis of open port liner-unfolded secondary mirror cover support struts.

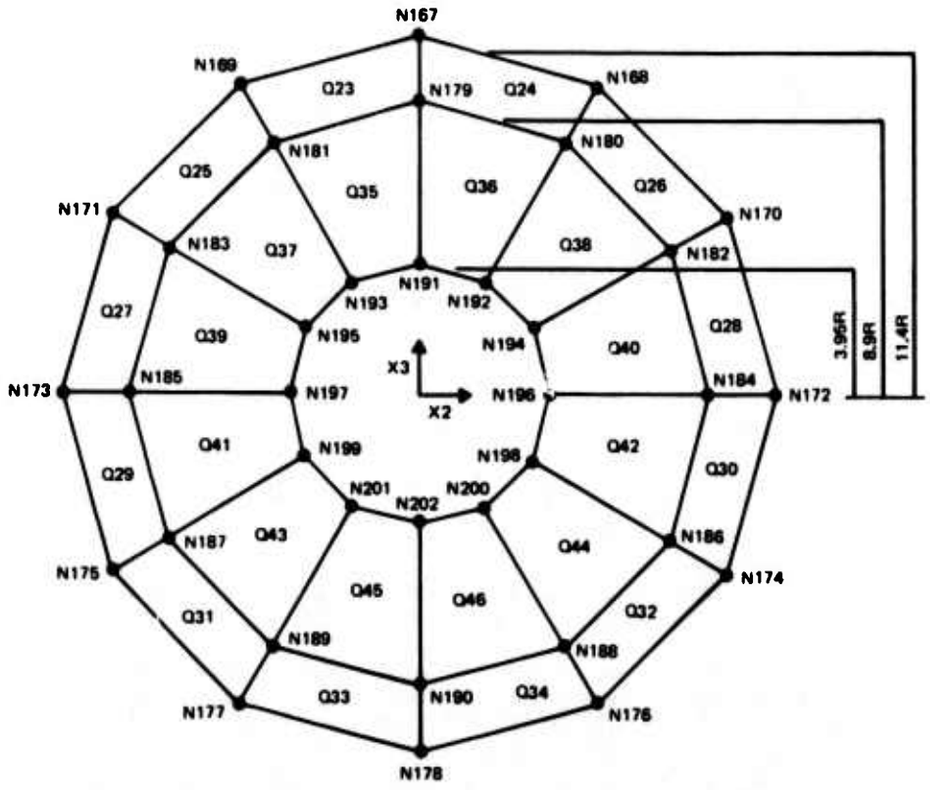

Figure A2.5.11. Mathematical model for STARDYNE analysis of APT open port liner-unfolded primary mirror cover and support straps.

TABLE A2.5.1. SCHEDULE OF APT OPEN PORT LINER STARDYNE MODEL BEAMS AND PLATES

Component	Material	Beams	Beam Property	Tri Plates	Quad Plates	Plate Thick
Aerofence	6061-T6 A1	-	-	T1-T24	-	0.064
Liner Cylinder						
Cylinder Plating	2024-T4 A1	-	-	T25-T144	Q22	0.125
Cylinder Plating	2024-T4 A1	-	-	T272-T278	-	0.125
Longitudinal Liner Vent Reinforcement Beams	2024-T4 A1	B1-B15	1	-	-	-
Circumferential Liner Vent Reinforcement Beams	2024-T4 A1	B16-B27	2	-	-	-
Circumferential Liner Strain Gage Beams	2024-T4 A1	B28-B54	3	-	-	-
Liner Flange						
Flange Plating	6061-T6 A1	-	-	-	Q1-Q12	0.500
Gusset Plating	6061-T6 A1	-	-	T245-T271	Q13-Q21	0.125
Secondary Mirror Cover						
Cylinder Plating	6061-T6 A1	-	-	T163-T198	-	0.125
Front Cover Plating	6061-T6 A1	-	-	T199-T202	-	0.125
Circumferential Strain Gage Beams	6061-T6 A1	B55-B78	3	-	-	-
Secondary Mirror Cover Support Struts						
Strut Plating	2024-T4 A1	-	-	T203-T244	-	0.062
Front Edge Beams	2024-T4 A1	B79-B81	4	-	-	-
Rear Edge Beams	2024-T4 A1	B94-B96	5	-	-	-
Radial Strain Gage Beams	2024-T4 A1	B82-B93	6	-	-	-
Primary Mirror	6061-T6 A1	-	-	-	Q23-Q46	0.312
Primary Mirror Support Straps	2024-Tr A1	B97-B108	7	T309-T320	-	0.125

TABLE A2.5.2. SCHEDULE OF BEAM SECTION PROPERTIES

BEAM PROPERTY 1

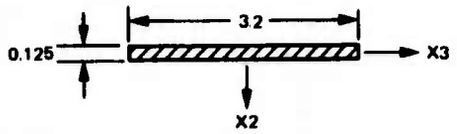

A = 0.4 IN^2
I2 = 0.341333 IN^4
I3 = 0.000521 IN^4
J = 0.002083 IN^4
SF2 = SF3 = 0.83

BEAM PROPERTY 2

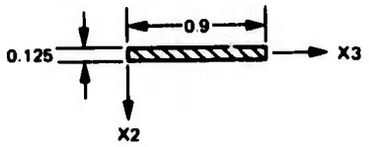

A = 0.1125 IN^2
I2 = 0.030375 IN^4
I3 = 0.000147 IN^4
J = 0.000586 IN^4
SF2 = SF3 = 0.83

BEAM PROPERTY 3

A = 0.012272 IN^2
I2 = 0.000012 IN^4
I3 = 0.000012 IN^4
J = 0.000024 IN^4
SF2 = SF3 = 0.901

BEAM PROPERTY 4

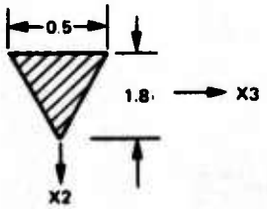

A2 = 0.45 IN^2
I22 = 0.00469 IN^4
I32 = 0.081 IN^4
J = 0.0106 IN^4
SF2 = SF3 = 0.87

BEAM PROPERTY 5

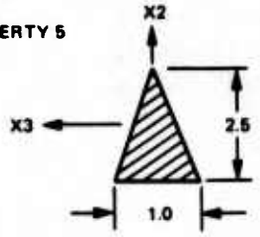

A = 1.25 IN^2
I2 = .0521 IN^4
I3 = 0.434 IN^4
J = 0.1116 IN^4
SF2 = SF3 = 0.87

BEAM PROPERTY 6

A = 0.003019 IN^2
I2 = 7.253E-7 IN^4
I3 = 7.253E-7 IN^4
J = 1.451E-6 IN^4
SF2 = SF3 = 0.901

BEAM PROPERTY 7

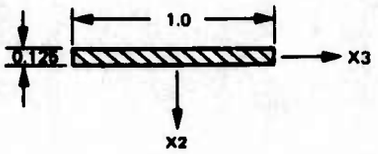

A2 = 0.125 IN^2
I2 = 0.0104 IN^4
I3 = 0.000163 IN^4
J = 0.000651
SF2 = SF3 = 0.901

APPENDIX 3

WEIBULL ANALYSIS OF APT ZnSe

AUTO ALIGNMENT INPUT WINDOW

IDC 277720.4/541

8 April 1974

The results of theoretical studies on the effect of nonuniform multiaxial stress fields encountered in simply-supported, uniformly loaded circular plates on the fracture of brittle materials are described. Derivations were carried out to determine the risk of rupture assuming the material obeyed the Weibull distribution function for volumetric flaw distribution.

The method has been used to predict the risk of rupture in the APT Zinc Selenide Auto Alignment Input Window for various pressures. The results of the analysis, using both the von Mises and maximum shear criteria for equivalent uniaxial stresses for multiaxial stress systems, is presented in Table 1.1.

The values of the Weibull parameters used in this analysis were derived by Dr. J. C. Wurst of the University of Dayton by performing a Weibull analysis on flexural strengths of 83 Raytheon CVD Zinc Selenide test bars obtained in four-point bending tests. The results of the test program are shown in Figure 1.1.

The applicable theory and GE 265 TimeSharing program listing, in XBASIC, are attached.

TABLE 1.1

WEIBULL ANALYSIS OF UNIFORMLY LOADED, SIMPLY-SUPPORTED CIRCULAR PLATE

PLATE RADIUS RO = 3.15
PLATE THICKNESS TO = .3
POISSON'S RATIO VO = .3
WEIBULL SHAPE PARAMETER M = 7.3
WEIBULL SCALE PARAMETER SO = 3545
WEIBULL LOCATION PARAMETER SU = O

PRESSURE	PLATE RELIABILITY VON MISES CRITERION	PLATE RELIABILITY MAX SHEAR CRITERION
1	1	1
2	1	1
3	1	1
4	1.	1.
5	.999999	.999999
6	.999998	.999997
7	.999994	.999992
8	.999983	.999978
9	.999961	.999949
10	.999916	.999889
11	.999831	.999778
12	.999681	.999581
13	.999428	.999249
14	.999018	.998711
15	.998376	.997868
16	.9974	.996587
17	.995956	.994691
18	.993868	.991954
19	.990914	.988083
20	.986814	.982718
21	.981226	.975415
22	.973735	.965646
23	.96385	.952792
24	.951006	.936151
25	.934565	.914951
26	.913831	.888385
27	.888082	.855653
28	.856603	.816041
29	.818754	.769015
30	.774047	.714342

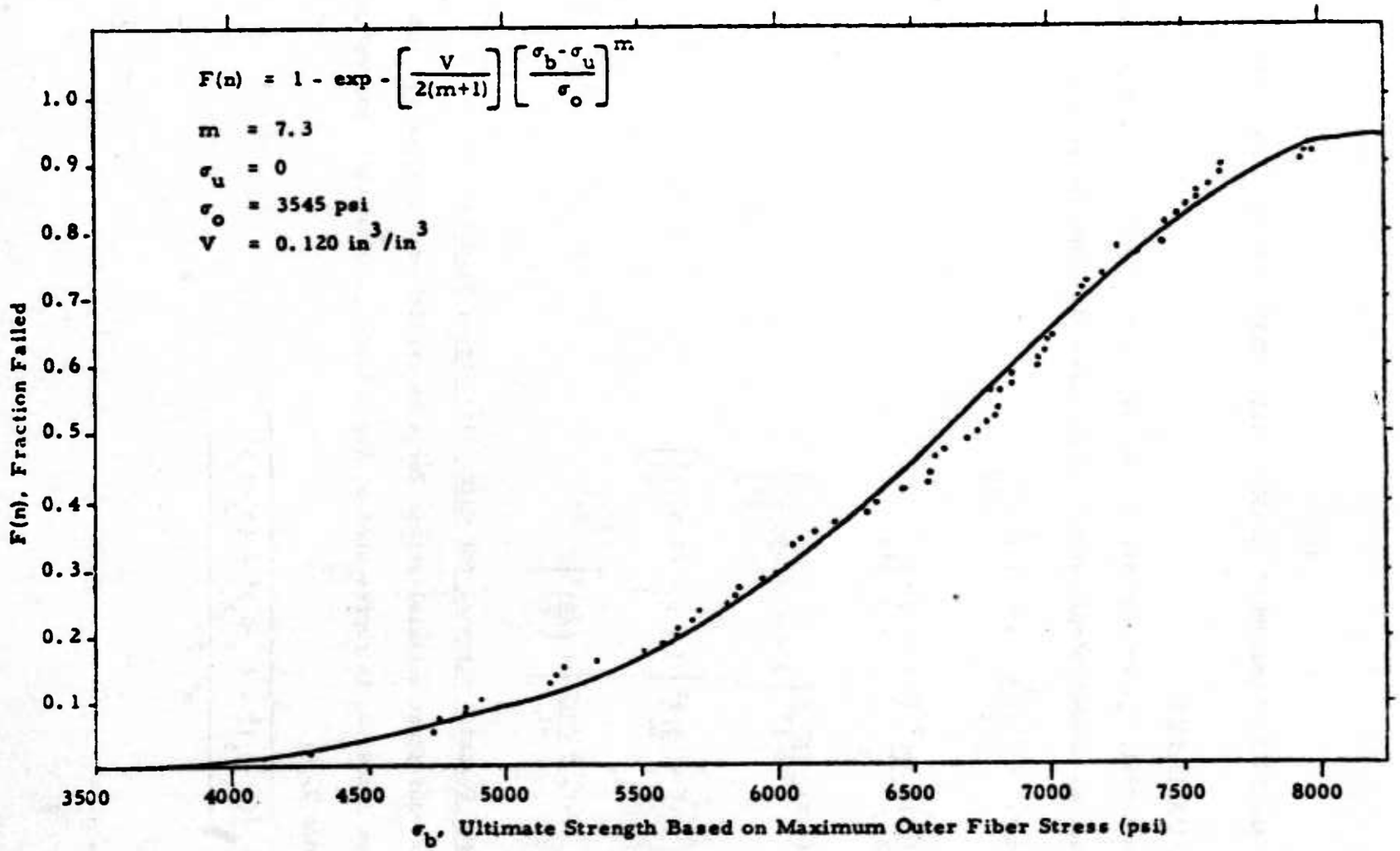

Figure 1.1. Weibull Cumulative Probability of Failure for 83 Zinc Selenide Four-Point Bend Test Bars.

THEORY

WEIBULL ANALYSIS OF UNIFORMLY LOADED, SIMPLY-SUPPORTED CIRCULAR PLATE

Stress Distribution

The radial, σ_r, tangential, σ_θ, and transverse shear , τ_{rz}, stresses in a uniformly loaded, simply-supported circular plate are (Reference 2):

1) $$\sigma_r(z,r) = \frac{3\ pR^2z}{4\ t^3}\ (3+\nu)\left(1-\frac{r^2}{R^2}\right)$$

2) $$\sigma_r\left(\frac{t}{2},r\right) = \frac{3pR^2}{8\ t^2}\ (3+\nu)\left(1-\frac{r^2}{R^2}\right)$$

3) $$\sigma_\theta\ (z,r) = \frac{3pR^2z}{4\ t^3}\left[3+\nu-(1-3\nu)\frac{r^2}{R^2}\right]$$

4) $$\sigma_\theta\left(\frac{t}{2},r\right) = \frac{3pR^2}{8t^2}\left[3+\nu-(1-3\nu)\frac{r^2}{R^2}\right]$$

5) $$\tau_{rz}\ (z,r) = \frac{3pr}{4t}\left[1-\left(\frac{2z}{t}\right)^2\right]$$

Equivalent Uniaxial Stresses for Multiaxial Stress Systems

The equivalent uniaxial stress for a multiaxial stress sytem per the von Mises criterion is represented by the following mathematical expression (Reference 3, 4):

6) $$\sigma = \sqrt{\frac{(\sigma_1-\sigma_2)^2+(\sigma_1-\sigma_3)^2+(\sigma_2-\sigma_3)^2}{2}}$$

where

7) $$\sigma_1 = \frac{\sigma_r}{2} + \tau$$

8) $$\sigma_2 = \frac{\sigma_r}{2} - \tau$$

9) $\sigma_3 = \sigma_\theta$

10) $\tau = \sqrt{\frac{\sigma_r^2}{4} + \tau_{rz}^2}$

The equivalent uniaxial stress for a multiaxial stress system per the maximum shear criterion is the absolute value of the largest difference in principal stresses, that is, (Reference 3, 4):

11) $\sigma = \text{Max}\,(|\sigma_1 - \sigma_2|, |\sigma_1 - \sigma_3|, |\sigma_2 - \sigma_3|)$

Analysis of Fracture Reliability Using Weibull Theory

For a uniaxial stress field induced by pure bending in a homogeneous isotropic material, governed by volumetric flow distribution, the percent failed, F(n), as a function of maximum outer fiber tensile stress, σ, is given by the Weibull equation (Reference 5):

12) $F(n) = 1 - e^{-B}$

where

13) $B = \frac{V}{2(m+1)} \left(\frac{\sigma - \sigma_u}{\sigma_o}\right)^m$

is the risk of rupture and

m = shape parameter or flaw density exponent

σ_u = location parameter or zero probability strength

σ_o = scale parameter

V = stressed volume

In a test program conducted by Dr. J. C. Wurst of the University of Dayton, the flexural strength of small zinc selenide test bars were measured in carefully

conducted four-point bending tests (Reference 6). On the basis of these tests, the strength of Raytheon CVD zinc selenide was characterized in terms of percent-failed as a function of maximum, outer fiber, tensile stress through Weibull Analysis. Figure 1 is a Weibull plot of flexural strength data for a set of 83 samples. For this set of 83 samples, the values of Weibull parameters were as follows:

$m = 7.3$

$\sigma_u = 0$

$\sigma_o = 3545$ psi

$V = 0.12$ in^3

For a uniformly loaded, simply-supported circular plate, the cross-section at any radius r is in a state of pure bending if the transverse shear stress can be neglected, and the risk of rupture in the infinitesimal volume, $2\pi rtdr$, becomes:

$$14) \quad B = \frac{1}{2(m+1)} \left[\frac{\sigma(\frac{t}{2}, r) - \sigma_u}{\sigma_o} \right]^m 2\pi rtdr$$

where $\sigma(\frac{t}{2}, r)$ is the equivalent uniaxial outer fiber stress at radius r. The risk of rupture in the entire plate volume then becomes

$$15) \quad B = \frac{1}{2(m+1)} \int_0^R \left[\frac{\sigma(\frac{t}{2}, r) - \sigma}{\sigma_o} \right]^m 2\pi rtdr$$

REFERENCES

1. B.S. Leo, "Thermal and Stress Analyses of the APT ZnSe Auto Alignment Input Window", HAC IDC 277740.1/179, 19 March 1973, Hughes Aircraft Company, Culver City, California.

2. S. Timoshenko, Theory of Plates and Shells, 2nd ed, McGraw-Hill, New York, 1959.

3. R. E. Peterson, Stress Concentration Design Factors, John Wiley & Sons, New York, 1953.

4. T.H. Lin, Theory of Inelastic Structures, John Wiley & Sons, New York, 1968.

5. N.A. Weil and I.M. Daniel, "Analysis of Fracture Probabilities in Nonuniformly Stressed Brittle Materials," Journal of the American Ceramic Society, V47, N6.

6. J.C. Wurst, "Thermal, Electrical, and Physical Property Measurements of Laser Window Materials," QPR5, June 1973 and QPR6, Nov 1973, Contract F33615-72-C-1257, Air Force. Material Laboratory, Wright-Patterson AFB, Ohio.

```
WEIBUL

1  READ RO,TO,VO,MO,OO,UO
5  PRINT "WEIBULL ANALYSIS OF UNIFORMLY LOADED SIMPLY-SUPPORTED CIRCULAR PLATE"
10 PRINT
15 PRINT "PLATE RADIUS RO = "RO
20 PRINT "PLATE THICKNESS TO = "TO
25 PRINT "POISSON'S RATIO VO = "VO
30 PRINT "WEIBULL SHAPE PARAMETER M = "MO
35 PRINT "WEIBULL SCALE PARAMETER SO = "OO
40 PRINT "WEIBULL LOCATION PARAMETER SU = "UO
45 PRINT
50 PRINT "PRESSURE", "PLATE RELIABILITY", "PLATE RELIABILITY"
55 PRINT "  ", "VON MISES CRITERION" , "MAX SHEAR CRITERION"
60 PRINT
65 FOR PO = 1 TO 30
70 B(1) = B(2) = 0
75 FOR R = 0.1*RO TO RO STEP .01*RO
80 S1 = 3/8*PO*(RO/TO)^2*(3 + VO)*(1-(R/RO)^2)
85 S2 = 0
90 S3 = 3/8*PO*(RO/TO)^2*(3 + VO - (1+3*VO)*(R/RO)^2)
95 S(1) = SQR(S1^2 +S2^2 +S3^2-S1*S2-S1*S3-S2*S3)
100 S4 = ABS(S1-S2)
105 S5 = ABS(S1-S3)
110 S6 = ABS(S2-S3)
115 S(2) = S4
120 IF S(2)>S5 THEN 130
125 S(2) = S5
130 IF S(2)>S6 THEN 140
135 S(2) = S6
140 FOR J = 1 TO 2
145 B(J) = B(J) + .062831853*RO*TO*R/2/(MO + 1)*(1-UO/S(J))*((S(J)-UO)/OO)^MO
150 NEXT J
155 NEXT R
160 PRINT PO,1/EXP(B(1))," ",1/EXP(B(2))
165 NEXT PO
170 DATA 3.15,.3,.3,7.3,3545,0
175 END
```

APPENDIX 4

STARDYNE STATIC ANALYSIS

OF THE APT PROTECTIVE DOOR

IDC 271222/399

6 August 1973

Reference: IDC 271222/265, "Structural Analysis of the APT System", by R. E. Holman, dated 5 February 1973

The attached report presents the results of an analysis of the protective door or eyelid which covers the Airborne Pointer and Tracker (APT) telescope window. MRI's STARDYNE Structural Analysis System of computer programs was used to evaluate the deflections and stresses induced by an 8 psi internal pressure on a 3/8 inch thick solid 2024-T4 aluminum eyelid.

The results of the analysis indicate that the eyelid can satisfactorily withstand a proof pressure of 1.5x8 = 12 psi without permanent set and a burst pressure of 3x8 = 24 psi without rupture. Maximum deflection normal to the eyelid surface for the 8 psi peak operating pressure was 0.12 inches. The minimum margin of safety was 0.08 for the mounting screw on the outer corner.

These results are predicated on a design with 160 ksi steel ¼-28 screws replacing the existing 10-32 screws and an additional ¼-28 screw added at each corner.

STRUCTURAL ANALYSIS OF THE APT PROTECTIVE DOOR

INTRODUCTION AND SUMMARY

This report presents the results of an analysis of the protective door or eyelid which covers the Airborne Pointer and Tracker (APT) telescope window. MRI's STARDYNE Structural Analysis System of computer programs was used to evaluate the deflections and stresses induced by an 8 psi internal pressure on a 3/8 inch thick solid 2024-T4 aluminum eyelid.

The results of the analysis indicate that the eyelid can satisfactorily withstand a proof pressure of 1.5x8 = 12 psi without premanent set and a burst pressure of 3x8 = 24 psi without rupture. Tables I and II present stress levels and deflections for critical sections of the eyelid. Maximum deflection normal to the eyelid surface for the 8 psi peak operating pressure was 0.12 inches. The minimum margin of safety was 0.08 for the mounting screw on the outer corner.

These results are predicated on a design with 160 ksi steel ¼-28 screws replacing the existing 10-32 screws and an additional ¼-28 screw added at each corner.

METHOD OF ANALYSIS

The eyelid was analyzed using MRI's STARDYNE Structural Analysis System of computer programs, available on CDC's 6600 CYBERNET System. It is a batch processing computer program that employs the finite element method wherein the three-dimensional continuous structure is represented mathematically by a system of finite elements interconnected at a finite number of nodal points where loads are applied and displacements are calculated. The finite element library includes beams, plates, cubes, tetrahedrons, rigid links, springs, and direct stiffness additions. The program uses the direct stiffness method to synthesize the elemental and system stiffness matrices and the normal mode method to determine dynamic responses for transient, sinusoidal, random, and acoustic excitation.

DESCRIPTION OF MODEL

The finite element, lumped mass, mathematical model of the eyelid is shown in Figures 1 through 6. This model consists of 119 nodes, 50 beams, 62 rigid links, 120 triangular plates, and 12 direct stiffness additions. Advantage was taken of symmetry to model only one-half of the structure. The APT Outer Elevation Gimbal model (reference) was cut at the vertical plane of symmetry with the appropriate restraints applied ($\delta_y = \vartheta_x = \vartheta_z = 0$). The resulting stiffness matrix was reduced to that for the ring of odd-numbered nodes, N99 through N121. This ring of nodes then formed the base structure to which the Eyelid structure was attached.

A concentric ring of nodes, connected to the base structure by rigid members, represents the eyelid bearing. A third concentric ring of nodes was used to model the ring carried on the eyelid bearing and to which the eyelid is attached. The only nodal restraints imposed on the Eyelid model were those required to maintain $\vartheta_y = \vartheta_x = \vartheta_z = 0$ at the plane of symmetry.

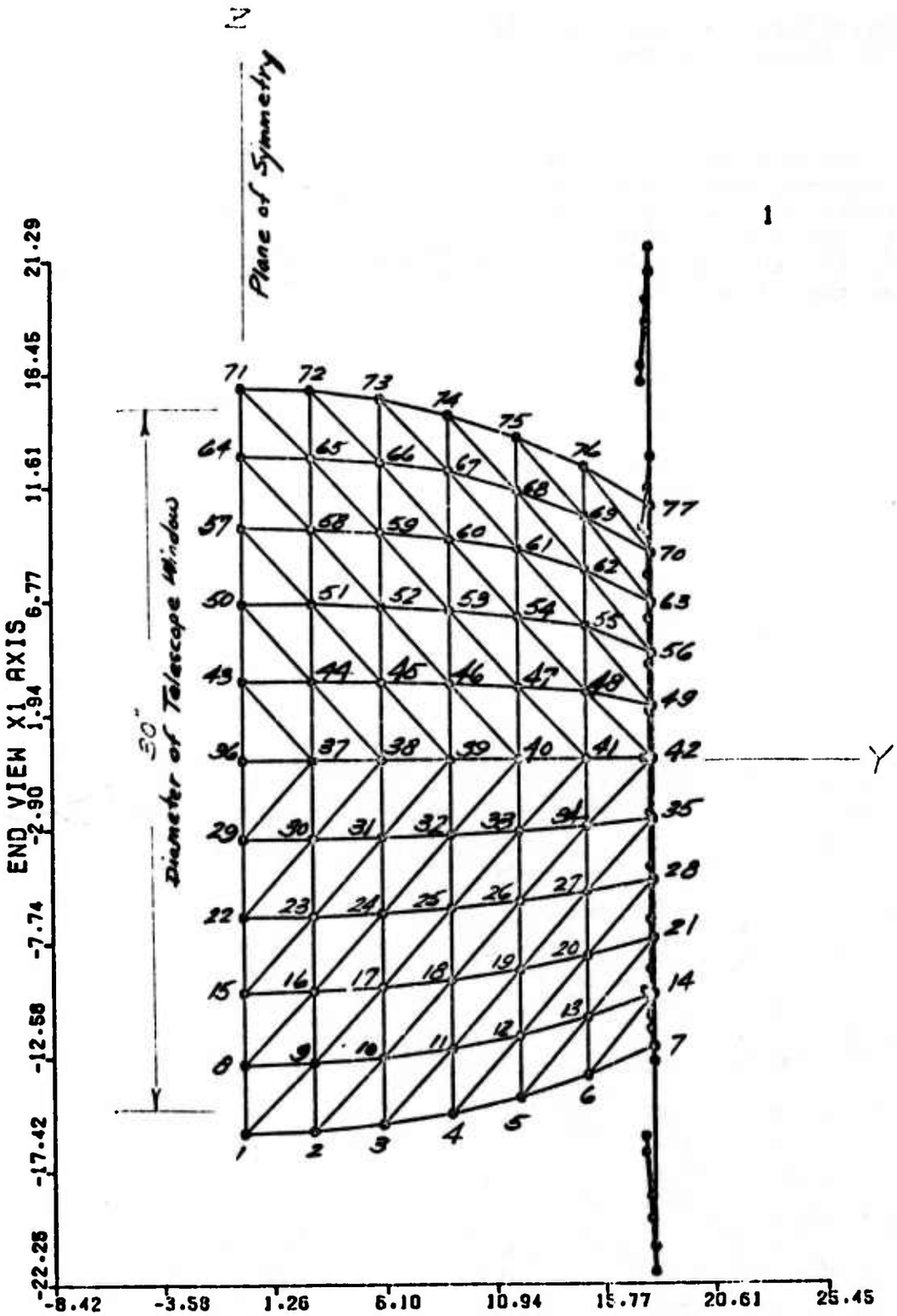

FIGURE 1

Math Model for STARDYNE Analysis of the APT Eyelid Structure (Nodal Point Numbers Shown)

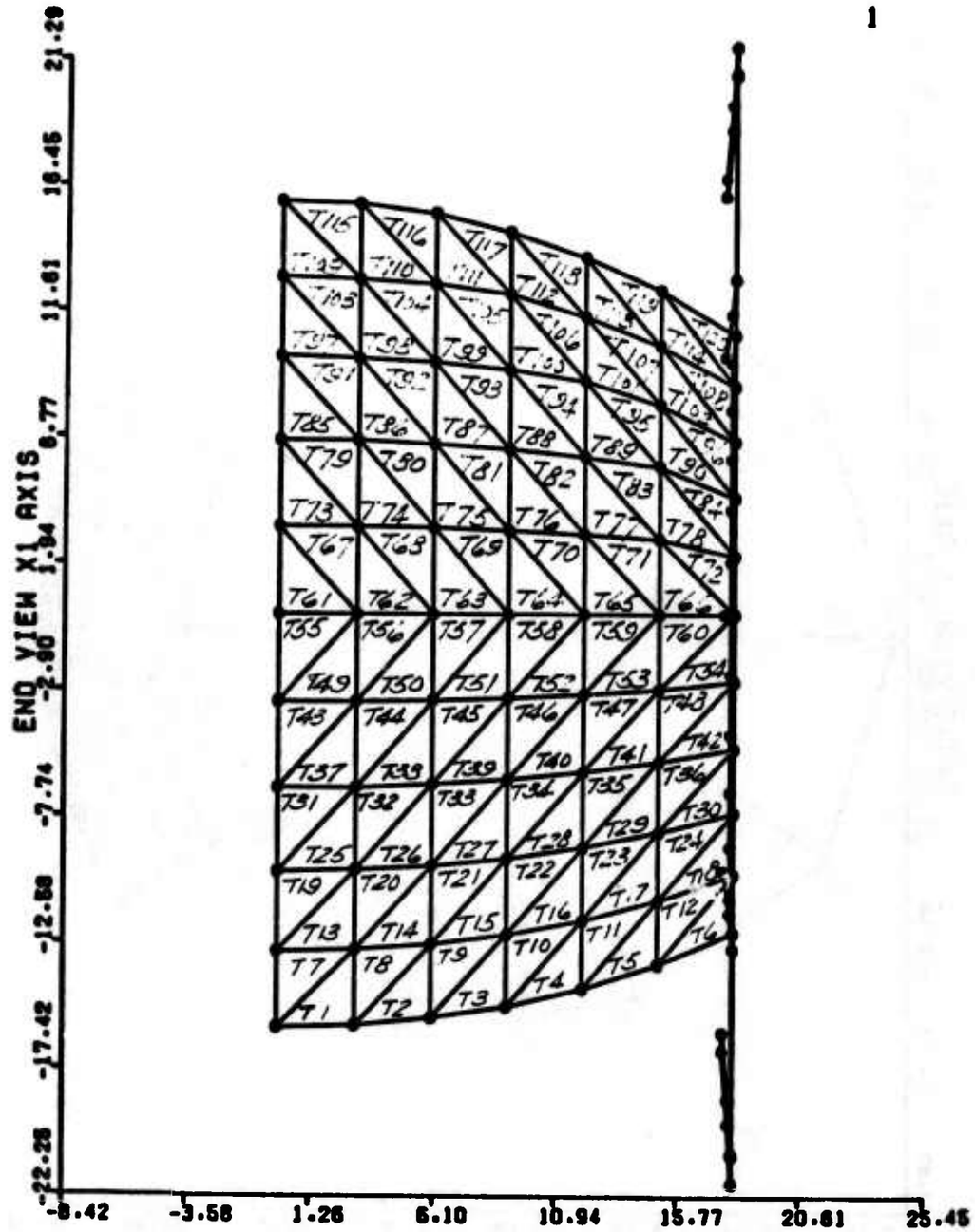

FIGURE 2

Math Model for STARDYNE Analysis of the
APT Eyelid Structure (Triangular Plate Elements Shown)

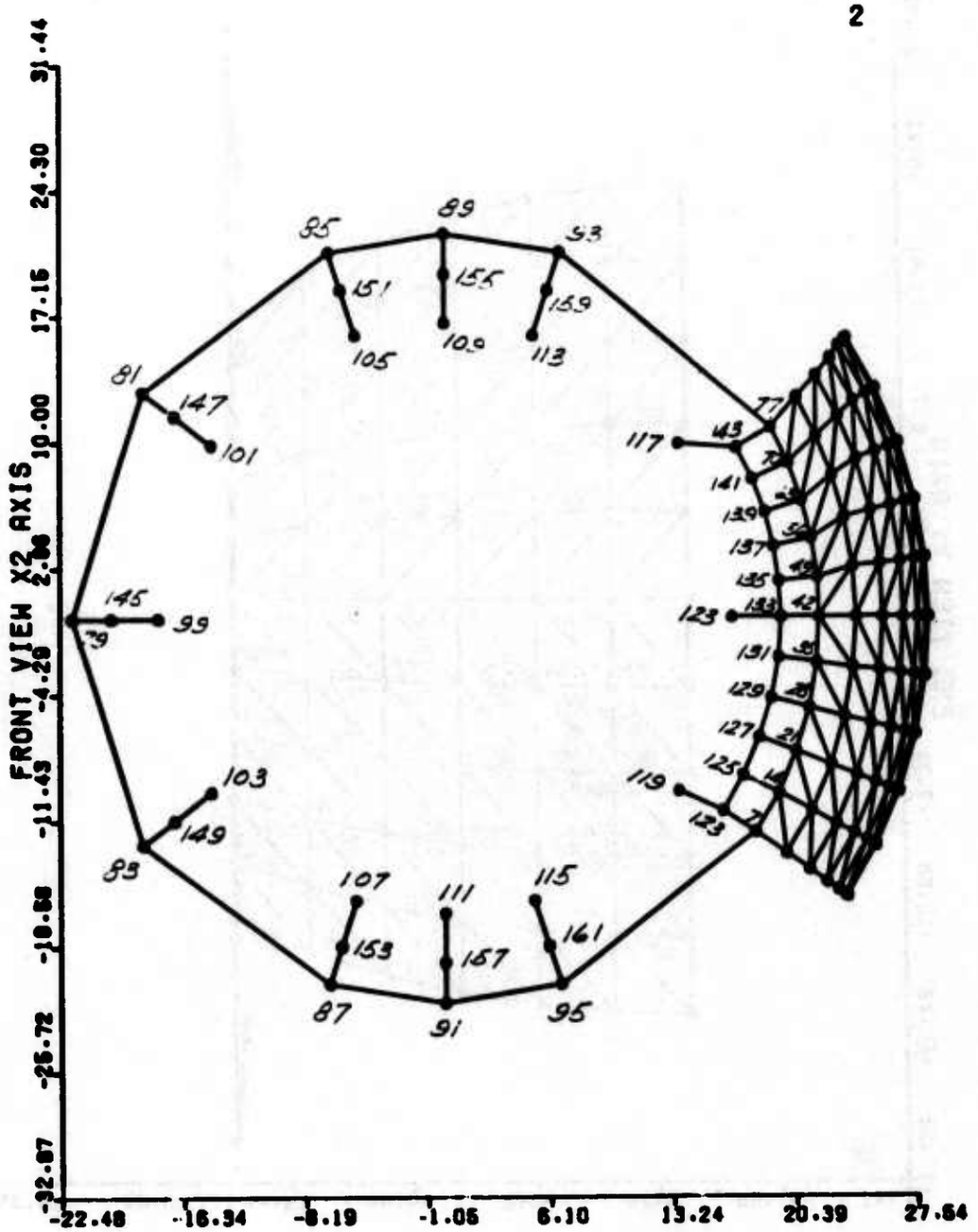

FIGURE 3

Math Model for STARDYNE Analysis of the APT Eyelid Structure (Nodal Point Numbers Shown)

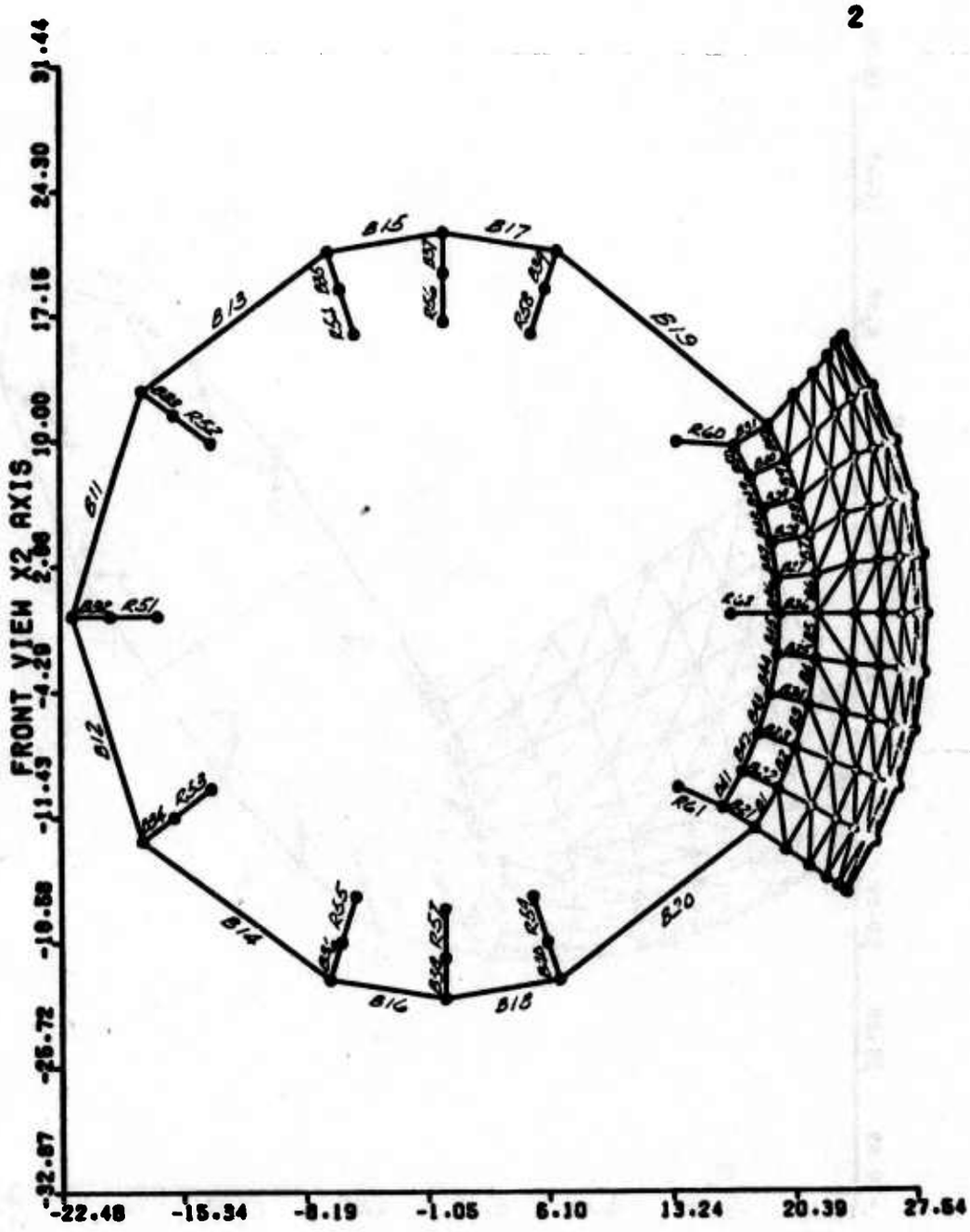

FIGURE 4

Math Model for STARDYNE Analysis of the APT Eyelid Structure (Beam Elements Shown)

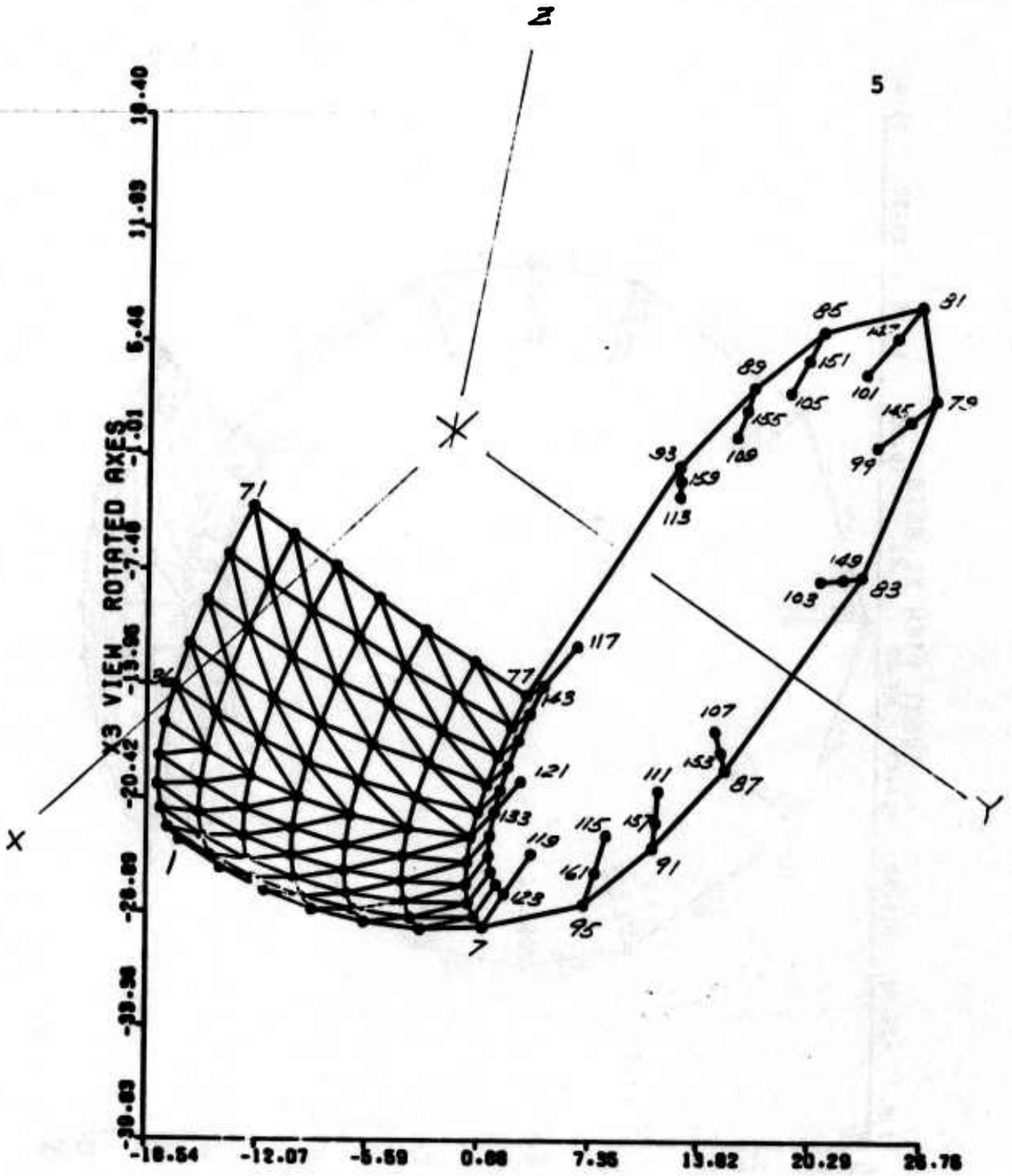

FIGURE 5

Math Model for STARDYNE Analysis of the
APT Eyelid Structure (Nodal Point Numbers Shown)

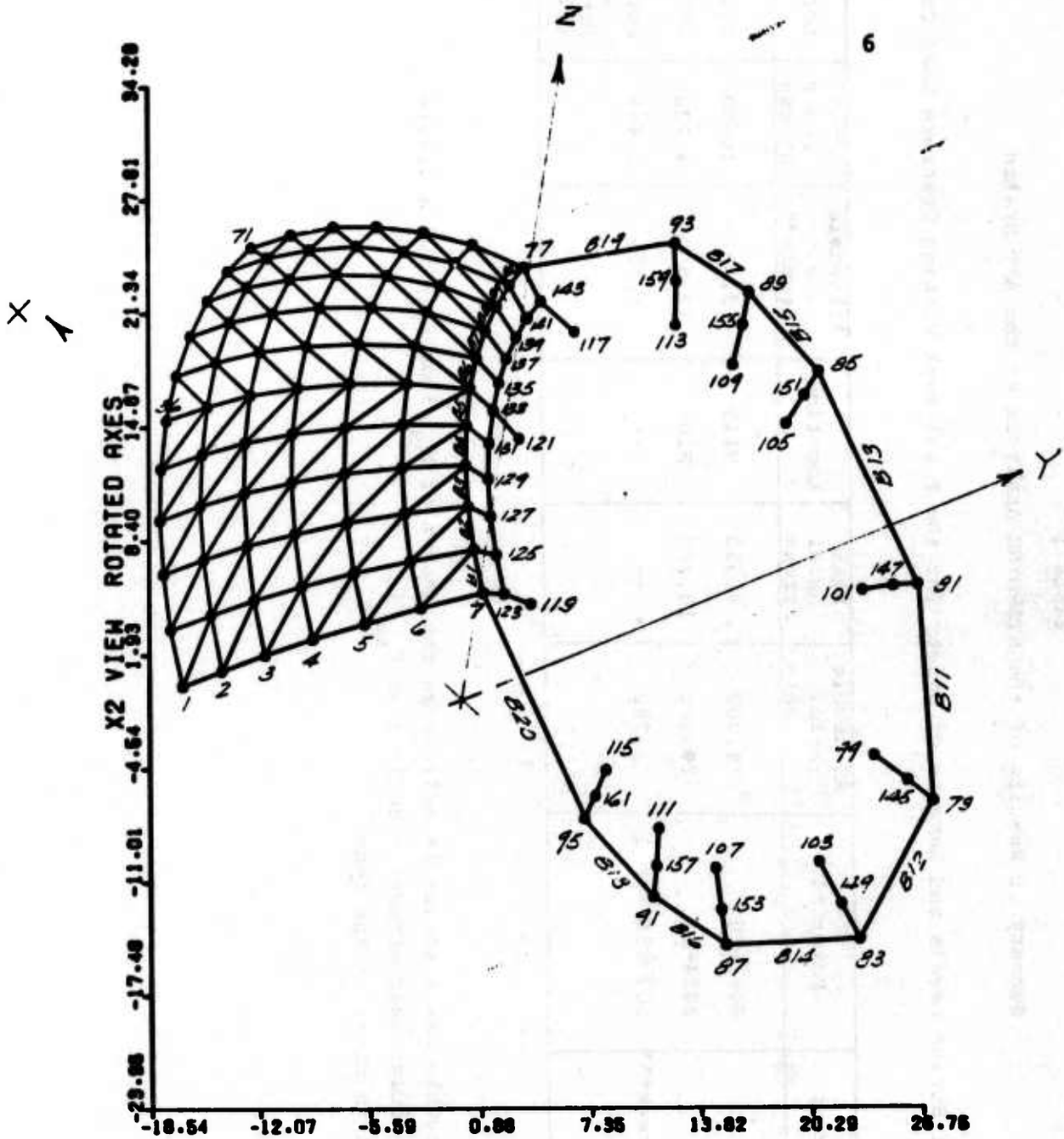

FIGURE 6

Math Model for STARDYNE Analysis of the
APT Eyelid Structure (Nodal Point Numbers Shown)

TABLE I

Summary of Results of the STARDYNE Analysis of the APT Eyelid

Critical Stress Levels and Margins of Safety for the 8 psi Peak Working Pressure Load Condition

Element Group	Material	Allowable Axial Stress*	Peak Axial Stress	Location	Allowable Shear Stress**	Peak Shear Stress	Location	M.S.
T1-T120	6061-T6	14,000	8,333	T119	9,000	4,000	T119	+.35
B1-B20	2024-T4	20,000	10,483	B10	12,000	4,230	B10	+.58
Mounting Screws***	160 KSI Steel	1,780	--	--	1,553	1,441	Corner of Eyelid (T120)	+.08

* The allowable axial stress is defined as the lesser of $F_{tu}/3$ or $F_{ty}/(1.5 \times 1.15)$.

** The allowable shear stress is defined as $F_{su}/3$.

*** Modified as noted in the text.

TABLE II

Summary of Results of the STARDYNE Analysis of the APT Eyelid

Critical Deflections for the 8 psi Peak Working Pressure Load Condition

Node Number	Deflection Normal to Eyelid Surface (Inches)	Rotation About Axis Tangent to Surface in X-Z Plane (Radians)	Y-Axis Deflection (Inches)
N1	.1081	.0	.0
N15	.0621	.0	.0
N36	.0458	.0	.0
N57	.0695	.0	.0
N71	.1236	.0	.0
N4	.0548	.0116	-.0153
N18	.0339	.0051	-.0056
N39	.0315	.0029	-.0029
N60	.0389	.0057	-.0062
N74	.0464	.0125	-.0147
N7	.0063	-.0023	-.0227
N21	.0021	-.0017	-.0216
N42	.0022	-.0013	-.0216
N63	.0020	-.0017	-.0231
N77	.0067	-.0023	-.0244

APPENDIX 5

APT OPEN PORT THERMAL ANALYSIS

SUMMARY

This is a study to determine the thermal response of various components within the APT turret subsequent to opening the window port. An attempt to bracket the response was made for three flight conditions - sea level hot, sea level cold, and 31,000 ft. cold. Components with large surface area/mass ratios, i.e., cylindrical liner, secondary mirror cover, have rapid thermal responses, whereas the other components have a notably slower response.

INTRODUCTION

Components in the APT ball are, during flight, exposed to the ambient when the port is open and the thermal response of each varies with respect to location, shape and physical properties. The purpose of this study was to determine the boundaries within which the thermal response of a sensitive component will lie since no convective heat transfer values are presently available for the interior of the ball.

ANALYSES

The following three cases were studied:

Case 1. Sea level hot, mach number = 0.5, temp = 103°F.
2. Sea level cold, mach number = 0.5, temp = -60°F
3. 31,000 ft. cold, mach number = 0.87, temp = -85°F

The components in the ball were divided into 23 thermal nodes and solution for Fourier's equation

where:

$$\frac{q'''}{\rho c_p} + \nabla^2 t = \frac{1}{\alpha}\frac{\partial t}{\partial \tau} \qquad (1)$$

q''' = heat generation per unit volume
ρ = density
c_p = specific heat capacity
t = temperature
τ = time
α = diffusivity

was obtained at each node by using HAC's CINDA-3G thermal program which solves Eq. (1) by the finite difference method.

Reliable data on convective heat transfer coefficients within cavities such as the APT ball are not reported in the literature. Therefore, it was decided to bracket the probable values by making assumptions with respect to flow patterns.

At one extreme, values representative of heat transfer coefficients obtainable under free convection conditions was used. The equation used, from Ref. 1, was applied to all surfaces where no direct airflow would occur, i.e., primary mirror, tracker imager, beam expander housing, and in the second case to all surfaces as a lower limit.

$$\bar{h} = 0.3\ (\Delta T)^{1/4} \qquad (2)$$

$\bar{h}$ = average heat transfer coefficient
ΔT = temperature difference between air and surface

The other extreme is represented by a condition where air flowed through the turret as if it was a duct open at both ends. Coefficients were calculated based on the particular surface geometry, air velocity within the duct was taken as that of the airplane speed.

These high coefficients were applied to those surfaces within the cylindrical liner, i.e., strut covers, liner, secondary mirror covers.

The front section of the secondary mirror cover was taken as a disc perpendicular to the air stream, film coefficient from Ref. 2. Aluminum strut covers were considered as flat plates parallel to the airflow, Ref. 3. The other surfaces are cylindrical and the tubular flow relations were used, Ref. 3.

Values of representative film coefficients under the three flight conditions analyzed are listed in Table 1. These values were applied in conjunction with Eq. (1) to obtain transient temperature responses of the components.

Internal air temperatures are external static where the low convective coefficients are used, and stagnation temperature where the high values are used.

The components of interest were:

1. Steel struts
2. Beam expander housing
3. Primary mirror
4. Cylindrical liner
5. Tracker/Imager body
6. Secondary mirror cover

Initial conditions were calculated for each case by a steady state analysis with internal air at 70°F and natural convection, and air external environment based on the flight condition.

RESULTS

Results of the analysis are shown in Figures 1 - 18, which show component temperature range as a function of time from opening the port. It is seen from Figs. 16 and 18 that the cylindrical liner and secondary mirror cover have short thermal responses due to their high surface to weight ratio. The other components have a notably slower response.

Table 1 - Heat Transfer Coefficients h ($^{BTU}/_{hr\ ft^2 °F}$)

	Surface	Condition: Sea Level Hot Atm h-High	Sea Level Hot Atm h-Low	Sea Level Cold Atm h-High	Sea Level Cold Atm h-Low	31,000 ft Cold Atm h-High	31,000 ft Cold Atm h-Low
1.	Secondary Mirror Cover, Disc	22	.7	21	.8	14	.5
2.	Strut Covers	84	.7	88	.8	50	.5
3.	Cylindrical Liner	50	.7	54	.8	31	.5
4.	Remainder	.7	.7	.8	.8	.5	.5

References 1) Perry, Chemical Engineers Handbook, 3rd Edition
2) Jakob, Proc. Phys. Soc. 59:726 (1947)
3) Eckert and Drake, Heat and Mass Transfer, 2nd Edition

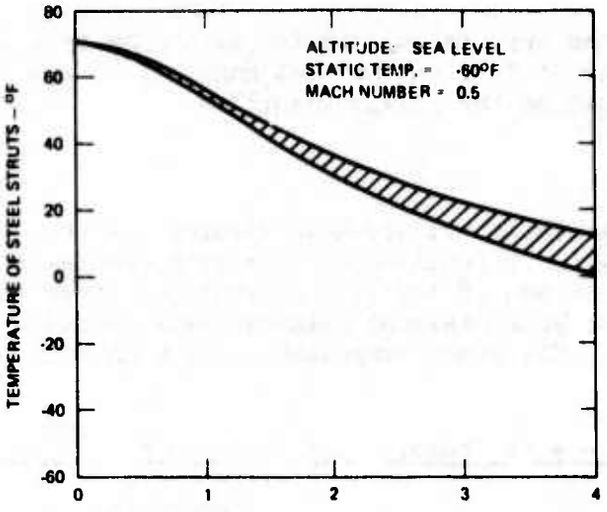

Figure 1. Temperature region of steel struts.

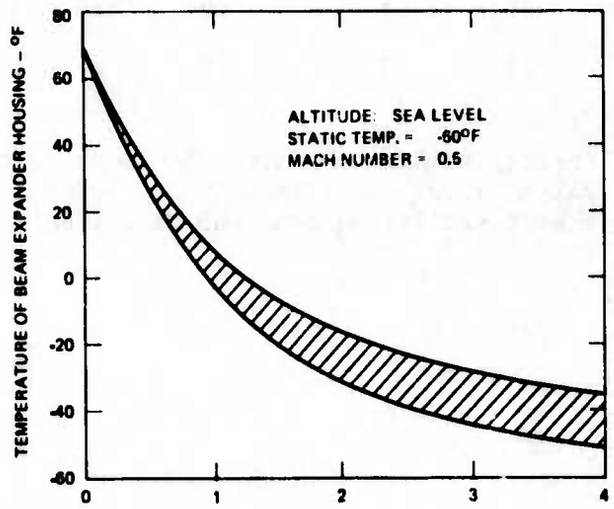

Figure 2. Temperature region of beam expander housing.

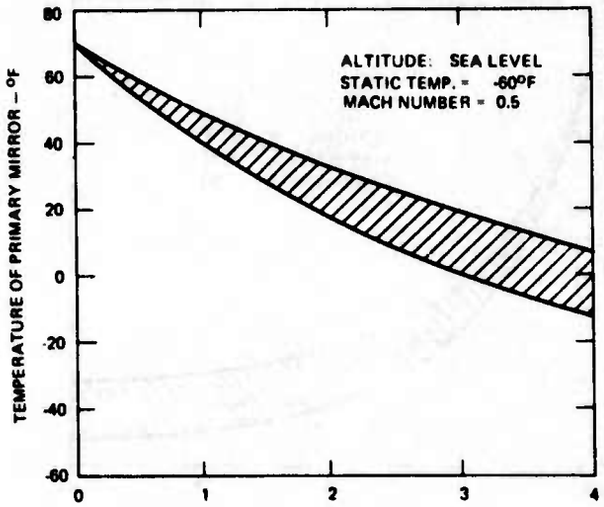

Figure 3. Temperature region of primary mirror.

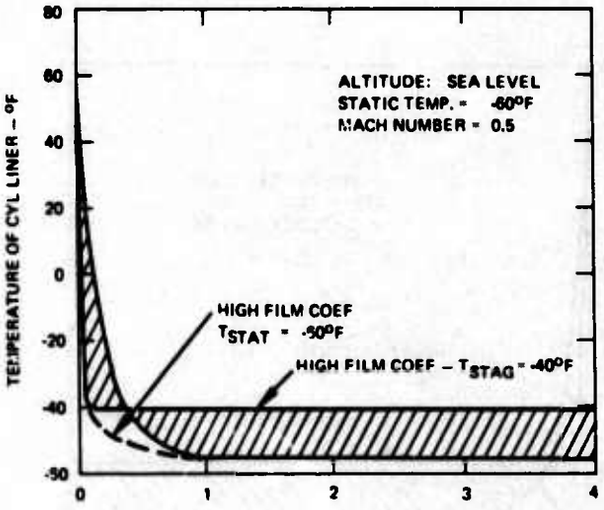

Figure 4. Temperature region of cylindrical liner.

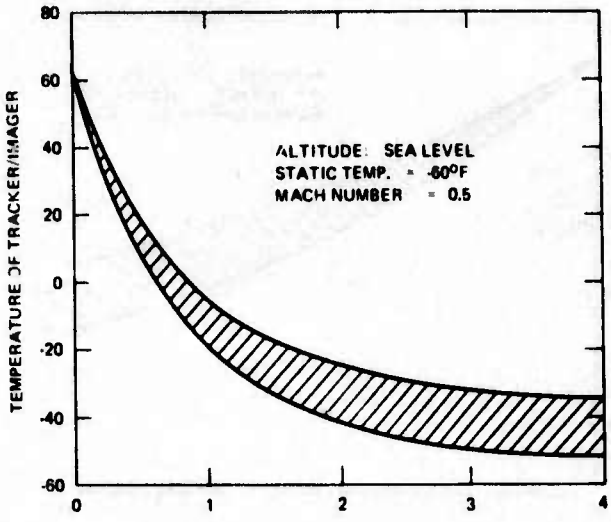

Figure 5. Temperature region of tracker/imager body.

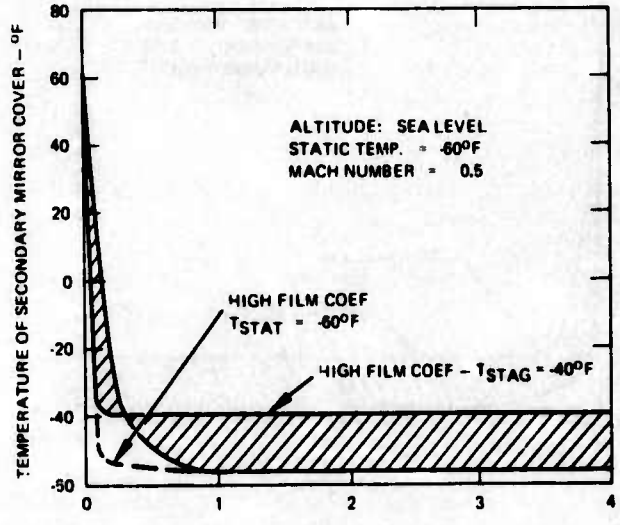

Figure 6. Temperature of secondary mirror cover.

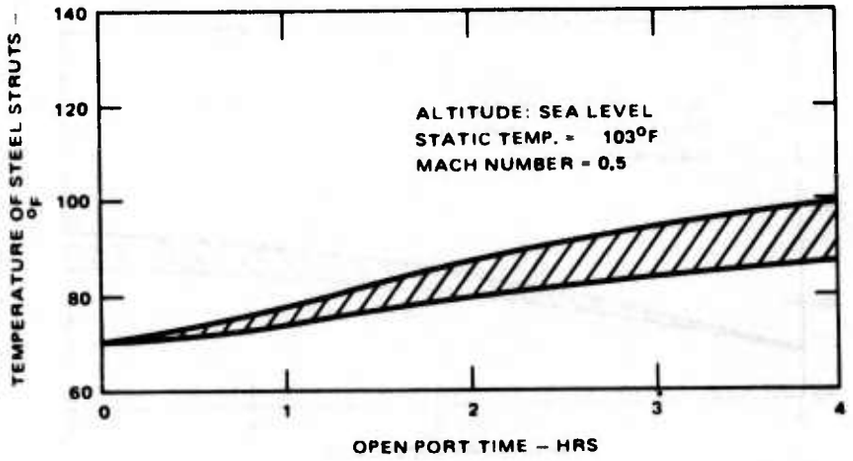

Figure 7. Temperature region of steel struts.

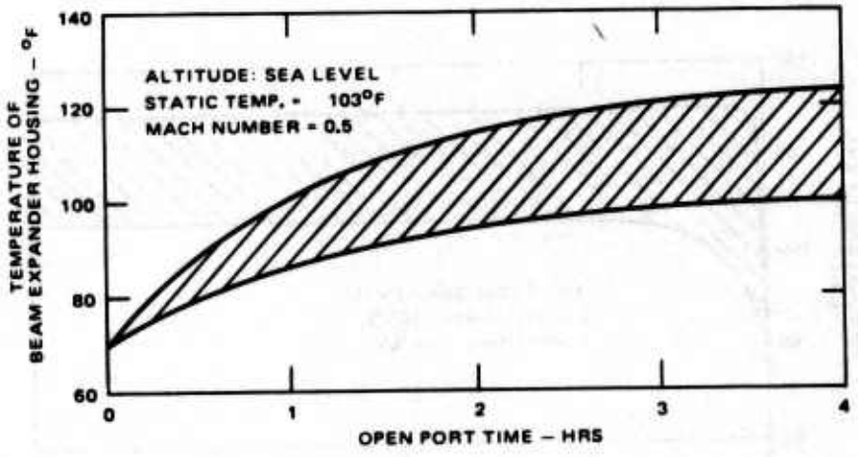

Figure 8. Temperature region of beam expander housing.

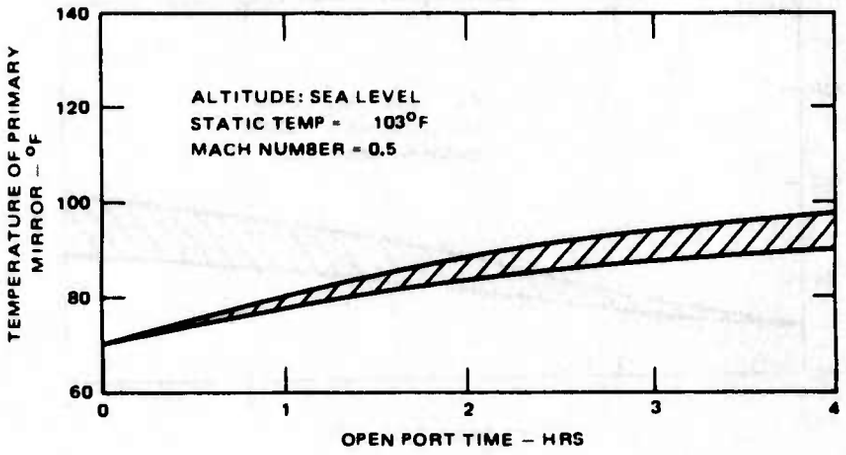

Figure 9. Temperature region of primary mirror.

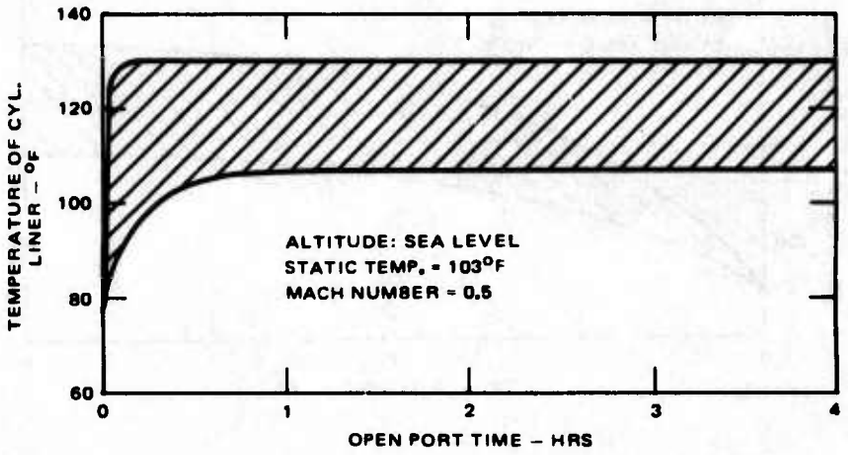

Figure 10. Temperature region of cylindrical liner.

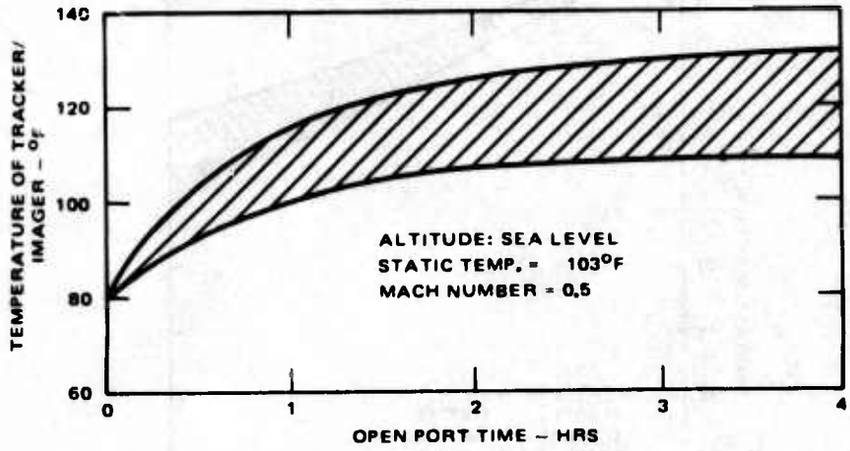

Figure 11. Temperature region of tracker/imager body.

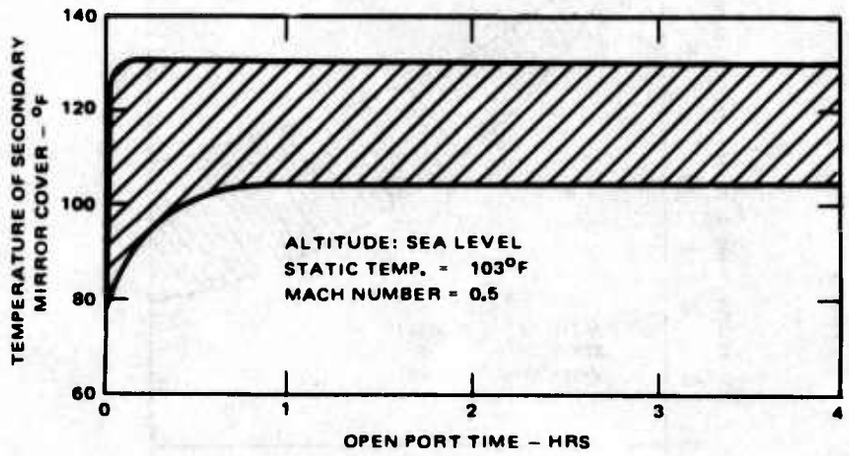

Figure 12. Temperature region of secondary mirror cover.

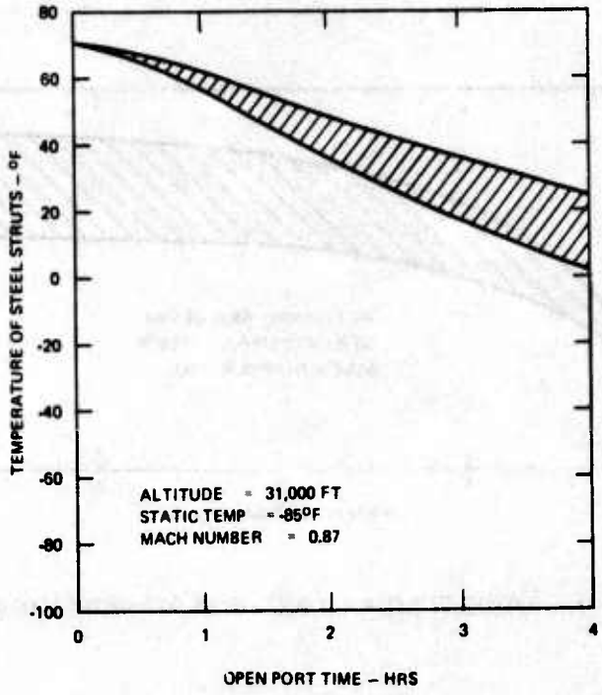

Figure 13. Temperature region of steel struts.

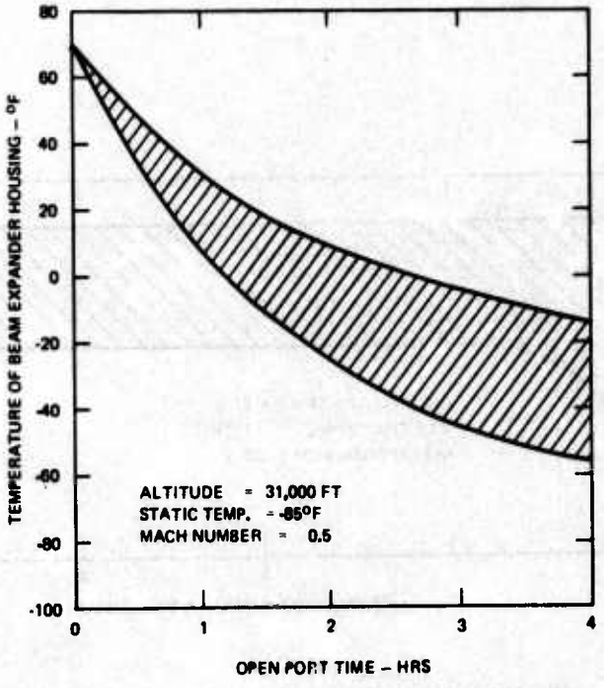

Figure 14. Temperature region of beam expander housing.

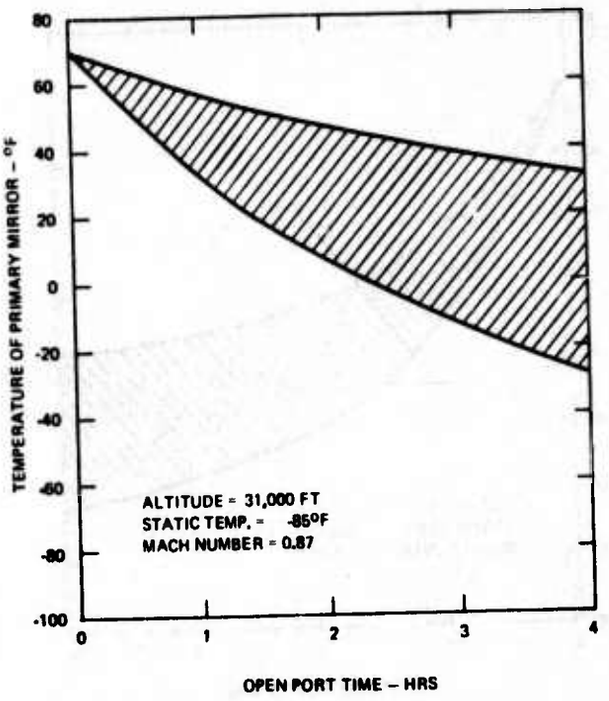

Figure 15. Temperature region of primary mirror.

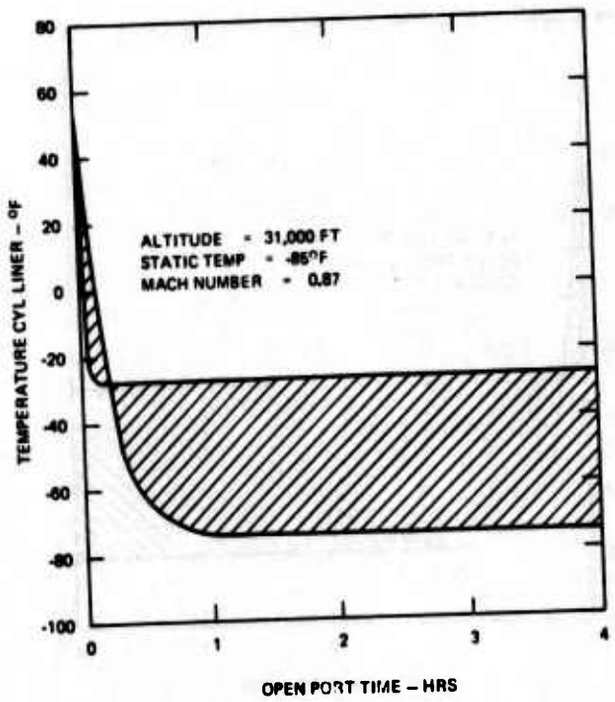

Figure 16. Temperature region of cylindrical liner.

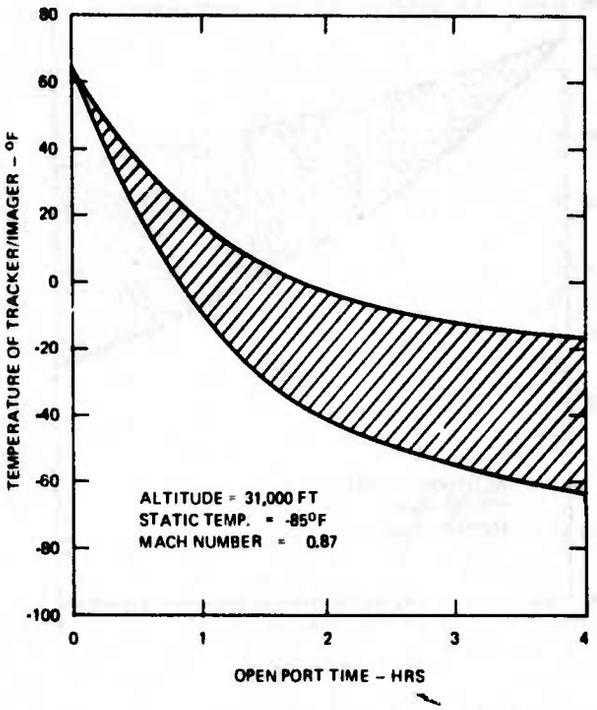

Figure 17. Temperature region of tracker/imager body.

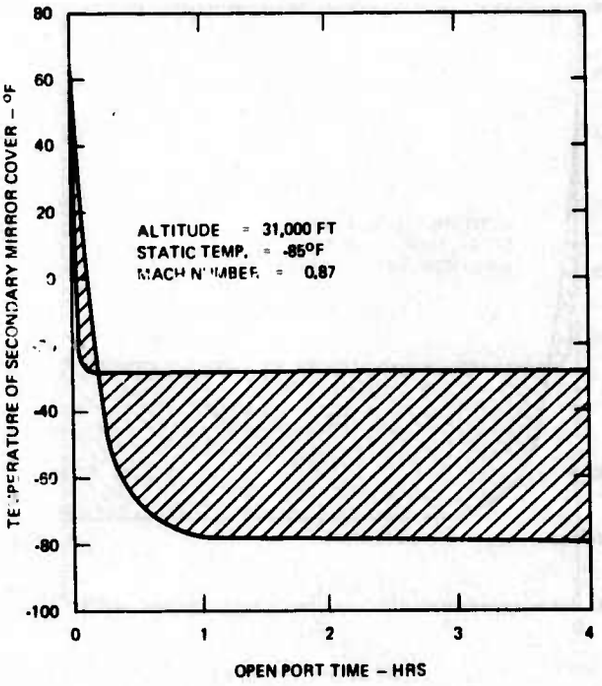

Figure 18. Temperature region of secondary mirror cover.

APPENDIX 6

APT OPEN PORT AERODYNAMIC ANALYSIS

APT Aerodynamic Flow Field Results

The APT open port liner and aerodynamic fence have been studied from both structural integrity and acoustic vibration viewpoints.

It is concluded that the present design is sound based upon available information from both the 0.3 scale wind tunnel test model and flight test bed.

Aerodynamic load on this protection cover will be small. But the disturbing torque about outer azimuth axis may become excessive. This is a situation that needs to be closely monitored.

This protection cover has been designed to avoid a possible 300 Hz acoustic excitation. It is also believed that APT open port should provide better acoustic absorption than test model because of various built-in acoustis resistances.

APT Open Port Flow Field and Acoustic Radiation Study

References:

1. 0.3-Scale Open Port ALL Turret Wind Tunnel Test Results, Capt. L. J. Otten end Lt. J. A. Devis, AFWL-TR-73-17, Vol. 1, April 1973 (Confidential)
2. The Dynamics and Thermodynamics of Compressible Fluid Flow, A. H. Shapiro, The Ronald Press, 1953
3. Principles of Aerodynamics, J. H. Dwinnell, McGraw-Hill, 1949
4. Boundary Layer Theory, H. Schlichting, McGraw-Hill, 1960
5. Basic Aerodynamic Noise Research, NASA SP-207, I. R. Schwartz Editor, NASA, 1969
6. "Wind Tunnel Experiments on the Flow Over Rectenguler Cavities at Subsonic and Trensonic Speeds," J. E. Rossiter, TR No. 64037 Royel Aircraft Esteblishment, 19o4

1.0 Introduction

This analysis is based primarily on the test results of the 0.3 scele model. It is realized that since standard sea level air had been used throughout the test program, Reynolds numbers of flight conditions have not been simulated.

However, steady state pressure distribution over the turret should be very similar to the test results et corresponding Mach numbers beceuse pressure coefficient is usually not sensitive to variations in Reynolds number for high Reynolds number air flow.

The difference in Reynolds number and temperature for the same Mach number does lead to different Prandtl number between flight test and wind tunnel model test. This indicates thet boundary layer flows of the two types of tests may not be "similar". Some deviations in fluctuating pressure field will be expected. According to recent flight envelope data received from AFWL, there is a possibility that rms disturbing torque about outer azimuth gimbal may become excessive (e.g., 2,700 in-lb for M = 0.75 at H $\gtrsim$ 20,000 ft) so that to cause the error in ezimuth engle more than 0.22 mrad.

Deviations between flight test end wind tunnel test under the same free stream Mach numbers will also be reelized because of the additional perturbations caused by the fuselage. For example, e 10% velocity perturbation at the nose of the eircraft may generate local sonic flow while M_∞ is below 0.65, which means shock end shear layer interection may happen much sooner than expected.

2.0 Flow Field Analysis

Configuration 17 of the wind tunnel test model is used as reference for this study. In this configuration, front fairing is removed for wider coverage, but the aft fairing is used to reduce wake formation.

The turret itself is a half-sphere and short cylinder combination. Ordinarily the flow pattern over a sphere or a cylinder is represented by the corresponding pressure distribuiton curve shown in Figure 1 and Figure 2 where the theoretical curves indicate non-viscous flow over these bodies.

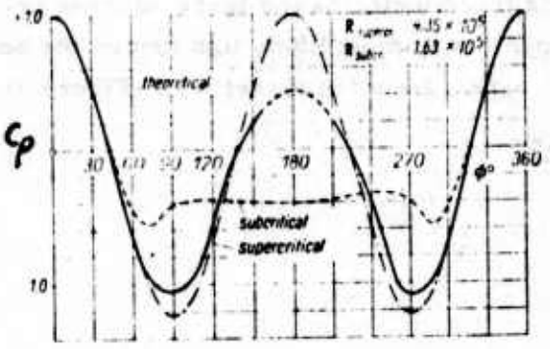

Figure 1. Pressure Distribution Around a Sphere

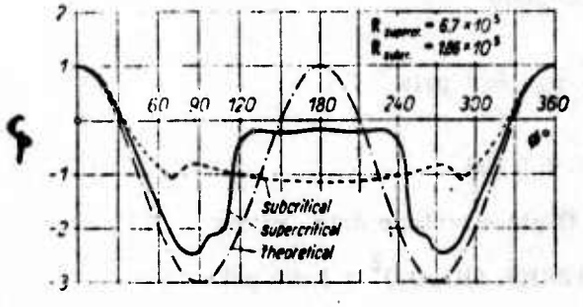

Figure 2. Pressure Distribution Around a Cylinder

The use of an aft fairing has greatly modified the flow field from that of a sphere. Results from wind tunnel tests indicate that pressure coefficients at different Mach numbers have had little changes. They all show a maximum value of

$$C_p \simeq 1.10 \text{ at stagnation point}$$

for high subsonic flow. While the peak negative pressure coefficients have always been near

$$C_p = -0.5$$

For $\theta_{Az} = 90^o$ and up. This trend indicates the large adverse pressure gradient produced by the open cavity most likely has forced the boundary over the aerodynamic fence to separate from the turret wall (Figure 3).

Maximum Dynamic Pressure

For isenhopic flow,

$$q = \frac{\gamma}{2} pM^2$$

since $\gamma = 1.4$

for air

this means that

$$q = 0.7pM^2$$

According to the flight envelope data (see Figure 4), the following case most likely will creat the dynamic pressure: of maximum magnitude:

$M_\infty = 0.75$ at 20.000'

$M_x = 1.02$

$q_\infty = 2.8$ psi, $p_\infty = 6.7$ psia

From these

$$p_o = p_\infty + q_\infty = 9.5 \text{ psi}$$

which, according to the flight envelope data, gives

$$q_x = 0.7\,(0.5128)(9.5)(1.02)^2 = 3.55 \text{ psi}$$

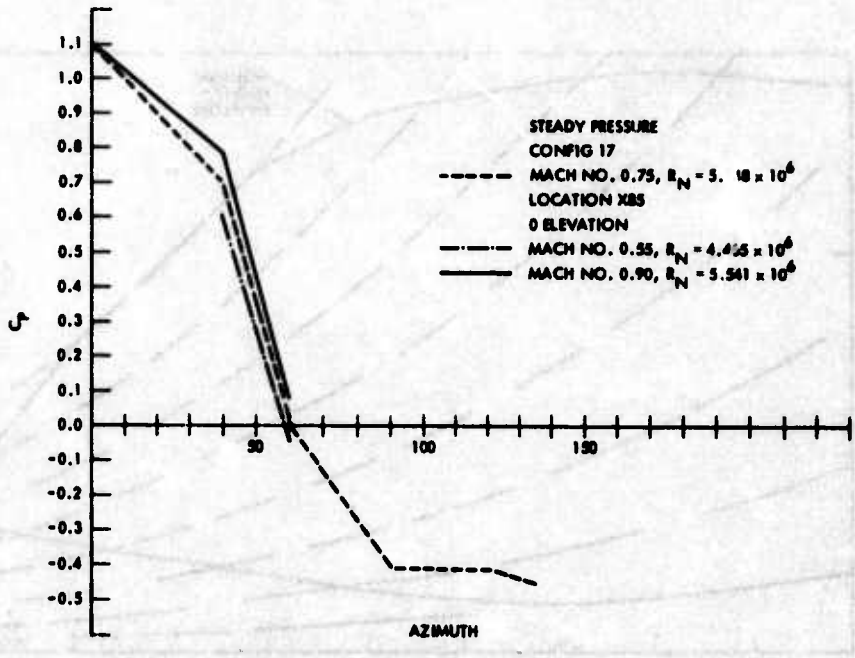

Figure 3. C_p,, Configuration 17, Position 6

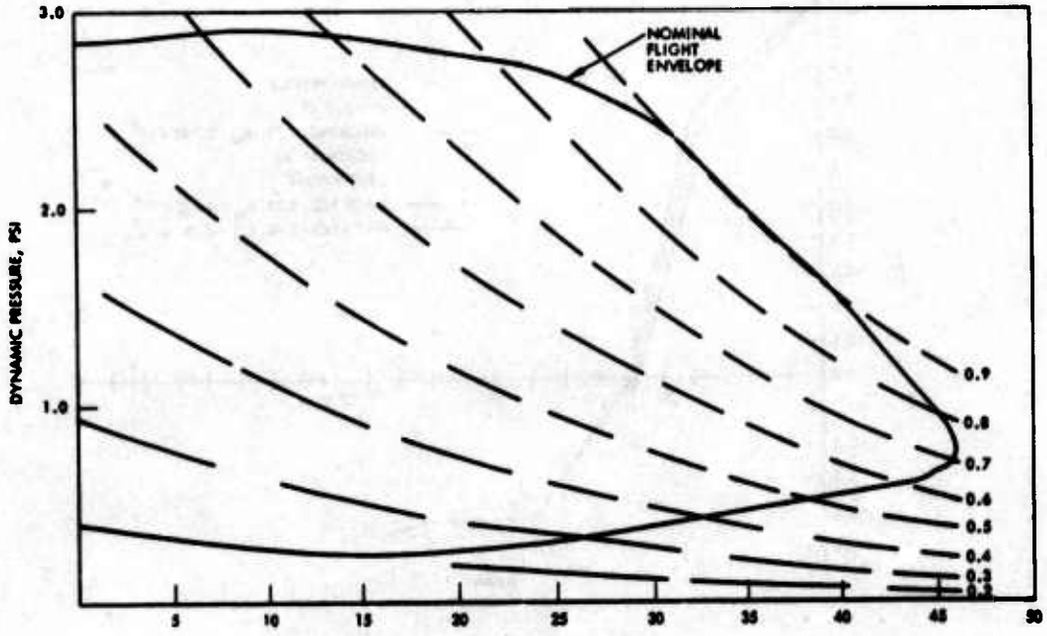

Figure 4. Dynamic pressure envelope.

In the design of aerodynamic fence, a maximum value of 4.00 psi is used. For a 50% porous fence this value is considered to be conservative.

Acoustic Vibrations

It appears that at low gimbal angles, air column inside the open and closed end pipe is excited by the boundary layer to vibrate at a broad band of frequencies. According to recent test on configuration 11, the random torque about outer azimuth axis has reached a value of

$$T_{o.a.} = 140 \text{ in-lb.}$$

for $\theta_{az} = 0^o$, $\theta_{el} = 28^o$. This means that for APT open port operation, a corresponding torque of

$$T'_{o.a.} = 9.59 \times 140 = 1,350 \text{ in-lb. at } 33,000'$$

can be realized. Since the maximum allowable disturbance torque for outer azimuth axis is 2,000 in-lb for 0 to 0.4 hz frequencies and 4,000 in-lb for 0.4 to 100 hz frequencies, this fluctuating torque should be carefully monitored. Using the dynamic pressure envelope of Figure 4, this disturbing torque may exceed 2,700 in-lb at lower flight altitude (e.g. 20,000 ft at $M_{\infty\infty} = 0.75$).

At higher gimbal angles, accoustic vibrations are more likely produced by vortex shedding. Because of the flow before the front lip of the cavity can be supersonic at higher free stream speed, this indicates that greater interaction between shock waves and shear layer flow. The predominant frequency for this type of vibration has been about 1,100 Hz for the 0.3 model, so that it is expected for APT a corresponding vibration of 330 Hz (Figure 5).

3.0 Mechanical Design

Aerodynamic Fence

Taking q = 4 psi

and $\ell = 1''$ for unsupported length.

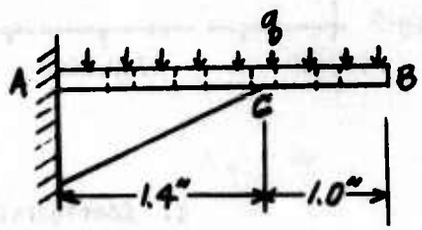

Figure 6. Aero. Fence

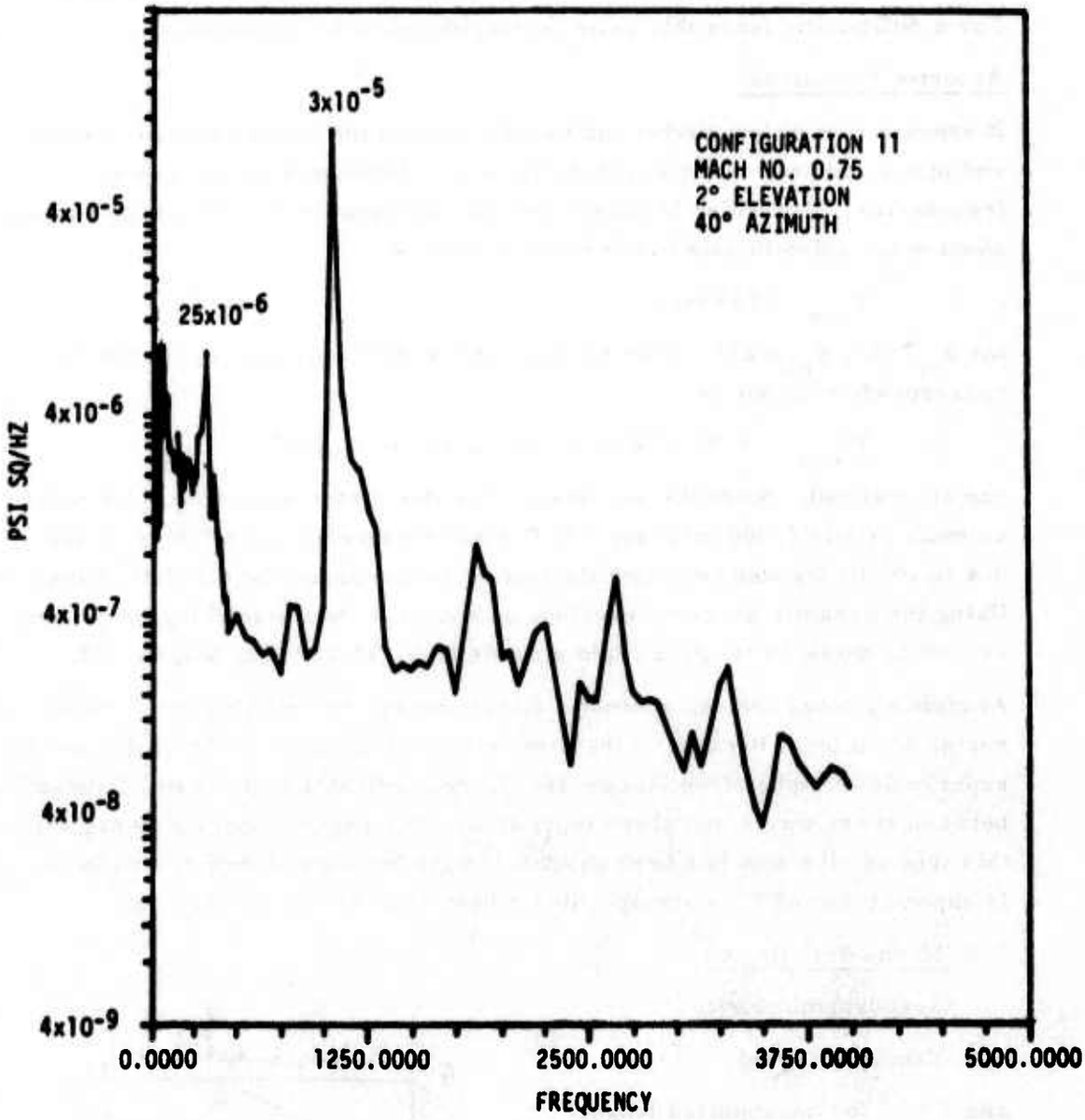

c. Configuration 11, 40 Degree Az

ACCOUSTIC RESONANCES AT HIGHER GIMBAL ANGLES

Figure 5

Bending moment at section C

$M_c = \frac{1}{2} q\ell^2 = 2$ in-lb/in. of screen

Cross sectional moment of inertia

$I = \frac{t^3}{12}$ in^4/in. of screen

Maximum bending stress is given by

$$J = \frac{M_c \left(\frac{t}{2}\right)}{I} = \frac{6 M_c}{t^2} = \frac{12}{t^2}$$

for $\frac{1}{16}$ in. solid plate, this is

$\sigma = 3{,}100$ psi

It is noted that section C is not really built-in. But in reality the dynamic pressure q is also a lot less than 4.0 psi because of the porosity of the screen. It is reasonable to assume that

$\sigma \leq 3{,}100$ psi

By considering a unit length of the fence as a cantilever beam, its fundamental frequency of vibration can be estimated to be

$$f > \frac{1}{2\pi}(3.52)\sqrt{\frac{10^7 \times \frac{1}{12}\left(\frac{1}{16}\right)^3 \times 386}{0.1\,(1.0)^4}} \approx 500 \text{ Hz}$$

Wind Load On Strut Covers

Consider the typical case of $H = 2.6^k$

$M = 0.9$

$q_\infty = 2.9$ psi

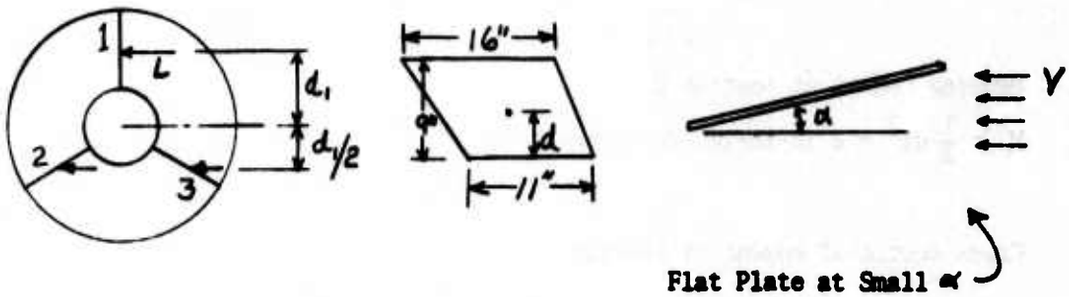

FIGURE 7

Aerodynamic Load On Strut Covers

since

$$A = \frac{1}{2}(11+16)(9) = 121 \text{ in}^2$$

the lift force on each strut is given by

$$L = C_L\, q\, A \approx (1.0)\, q\, A = (2.90)(121) = 350 \text{ lb}$$

and the moment on it is

$$M_1 = L\, d \quad 350\,(4.5) = 1{,}580 \text{ "-\#} \quad \text{(Moment on \#1 strut)}$$

so that the total moment due to wind load is

$$M = M_1 + \frac{1}{2} M_1 = \frac{1}{2} M_1 = 790 \text{ "-\#}$$

For the present strut cover of 3×10^{-3} inch thick, this means maximum flexural stress of

$$\sigma = \frac{790}{h \text{ (cross sectional area)}} \approx 2{,}000 \text{ psi}$$

Force And Deflection Of The End Plate

The wind pressure, p = 2 psi gives

Total pressure on plate

$$P = pA \approx 2\pi\,(9^2 - 4^2) = 410 \text{ \#}$$

Elongation of supports (unstiffened)

$$\delta_1 = \frac{P}{E_A} = \frac{410\,(8)}{10^7\,(\frac{1}{8})(1)(12)} = 2.2 \times 10^{-4} \text{ in}$$

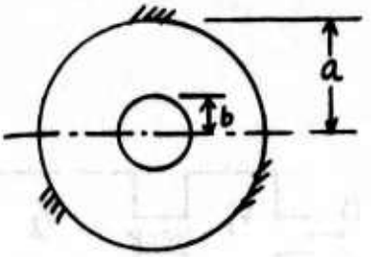

Figure 8 Deflection Of Plate Due To Distributed Load

According to Timoshenko,

$$\delta = K_1 \frac{P a^4}{E h^3}$$

with

$K_1 = 0.060$ for the present construction, and

$h = .25"$

$p = 2$ psi

so that

$$\delta = 0.06 \frac{2 \times (9)^4}{10^7 (.25)^3} = (.12)(.9)^4 (4)^3 10^{4-7} = 5 \times 10^{-3} \text{in.}$$

which means that the deflection is small even if the aerodynamic load is doubled.

Resonance Frequency Of Cylindrical Liner (Bending Mode)

Before gassets are used, its bending mode vibration has a frequency of

$$f = \frac{1}{2\pi} \frac{12{,}200 \times 386}{1.5} = 282 \text{ Hz}$$

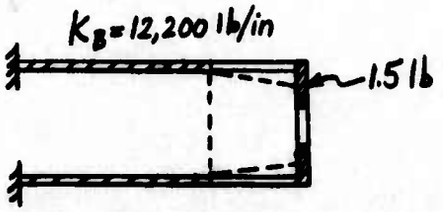

Figure 9. Liner Vibration

This resonance frequency is probably close to one of the dominant accoustic excitation frequency which is expected to be in the neighborhood of 330 Hz to 370 Hz. Thus, it is recommended to stiffen each of the bracket with a suitable gasset. Doing so, the final bending vibration of the end plate will have a frequency exceeding 500 Hz.

Accoustic Absorption

The telescope cavity can be viewed as Volume V_1, and the rest of the space inside the turret may be viewed as equivalent to V_2, the sum of all the large and small openings on the porous liner as well as the telescope itself can be considered as the neck of the Helmholtz resonator.

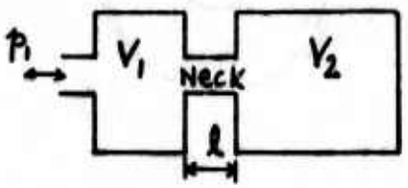

Figure 10 a

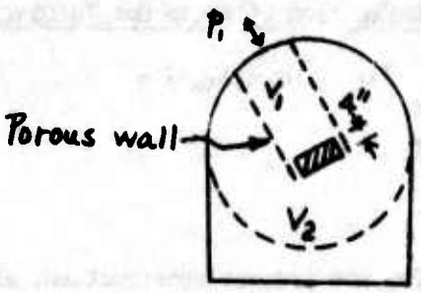

Fig. 10b Physical Model

Equivalent Low Pass Fluid Filter

case 1 Porous Wall ($\frac{1}{4}$" screen, A = 20 in^2)

$$f_1 \text{ (cutoff freq.)} = \frac{2C}{2\pi}\sqrt{\frac{A\ (Neck)}{(V_1 + V_2)\,l}} \approx \frac{12{,}000}{\pi}\sqrt{\frac{20}{1.4 \times 10^5 (\frac{1}{4})}} \approx 91 \text{ Hz}$$

case 2 Slot Between Primary Mirror And Telescope Tube

$$f_2 \text{ (cutoff freq.)} \approx \frac{12{,}000}{\pi}\sqrt{\frac{24}{1.4 \times 10^5 \times 4}} \approx 28 \text{ Hz}$$

4.0 Window Cover Pneumatic Seal

Figure 11 is a schematic of the bottle and seal. The seal will be completely inflated when its pressure reaches 24 psi. The bottle is designed to supply enough air at an initial pressure of 2,100 psi. The design data is:

V_B = 22 in^3

$(\rho_B)_0$ = 2,100 psi

V_S = 24 in^3

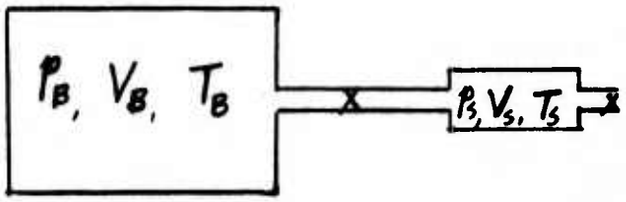

Figure 11. Window Pneumatic Seal

Consider the process to be isothermal, then for 40 shots, it requires a volume of high pressure air to be given by

$$P'_B V'_B = \rho_S (40 V_S)$$

$$\text{or } V_B' = \frac{40 \rho_S V_S}{\rho_B'} \qquad \rho'_B = \rho_B$$

$$= \frac{40 (24 + 14.7) (22)}{2100 + 14.7}$$

which means that the final bottle pressure will be

$$\rho_f = \left(\frac{22 - 16.1}{22} \right) (2114.7) = 560 \text{ psi}$$

Since leakage and temperature changes are not considered here, the real final pressure inside the supply bottle should be lower than this.

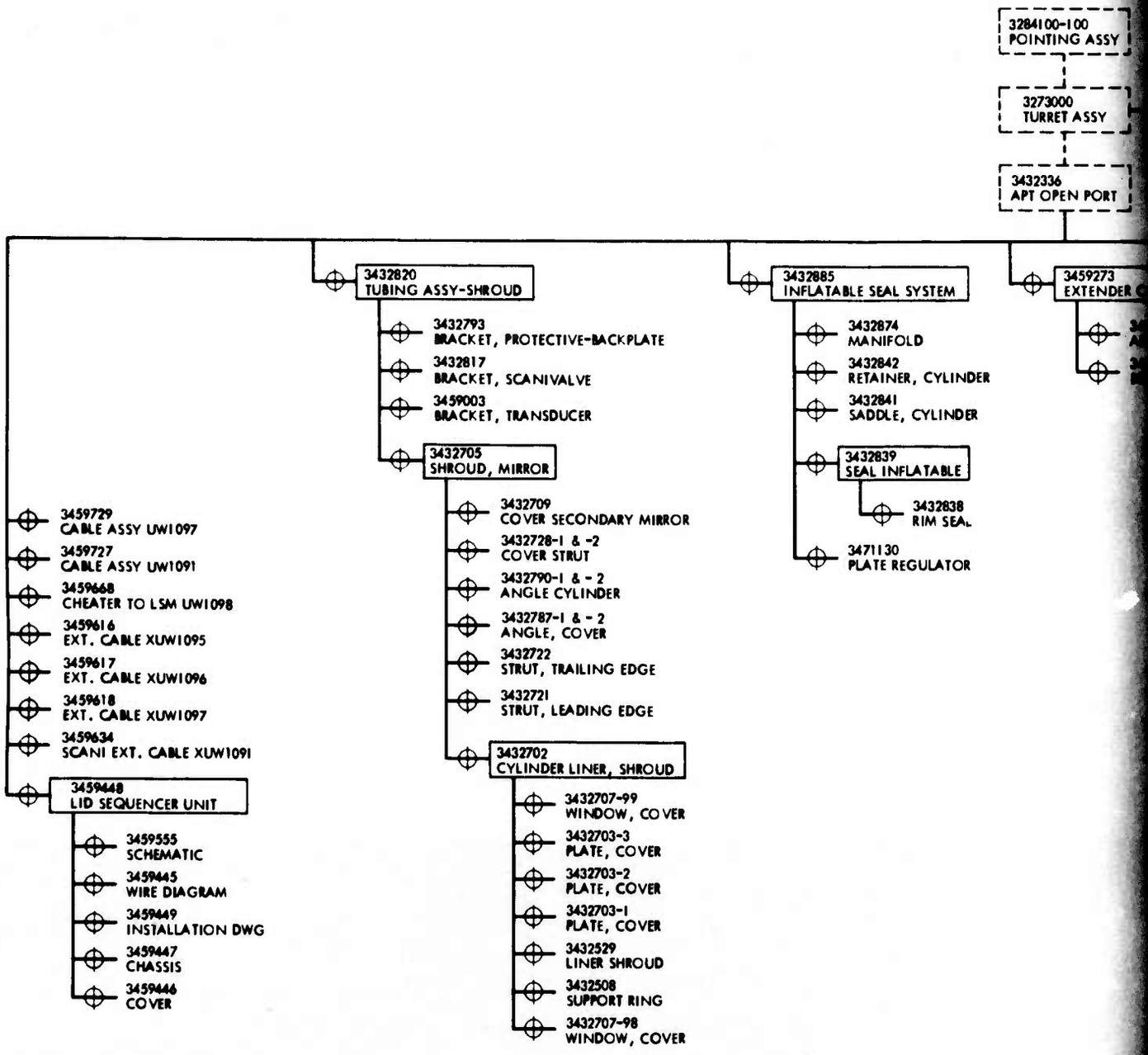

2

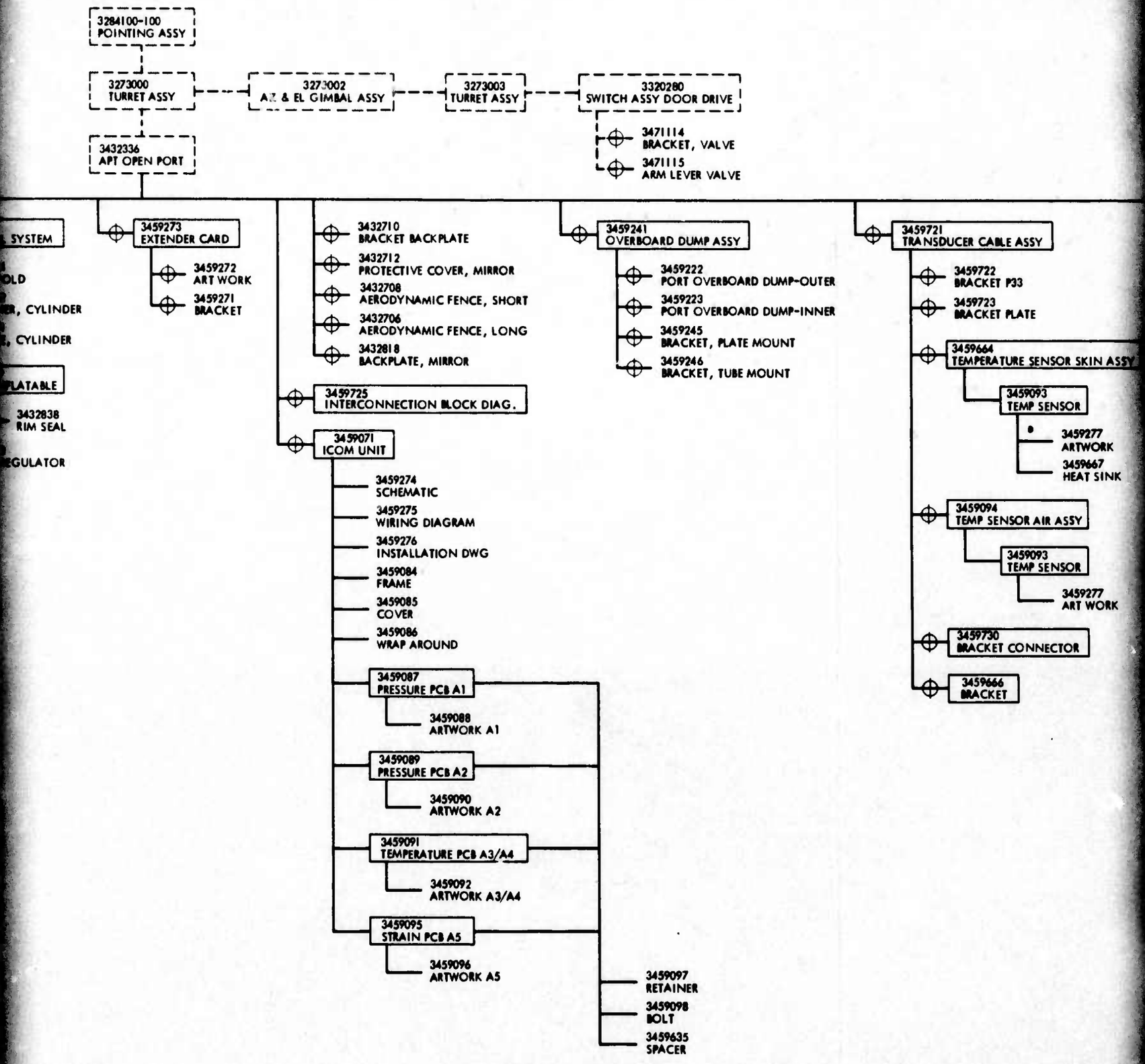
3284100-100
POINTING ASSY
3273000
TURRET ASSY
3273002
AZ & EL GIMBAL ASSY
3273003
TURRET ASSY
3320280
SWITCH ASSY DOOR DRIVE
3471114
BRACKET, VALVE
3471115
ARM LEVER VALVE
3432336
APT OPEN PORT
SYSTEM
OLD
R, CYLINDER
, CYLINDER
LATABLE
3432838
RIM SEAL
EGULATOR
3459273
EXTENDER CARD
3459272
ART WORK
3459271
BRACKET
3432710
BRACKET BACKPLATE
3432712
PROTECTIVE COVER, MIRROR
3432708
AERODYNAMIC FENCE, SHORT
3432706
AERODYNAMIC FENCE, LONG
3432818
BACKPLATE, MIRROR
3459725
INTERCONNECTION BLOCK DIAG.
3459071
ICOM UNIT
3459274
SCHEMATIC
3459275
WIRING DIAGRAM
3459276
INSTALLATION DWG
3459084
FRAME
3459085
COVER
3459086
WRAP AROUND
3459087
PRESSURE PCB A1
3459088
ARTWORK A1
3459089
PRESSURE PCB A2
3459090
ARTWORK A2
3459091
TEMPERATURE PCB A3/A4
3459092
ARTWORK A3/A4
3459095
STRAIN PCB A5
3459096
ARTWORK A5
3459097
RETAINER
3459098
BOLT
3459635
SPACER
3459241
OVERBOARD DUMP ASSY
3459222
PORT OVERBOARD DUMP-OUTER
3459223
PORT OVERBOARD DUMP-INNER
3459245
BRACKET, PLATE MOUNT
3459246
BRACKET, TUBE MOUNT
3459721
TRANSDUCER CABLE ASSY
3459722
BRACKET P33
3459723
BRACKET PLATE
3459664
TEMPERATURE SENSOR SKIN ASSY
3459093
TEMP SENSOR
3459277
ARTWORK
3459667
HEAT SINK
3459094
TEMP SENSOR AIR ASSY
3459093
TEMP SENSOR
3459277
ART WORK
3459730
BRACKET CONNECTOR
3459666
BRACKET

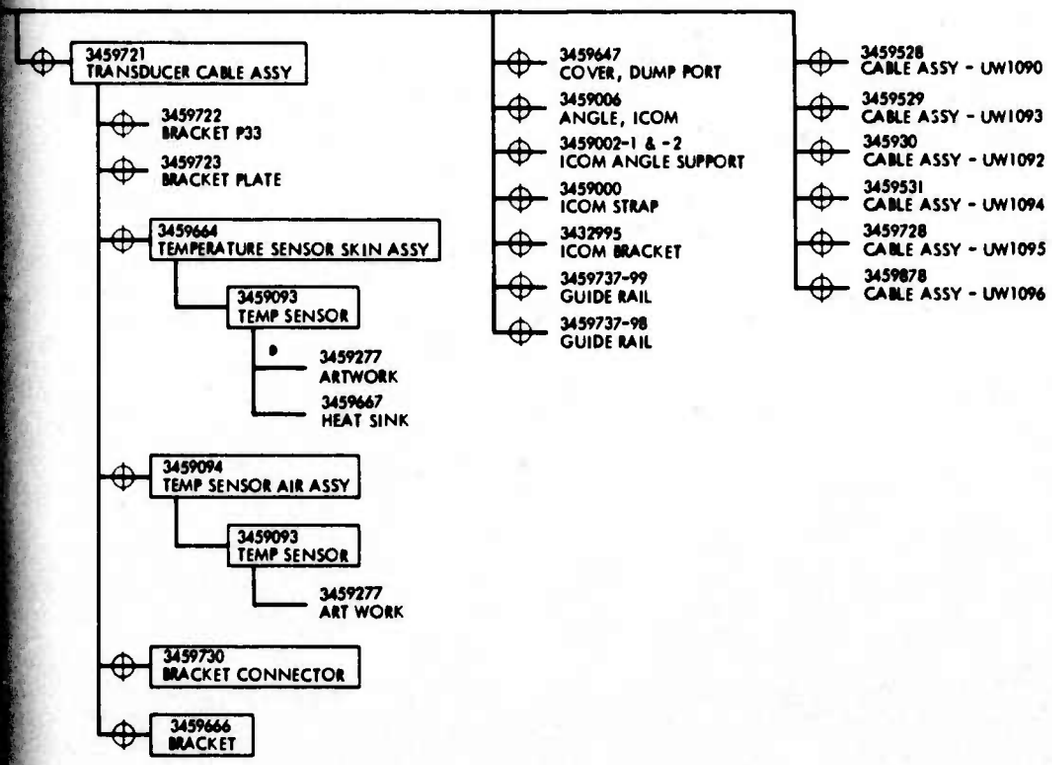

Figure 1-3. Open Port drawing breakdown.

DISTRIBUTION

HQ USAF (AFRDPS/Lt Col Chiota)	1	USAFA (P. Ravelli)	1
HQ USAF (INAKA/Lt Col Truesdell)	1	USAFA (M. Elnick)	1
AFSC (XRLW/Maj Walton)	1	USAEC (AMSEL-XL-H/R. Buser)	1
AFSC (DLCAW/Capt Pulley)	1	Off of the Ch R&D (DARD-ARS-P)	1
SAMSO (XRTD/Capt DeMaio)	1	Off of the Ch R&D (DARD-DD)	1
SAMSO (DY/Col Johnson)	1	Asst Ch of Staff (DAFD-AD/Maj Bradley)	1
AFAL (CA/Dr. Eppers)	1	Asst Ch of Staff (DAFD-SDF/1TC Fryan)	1
AFAL(TEL (405B)/Capt Matassov)	1	Safeguard Sys Off (Mr. Bast, Jr.)	3
AFAL (WRW/Mr. Toto)	1	ABMDA (RDMC-NC/Mr. Zlotnick)	1
AFAL (TEO/Mr. Hutchinson)	1	Rock Island Arsenal (SARRI-LR/McGarvey)	1
AFAL (RWI/G. Fitzgibbon)	1	USAME R&D (SMEFB-MW)	1
RADC (OCSE/Mr. Urtz)	1	USAMC (AMSMI-RNS)	1
RADC (OCTM/Mr. Rehm)	1	USAMC (AMSMI-RGN)	1
RADC (OCTM-1/Mr. Ogrodnik)	1	USAMC (AMCRD-T/Dr. Stefanye)	1
ESD (XRT/A. Anderson)	1	USAMC (AMCRD-T/Mr. Chernoff)	1
AFML (LPJ/Maj Elder)	1	USAMC (AMCRD-T/Dr. Zarwyn)	1
AFML (LPO/Dr. Frederick)	1	Armament Command (AMSAR-RDT)	1
AFRPL (LKCG/B. Bornhorst)	1	Air Def School (ATSA-CTD-MS/Capt Poage)	1
AFAPL (CC/D. Cheatom, Jr.)	1	T&E Command (AMSTE-ME/Dr. Pentz)	1
CINCSAC (INEP)	1	USA Ord Ctr & School (ATSL-CTD-MS-R/	
ARL (AP/Lt Col Duggins)	1	LTC Stewart)	1
AFFDL (FX/Dr. VanKuren)	1	Off Nav Rsch (F. Quelle)	1
AFFTD (PDTR/Lt Faehl)	1	NRL (Dr. Linvingston/Code 5560)	1
AFFTD (ETEO/R. Buxton)	1	NRL (Dr. Shenker/Code 5507)	1
AF Academy (FJSRL/Capt Asher)	1	NRL (Mr. McLaughlin/Code 5560)	1
CIGTF (Col Clark)	1	NRL (Dr. Walsh/Code 5503)	1
AFWL (HO)	1	NRL (Dr. Connolly, Jr./Code 5503C)	1
AFWL (SUL)	2	NRL (Dr. Schriempf/Code 6330)	1
AFWL (LRL)	1	NRL (Dr. Wenzel/Code 6461)	1
AFWL (LRP)	1	NRL (Dr. Rice/Code 6130)	1
AFWL (LRE)	1	NRL (Dr. Milton/Code 6504-3)	1
AFWL (LRO)	5	NRL (Mr. Anderson/Code 6550)	1
AFWL (DY)	1	ONR (421/F. Isackson)	1
AFWL (PG)	5	ONR (W. Condell)	1
AFWL (AL)	1	HELPO (PMO-405/Capt Wilson)	1
AFWL (ALO)	3	NOL (Dr. Schindel/Code 310)	1
AUL (LDE)	1	NOL (Dr. Harris/Code 313)	1
AFEWC	1	NOL (Mr. Enkenhus/Code 034)	1
Dep Ch of Staff for Ops		NOL (Mr. Wise/Code 047)	1
(DAMO-RQD/LTC Mayhew)	1	NOL (Mr. Nikirk/Code 422)	1
(DAMO-RQD/LTC Fox)	1	NWC (Bittel/Code 3014)	1
USAMC R&D (W. Jennings)	1	NWC (Niccum/Code 5114)	1
USAMC R&D (AMSMI-RGN/G. Scheiman)	1	Nav Ops (OP-982F3/Capt Greeley)	1
ABMDA (CRDABH-O)	1	Nav Material (Dev (Mr. Gaylord/MAT032B)	1
ABMDA (ATC-R/D. Schenk)	1	NMC (Gibbs/Code 5352)	1
ABMDA (ATC-M/A. Carmichael)	1	Nav Postgrad School (Lib/Code 2124)	1
ABMDA (ATC-O/W. Davies)	1	ARPA (S. Lukasik)	1
BRL (E. Alcarez)	1	ARPA (STO)	2
BRL (R. Eichelberger)	1	ARPA (TIO)	1
BRL (F. Allen)	1	DDC (TCA)	2
USACDC, Air Def Agency	1	DIA (DT 1D/S. Berler)	1
USACDC, Dir Mat/Msl Div	1	ODDR&E (Dr. Cooper)	1

DISTRIBUTION

CIA (Mr. Nall)	1	LMSC (B. Dunn)	1
ERDA (Dr. Killion)	1	LASL (Dr. Boyer)	1
NASA (Dr. Dunning, Jr)	1	LASL (Dr. Judd)	1
NASA (Mr. McKenzie)	1	Lulejian & Asso	1
NASA (Dr. Billman)	1	Lockheed (Lunsford)	1
NASA (R. Saunders III)	1	Math Sci NW (Mr. Rose)	1
NSA (Mr. Foss)	1	Math Sci NW (Dr. Hertzberg)	1
Analytic Services (Dr. Davis)	1	Martin-Marietta (Mr. Chapin)	1
Aerojet Electro-Sys (E. Dryden)	1	Martin-Marietta (Mr. Giles)	1
Aerospace (Dr. Milburn)	1	Martin-Marietta (Mr. Wudell)	1
Aerospace (Dr. Warren)	1	MIT (Dr. Edelberg)	1
Airesearch Manuf (Mr. Stancliffe)	1	MIT (Dr. Marquet)	1
Atlantic Res (Mr. Naismith)	1	MIT (Dr. Freedman)	1
AVCO (Dr. Sutton)	1	MIT (Dr. Dinneen)	1
AVCO (Dr. Dougherty)	1	MIT (Dr. Rediker)	1
Battelle (Mr. Tietzel/STOLAC)	1	MIT (Dr. Kingston)	1
Bell Aerospace (Dr. Solomon)	1	McDonnell Douglass Astro (Klevatt)	1
Boeing (Gamble/Org 2-1360 MS 8C-88)	2	McDonnell Douglas Res (Dr. Ames)	1
C.S. Draper (K. Fertig)	1	MITRE (A. Cron)	1
Electro-Optical Sys (Dr. Jensen)	1	Phy Sci (Dr. Pirri)	1
Environ Rsch (R. Kauth)	1	Northrop (Dr. Hasserjian)	1
ESL (A. Einhorn)	1	Northrop (Mr. Wenninger)	1
GDC (F. Kuffer)	1	Northrop (Mr. Longmire)	1
EG (Mr. East)	1	Pacific Sierra Rsch (Dr. Lutomirski)	1
GE (Dr. Anderson)	1	Perkin Elmer (N. Schnog)	1
GE (Dr. Sigismonti)	1	P&W Aircraft (Dr. Sziklas)	1
GE (Mr. Harrington)	1	RAND (Dr. Culp/Mr. Carter/H. Liefer)	1
General Rsch (Dr. Holbrook)	1	Raytheon (Dr. Horrigan)	1
General Rsch (Dr. Crimi)	1	Raytheon (Dr. Statz)	1
Hercules (Dr. Voris)	1	Raytheon (Dr. Mehlhorn)	1
Hercules (Dr. Preckel)	1	Raytheon (Dr. Sonnenschien)	1
Hughes Rsch (Dr. Foster)	1	RCA (Mr. Mayman)	1
Hughes Rsch (Dr. Chester)	1	RRI (Dr. O'Neill)	1
Hughes Rsch (Dr. Entulov)	1	RRI (Dr. Bose)	1
Hughes Rsch (Dr. Picus)	1	RRI (HPEGL Lib)	1
Hughes Aircraft (Dr. Alcalay)	1	RRI (Dr. Skurnick)	3
Hughes Aircraft (Dr. Peressini)	1	R&D Asso (Dr. LeLevier)	1
Hughes Aircraft (Dr. Fitts)	1	R&D Asso (Dr. Hundley)	1
Hughes Aircraft (Mr. Welch)	1	RI (Mr. Kumagai)	1
Hughes Aircraft (Dr. Yates)	1	RI (Mr. Hovda)	1
Inst for Def Anlys (Dr. Schnitzler)	1	RI (Mr. Kraus)	1
Inst for Def Anlys (Dr. Musa)	1	Sandia Labs (Dr. Narath)	1
ITT Gilfillan (T. Dixon)	1	W.J. Asso (F. French)	1
JHU (Dr. Stone)	1	SRI (Dr. Armistead)	1
JHU (Dr. Gorozdos)	1	SRI (Mr. Malick)	1
JHU (R. Bruns)	1	Sci Applications	1
LLL (Dr. Kidder)	1	Sci Applications (Dr. Asmus)	1
LLL (Dr. Teller)	1	Sci Appli (Mr. Peckham)	1
LLL (Dr. Fleck)	1	Sci Appli (Dr. Meredith	1
LLL (Dr. Emmett)	1	Sys Consultants (Dr. Keller)	1
LLL (Mr. Haussmann)	1	Sys Sci & Software (Mr. Klein)	1

DISTRIBUTION

TI (MS 208/Dr. Coale)	1
Thiokol Chemical (Mr. Hansen)	1
TRW (Mr. Campbell)	1
UARL(Mr. McLafferty)	3
UARL(Mr. Angelbeck)	1
UARL (Mr. Grose)	1
UAC P&W (Dr. Schmidtke)	1
UAC P&W (Mr. Pinsley)	2
VARIAN Asso (Mr. Quinn)	1
Vought Sys LTV Aerospace (Mr. Simpson)	1
Westinghouse (W. List)	3
Westinghouse (Dr. Riedel)	1
Westinghouse (Mr. Hundstad)	1
MIT/Lincoln Lab/Code LRO/AFWL/KAFB	5
OSU (Prof Sebesta)	1
Aeronutronic Ford (Mr. Verble)	1
Analytic Sci (A. Gelb)	1
USA Tng & Doctrine (ATCD-CF)	1
Combined Arms Cntr (PROV)	1
Offl Record Cy (LRO/Maj Boesen)	1